Identifying Genetic Regulators of Dispersion in *Candida albicans* Biofilms

By

Stephanie H Geller

A dissertation submitted in partial fulfillment of
the requirements for the degree of

Doctor of Philosophy

(CELLULAR AND MOLECULAR BIOLOGY)

at the
UNIVERSITY OF WISCONSIN-MADISON
2023

Date of final oral examination 05/03/2023

The dissertation is approved by the following members of the Final Oral Committee:

Megan N. McClean, Associate Professor, Biomedical Engineering
Audrey Gasch, Professor, Genetics
Christina Hull, Professor, Biomolecular Chemistry and Medical Microbiology & Immunology
Mark Mandel, Associate Professor, Medical Microbiology & Immunology
Jeniel Nett, Associate Professor, Medical Microbiology & Immunology

Acknowledgements

I would like to begin by thanking my advisor, Dr. Megan McClean for all the help and encouragement throughout these years together. When I started in her lab as an intern I had very little experience working in a lab. With such grace she taught me the ropes of how to be and think like a scientist. I would not have been able to complete this thesis without her help. I would also like to thank my committee members, Dr. Christina Hull, Dr. Mark Mandel, Dr. Jeniel Nett, and Dr. Audrey Gasch for their stimulating discussions and valuable feedback.

I would like to thank the past and current members of the McClean lab for their support and creating an environment where it is easy for a scientist to grow. The game nights, Game of Thrones marathons, and lunches at the library were always helpful after hard days in lab. Specifically, I would like to thank Taylor Scott for the helpful discussions and valuable feedback, Neydis Morales Moreno for encouragement through many failed experiments, and Kieran Sweeney for help analyzing data, giving constructive feedback, and always encouraging me to get out of my comfort zone. Additionally, I thank Luke Voce for help developing the underoil microfluidic tool for use in *C. albicans*.

I am also grateful for the Andes and Nett lab members, specifically Robert Zarnowski, and Chad Johnson, for their help to understand *Candida albicans* and teaching me how to study this organism. Bringing a new organism into a lab is never easy, but their guidance made the process very smooth. I would also like to thank our collaborators David Beebe, Chao Li, and Grace Li for the development of the underoil microfluidic system and helpful discussions. I also appreciate the Carbone Cancer Center Flow Cytometry lab, Gene Expression Center, and Bioinformatic Resource Center for their assistance in my countless experiments.

Lastly, I would like to thank my family: my parents Jack and Diane, my siblings Sam, Katy, and Sarah, and my brother-in-law Steve. Thank you for always lending an ear on the hard days and excitingly celebrating with me on the good days. They have always encouraged me to continue learning and reminded me of my capabilities when I doubted them.

This research was supported by the National Institutes of Health and Burroughs Wellcome Fund.

Abstract

Candida albicans is an opportunistic fungal pathogen that causes severe systemic infections in immunocompromised individuals and those with implanted medical devices. Infection severity can range from mucosal or dermal infections to life threatening systemic infections with mortality rates reaching up to 25%. Most *C. albicans* infections stem from biofilm development that leads to tissue damage and illness in the host. Biofilms develop from planktonic yeast cells adhering to a surface and changing their gene expression to initiate biofilm development by forming hyphae. The biofilm continues to develop with cells replicating and secreting an extracellular matrix that serves to protect and facilitate communication within the biofilm. Once the biofilm is established, hyphae begin budding off yeast that leave the biofilm in a process called dispersion. Dispersed cells are primed to continue infection with upregulated gene expression in genes related to virulence, including drug resistance and host cell adhesion and invasion genes. Despite dispersed cells being more virulent than planktonic cells, little is known about dispersion compared to early stages of biofilm development such as biofilm adhesion and initiation. This is due, in part, to an absence of appropriate tools for studying dispersion.

Current genetic tools are inadequate for studying dispersion because they lack temporal and spatial control. Static mutations can often disrupt biofilm formation, making it impossible to distinguish inadequate biofilm formation from dispersion defects. Current inducible systems rely on changes in media to add or remove inducers and therefore lack spatial and temporal control, depending on the assay. Optogenetics, which uses genetically-encoded light-controlled effector proteins, can be used to spatiotemporally control gene expression in individual cells and biofilms and would be very useful in studying dispersion. In Chapters 2-4, I discuss the development of optogenetic tools in both *S. cerevisiae* and *C. albicans.*

Large scale screens have been successful in identifying genes involved in biofilm formation in *C. albicans.* However, these same assays are not suitable for assessing dispersion, and assays developed specifically for measuring dispersion are not suitable for screening large mutant libraries in a biologically relevant flow environment. Thus, identification of genes regulating dispersion has lagged far behind other aspects of biofilm formation and development. In Chapter 5 I introduce an underoil microfluidic assay that can be used to screen many samples at once under flow conditions.

Lastly, to discover additional genes that affect dispersion, I developed an assay and screened a large transcription factor mutant library for dispersion phenotypes, described in Chapter 6. From this screen I identified one mutant that was highly dispersive. I used RNA sequencing to look at gene expression differences between different stages of biofilm development and between this mutant and its wildtype parent strain. Using this dataset, I identified genes in the carbohydrate transport and utilization pathways that were upregulated in the mutant strains compared to the parent strain. The gene expression data indicate that these same pathways are enriched/upregulated in dispersed cells relative to biofilm cells.

This dissertation contributes to a better understanding of dispersion in the human fungal pathogen *Candida albicans* by developing tools to study the process of dispersion and using these tools to identify dispersion mutants and the genes now implicated in the process of dispersion.

Table of Contents

List of Figures

Chapter 1

Chapter 2

Chapter 3

Chapter 4

Chapter 5

Chapter 6

List of Tables

Chapter 2

Chapter 3

Chapter 4

Chapter 5

Chapter 6

Chapter 1: Introduction

Stephanie H. Geller wrote this chapter.

Abstract

Candida albicans is an opportunistic pathogen that causes deadly infection in immunocompromised individuals and those with implanted medical devices. *C. albicans* biofilms will grow on surfaces such as medical devices and disseminate or disperse into the body causing downstream infections. It is known that strains that are deficient in dispersion are less virulent than those that can disperse. However, there are no drugs that target the process of dispersion nor are there ideal tools for studying dispersion. Accordingly, the process of dispersion is poorly understood on a transcriptomic level and only a few genes have been confirmed to effect dispersion. In this Chapter, I outline what is known about *C. albicans* biofilm formation and dispersion. I also highlight which drugs are available to treat infections and what tools are available for studying biofilm development and dispersion. In Chapter 2, I discuss an optogenetic tool for repressing gene expression in *Saccharomyces cerevisiae* in response to light. In chapter 3, I introduce another optogenetic tool for inducing gene expression in *S. cerevisiae* in response to light. In Chapter 4, I introduce a toolkit for the easy assembly of genetic tools for *C. albicans*. I also characterize promoters and terminators that can be used for tool development. In Chapter 5, I introduce a new underoil microfluidic assay for studying dispersion, which unlike current assays, allows flow and visualization during biofilm growth. In Chapter 6, I describe a screen of transcription factor mutants for a dispersive phenotype and subsequent studies of a particularly interesting mutant. Lastly, in Chapter 7, I discuss my conclusions from this work and future directions for these projects.

Overview

C. albicans is an opportunistic pathogen that lives commensally in the oral cavities of 75% of people, the gastrointestinal tract of 80% of people, and the genitourinary tract of 70% of people [1]–[3]. Despite its prevalence, *C. albicans* can become invasive and cause deadly infections in immunocompromised individuals such as neonate patients and chemotherapy patients, or those with an implanted medical device [4]. It is responsible for 54% of fungal infections and severe infections have mortality rates as high as 25% [5]. Infections can range from dermal and mucosal infections, such as oral thrush and vaginal yeast infections, to more serious systemic infections. *C. albicans* biofilms adhere particularly well to the surfaces of medical devices such as catheters, pacemakers, and dentures. Currently, such infections are treated by removing the compromised medical device and applying high doses of antifungals [6]. Moreover, Candida infections can lead to an additional 3-13 days in the hospital and up to $29,000 in healthcare costs for treatment [7], [8].

In most cases, *C. albicans* infections are caused by the establishment of biofilms that destroy host tissue and cause illness in the host. Biofilms are organized groups of cells and the NIH reports that 80% of microbial infections are in some way due to biofilms [9]. The development of *C. albicans* biofilms begins with planktonic cells adhering to a surface (Fig 1). Biofilm initiation then occurs as the cells then undergo morphology and gene expression changes to reach a hyphal state [4], [10], [11]. The biofilm continues to develop by replicating hyphal form cells until it reaches maturation. During this process, the biofilm becomes encased in an extracellular matrix (ECM) formed as Candida cells secrete a mixture of DNA, lipids, carbohydrates, and proteins [12]. This ECM both protects the biofilm from its environment—it helps confer antifungal resistance and

protection from host immune cells—and allows communicate within the biofilm via extracellular vesicles [13]. It was traditionally thought that the process of dispersion then begins after the biofilm matures. During dispersion, the hyphal cells begin budding yeast form cells that can leave the biofilm and develop downstream biofilms [11], [14]–[16]. However, Uppuluri, *et al* showed that dispersion occurs throughout biofilm maturation as opposed to once maturation is complete [10], [17].

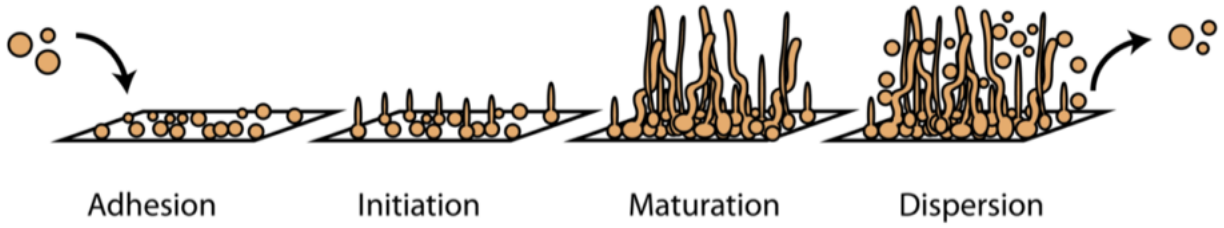

Figure 1. *Candida albicans* biofilm lifecycle. Biofilm development begins with a planktonic yeast cell adhering to a surface such a medical device. These cells then begin biofilm initiation by changing their growth into a hyphal morphology. The biofilm continues to grow and the cells excrete an extracellular matrix that protects the biofilm and allows communication within the biofilm. The biofilm then reaches maturation and starts dispersing yeast form cells that can travel and cause downstream infections.

For *C. albicans*, cell adhesion, biofilm initiation, and biofilm virulence are well studied. Searching PubMed for the keywords "*Candida* adhesion", "*Candida* biofilm initiation", and "*Candida* virulence" yields a combined 9,605 results. However, searching for "*Candida* dispersion" yields only 692 results, which include articles that simply mention dispersion as a stage in the lifecycle, or review articles. One may think that there are fewer studies of *Candida* dispersion because it does not affect *Candida* virulence. However, Uppuluri, *et al* (2010) show that strains deficient in dispersion are less virulent than wildtype [10]. This suggests that dispersion plays a role in the

virulence of a strain during infection. Instead, I believe that the lack of knowledge of dispersion is a consequence of the lack of tools available for studying this process, as elaborated later in this chapter. With microbial drug resistance on the rise, it is necessary to discover more druggable targets that affect biofilm growth [18]–[20]. The process of dispersion should be investigated for druggable targets since it is known to affect virulence.

Despite the fact that there are over 9 million fungal infections in the US per year, there are currently only 4 main classes of drugs available to treat fungal infections: polyenes, pyrimidine analogues, azoles, and echinocandins [18]. In contrast, there are 6 classes of drugs, and over a hundred drugs, available to treat bacterial infections. Polyenes like amphotericin B and nystatin target the ergosterol pathway to create pores in the cell membrane while pyrimidine analogues like 5-flucytosine halts DNA replication and cellular functions. Pyrimidine analogues are never used as a sole therapy due to likelihood of resistance and are often paired with a polyene for treatment [18]. Azoles and echinocandins constitute the most used classes of anti-fungal drugs. Azoles are the largest class of anti-fungals and target the ergosterol pathway to weaken the membrane, thereby halting some membrane functions and cell growth. Echinocandins target the cell membrane by inhibiting β-(1,3) glucan synthase which is an essential enzyme in the membrane as well. Most anti-fungal drugs target the ergosterol pathway as there are structural differences in its enzymes between eukaryotic fungal cells and eukaryotic host cells, leading to minimal effects to the host cells [21]. With fungal resistance on the rise, especially with the discovery of *Candida auris*, there is a need for additional drugs that target different areas of biofilm development.

Current knowledge of *C. albicans* dispersion

While our understanding of *C. albicans* dispersion is limited, recent studies have provided some foundational information. Firstly, we know that dispersed cells are yeast form cells that bud from hyphal form cells and leave to create additional biofilms [10]. Next, we know that the process of dispersion is highly dependent on its environment such as carbon source and concentration, pH, and the presence of quorum sensing molecules [10]. Additionally, we know that dispersed cells are primed for infection: they have the ability to adhere, develop biofilms, and can even damage host cells better than their planktonic counterparts [10]. Dispersed cells are also more virulent than planktonic cells, as mice injected with dispersed cells succumb to infection faster than those injected with planktonic cells [10]. Despite this, we currently know of few genes that affect dispersion. Uppuluri, *et al* used an inducible Tet system to show an increase in dispersion when biofilms grown for 24 hours without PES1 expression were switched to overexpressing the gene [10]. Uppuluri, *et al* also saw that repressing UME6 led to more dispersion. Biofilms grown for 24 hours with NRG1 repressed and then released from repression caused increased biofilm dispersion versus wildtype SC5314 [22]. Lastly, HSP90 repression was shown to decrease the number of cells dispersed from a biofilm; in addition, the dispersed cells had reduced viability compared to the same strain without doxycycline-mediated repression [23].

Uppuluri, *et al* used RNA-seq to measure gene expression in planktonic cells, biofilm cells, and dispersed cells and found different expression profiles for many genes [17]. They collected the cells for RNA-seq using a macro-flow assay developed by their lab [24], [25]. In this assay, biofilms are grown on a silicone sheet while fresh media is flown over the biofilm. Biofilm cells

were collected after 24 hours of growth on the silicone sheet and dispersed cells were collected in the flow through after 24 hours. Multiple replicates were pooled to ensure enough RNA for sequencing. Lastly, planktonic cells were "age matched" by growing in flasks for 24 hours in the same media (YNB-1% glucose). One caveat from this study is that dispersed cells sat in a vat of fresh media for up to 24 hours after being released, which may have affected gene expression. However, this study did show that gene expression in dispersed cells differed from planktonic or biofilm cell and genes typically associated with virulence were upregulated in dispersed cells compared to biofilm cells. The dispersed cells also showed increased expression for genes associated with methionine biosynthesis genes, aromatic amino acid metabolism, ergosterol biosynthesis, adhesion, small-molecule efflux and drug resistance, chitin synthesis, glycerol biosynthesis, and ribosome biosynthesis. The dispersed cells were also shown to strongly express genes associated with the gluconeogenesis pathway comparatively to their parent cells, which strongly expressed glycolysis pathway genes. Lastly, the tricarboxylic acid pathway was highly upregulated in dispersed cells compared to biofilm cells. Overall, virulence genes and many biosynthesis pathways were upregulated in dispersed cells, as in biofilm cells, but carbon metabolism gene profiles more closely resembled age matched planktonic cells.

Tools and assays available for studying the *Candida albicans* biofilm lifecycle and dispersion

There are currently both *in vivo* and *in vitro* assays for studying *C. albicans* biofilm development and virulence. In vivo models include the rat, the mouse, the fruit fly *Drosophila melanogaster*, the nematode *Caenorhabditis elegans*, and the larvae of the moth *Galleria mellonella* [26]–[29]. These models can be used to evaluate strain virulence, infection dissemination, and interactions with host immune cells. Use of non-mammalian hosts is beneficial due to their ease of handling

and cost, but caution should be taken when interpreting their results. Prior works indicate that results between mammalian and non-mammalian hosts are not always compatible [26]. Within the rat and mouse models there are many routes for infection such as a urinary catheter route, a vaginal route, an oral route, an intra-veinous tail injection, and recently a subdermal ear route [2], [30]–[34]. This allows researchers to investigate infections comparable to those found in humans.

Many *in vitro* assays have been developed to study biofilm development. The 96-well biofilm assay is the most used because it is inexpensive and easy to use. This assay involves seeding cells in a 96-well microtiter plate, growing biofilms to maturation, and using a colorimetric assay to determine relative biofilm growth [4], [35], [36]. Other assays include use of large roller bottles, flow cells, static growth on a silicone sheets, and nano-biofilm microarrays [24], [37]–[40]. There are few assays for studying dispersion specifically. These assays include the 96-well microtiter standard or sustained dispersion assay, a macro-scale flow assay, and a microfluidic flow assay [24], [37], [41], [42]. Each of these assays has benefits and limitations in their ability to visualize biofilm growth, apply flow for biological relevance, retrieve cells for downstream analysis, or operate at high throughput.

Genetic tools are used to study the effects of different genes on dispersion. The genetic tools available for *C. albicans* consist mostly of overexpression or deletion strains [43]–[48]. In recent CRISPR-based systems, Cas9 has been used for gene mutations and nuclease-dead dCas9 has been used to repress specific genes [49]–[51]. When studying dispersion, inducible expression systems are preferable to static mutations as they provide the ability to tune expression throughout biofilm development. Static mutations of gene expression may hinder the investigation of late-stage

processes like dispersion via changes to early-stage processes such as adhesion or hyphal initiation. Thankfully, *Candida* libraries with genes under inducible promoters allow for temporal control of gene expression [43], [52], [53]. Most of these strains use Tet-based systems to either induce or repress gene expression in the presence of tetracycline. The promoters pPCK1, pMAL2, pGAL1 and pMET3 can also be used to perturb gene expression in response to succinate, maltose, glucose, or methionine, respectively [54]–[58].

Conclusions

C. albicans is an infectious pathogen with a complex, multi-stage life cycles. Dispersion is a key step of that lifecycle that contributes to virulence. However, current tools for growing and perturbing *C. albicans* are not ideally suited for studying dispersion.

For example, existing gene induction systems like Tet-On provide little spatial control. Since it is known that gene expression differs across a biofilm, a tool capable of perturbing genes with spatial control would be helpful in studying dispersion [17]. Moreover, removing chemical inducers from *Candida* cultures can require many washes, each of which risks disrupting the biofilm being studied. An inducer that is easy to add or remove without disrupting the biofilm would make it easier to study the process of dispersion. An optogenetic system featuring genetically encoded, light-controlled effector proteins can meet all these requirements. Optogenetic systems have already been used extensively in other organisms to allow spatiotemporal control of gene expression and have recently been introduced into *C. albicans* to studying protein to protein interactions [59], [60]–[63]. An optogenetic gene induction system could be used to study dispersion in *C. albicans* by activating different genes only at select stages of the *Candida* life

cycle and would allow spatial control to investigate where in a biofilm such genes may be important.

Therefore in Chapters 1-3, I discuss novel optogenetic tools I have built with the aim of studying dispersion in *C. albicans*. Chapter 1 describes an optogenetic repression tool implemented in *S. cerevisiae* that combines the DNA binding protein dCas9 with a light activatable nuclear localization signal (NLS). In blue light, the light-controlled dCas9 construct enters the nucleus, binds DNA, and sterically hinders downstream transcription. Chapter 2 discusses an optogenetic tool built for inducing gene expression in *S. cerevisiae*. In this tool, the light responsive proteins CRY2 and CIB1 are fused to a DNA binding domain and an activation domain, respectively. Accordingly in response to blue light, CRY2 and CIB1 dimerize to recruit the activation domain to a gene of interest. In this chapter, I also discuss an orthogonal DNA binding domain, Zif268, and its complementary promoter, pZif, which were developed to decrease off target binding of our optogenetic tool. These optogenetic tools were developed in *S. cerevisiae* because it is a less complex organism (haploid) in which many components of the optogenetics tools have already been used successfully. In Chapter 4, I discuss a toolkit that I developed for assembling optogenetic tools in *C. albicans* and the characterization of promoters and terminators from *S. cerevisiae* for use in *C. albicans*. I also discuss the optogenetic tool that we developed for controlling gene expression and lastly, we investigate the functionality of the DNA binding domain ZIF268 in *C. albicans*.

The study of *Candida* dispersion is also limited by a lack of assays that allow the visualization of biofilm growth, the application flow through the biofilm, the retrieval of cells for downstream

analysis, or the high-throughput screening of large libraries with unknown characteristics. Therefore in Chapter 5, I explore the use of underoil microfluidics for studying dispersion. I describe the differences in biofilm growth between the underoil microfluidic assay and a standard 96-well microplate assay and discuss the ability to add flow through the biofilm in the underoil microfluidic assay. I also show how underoil valves can be used to add flow through the biofilm at selected times and that this flow is sufficient to move dispersed cells from a biofilm.

While there has been extensive research on *C. albicans* virulence and biofilm development, dispersion is by comparison poorly understood. A few genes and environmental factors are known to affect dispersion, but a large library screen of dispersion has not been published to date. Thus in Chapter 6, I discuss the screening of a transcription factor mutant library for altered dispersion phenotypes and the identification of mutants with an increased dispersion phenotype versus its parent strain, with a special focus on a specific mutant (*rob1Δ/Δ*) with a hyper-dispersion phenotype. I then discuss the subsequent RNA sequencing experiment of the different stages of biofilm development including dispersion in *rob1Δ/Δ* and the parent strain.

Lastly, Chapter 7 discusses my conclusions from this work and potential future directions for the study of *C. albicans* dispersion. The tools developed in this work will allow researchers to investigate new questions on the development and dispersion of *Candida* biofilms. Moreover, the RNA-seq measurements presented here open additional avenues for understand the genes driving dispersion. With this information we can begin to fill the gap in knowledge of the process of dispersion, which can lead to a better understanding of *C. albicans* infections.

References

[1] M. A. Kabir, M. A. Hussain, and Z. Ahmad, "*Candida albicans*: A Model Organism for Studying Fungal Pathogens," ISRN Microbiol., vol. 2012, pp. 1–15, Sep. 2012.

[2] A. Akpan and R. Morgan, "Oral candidiasis," Postgrad. Med. J., vol. 78, no. 922, p. 455, Aug. 2002.

[3] A. K. Nash et al., "The gut mycobiome of the Human Microbiome Project healthy cohort," Microbiome, vol. 5, no. 1, p. 153, Nov. 2017.

[4] G. Wall, D. Montelongo-Jauregui, B. Vidal Bonifacio, J. L. Lopez-Ribot, and P. Uppuluri, "*Candida albicans* biofilm growth and dispersal: contributions to pathogenesis," Curr. Opin. Microbiol., vol. 52, pp. 1–6, Dec. 2019.

[5] E. Rayens and K. A. Norris, "Prevalence and Healthcare Burden of Fungal Infections in the United States, 2018," Open Forum Infect. Dis., vol. 9, no. 1, Jan. 2022.

[6] C. J. Nobile and A. D. Johnson, "*Candida albicans* Biofilms and Human Disease," Annu. Rev. Microbiol., vol. 69, no. 1, p. 71, Oct. 2015.

[7] J. Morgan et al., "Excess mortality, hospital stay, and cost due to candidemia: a case-control study using data from population-based candidemia surveillance," Infect. Control Hosp. Epidemiol., vol. 26, no. 6, pp. 540–547, Jun. 2005.

[8] "FLUCONAZOLE-RESISTANT CANDIDA 3,400 FLUCONAZOLE-RESISTANT."

[9] C. J. Nobile and A. D. Johnson, "Candida albicans Biofilms and Human Disease.," Annu. Rev. Microbiol., vol. 69, pp. 71–92, 2015.

[10] P. Uppuluri et al., "Dispersion as an important step in the Candida albicans biofilm developmental cycle.," PLoS Pathog., vol. 6, no. 3, p. e1000828, Mar. 2010.

[11] C. J. Nobile and A. D. Johnson, "Candida albicans Biofilms and Human Disease," Annu. Rev. Microbiol., 2014.

[12] J. E. Nett and D. R. Andes, "Contributions of the Biofilm Matrix to Candida Pathogenesis," J. Fungi, vol. 6, no. 1, Mar. 2020.

[13] R. Zarnowski et al., "Coordination of fungal biofilm development by extracellular vesicle cargo," Nat. Commun. 2021 121, vol. 12, no. 1, pp. 1–9, Oct. 2021.

[14] M. Gulati and C. J. Nobile, "Candida albicans biofilms: development, regulation, and molecular mechanisms.," Microbes Infect., vol. 18, no. 5, pp. 310–21, May 2016.

[15] V. Amann et al., "Increased Activities against Biofilms of the Pathogenic Yeast Candida albicans of Optimized Pom-1 Derivatives," Pharmaceutics, vol. 14, no. 2, p. 318, Feb. 2022.

[16] J. Talapko et al., "Candida albicans—The Virulence Factors and Clinical Manifestations of Infection," J. Fungi, vol. 7, no. 2, pp. 1–19, Feb. 2021.

[17] P. Uppuluri et al., "Candida albicans Dispersed Cells Are Developmentally Distinct from Biofilm and Planktonic Cells.," MBio, vol. 9, no. 4, pp. e01338-18, Sep. 2018.

[18] S. Costa-de-oliveira and A. G. Rodrigues, "Candida albicans Antifungal Resistance and Tolerance in Bloodstream Infections: The Triad Yeast-Host-Antifungal," Microorganisms, vol. 8, no. 2, Feb. 2020.

[19] T. M. Rawson et al., "Optimizing antimicrobial use: challenges, advances and opportunities," Nat. Rev. Microbiol. 2021, pp. 1–12, 2021.

[20] Y. Lee, E. Puumala, N. Robbins, and L. E. Cowen, "Antifungal Drug Resistance: Molecular Mechanisms in Candida albicans and beyond," Chem. Rev., vol. 121, no. 6, pp. 3390–3411, Mar. 2021.

[21] G. C. d. O. Santos et al., "Candida infections and therapeutic strategies: Mechanisms of action for traditional and alternative agents," Front. Microbiol., vol. 9, no. JUL, p. 1351, Jul. 2018.

[22] P. Uppuluri, C. G. Pierce, D. P. Thomas, S. S. Bubeck, S. P. Saville, and J. L. Lopez-Ribot, "The transcriptional regulator Nrg1p controls Candida albicans biofilm formation and dispersion.," Eukaryot. Cell, vol. 9, no. 10, pp. 1531–7, Oct. 2010.

[23] N. Robbins et al., "Hsp90 governs dispersion and drug resistance of fungal biofilms.," PLoS Pathog., vol. 7, no. 9, p. e1002257, Sep. 2011.

[24] P. Uppuluri and J. L. Lopez-Ribot, "An easy and economical in vitro method for the formation of Candida albicans biofilms under continuous conditions of flow.," Virulence, vol. 1, no. 6, pp. 483–7, 2010.

[25] P. Uppuluri, A. K. Chaturvedi, and J. L. Lopez-Ribot, "Design of a simple model of Candida albicans biofilms formed under conditions of flow: development, architecture, and drug resistance," Mycopathologia, vol. 168, no. 3, pp. 101–109, 2009.

[26] E. Segal and M. Frenkel, "Experimental In Vivo Models of Candidiasis," J. Fungi, vol. 4, no. 1, Mar. 2018.

[27] H. R. Conti, A. R. Huppler, N. Whibley, and S. L. Gaffen, "Animal Models for Candidiasis," Curr. Protoc.

Immunol., vol. 105, no. SUPPL.105, p. 19.6.1, 2014.
[28] M. Řičicová et al., "Candida albicans biofilm formation in a new in vivo rat model," Microbiology, vol. 156, no. Pt 3, pp. 909–919, 2010.
[29] A. Desalermos, B. B. Fuchs, and E. Mylonakis, "Selecting an Invertebrate Model Host for the Study of Fungal Pathogenesis," PLoS Pathog., vol. 8, no. 2, Feb. 2012.
[30] R. S. Wakade, L. C. Ristow, M. Wellington, and D. J. Krysan, "Intravital imaging based genetic screen reveals the transcriptional network governing Candida albicans filamentation during mammalian infection," Elife, vol. 12, Feb. 2023.
[31] J. E. Nett et al., "Rat Indwelling Urinary Catheter Model of Candida albicans Biofilm Infection," Infect. Immun., vol. 82, no. 12, p. 4931, 2014.
[32] A. Cassone and J. D. Sobel, "Experimental Models of Vaginal Candidiasis and Their Relevance to Human Candidiasis," Infect. Immun., vol. 84, no. 5, p. 1255, May 2016.
[33] D. Frank and N. Carpino, "Induction and analysis of systemic *C. albicans* infections in mice," Methods Cell Biol., vol. 168, pp. 315–327, Jan. 2022.
[34] N. V. Solis and S. G. Filler, "Mouse Model of Oropharyngeal Candidiasis," Nat. Protoc., vol. 7, no. 4, p. 637, Apr. 2012.
[35] C. G. Pierce, P. Uppuluri, S. Tummala, and J. L. Lopez-Ribot, "A 96 Well Microtiter Plate-based Method for Monitoring Formation and Antifungal Susceptibility Testing of Candida albicans Biofilms," J. Vis. Exp., no. 44, 2010.
[36] L. Sherry et al., "Biofilms formed by Candida albicans bloodstream isolates display phenotypic and transcriptional heterogeneity that are associated with resistance and pathogenicity," BMC Microbiol., vol. 14, no. 1, pp. 1–14, Jul. 2014.
[37] A. McCall and M. Edgerton, "Real-Time Approach to Flow Cell Imaging of Candida albicans Biofilm Development.," J. fungi (Basel, Switzerland), vol. 3, no. 1, Mar. 2017.
[38] S. A, U. P, L.-R. J, and R. AK, "Development of a high-throughput Candida albicans biofilm chip," PLoS One, vol. 6, no. 4, 2011.
[39] A. Srinivasan, K. P. Leung, J. L. Lopez-Ribot, and A. K. Ramasubramanian, "High-Throughput Nano-Biofilm Microarray for Antifungal Drug Discovery," MBio, vol. 4, no. 4, Jun. 2013.
[40] R. Zarnowski, H. Sanchez, and D. R. Andes, "Large-scale production and isolation of Candida biofilm extracellular matrix," Nat. Protoc. 2016 1112, vol. 11, no. 12, pp. 2320–2327, Oct. 2016.
[41] M. B. Lohse, M. Gulati, A. V. Arevalo, A. Fishburn, A. D. Johnson, and C. J. Nobile, "Assessment and optimizations of Candida albicans in vitro biofilm assays 1," 2017.
[42] C. J. Nobile et al., "A histone deacetylase complex mediates biofilm dispersal and drug resistance in Candida albicans.," MBio, vol. 5, no. 3, pp. e01201-14, Jun. 2014.
[43] R. Wang, J. Liu, Y. Liu, Q. Lv, and L. Yan, "Application of the Mutant Libraries for Candida albicans Functional Genomics," Int. J. Mol. Sci., vol. 23, no. 20, p. 12307, Oct. 2022.
[44] S. M. Noble and A. D. Johnson, "Strains and Strategies for Large-Scale Gene Deletion Studies of the Diploid Human Fungal Pathogen Candida albicans," Eukaryot. Cell, vol. 4, no. 2, p. 298, Feb. 2005.
[45] O. R. Homann, J. Dea, S. M. Noble, and A. D. Johnson, "A phenotypic profile of the Candida albicans regulatory network," PLoS Genet., vol. 5, no. 12, Dec. 2009.
[46] D. Xu et al., "Genome-Wide Fitness Test and Mechanism-of-Action Studies of Inhibitory Compounds in Candida albicans," PLOS Pathog., vol. 3, no. 6, p. e92, Jun. 2007.
[47] C. J. Nobile and A. P. Mitchell, "Regulation of cell-surface genes and biofilm formation by the *C. albicans* transcription factor Bcr1p," Curr. Biol., vol. 15, no. 12, pp. 1150–1155, Jun. 2005.
[48] D. A. Davis, V. M. Bruno, L. Loza, S. G. Filler, and A. P. Mitchell, "Candida albicans Mds3p, a Conserved Regulator of pH Responses and Virulence Identified Through Insertional Mutagenesis," Genetics, vol. 162, no. 4, pp. 1573–1581, Dec. 2002.
[49] L. Wensing, J. Sharma, D. Uthayakumar, Y. Proteau, A. Chavez, and R. S. Shapiro, "A CRISPR Interference Platform for Efficient Genetic Repression in Candida albicans.," mSphere, vol. 4, no. 1, pp. e00002-19, Feb. 2019.
[50] N. Nguyen, M. M. F. Quail, and A. D. Hernday, "An Efficient, Rapid, and Recyclable System for CRISPR-Mediated Genome Editing in Candida albicans," mSphere, vol. 2, no. 2, pp. e00149-17, Apr. 2017.
[51] V. K. Vyas, M. I. Barrasa, and G. R. Fink, "A Candida albicans CRISPR system permits genetic engineering of essential genes and gene families.," Sci. Adv., vol. 1, no. 3, p. e1500248, 2015.
[52] T. Roemer et al., "Large-scale essential gene identification in Candida albicans and applications to antifungal drug discovery," Mol. Microbiol., vol. 50, no. 1, pp. 167–181, Oct. 2003.

[53] Y. N. Park and J. Morschhäuser, “Tetracycline-Inducible Gene Expression and Gene Deletion in Candida albicans,” Eukaryot. Cell, vol. 4, no. 8, p. 1328, Aug. 2005.
[54] C. E. Leuker, A. Sonneborn, S. Delbrück, and J. F. Ernst, “Sequence and promoter regulation of the PCK1 gene encoding phosphoenolpyruvate carboxykinase of the fungal pathogen Candida albicans,” Gene, vol. 192, no. 2, pp. 235–240, Jun. 1997.
[55] R. S. Care, J. Trevethick, K. M. Binley, and P. E. Sudbery, “The MET3 promoter: a new tool for Candida albicans molecular genetics,” Mol. Microbiol., vol. 34, no. 4, pp. 792–798, 1999.
[56] S. E. Eckert and F. A. Mühlschlegel, “Promoter regulation in Candida albicans and related species,” FEMS Yeast Res., vol. 9, no. 1, pp. 2–15, Feb. 2009.
[57] D. H. Brown, I. V. Slobodkin, and C. A. Kumamoto, “Stable transformation and regulated expression of an inducible reporter construct in Candida albicans using restriction enzyme-mediated integration,” Mol. Gen. Genet., vol. 251, no. 1, pp. 75–80, 1996.
[58] T. Srikantha et al., “The sea pansy Renilla reniformis luciferase serves as a sensitive bioluminescent reporter for differential gene expression in Candida albicans,” J. Bacteriol., vol. 178, no. 1, pp. 121–129, 1996.
[59] P. M. Silva, C. Puerner, A. Seminara, M. Bassilana, and R. A. Arkowitz, “Secretory Vesicle Clustering in Fungal Filamentous Cells Does Not Require Directional Growth,” Cell Rep., vol. 28, no. 8, pp. 2231-2245.e5, Aug. 2019.
[60] E. M. Zhao, M. A. Lalwani, J. M. Chen, P. Orillac, J. E. Toettcher, and J. L. Avalos, “Optogenetic Amplification Circuits for Light-Induced Metabolic Control,” ACS Synth. Biol., vol. 10, no. 5, pp. 1143–1154, May 2021.
[61] N. Moreno Morales, M. T. Patel, C. J. Stewart, K. Sweeney, and M. N. McClean, “Optogenetic Tools for Control of Public Goods in Saccharomyces cerevisiae,” mSphere, vol. 6, no. 4, Aug. 2021.
[62] F. Salinas, V. Rojas, V. Delgado, E. Agosin, and L. F. Larrondo, “Optogenetic switches for light-controlled gene expression in yeast,” Appl. Microbiol. Biotechnol., vol. 101, no. 7, pp. 2629–2640, Apr. 2017.
[63] H. Liu, G. Gomez, S. Lin, S. Lin, and C. Lin, “Optogenetic Control of Transcription in Zebrafish,” PLoS One, vol. 7, no. 11, p. 50738, Nov. 2012.

Chapter 2: Optogenetic Repressors of Gene Expression in Yeasts Using Light-Controlled Nuclear Localization

The contents of this chapter are published:

Geller SH, Antwi EB, Di Ventura B, McClean MN. Optogenetic Repressors of Gene Expression in Yeasts Using Light-Controlled Nuclear Localization. Cell Mol Bioeng. 2019 Sep 24;12(5):511-528. doi: 10.1007/s12195-019-00598-9. PMID: 31719930; PMCID: PMC6816687.

Stephanie H Geller and Megan N McClean designed the experiments and analyzed the data. Stephanie H Geller and Enoch B Antwi cloned plasmids. Stephanie H Geller completed flow cytometry, timelapse microscopy, and drug sensitivity experiments. Stephanie H Geller, and Megan N McClean wrote the manuscript. All authors revised the manuscript and approved the final version.

Abstract

Introduction

Controlling gene expression is a fundamental goal of basic and synthetic biology because it allows insight into cellular function and control of cellular activity. We explored the possibility of generating an optogenetic repressor of gene expression in the model organism *Saccharomyces cerevisiae* by using light to control the nuclear localization of nuclease-dead Cas9, dCas9.

Methods

The dCas9 protein acts as a repressor for a gene of interest when localized to the nucleus in the presence of an appropriate guide RNA (sgRNA). We engineered dCas9, the mammalian transcriptional repressor Mxi1, and an optogenetic tool to control nuclear localization (LINuS) as parts in an existing yeast optogenetic toolkit. This allowed expression cassettes containing novel dCas9 repressor configurations and guide RNAs to be rapidly constructed and integrated into yeast.

Results

Our library of repressors displays a range of basal repression without the need for inducers or promoter modification. Populations of cells containing these repressors can be combined to generate a heterogeneous population of yeast with a 100-fold expression range. We find that repression can be dialed modestly in a light dose- and intensity-dependent manner. We used this library to repress expression of the lanosterol 14-alpha-demethylase Erg11, generating yeast with a range of sensitivity to the important antifungal drug fluconazole.

Conclusions

This toolkit will be useful for spatiotemporal perturbation of gene expression in *S. cerevisiae*. Additionally, we believe that the simplicity of our scheme will allow these repressors to be easily modified to control gene expression in medically relevant fungi, such as pathogenic yeasts.

Introduction

The modified type II CRISPR (clustered regularly interspersed palindromic repeats) system from bacteria serves as a versatile platform for genome editing [23,25] and transcriptional modulation [50] due to its ability to be targeted to specific DNA sequences using complementary guide RNAs [25]. This single RNA-single protein CRISPR system is derived from the natural adaptive immune response of bacteria and archaea. In the type II CRISPR/Cas system, a ribonucleoprotein complex formed from a single protein (Cas9), a short CRISPR RNA (crRNA), and a trans-acting crRNA (tracrRNA) can carry out efficient crRNA-directed recognition and site-specific cleavage of foreign DNA [9,25]. This system was further simplified by the development of a chimeric single-guide RNA (sgRNA) and a Cas9 protein from the *Streptococcus pyogenes* CRISPR. Together these two components are sufficient for targeting the Cas9 protein to a specific DNA sequence dictated entirely by the sgRNA which is complementary to it.

In addition to functioning as a site-specific nuclease, the endonuclease domains of the Cas9 protein can be mutated to create a programmable RNA-dependent DNA binding protein [50]. Targeting of the catalytically inactive Cas9 protein (nuclease-dead or dCas9) to the promoter or coding region of a gene can block transcription initiation or sterically block RNA polymerase binding or elongation, leading to suppression of transcription. Nuclease-dead dCas9 is attractive as a repressor, as Cas9 is known to have a long residence time (on the order of hours) when guide RNAs with full complementarity to the genomic target are utilized [39]. Use of dCas9 as a repressor at endogenous loci avoids the need for extensive engineering or circuitry as repression requires only two components: dCas9 and the sgRNA. When dCas9 is used to block transcription in bacteria, gene repression up to 99.9% is possible [50]. Using dCas9 and a single gRNA in yeast

has been shown to have only modest effects on gene expression regulation ranging from no effect to 2–3 fold repression, [8,12,62] though Gilbert and colleagues reported up to 18-fold downregulation of reporter gene activity [18,32]. The repressor ability of dCas9 can be increased by addition of a yeast or mammalian transcriptional repressor domain. The mammalian transcriptional repressor, Mxi1, is reported to interact with the chromatin modifying histone deacetylase Sin3 homolog in yeast [18,54]. Targeting repression with dCas9-Mxi1 has been shown to repress reporter gene activity up to 53-fold [18]. Other fusions with different repressive domains have been tested, with most failing to achieve as strong a repression as Mxi [14] (though see Lian, *et al.* for an exception[35]).

The ability to temporally and spatially control the repressive ability of dCas9 and dCas9-Mxi1 fusions would enable the study and control of gene function at specific times and places in individual or populations of yeast cells [15]. A relatively straightforward approach to temporally control dCas9 activity is to regulate its transcription through an inducible promoter [11,19]. It is also possible to regulate dCas9 by controlling expression of the guide RNA, for example, through drug-inducible sgRNA expression [2,28]. However, these approaches have slow response times due to the timescale required for transcription and translation [19]. To circumvent these issues, post-translational control methods have been developed [15]. Insertion of ligand-responsive inteins and hormone-binding domains into Cas9 have been used to make the activity of the protein controllable with addition of small molecules [7,36,46]. Strategies based on chemically induced dimerization of split protein fragments, for example the rapamycin-mediated dimerization of FK506 binding protein 12 (FKBP) and FKBP rapamycin binding domain (FRB), [13] also reconstitute Cas9 activity in the presence of a small molecule [64]. Small molecule-mediated

inhibition or degradation of Cas9 add variety to the repertoire of control approaches [29,41,51,52,55]. It is also possible to control Cas9 activity through chemical control of the guide RNA activity [31,37,61].

Optical approaches have the added advantage of allowing for spatial precision, so that dCas9 repressive activity can be triggered in specific places as well as at specific times. Spatial control is important for understanding the role of gene expression in regulating spatially heterogeneous processes, such as the development of a fungal biofilm. Light-inducible approaches have largely mimicked the chemical approaches including complementation of Cas9 fragments, light-induced two-hybrid systems, and photolysis of a caged unnatural amino acid [20,43,44,49]. Development of these systems required extensive engineering and screening in addition to the expression of multiple genes, e.g. fusions of photo-associating domains with Cas9 fragments.

In this article, we explore the possibility of using light-induced nuclear localization to optogenetically control the activity of dCas9 variants in a single polypeptide format. Repressors require access to the nucleus to function, and control of localization is a conceptually simple method of regulation that might allow for control of different Cas9 variants as well as control in diverse eukaryotic species. We put the nuclear accumulation of the dCas9 or dCas9-Mxi1 repressors under optogenetic control using LINuS, an optogenetic tool for controlling the nuclear localization of proteins of interest with blue light [45]. By testing different configurations of the dCas9, Mxi1, and LINuS domains we were able to achieve weak light-controlled repression. Our results suggest future directions to improve repression through optical control of nuclear localization. To improve the utility of our tool, we engineered the repressors into an existing yeast

optogenetic toolkit [1,33] to allow for rapid construction and integration of the repressor targeted to a gene of interest through an appropriate guide RNA. Interestingly, we found that basal (dark) repression by different repressor configurations allowed us to create populations of yeast with gene expression spanning a 100-fold range. This could be a powerful tool for generating heterogeneous populations of cells and studying their response to stimuli, including stress and drug treatment. This work provides a useful foundation for developing an optogenetic toolkit for repressing gene expression at a *S. cerevisiae* gene of interest. We expect that the simplicity of our scheme will allow it to be adapted to other important fungal organisms, including Candida albicans, to allow the role of gene expression in biofilm formation, drug resistance, and virulence to be better studied.

Results

Generation of a Light-Inducible Repressor Using LINuS

We used the promoter of the TEF1 gene as a proof-of-principle target of repression. TEF1 codes for the translational elongation factor EF-1α [53]. Loss of function of TEF1 is buffered by the presence of a paralog, TEF2. It has previously been shown that targeting dCas9 to the TEF1 promoter leads to repression of gene expression due to steric hinderance [18,24]. We verified that a constitutively localized dCas9 (dCas9 containing a C-terminal SV40 NLS [18]) induced repression in our TEF1-GFP reporter strain when co-transformed with an appropriate guide RNA (sgTEF1) under the control of the SNR52 RNA polymerase III promoter (Supplemental Fig. 1) [18].

In order to control the nuclear concentration of the dCas9 repressor, we removed the SV40 NLS and fused dCas9 to LINuS, an optogenetic tool that allows blue light control of nuclear import of proteins of interest [45]. LINuS is based on the second Light Oxygen Voltage (LOV) domain

of Avena sativa phototrophin 1 (AsLOV2). A nuclear localization signal (NLS) is introduced into the C-terminal Jα helix of the AsLOV2 domain such that, when the Jα helix unfolds and undocks from the AsLOV2 core in response to blue (~ 450 nm to 495 nm) light absorption, the NLS can be recognized and bound by endogenous importins (Fig. 1a). We experimented with fusing LINuS to both dCas9 and dCas9 tagged with the red fluorescent protein mCherry (dCas9-mCherry) (Fig. 1b) to allow blue light-mediated nuclear localization and repression by dCas9 (Fig. 1c). Plasmids containing either dCas9-LINuS or dCas9-mCherry-LINuS were co-transformed with a plasmid carrying the sgTEF1 guide RNA [18] into yeast expressing the Tef1 protein tagged with GFP (Tef1-GFP). Repression of gene expression was assayed by flow cytometry. We verified for all blue light stimulation experiments that repression was not due to photobleaching. Indeed, stimulation with maximal (100 $\mu W/cm^2$) blue light for up to 12 h does not lead to detectable photobleaching (Supplemental Fig. 2).

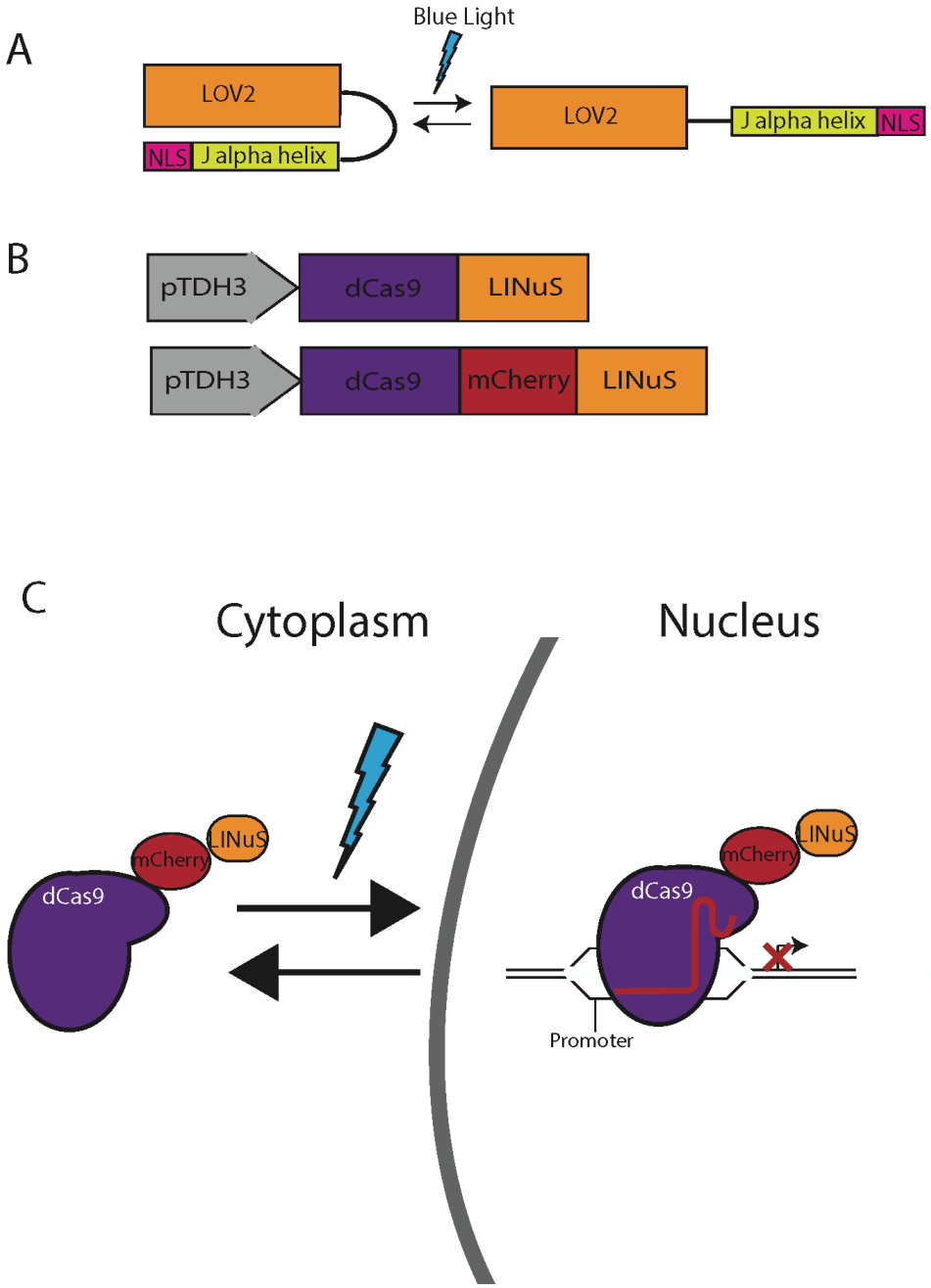

Figure 1. A. In the dark state, the Jα helix in LINuS is folded and interacts with the AsLOV2 core domain. This sequesters the nuclear localization signal (NLS) and prevents it from interacting with importins. Upon blue light exposure, the Jα helix unfolds rendering the NLS accessible. B. Schematic of the dCas9-LINuS and dCas9-mCherry-LINuS used in this study. pTDH3 is a

constitutively strong promoter. C. Blue light induces unfolding of the Jα helix, allowing endogenous importins to interact with the nuclear localization signal allowing dCas9-mCherry-LINuS to be imported into the nucleus where it sterically inhibits transcription by binding to promoters or coding regions as guided by the appropriate sgRNA.

In dark conditions, when the NLS within LINuS is photocaged, we observed in the dCas9-LINuS-expressing cells a small (1.5-fold) but significant repression of gene expression (Supplemental Fig. 3). We attribute this basal repression to the known low levels of unfolding of the LOV2 Jα helix even in the dark, which leads to accumulation of the repressor in the nucleus [59]. Fusion of dCas9 to mCherry alleviates this basal repression, perhaps due to increased protein size or accessibility of the NLS. Exposing the cells containing both dCas9-mCherry-LINuS and sgTEF1 to 100 $\mu W/cm^2$ blue light (470 nm) resulted in a modest (1.6-fold), but significant light-induced repression in Tef1-GFP protein levels (Fig. 2). In an attempt to reduce the leakiness of the system, we added a nuclear export signal (NES) to the constructs. The NES is constitutively active, and therefore able to bring the proteins that are imported in the nucleus during the dark phase back into the cytosol [45]. We selected two NESs with different strengths, namely the stronger PKIt and the weaker SNUPN. Both NESs reduced the level of light-induced repression (Supplemental Fig. 4). Addition of the PKIt NES also reduced the level of basal repression in the dark while the SNUPN NES did not. This result suggests that even small amounts of basal (dark) nuclear dCas9 in the dCas9-SNUPN-mCherry-LINuS fusion are enough to cause basal repression of gene expression. Weak basal repression of TEF1 by the dCas-mCherry-LINuS and dCas9-SNUPN-mCherry-LINuS constructs did not cause a measurable growth defect, in contrast to strong repression by

dCas9-Mxi1 which caused a significant reduction in cell growth (Supplemental Fig. 5a, b).

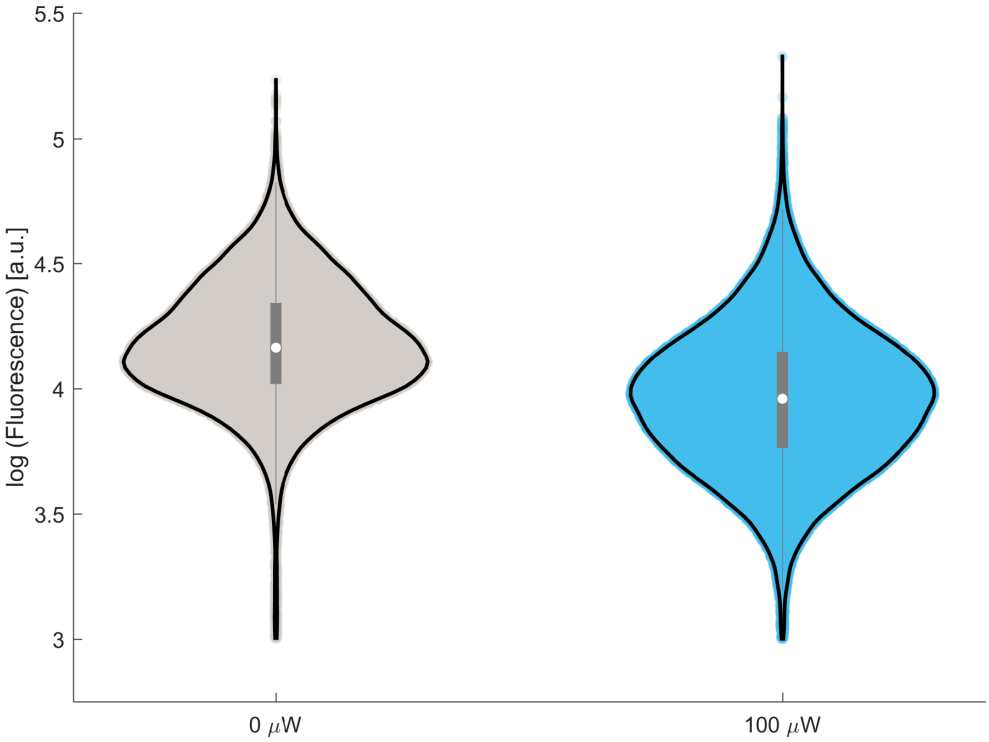

Figure 2. Growth in 100 µW/cm2 blue light induces a significant 1.6-fold repression of Tef1-GFP expression from the TEF1 promoter (median population fluorescence, $n = 3$, $p < 0.00005$, Welch's T test) relative to growth in the dark. Violin plots of Tef1-GFP fluorescence in representative populations indicate that there is significant overlap between gene expression in the blue light population and the dark population.

We attempted to measure the nuclear localization of our dCas9-mCherry-LINuS construct but found that the mCherry signal was weak and difficult to measure. We therefore tagged dCas9 with a brighter red fluorescent protein, mRuby2, which is approximately 2.5 times as bright as mCherry [57]. We generated the dCas9-mRuby2-LINuS construct utilizing the yeast toolkit cloning format

discussed below. Using a yeast strain with a fluorescently labelled nucleus (Nhp6a-iRFP) we were able to visualize the co-localization of dCas9-mRuby2-LINuS to the nucleus in response to stimulation with blue light (Fig. 3). We found that dCas9-mRuby2-LINuS localized to the nucleus within minutes, and stayed there, consistent with its lack of an NES. However, there was also clearly some dCas9-mRuby2-LINuS nuclear localization in the dark, in agreement with the Tef1-GFP expression data (Supplemental Fig. 3).

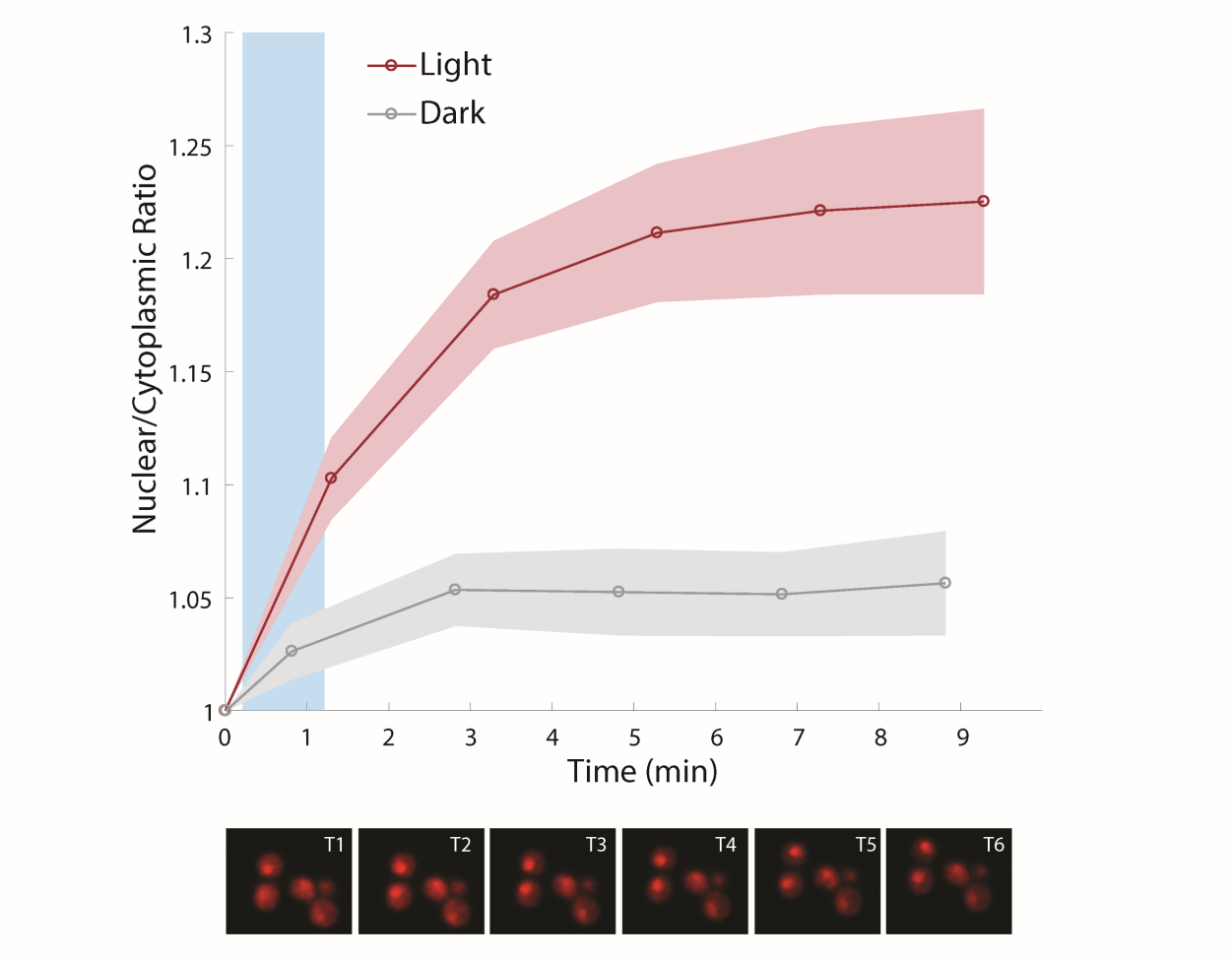

Figure 3. In response to stimulation with blue light, dCas9-mRuby2-LINuS localizes to the nucleus in *S. cerevisiae*. Cells were stimulated with 1 W/cm2 blue light for 1 min (blue bar). Time points T1-T6 are 0, 1.3, 3.3, 5.3, 7.3, 9.3 min respectively. Localization is measured by comparing the nuclear mRuby2 signal (co-localized with Nhp6A-iRFP) to the cytoplasmic signal in individual

cells (n = 108, 143 for light and dark respectively). Fold-change is measured relative to the T = 0 nuclear to cytoplasmic signal and error bars represent the 95% confidence interval.

The Mammalian Transcriptional Repressor Mxi1 Increases Light-Induced Repression and Variability of Gene Expression Within the Population

We sought to improve the repressive ability of our construct by adding the mammalian transcriptional repressor domain Mxi1 [18]. In our TEF1-GFP strain, dCas9-NLS-Mxi1 in combination with the sgTEF1 guide led to 52-fold repression in Tef1-GFP expression (Supplemental Fig. 1), consistent with previous results [18]. We hypothesized that the order of dCas9, Mxi1 and LINuS in the fusion would be important to ensuring function of all three elements. We therefore created three different fusion proteins: Mxi1-dCas9-mCherry-LINuS, dCas9-Mxi1-mCherry-LINuS and dCas9-mCherry-LINuS-Mxi1 (Fig. 4). The N-terminal fusion of Mxi1 to dCas9 resulted in a protein that caused very modest basal repression and no additional light-induced repression (Supplemental Fig. 6) at 25 $\mu W/cm^2$ light. We therefore focused on the dCas9-Mxi1-mCherry-LINuS and dCas9-mCherry-LINuS-Mxi1 fusions. The dCas9-Mxi1-mCherry-LINuS fusion produced 5-fold repression (Fig. 5a). However, this repression occurred in both the light and the dark, and we could not induce further repression by growing the cells in 25 $\mu W/cm^2$ light.

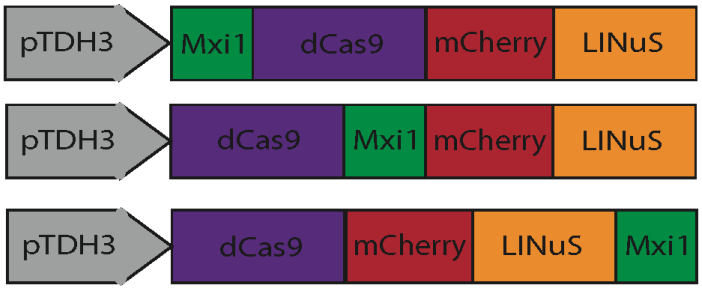

Figure 4. In order to explore how the orientation of the Mxi1 repressor domain affected our ability to make a light-inducible repressor we made three fusion proteins with Mxi1 in different orientations: Mxi1-dCas9-mCherry-LINuS, dCas9-Mxi1-mCherry-LINuS and dCas9-mCherry-LINuS-Mxi1.

Though dCas9-Mxi1-mCherry-LINuS reduced expression of Tef1-GFP from the TEF1 promoter, there was still significant overlap in the range of the repressed (dCas9-Mxi1-mCherry-LINuS + sgTEF1) and unrepressed (dCas9-Mxi1-mCherry-LINuS + no guide) populations (Fig. 5b). Subpopulations of yeast that express specific genes at lower levels can serve as reservoirs of phenotypic heterogeneity important for surviving environmental perturbations and drug treatments [3,34]. The relative fraction of a population considered a low expresser can be defined by a relevant subpopulation ratio [3]. Using the 25th and 75th quartiles of the uninduced population to define low- and high-expressors respectively, we define N_L as the fraction of the population in the low state and N_H as the fraction of the population in the high state. The subpopulation ratio (N_L/N_H) increases 60-fold due to repression by dCas9-Mxi1-mCherry-LINuS, indicating that this construct, though not light-inducible, could be used to understand the consequences of changing the ratios of low- and high-expressors in populations of *S. cerevisiae*.

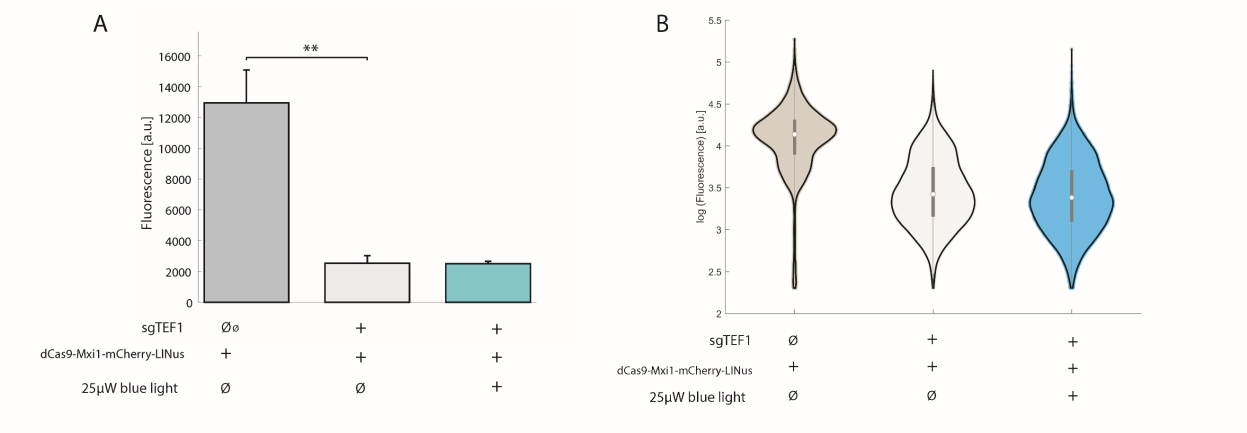

Figure 5. Yeast strains carrying dCas9-Mxi1-mCherry-LINuS with or without the sgTEF1 guide RNA were compared for repression in light and dark. A. Co-transformation of dCas9-Mxi1-mCherry-LINuS with sgTEF1 leads to a 5-fold repression in median Tef1-GFP expression with or without light relative to the no guide control (median fluorescence, $n = 3$, $p < 0.01$, Welch's t-test). B. Violin plots demonstrate the increase in expression range in the dCas9-Mxi1-mCherry-LINuS + sgTEF1 strains with or without light relative to the control. Violin plots represent median, interquartile range, and 95% confidence interval on a representative population of cells (biological replicates).

In contrast, the dCas9-mCherry-LINuS-Mxi1 construct showed less basal repression in the dark than the dCas9-Mxi1-mCherry-LINuS construct and a modest light-induced repression when grown in both 25 µW/cm^2 (data not show) and 130 µW/cm^2 blue light (Fig. 6). An examination of the fluorescence distributions indicates that light increases the population of cells in a low-expressing state but also leaves a substantial fraction of the population in the high expressing state. Indeed, in response to blue light the dCas9-mCherry-LINuS-Mxi1 cells start to show bimodality in expression levels. This is potentially due to plasmid maintenance, as yeast strains maintaining two low-copy CEN6/ARS4 plasmids have been shown to display bimodality in expression [33]. However, when comparing all of our dCas9 constructs, we have only seen the emergence of bimodality in strains with the Mxi1 repressor. The Mxi1 repressor is known to interact with

chromatin remodelers, [54] and perhaps converts a fraction of the population into a more deeply repressed state, leading to expression bimodality [48].

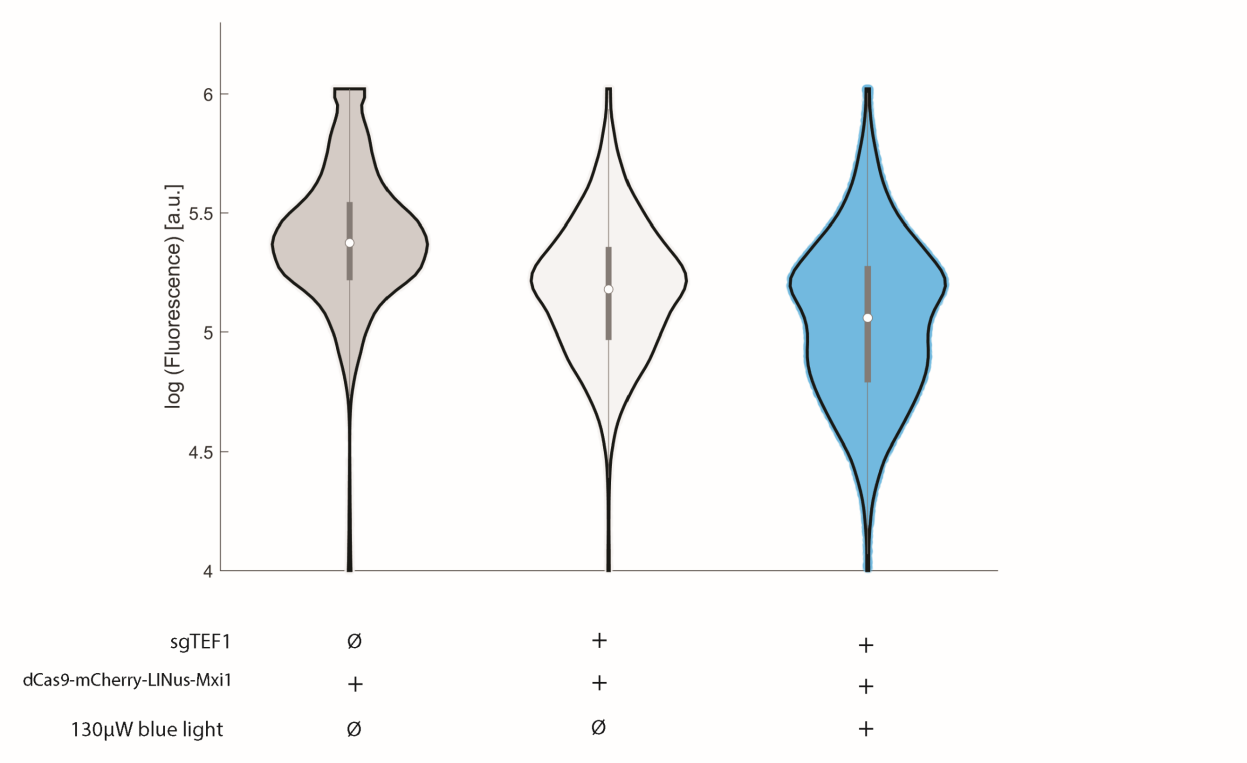

Figure 6. Yeast strains carrying dCas9-mCherry-LINuS-Mxi1 with or without the sgTEF1 guide RNA were compared for repression in light and dark. Co-transformation of dCas9-mCherry-LINuS-Mxi1 with sgTEF1 led to basal repression (1.7 fold) in the dark but light was able to cause a significant moderate increase in repression (1.3 fold, $n = 3$, $p < 0.0001$, Welch's t-test). Violin plots represent median, interquartile range, and 95% confidence interval on a representative population of cells with or without 130 µW/cm2 blue light.

Modulation of Light Duty Cycle Regulates Expression Level Through the dCas9-mCherry-LINuS Repressor

We next explored the tunability of our dCas9-mCherry-LINuS repressor as a function of duty cycle. Cells containing dCas9-mCherry-LINuS and the sgTEF1 guide were grown for 12 h in the light plate apparatus at either 15 µW/cm^2 or 135 µW/cm^2 light intensity. Duty cycle was varied at

0%, 5%, 25%, 50%, 75%, and 100% corresponding to 1 s on/19 s off; 5 s on/15 s off; 10 s on/10 s off; 15 s on/5 s off and constantly on. Maximal repression occurred for constant light at 135 $\mu W/cm^2$ (1.5-fold) corresponding to the same maximal repression we saw previously with the dCas9-mCherry-LINuS repressor. We could continuously change repression between minimal and maximal levels by varying the duty cycle (Figs. 7a and 7b). By changing duty cycle, we noticed that we could change the relative fraction of the population at the highest and lowest levels of fluorescence. Defining the subpopulation ratio as above (N_L/N_H), we saw that, despite a maximal change in median fluorescence of 1.5-fold, we were able to increase the subpopulation ratio up to 6-fold (Fig. 7c). This relationship holds when defining the subpopulation ratio using different thresholds (Supplemental Fig. 7). Thus by tuning the light duty cycle we can modulate the distribution of low expressors in the population, which may allow us to better understand the importance of relative expression populations [3].

A

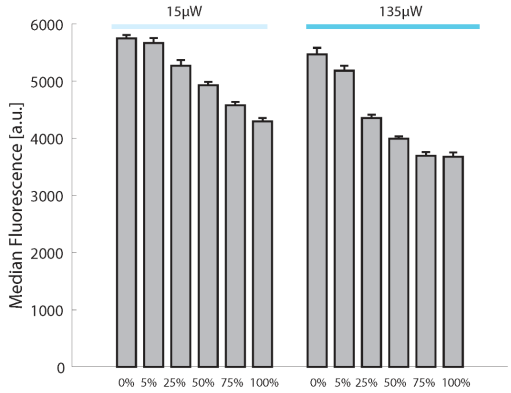
15µW
135µW
Median Fluorescence [a.u.]
6000
5000
4000
3000
2000
1000
0
0% 5% 25% 50% 75% 100%
0% 5% 25% 50% 75% 100%

B

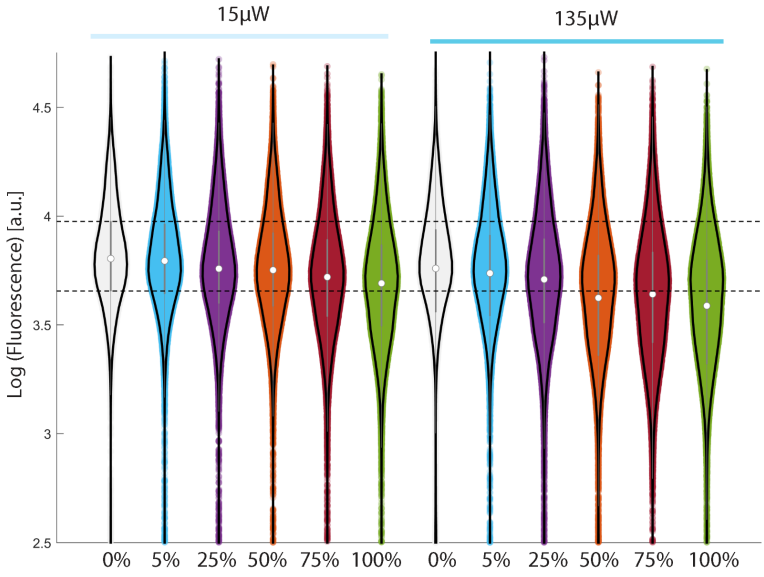
15µW
135µW
Log (Fluorescence) [a.u.]
4.5
4
3.5
3
2.5
0% 5% 25% 50% 75% 100% 0% 5% 25% 50% 75% 100%

C

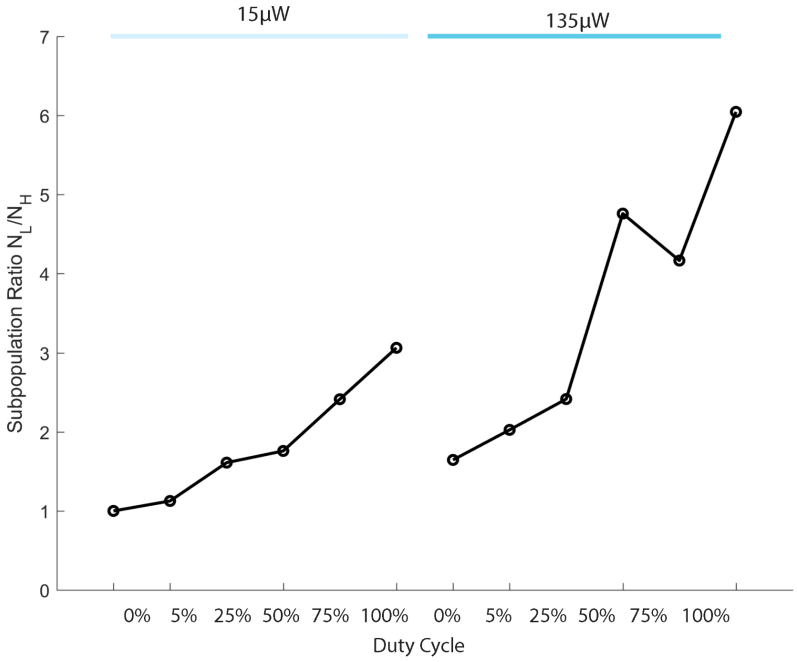
15µW
135µW
Subpopulation Ratio N_L/N_H
7
6
5
4
3
2
1
0
0% 5% 25% 50% 75% 100% 0% 5% 25% 50% 75% 100%
Duty Cycle

Figure 7. Duty cycle increases repression and expression variability in strains carrying the dCas9-mCherry-LINuS repressor. A. Strains carrying dCas9-mCherry-LINuS and the sgTEF1 guide RNA were exposed to cycles of 15 μW/cm2 or 135 μW/cm2 blue light at increasing duty cycle (0% off 5% 1 s on/19 s off, 25% 5 s on/15 s off, 50% 10 s on 10 s off 75% 15 s on 5 s off 100% on). Increasing duty cycle increases repression up to a maximum of 1.5-fold. Error bars represent 95% confidence intervals on the average of the median fluorescence from n = 3 biological replicates. B. Duty cycle increases the population of low expressing cells while leaving a significant fraction of the population distributed through the wild-type (dark) expression levels. Dashed lines represent the first and third quartile for cells carrying dCas9-mCherry-LINuS/sgTEF1 in the dark. C. Plotting the subpopulation ratio (N_L/N_H) shows that increasing light dosage increases the ratio of low expressors to high expressors in the population (up to 6-fold for dCas9-mCherry-LINuS-Mxi1).

Modulation of Light Intensity Regulates Expression Level Through the dCas9-mCherry-LINuS and dCas9-mCherry-LINuS-Mxi1 Repressors

We also wanted to understand the dynamic range achievable by modulating light intensity. We included the dCas9-mCherry-LINuS-Mxi1 strains to determine how the chromatin remodeler affects our ability to repress gene expression. Cells containing dCas9-mCherry-LINuS or dCas9-mCherry-LINuS-Mxi1 and the sgTEF1 guide (as well as guideless controls) were grown for 13 h at the indicated light intensities. No change in expression was evident in no-guide controls grown at different light intensities (Supplemental Fig. 8). Maximal repression for the dCas9-mCherry-LINuS (1.7-fold) and the dCas9-mCherry-LINuS-Mxi1 (2-fold) strains occurred at 100 μW/cm^2 (Figs. 8a and and 8b). We determined that further illumination at 200 μW/cm^2 and 300 μW/cm^2 did not increase repression (data not shown). Plotting the subpopulation ratio (N_L/N_H)

shows that dCas9-LINuS-Mxi1 allows us to change the ratio of low to high expressors by 10-fold, despite a mere 2-fold change in median expression level (Fig. 8c).

A

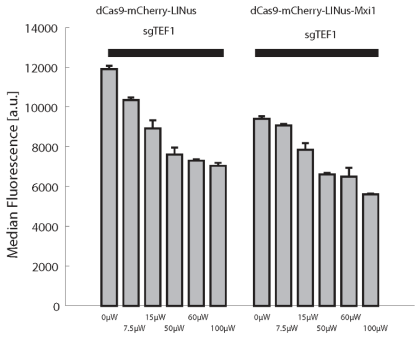
dCas9-mCherry-LINus
sgTEF1
dCas9-mCherry-LINus-Mxi1
sgTEF1
Median Fluorescence [a.u.]
14000
12000
10000
8000
6000
4000
2000
0
0μW
7.5μW
15μW
50μW
60μW
100μW

B

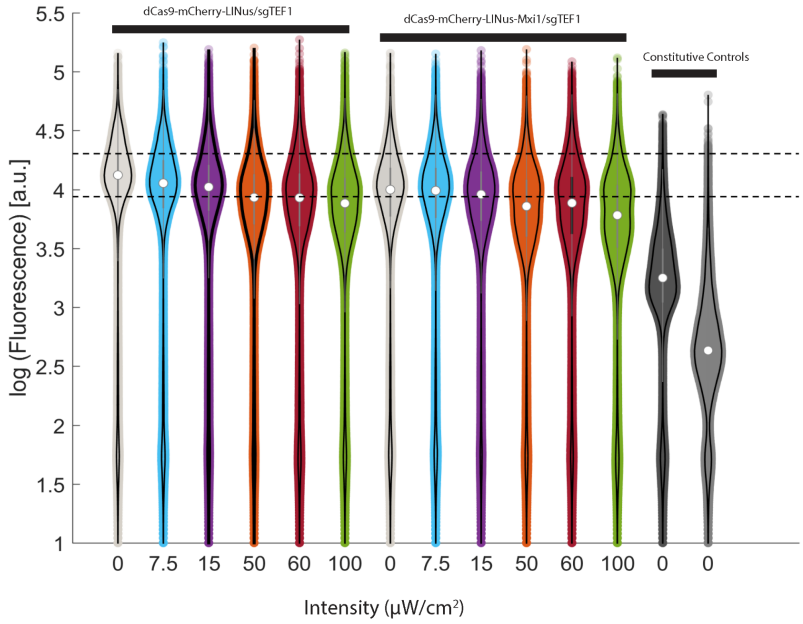
dCas9-mCherry-LINus/sgTEF1
dCas9-mCherry-LINus-Mxi1/sgTEF1
Constitutive Controls
log (Fluorescence) [a.u.]
5.5
5
4.5
4
3.5
3
2.5
2
1.5
1
0 7.5 15 50 60 100 0 7.5 15 50 60 100 0 0
Intensity (μW/cm²)

C

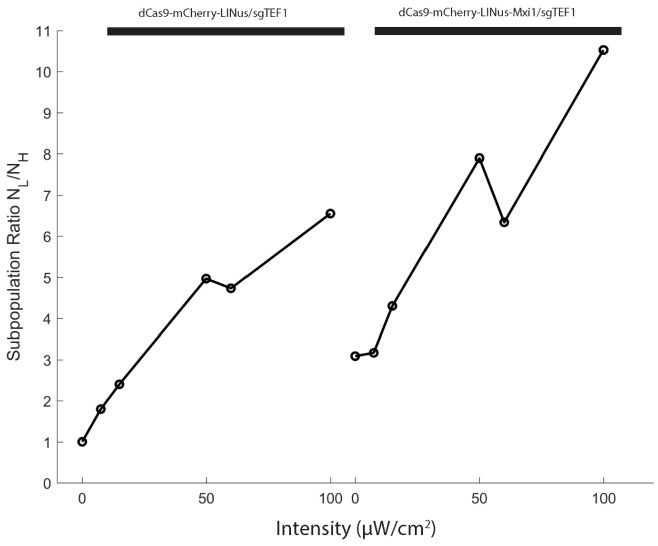
dCas9-mCherry-LINus/sgTEF1
dCas9-mCherry-LINus-Mxi1/sgTEF1
Subpopulation Ratio N_L/N_H
11
10
9
8
7
6
5
4
3
2
1
0
0 50 100 0 50 100
Intensity (μW/cm²)

Figure 8. Light intensity increases repression and expression variability in strains carrying the dCas9-mCherry-LINuS and dCas9-mCherry-LINuS-Mxi1 repressors. A. Strains carrying dCas9-mCherry-LINuS or dCas9-mCherry-LINuS-Mxi1 and the sgTEF1 guide RNA were exposed to increasing light intensities. Increasing light intensity increases repression in both the dCas9-mCherry-LINuS repressor and the dCas9-mCherry-LINuS-Mxi repressor, consistent with previous results. Error bars represent 95% confidence intervals on the average of the median fluorescence from n = 3 biological replicates. B. Light intensity increases the population of low expressing cells while leaving a significant fraction of the population distributed through the wild-type (dark) expression levels. Dashed lines represent the first and third quartile for cells carrying dCas9-mCherry-LINuS/sgTEF1 in the dark. The most variable population is dCas9-mCherry-LINuS-Mxi1 at 100 μW/cm2. This population has significant overlap with both the dark population as well as the constitutively repressed (dCas9/sgTEF1) population. Controls (dCas9 +sgTEF1, dark grey) and dCas9-Mxi1 +sgTEF1, light grey) are shown for comparison. C. Plotting the subpopulation ratio (N_L/N_H) shows that increasing light intensity increases the ratio of low expressors to high expressors in the population (up to 10-fold for dCas9-mCherry-LINuS-Mxi1). The controls (dCas9, dCasi-Mx1) change the subpopulation ratio (N_L/N_R) 450- and 1500-fold respectively and are therefore not shown on this plot.

Incorporation of the Light-Inducible Repressors into a Yeast Optogenetic Toolkit

The utility of our tool depends on the ability to rapidly integrate both the desired repressor (dCas9 variants) and an appropriate guide RNA targeting the gene of interest into the desired yeast strain. In order to make this possible, we implemented the unique aspects of our toolkit as “parts” in an existing yeast optogenetic toolkit format (Fig. 9) [1,33]. In the toolkit format, each part is characterized as a type (e.g. promoter types, coding sequence types, terminator types) based on function and location in the complete gene expression cassette (Fig. 9). The yeast toolkit [33] contains a part that can be modified to integrate the appropriate guide RNA with

complementarity to the desired genomic region (234 Combination Parts). Parts can be assembled into cassettes, fully assembled transcriptional units which express a single component, e.g. dCas9-mRuby2-LINuS, and then further assembled into multigene plasmids which contain both the dCas9-based repressor and the required guide RNA. The implementation of the essential elements (dCas9, LINuS, Mxi1, LINuS-Mxi1, see Supplemental Table S5) as parts allows us to build multigene plasmids containing the light-controlled repressor and appropriate guide in as little as 2 days using a Golden Gate cloning scheme.

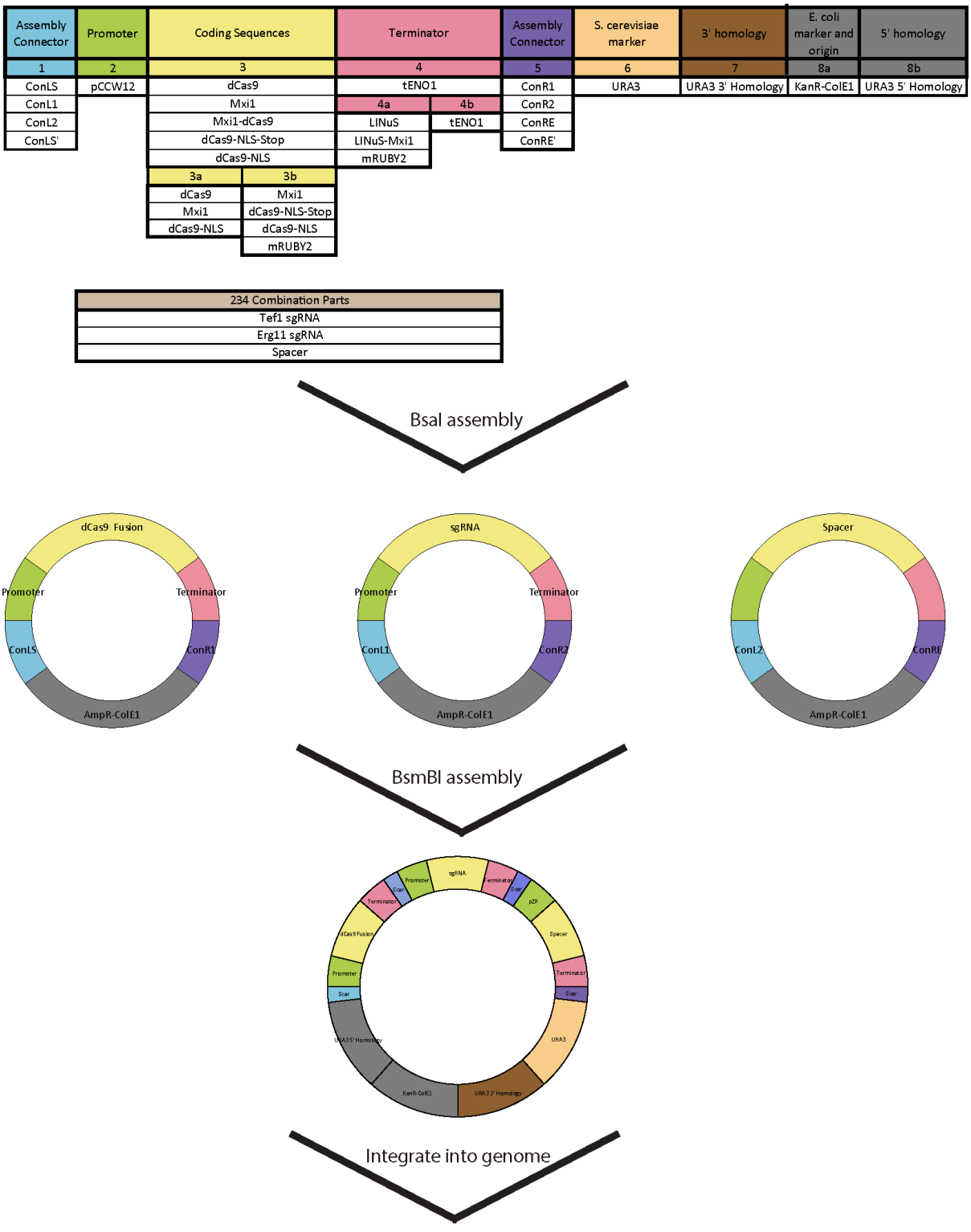

Figure 9. We generated dCas9, LINuS, and Mxi1 as either coding sequence or terminator parts, with and without stop codons and constitutive NLSs to allow for versatile repressors to be constructed using the toolkit. Part plasmids contain unique upstream and downstream BsaI-

generated overhangs to assemble into the appropriate position in “Cassette” plasmids. Cassette plasmids are fully functional transcriptional units that are further assembled into multigene plasmids using BsmBI assembly and appropriate Assembly Connectors. This figure utilizes the color scheme and organization from Lee, *et al*.[33] and An-Adirrekun, *et al*.[1] to illustrate how the new optogenetic components integrate with the existing yeast toolkit. (P, Promoter; T, Terminator; S, Scar)

Using the toolkit, we reconstructed five repressors containing varying configurations of dCas9, LINuS, mRuby2, and Mxi1 (Fig. 10a) based on our initial results with the LINuS and Mxi1 configurations. We found that dCas9-mRuby2 was a more effective constitutive repressor than dCas9 alone (Fig. 10a, Supplemental Fig. 9), perhaps due to increased steric hindrance. All constructs containing LINuS showed light-induced repression at 100 $\mu W/cm^2$ similar to that seen for our original mCherry constructs ranging from 1.2 (dCas9-mRuby2-LINuS) to 1.3-fold (dCas9-mRuby2-LINuS-Mxi1) (data not shown). We found that the repressors showed varying levels of basal (dark) repression ranging from 2- to 20-fold (Fig. 10a). We took advantage of this basal repression to in silico generate a population of yeast cells with expression varying over a 100-fold range (Figs. 10a and 10b) by sampling from each of the repressor populations.

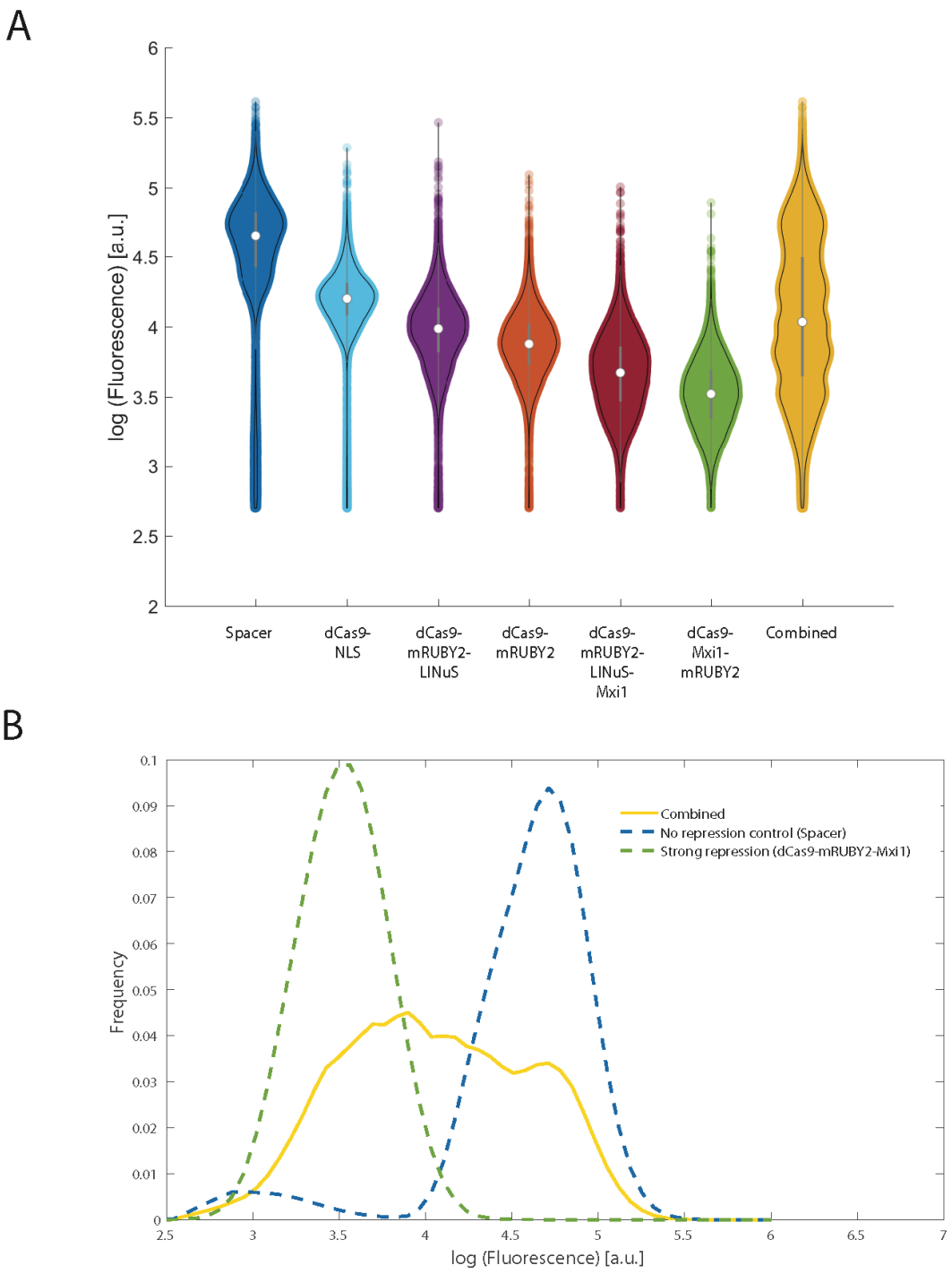

Figure 10. A. Basal (dark) repression of Tef1-GFP varies in the different repressor configurations. Each violin plot represents median, interquartile range, and 95% confidence interval on a representative population of cells (three biological replicates). B. By randomly combining cells from each population, we can in silico generate a population of cells with expression varying over

a 100-fold range, from the highest values to the most repressed (dCas9-Mxi1-mRuby2) values ("Combined").

Generation of Yeast Strains with Varying Sensitivity to Fluconazole

Though we did not set out to make repressors with varying levels of basal (dark) activity, this finding presented us with the opportunity to generate yeast with varying levels of (dark) repression for important drug resistance genes. As a proof-of-principle, we generated multigene cassettes containing the five repressors shown in Fig. 10a and a guide RNA targeting the gene ERG11 [58]. The ERG11 gene encodes lanosterol 14-alpha-demethylase, the enzyme which catalyzes C-14 demethylation of lanosterol to form 4,4″-dimethyl cholesta 8,14,24-triene-3-beta-ol in the ergosterol biosynthesis pathway in *S. cerevisiae* [27]. Mutants in the ERG11 gene are known to be sensitive to fluconazole, an antifungal medication that targets ergosterol synthesis and is widely used to treat a number of fungal infections [30]. A spot test demonstrated that these strains, each containing a different repressor, exhibited a > 10-fold range of sensitivity to fluconazole in line with the expression differences in Tef1-GFP from the TEF1 promoter seen in Fig. 10a (Fig. 11). Strains without a dCas9 repressor construct (Fig. 11) or containing dCas9 repressors without a guide RNA showed no increased sensitivity to fluconazole (Supplemental Fig. 10a). The various repressors with the ERG11 guide showed no difference in growth on plates lacking fluconazole (Supplemental Fig. 10b). We also tested repression of ERG25, C-4 methyl sterol oxidase, another enzyme involved in ergosterol biosynthesis. Repression of ERG25 has been shown to cause increased resistance to fluconazole, [58] but we could not detect this effect in our assays (data not shown).

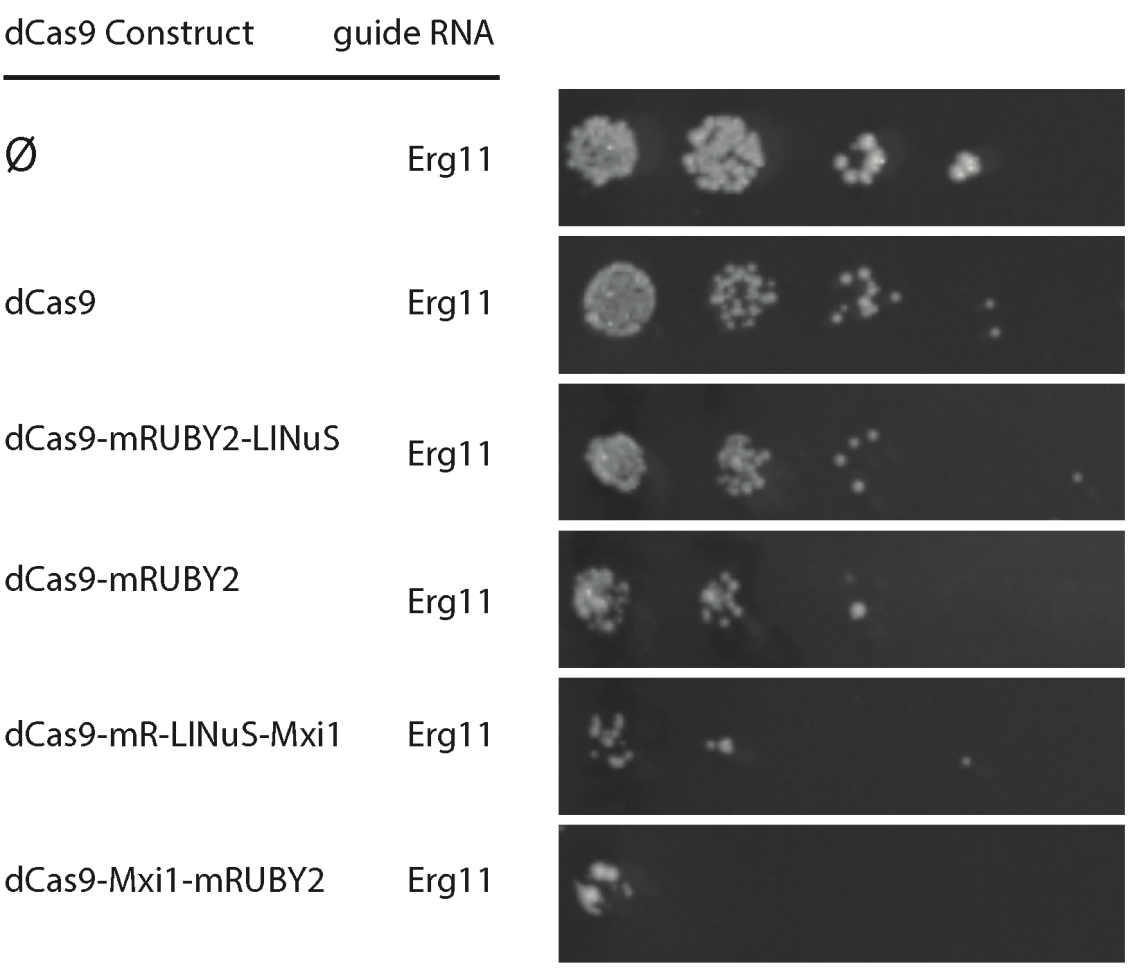

Figure 11. Repressors in Fig. 10 were assembled into multigene cassettes containing a guide RNA for the ERG11 gene. Repression of ERG11 confers sensitivity to the antifungal drug fluconazole. Dilutions (1:1, 1:10, 1:100, 1:1000 left to right) of cells were spotted onto plates containing 32 mg/mL fluconazole and grown in ambient light. The strain without a repressor shows no additional fluconazole sensitivity relative to wild-type cells. Sensitivity in strains carrying the dCas9 repressors agrees qualitatively with the repression of Tef1-GFP seen in Fig. 10a.

Discussion

In this study, we demonstrated that light-controlled nuclear localization of dCas9 achieved by fusing it to the light-inducible nuclear localization tool LINuS [45] can be used to manipulate gene

expression in populations of *S. cerevisiae* yeast cells. Moreover, we showed that the construct bearing an additional repressor domain (Mxi1) more strongly repressed gene expression. We selected the model protein Tef1 (translational elongation factor EF-1) because it has commonly been utilized to characterize the dCas9 and dCas9-Mxi1 repressors in *S. cerevisiae*. However, our choice of dCas9 as the DNA binding element means that specificity of the repressor can be changed by modifying the co-expressed guide RNA. To make creation of cassettes containing both the repressor of choice and an appropriate guide RNA (sgRNA) a rapid and simple process, we have integrated the essential elements of our repressors into "parts" that can be used with an existing yeast toolkit [34] to generate episomal or integrating constructs using a Golden Gate cloning scheme. Using this strategy, we can assemble and verify a repressor to target a gene of interest in less than 2 weeks. We demonstrated this by targeting the ERG11 gene and demonstrating a range of drug sensitivity due to variable basal repression (discussed further below).

The light-induced repression achieved by our repressors over the timescale we have studied is relatively modest (up to 2-fold). We hypothesize that basal repression, as well as time for dilution of the existing Tef1-GFP protein, leads to this low level of light-inducible repression. This suggests future avenues for improving the light inducibility of our repression including utilizing stronger nuclear localization signals, tethering of dCas9 in the cytoplasm to reduce basal repression, tuning expression levels of the dCas9 repressors, and balancing LINuS with a different nuclear export signal. Despite being modest, the light-inducible repression achieved is still enough to change the relative proportions of high- and low-expressors in populations of yeast up to 6-fold (dCas9-mCherry-LINuS) or 10-fold (dCas9-mCherry-LINuS-Mxi1).

We discovered that our different repressor constructs, in addition to light-inducible repression, show a 20-fold range in median basal (dark) gene repression. Using a combination of these repressors, we demonstrated that we can generate populations of yeast that repress the expression of Tef1-GFP over a 100-fold range (Fig. 10). Yeast promoters used in metabolic engineering naturally span a 1000-fold expression range [33]. However, generation of expression heterogeneity by transforming a library of repressors is attractive as it requires modification of only one genetic locus (with a dCas9 repressor and guide RNA) and does not require modifying the promoter of the gene of interest. We are particularly excited to use this basal repression to better understand the emergence of drug sensitivity and resistance, particularly in fungal populations. Fungal and human cells share very similar cellular structures and machineries, making it difficult to find drugs that aggressively target the fungal cell without significant toxicity in humans. Only four major classes (azoles, echinocandins, polyenes, and nucleoside analogs) of fungal drugs exist, making fungal drug resistance an emerging health concern. Gene expression variability is known to play a role in promoting yeasts' ability to evolve and adapt to drug treatment [3,42]. We demonstrated using our repressors that we could generate yeast with a > 10-fold range of fluconazole resistance (Fig. 11). The simplicity of our scheme should allow it to be adopted in other organisms, particularly pathogenic fungi, where promoter engineering to study the importance of gene expression on drug resistance and sensitivity is much more difficult than in *S. cerevisiae*.

Materials and Methods

Yeast Strains and Growth Conditions

All yeast strains used in this study are listed in the supplemental information (Supplemental Table S1). The strain background used in this study is FY HAP1^{+}, [22,63] or BY4741 [4]. TEF1-GFP and TEF1-mCherry reporter strains were created to test the function of the light-inducible

repressors. We utilized yeast strain yMM1032 (FY Matα ura3Δ0 his3Δ200 leu2Δ0 lys2-1280 trp1Δ63 HAP1^{+}) and tagged the TEF1 gene at its endogenous locus by amplifying either mCherry-hphMX or GFP-KanMX with primers containing appropriate homology downstream to the native TEF1 (Supplemental Table S1) and transforming this product using standard lithium-acetate transformation [17]. After selection on appropriate media (YPD agar + 300 µg/mL Hygromycin B or 200 µg/mL G418) and confirmation by colony PCR and confirmation of tagging by Sanger sequencing we obtained yMM1384 (FY Matα ura3Δ0 his3Δ200 leu2Δ0 lys2-1280 trp1Δ63 HAP1 + TEF1-mCherry-hphMX) and yMM1385 (FY Matα ura3Δ0 his3Δ200 leu2Δ0 lys2-1280 trp1Δ63 HAP1 + TEF1-GFP-KanMX). To test for light-induced nuclear-localization of our dCas9 LINuS fusion proteins we obtained a strain with a fluorescently labelled nucleus by utilizing yeast strain yMM84 (Matα ura3Δ0 his3Δ1 leu2Δ0 lys2Δ0) and tagging the nuclear protein Nhp6A by amplifying iRFP with primers containing appropriate homology downstream to the native NHP6A (Supplemental Table 1) and proceeding with transformation and verification as described for TEF1 tagging.

Standard yeast media was used for all experiments [6]. Yeast strains for transformation were grown to mid-log in YPD. Once transformed, yeast strains containing plasmids were maintained on appropriate Synthetic Complete (SC) media lacking amino acids needed to select for the plasmids (i.e. SC-URA-LEU). Selective SC consisted of yeast nitrogen base (BD Difco #291940), amino acid mix with appropriate amino acids dropped out and a final concentration of 2% glucose. Yeast assayed for fluorescence via flow cytometry were grown in low fluorescence media lacking riboflavin and folic acid as previously described [40,56] with the modification that we used a commercially available low fluorescence yeast nitrogen base (Formedium #CYN6501).

Plasmid Construction

All plasmids use in this study are listed in Supplemental Table S2. Plasmids were constructed using recombination-mediated plasmid construction as previously described [10,38,47]. The backbone plasmids, donor plasmids, and primers used are listed in Supplemental Table S4. Briefly, appropriate primers were used to amplify from donor DNA a cassette containing appropriate overhangs to recombine with the linearized backbone. Insert(s) and backbones were transformed into yeast strain yMM1032 and selected on SC-URA or SC-LEU to select for yeast containing appropriately repaired plasmid. Plasmids from separate colonies were then prepped from yeast using the Zymoprep Yeast Plasmid Miniprep Kit (ZymoResearch #D2004) and transformed into chemically competent DH5alpha E. coli to be further amplified. Plasmids were then prepped from E. coli and correct plasmid construction was confirmed by restriction enzyme digest followed by Sanger sequencing.

Induction of Repression and Blue Light Delivery

Blue light induction of repression was done in one of two ways. Cultures of yeast were either exposed to blue light on [1] a Light Plate Apparatus (LPA)16 in a dark coffin-shaker (250 rpm) at 30°C or [2] in culture tubes on a roller drum inside a light-proof 30°C incubator using LEDs fitted to the incubator and roller drum using custom hardware. Light intensity was measured using a standard photodiode power sensor and power meter (Thorlabs #S120VC, Thorlabs #PM100D). For illumination via LPA yeast cells carrying appropriate plasmid combinations were grown overnight to saturation and then diluted to an OD_{600} of 0.01. Cells were grown overnight (12–16 h) in a black 24-well polystyrene assay plate (Artic White, AWLS-303008) on the LPA. One glass microbead (Fisher Scientific 11-312A 3 mm or 11-312B 4 mm) was added to each well of the plate

to increase aeration. All LPAs utilized in this study were calibrated as described in Sweeney, *et al.* [60] so that uniform light doses could be delivered between LPAs and between experiments. LPAs were programmed to deliver varying light intensities or duty cycles as described in the main text. For illumination via custom hardware on the roller drum, yeast cells carrying appropriate plasmid combinations were grown overnight to saturation and then diluted to an OD_{600} of 0.01. Cells were grown overnight (12–16 h) in either clear (Falcon #1495970C) or black (Millipore Sigma LightSafe # TB1500) 15 mL conical tubes capped with aluminum foil to allow for gas exchange. Tubes were placed on a roller drum in an incubator fitted with blue LEDs in a custom configuration. An average illumination of ~ 25 μW/cm^2 was measured for cultures grown in this configuration. At each light intensity and for each dCas9 construct, we performed experiments in at least triplicate with biological replicates (individual colonies from the transformation with dCas9).

Time-Course of Repression

Cultures were grown in low fluorescence media without leucine or uracil (LFM-L-U). Yeast strain yMM1385 transformed with dCas9 repressors (pMM469, 472, 488, or 499) and a guide RNA or empty control (pMM473 or pMM7) was grown overnight in black 15 mL conical tubes. In the morning, cells were diluted to OD_{600} 0.01 and 1 mL of this diluted culture was transferred to the Light Plate Apparatus (LPA) with a glass bead (Fisher Scientific 11-312A 3 mm or 11-312B 4 mm). Cultures were grown at 30°C in a light-proof coffin shaker at 100 μW/cm^2 blue light and samples were taken every 4 h. At each timepoint, 50 μL of culture was removed and stored in 150 μL of PBS2 + 2% Tween-20 at 4°C. After 24 h all samples were taken for flow cytometry as described below.

Multiple dilution experiments were performed in LFM-L-U. Yeast strain yMM1385 transformed with dCas9 repressors (pMM469, 472, 488, or 499) and a guide RNA or empty control (pMM473 or pMM7) was grown overnight in black 15 mL conical tubes. In the morning, cells were diluted to OD_{600} 0.01 and 1 mL of this diluted culture was transferred to the Light Plate Apparatus (LPA) with a glass bead (Fisher Scientific 11-312A 3 mm or 11-312B 4 mm). Cultures were grown at 30°C in a light-proof coffin shaker at 100 μW/cm^2 blue light and samples (50 μL) were taken every 6 h. After 12 h samples were diluted to an OD_{600} of ~ 0.01. Flow cytometry was carried out every 24 h. Rainbow beads (Thermo Fisher Scientific #556286) were used to calibrate the voltage settings on the flow cytometer so that samples could be compared between days.

Flow Cytometry

Repression and gene expression variability of Tef1-GFP was assayed by fluorescence using flow cytometry. Two different cytometry instruments were employed. Samples analyzed using a BD LSRII multi-laser analyzer (488 nm laser and 505 LP dichroic filter) were grown overnight to saturation and diluted back to OD_{600} 0.01. Blue light was delivered as described above for 16 h. Cells were then diluted by adding 250 μL of culture to 800 μL of PBS/0.1% Tween-20 and kept on ice until measurement. Samples analyzed on an Attune NxT Flow Cytometer were grown overnight to saturation and diluted back to OD_{600} 0.01. Blue light was delivered for 12–16 h as described above. To prepare for cytometry, 50 μL of culture was diluted into 150 μL of PBS/0.1% Tween-20 in a 96-well plate (Corning #3788) and kept on ice until measurement. Samples were analyzed on the Attune using a 96-well autosampler and the 488 nm laser and 530/30 filter.

Quantification of Flow Cytometry Data

Flow cytometry data was analyzed using FlowJo or custom-written MATLAB code. Samples were gated by forward and side-scatter to include single cells. Samples were then gated by fluorescence based on non-fluorescent control strains. Unless otherwise indicated, the median fluorescence value was used to quantify the fluorescence of a population of cells. Appropriate statistical tests were used to determine the significance of changes in fluorescence, as described in the main text and figure captions where appropriate.

Localization of dCas9-mRUBY2-LINuS

To generate strains containing fluorescently tagged dCas9 fused to LINuS we created plasmid pMM771 (ConLS-pCCW12-dCas9-mRuby-LINuS-tENO1-ConRE-Ura3-Ura3'-ColE1-KanR-Ura5') using the yeast toolkit construction scheme (see below), digested this plasmid with NotI and transformed the resulting linear DNA into yMM1442 (MAT alpha his3Δ1 leu2Δ0 lys2Δ0 MET15 ura3Δ0 NHP6A-iRFP) using standard yeast transformation techniques as described above. Confirmed transformants were grown overnight in black 15 mL conical tubes in low fluorescence media lacking uracil (LFM-U). Overnight cultures were then diluted to OD_{600} 0.05 and grown for ~ 5 h. Optical 96-well plates (Nunc #265300) were then coated with 30 µL of 2 mg/mL concanavalin A as previously described [21] and incubated at room temperature for 5 min. Then 100 µL of culture was added to the wells and allowed to settle for 10 min. Excess culture was removed and cells were washed with fresh LFM-U to remove nonadherent cells followed by the addition of 100 µL of fresh LFM-U. Cells were imaged and stimulated on a Nikon Eclipse-TI inverted microscope using a ×40 air objective (Nikon 40x Plan Apo) and Clara CCD camera (Andor DR328G, South Windsor, Connecticut, United State of America). Cells were stimulated

with 470 nm blue light (Chroma 49002 GFP filter Cube, 470/40x) at ND16, resulting in a light intensity of 1.0 W/cm^2. mRUBY2 fluorescence was visualized at excitation 560 nm and 630 nm emission (Chroma 96365, ex560/40x, em630/75 m) and iRFP was visualized at 650 nm excitation, 720 nm emission (Chroma 49006, ex650/45x, em720/60 m). For the dark control, mRUBY2 and iRFP images were taken every 2 min for 8 min. For the blue light stimulated samples, the program was the same, except that cells were stimulated with blue light for 1 min after the first image was taken, followed by mRUBY2 and iRFP images for 8 min.

Growth Curve

Cells were grown to an OD_{600} of 0.2–0.7 then diluted to an OD_{600} of 0.05 and put in a 96-well plate (Corning #3370). Growth curves were generated by a Tecan Infinite M1000 plate reader. Cells were grown for 60 h with continuous double orbital shaking (120 rpm) and OD_{600} readings taken every 30 min. Four readings were taken for each well for every time point. Growth rate μ was determined for the culture in each well (except for the dCas9-Mxi1 samples) by fitting the log-transformed OD_{600} readings to the modified Gompertz equation described in Reference [65] using the Trust Region Reflective algorithm implemented in SciPy [5,26]. The dCas9-Mxi1 strains grew too slowly to fit well to the Gompertz equation, and so μ was not determined for these strains. We observed that in some cases the early time points were too dilute to give consistent readings in the Tecan so rather than normalizing by the starting reading as described in Zwietering, *et al*. [65], we added a fourth parameter N_0 to represent the starting concentration and fit the equation $y = A \exp(-\exp(\mu * e * (\lambda - t)/A + 1)) + \log N_0$ where y is the log-transformed OD_{600} readings.

Domestication and Creation of yOTK Parts Plasmids

Part plasmids added to the yeast optogenetic toolkit (yOTK) [1,33] format are shown in Supplemental Table S5. To comply with the yeast optogenetic toolkit (yOTK) format parts must be domesticated by removal of BsmBI, BsaI, and NotI restriction enzyme sites. dCas9 (pMM386) was mutated using the Q5 mutagenesis kit and protocol to remove an internal BsaI site. The restriction enzyme site went from GAGACC to GAAACC. This was confirmed using Sanger sequencing and resulted in pMM814.

Part plasmids were constructed using Golden Gate assembly as previously described [33]. Briefly, the region of interest was amplified using PCR with appropriate primers allowing for Golden Gate Assembly by adding a BsmBI digestion site. This product was then combined with the entry vector (pMM452) at a 1:1 molar ratio (20 fmol of both) as well as 1 µL of T4 ligase buffer, 0.5 µL of T7 ligase, and 0.5 µL of BsmBI. This reaction was put in a thermocycler with the following protocol: 25 cycles of 2 min at 42°C and 5 min at 16°C, then 10 min at 60°C and 10 min at 80°C. This reaction was then transformed into E. coli, plasmids were confirmed by screening for white colonies and then prepped for confirmation by restriction enzyme digestion followed by Sanger sequencing.

To create guide RNA parts to target dCas9 constructs to specific genomic loci, guide RNAs (sgRNAs) were constructed according to Reference [33]. Oligos were annealed together by adding 0.5 µL of the top oligo (100 µM), 0.5 µL of the bottom oligo (100 µM), 5 µL of 10x T4 Ligase Buffer, 1 µL of T4 polynucleotide Kinase, and 43 µL of H_20. This was run in the thermocycler for 30 min at 37°C, 5 min at 95°C, and slowly cooled to 4°C. Then 2 µg of the sgRNA entry vector (pMM736) was digested with 1 µL BsmBI, 5 µL 10x NEB3.1, and H_2O to 50 µL. This was

digested for 1 h at 55°C. Then 1 µL of alkaline phosphatase (CIP, New England Biolabs #M0290) was added and incubated for 1 h at 37°C. The backbone was purified using the GeneJet gel extraction protocol. Then, 0.5 µL of the annealed oligos, 0.5 µL of T4 DNA ligase, 1 µL of 10x T4 DNA ligase buffer, 20–40 ng of vector and H_2O to 10 µL were combined. This was run in the thermocycler for 30 min at 16°C, 10 min at 65°C, and cooled to 25°C, 5 µL of the ligated sgRNA was transformed into chemically competent E. coli, plasmids were confirmed by screening for white colonies and then prepped for confirmation by restriction enzyme digestion followed by Sanger sequencing.

Golden Gate Assembly of Cassette and Multigene Plasmids

Part plasmids (Supplemental Table S5) were used to construct cassette plasmids (consisting of transcriptional units, i.e., promoter-coding sequence-terminator, Supplemental Table S6) and multigene plasmids (consisting of multiple transcriptional units linked together through assembly connectors with appropriate homology to integrate into the yeast genome, Supplemental Table S7). These were assembled using BsaI or BsmBI assembly as outlined in Lee, *et al*.[33] and An-Adirekkun, *et al*.[1] NEB Golden Gate assembly mix (E1600) was used for BsaI assembly. The 10 µL Golden Gate reaction mixture consisted of 1 µL of NEB Golden Gate Buffer (10x), 0.5 µL NEB Golden Gate assembly mix, 20 fmol of each plasmid, and water. We found that using commercially available NEB Golden Gate assembly mixture, as opposed to using BsaI, T7 Ligase, and T4 Ligase buffer, increases the reaction efficiency greatly. For BsmBI assembly, the protocol was adapted from Lee, *et al* [33] and each 10 µL BsmBI reaction mixture consisted of 0.5 µL BsmBI, 0.5 µL T7 Ligase, 1 µL T4 Ligase buffer, 20 fmol of each plasmid, and H_2O.

The thermocycler program was adapted from Lee, *et al*. [33] and consisted of 20-30 cycles of digestion and ligation (2 min at 37–42°C; 5 min at 16°C) followed by a final digestion (55–60°C) and a heat inactivation step (80°C for 10–20 min). For final cassettes with internal BsaI cut sites (i.e., integration vectors), the reaction was ended with ligation, and final digestion and inactivation steps were omitted. 5 μL of reaction mixture was then transformed into DH5α competent E. coli cells and plated on LB plates with appropriate antibiotics. Plasmids were then extracted, digested with BsmBI or NotI-HF as a first-pass test, and sequenced with appropriate primers for final verification. For both BsaI and BsmBI assemblies, the efficiencies were found to be at least 50%. However, final cassettes with internal BsaI cut sites have notably lower assembly efficiency.

Assessment of Fluconazole Resistant Phenotypes

Yeast strains (yMM1518-1524, Supplemental Table S1) carrying different dCas9 constructs as well as an ERG11 sgRNA were grown overnight in black 15 mL conical tubes in low fluorescence media without uracil (LFM-U). These overnight cultures were diluted to an OD_{600} of 0.1 and serially diluted 1:10, 1:100, 1:1000. A spot analysis was performed by frogging these dilutions onto a synthetic complete agar plate lacking uracil (SC-U) with or without 32 mg/mL fluconazole (Sigma-Aldrich #1271700). The working stock of fluconazole was dissolved in DMSO, and equal amounts of DMSO were added to both the control and fluconazole plates. Strains were grown at room temperature in ambient (~ 45 μW/cm^2, 488 nm wavelength) light for 3 days before imaging.

References

1. Anadirekkun J, Stewart C, Geller S, Patel M, Melendez J, Oakes B, Noyes M, McClean M. A yeast optogenetic toolkit (yOTK) for gene expression control in Saccharomyces cerevisiae. BioRxiv. 2019 doi: 10.1101/663393.
2. Aubrey B, Kelly G, Brennan KAM, O'Connor L, Milla L, Wilcox S, Tai L, Strasser A, Herold M. An inducible lentiviral guide RNA platform enables the identification of tumor-essential genes and tumor-promoting mutations in vivo. Cell Reports. 2015;10:1422–1432. doi: 10.1016/j.celrep.2015.02.002.

3. Bódi Z, Farkas Z, Nevozhay D, Kalapis D, Lázár V, Csörgö B, Nyerges Á, Szamecz B, Fekete G, Papp B, Araújo H, Oliveira J, Moura G, Santos M, Székely T, Jr, Balázsi G, Pál C. Phenotypic heterogeneity promotes adaptive evolution. PLOS Biology. 2017;15(5):e2000644. doi: 10.1371/journal.pbio.2000644.
4. Brachmann C, Davies A, Cost G, Caputo E, Li J, Heiter P, Boeke J. Designer deletion strains derived from Saccharomyces cerevisiae S288C: a useful set of strains and plasmids for PCR-mediated gene disruption and other applications. Yeast. 1998;14:115–132. doi: 10.1002/(SICI)1097-0061(19980130)14:2<115::AID-YEA204>3.0.CO;2-2.
5. Branch M, Coleman T, Li Y. A Subspace, Interior, and Conjugate Gradient Method for Large-Scale Bound-Constrained Minimization Problems. SIAM Journal of Scientific Computing. 1999;21(1):1–23. doi: 10.1137/S1064827595289108.
6. Burke D, Amberg DC, Stearns T. Methods in Yeast Genetics: A Cold Spring Harbor Laboratory Course Manual. Woodbury, NY: Cold Spring Harbor Laboratory Press; 2000.
7. Davis K, Pattanayak V, Thompson D, Zuris J, Liu D. Small molecule-triggered Cas9 protein with improved genome-editing specificity. Nature Chemical Biology. 2015;11:316–318. doi: 10.1038/nchembio.1793.
8. Deaner M, Mejia J, Alper HS. Enabling graded and large-scale multiplex of desired genes using a dual-mode dCas9 activator in Saccharomyces cerevisiae. ACS Synthetic Biology. 2017;6:1931–1943. doi: 10.1021/acssynbio.7b00163.
9. Deltcheva E, Chylinski K, Sharma CM, Gonzales K, Chao Y, Pirzada ZA, Eckert MR, Vogel J, Charpentier E. CRISPR RNA maturation by trans-encoded small RNA and host factor RNase III. Nature. 2011;471(7340):602–607. doi: 10.1038/nature09886.
10. Dexter J, Xu P, Gunawardena J, McClean M. Robust network structure of the Sln1-Ypd1-Ssk1 three-component phospho-relay prevents unintended activation of the HOG MAPK pathway in Saccharomyces cerevisiae. BMC Systems Biology. 2015;9(1):17. doi: 10.1186/s12918-015-0158-y.
11. Dow L, Fisher J, O'Rourke K, Muley A, Kastenhuber E, Livshits G, Tschaharganeh D, Socci N, Lowe S. Inducible in vivo genome editing with CRISPR-Cas9. Nature Biotechnology. 2015;33:390–394. doi: 10.1038/nbt.3155.
12. Farzadfard F, Perli SD, Lu TK. Tunable and multifunctional eukaryotic transcription factors based on CRISPR/Cas. ACS Synthetic Biology. 2013;2(10):604–613. doi: 10.1021/sb400081r.
13. Fegan A, White B, Carlson J, Wagner C. Chemically controlled protein assembly: Techniques and applications. Chemical Reviews. 2010;110:3315–3336. doi: 10.1021/cr8002888.
14. Gander M, Vrana J, Voje W, Carothers J, Klavins E. Digital logic circuits in yeast with CRISPR-dCas9 NOR gates. Nature Communications. 2017;8:15459. doi: 10.1038/ncomms15459.
15. Gangopadhyay S, Cox K, Manna D, Lim D, Maji B, Zhou Q, Coudhary A. Precision Control of CRISPR-Cas9 Using Small Molecules and Light. Biochemistry. 2019;58:234–244. doi: 10.1021/acs.biochem.8b01202.
16. Gerhardt KP, Olson EJ, Castillo-Hair SM, Hartsough LA, Landry BP, Ekness F, Yokoo R, Gomez EJ, Ramakrishnan P, Suh J. An open-hardware platform for optogenetics and photobiology. Scientific Reports. 2016;6:35363. doi: 10.1038/srep35363.
17. Gietz RD, Schiestl RH. High-efficiency yeast transformation using the LiAc/SS carrier DNA/PEG method. Nature Protocols. 2007;2(1):31–34. doi: 10.1038/nprot.2007.13.
18. Gilbert LA, Larson MH, Morsut L, Liu Z, Brar GA, Torres SE, Stern-Ginossar N, Brandman O, Whitehead EH, Doudna JA, Lim WA, Weissman JS. CRISPR-mediated modular RNA-guided regulation of transcription in eukaryotes. Cell. 2013;154(2):442–451. doi: 10.1016/j.cell.2013.06.044.
19. Gonzalez F, Zhu Z, Shi Z, Lelli K, Verma N, Li Q, Huangfu D. An iCRISPR platform for rapid, multiplexable, and inducible genome editing in human pluripotent stem cells. Cell Stem Cell. 2014;15:215–226. doi: 10.1016/j.stem.2014.05.018.
20. Hemphill J, Borchardt E, Brown K, Asokan A, Deiters A. Optical control of CRISPR/Cas9 gene editing. Journal of the American Chemical Society. 2015;137:5642–5645. doi: 10.1021/ja512664v.
21. Hersen P, McClean M, Mahadevan L, Ramanathan S. Signal processing by the HOG MAP kinase pathway. Proceedings of the National Academy of Sciences. 2008;105(20):7165–7170. doi: 10.1073/pnas.0710770105.
22. Hickman MJ, Winston F. Heme levels switch the function of Hap1 of Saccharomyces cerevisiae between transcriptional activator and transcriptional repressor. Molecular and Cellular Biology. 2007;27(21):7414–7424. doi: 10.1128/MCB.00887-07.

23. Hsu P, Lander E, Zhang F. Development and applications of CRISPR-Cas9 for genome engineering. Cell. 2014;157:1262–1278. doi: 10.1016/j.cell.2014.05.010.
24. Jensen M. Design principles for nuclease-deficient CRISPR-based transcriptional regulators. FEMS Yeast Research. 2018 doi: 10.1093/femsyr/foy039.
25. Jinek M, Chylinski K, Fonfara I, Hauer M, Doudna JA, Charpentier E. A programmable dual-RNA–guided DNA endonuclease in adaptive bacterial immunity. Science. 2012;337(6096):816–821. doi: 10.1126/science.1225829.
26. E. Jones, E. Oliphant, and P. Peterson. SciPy: Open Source Scientific Tools for Python. 2001. http://www.scipy.org/. Accessed 26 Feb 2019.
27. Karst F, Lacrout F. Ertosterol biosynthesis in Saccharomyces cerevisiae: mutants deficient in the early steps of the pathway. Molecular Genetics and Genomics. 1977;154(3):269–277. doi: 10.1007/BF00571282.
28. Kiani S, Beal J, Ebrahimkhani M, Huh J, Hall R, Xie Z, Li Y, Weiss R. CRISPR transcriptional represion devices and layered circuits in mammalian cells. Nature Methods. 2014;11:723–726. doi: 10.1038/nmeth.2969.
29. Kleinjan D, Wardrope C, Nga Sou S, Rosser S. Drug-tunable multidimensional synthetic gene control using inducible degron-tagged dCas9 effectors. Nature Communications. 2017;8:1191. doi: 10.1038/s41467-017-01222-y.
30. Kontoyiannis D, Sagar N, Hirschi K. Overexpression of Erg11p by the regulatable GAL1 promoter confers fluconazole resistance in Saccharomyces cerevisiae. Antimicrobial Agents and Chemotherapy. 1999;43(11):2798–2800. doi: 10.1128/AAC.43.11.2798.
31. Kundert K, Lucas J, Watters K, Fellmann C, Nh A, Heineike B, Fitzsimmons C, Oakes B, Qu J, Prasad N, Rosenberg O, Savage D, El-Samad H, Doudna J, Kortemme T. Controlling CRISPR-Cas9 with ligand-activated and ligand-deactivated sgRNAs. Nature Communications. 2019;10:2127. doi: 10.1038/s41467-019-09985-2.
32. Lawhorn I, Ferreira J, Wang C. Evaluation of sgRNA target sites for CRISPR-mediated repression of TP53. PloS ONE. 2014;9(11):e113232. doi: 10.1371/journal.pone.0113232.
33. Lee ME, Deloache W, Cervantes D, Dueber J. A highly characterized yeast toolkit for modular, multipart assembly. ACS Synthetic Biology. 2015;4(9):975–986. doi: 10.1021/sb500366v.
34. Li S, Giardina D, Siegal M. Control of nongenetic heterogeneity in growth rate and stress tolerance of Saccharomyces cerevisiae by cyclic AMP-regulated transcription factors. PLoS Genetics. 2018;14(11):e1007744. doi: 10.1371/journal.pgen.1007744.
35. Lian J, HamediRad M, Hu S, Zhao H. Combinatorial metabolic engineering using an orthogonal tri-functional CRISPR system. Nature Communications. 2017;8:1688. doi: 10.1038/s41467-017-01695-x.
36. Liu K, Ramli M, Woo C, Wang Y, Zhao T, Zhang X, Yim G, Chong B, Gowher A, Chua M, Jung J, Lee J, Tan M. A chemical-inducible CRISPR–Cas9 system for rapid control of genome editing. Nature Chemical Biology. 2016;12:980–987. doi: 10.1038/nchembio.2179.
37. Liu Y, Zhan Y, Chen Z, He A, Li J, Wu H, Liu L, Zhuang C, Lin J, Guo X, Zhang Q, Huang W, Cai Z. Directing cellular information flow via CRISPR signal conductors. Nature Methods. 2016;13:938–944. doi: 10.1038/nmeth.3994.
38. Ma H, Kunes S, Schatz P, Botstein D. Plasmid construction by homologous recombination in yeast. Gene. 1987;58:201–216. doi: 10.1016/0378-1119(87)90376-3.
39. Ma H, Tu L-C, Naseri A, Huisman M, Zhang S, Grunwald D, Pederson T. CRISPR-Cas9 nuclear dynamics and target recognition in living cells. Journal of Cell Biology. 2016;214(5):525–537.
40. Melendez J, Patel M, Oakes BL, Xu P, Morton P, McClean MN. Real-time optogenetic control of intracellular protein concentration in microbial cell cultures. Integrative Biology. 2014;6(3):366–372. doi: 10.1039/c3ib40102b.
41. Natsume T, Kanemaki M. Conditional degrons for controlling protein expression at the protein level. Annual Reviews of Genetics. 2017;51:83–102. doi: 10.1146/annurev-genet-120116-024656.
42. Nevozhay D, Zal T, Balazsi G. Transferring a synthetic gene circuit from yeast to mammalian cells. Nature Communications. 2013;4:1451. doi: 10.1038/ncomms2471.
43. Nihongaki Y, Kawano F, Nakajima T, Sato M. Photoactivatable CRISPR-Cas9 for optogenetic genome editing. Nature Biotechnology. 2015;33:755–760. doi: 10.1038/nbt.3245.
44. Nihongaki Y, Yamamoto S, Kawano F, Suzuki H, Sato M. CRISPR-Cas9 based photoactivatable transcription system. Chemical Biology. 2015;22:169–174. doi: 10.1016/j.chembiol.2014.12.011.

45. Niopek D, Benzinger D, Roensch J, Draebing T, Wehler P, Eils R, DiVentura B. Engineering light-inducible nuclear localization signals for precise spatiotemporal control of protein dynamics in living cells. Nature Communications. 2014;5:4404. doi: 10.1038/ncomms5404.
46. Oakes B, Nadler D, Flamholz A, Christof F, Staahl B, Doudna J, Savage D. Profiling of engineering hotspots identifies an allosteric CRISPR-Cas9 switch. Nature Biotechnology. 2016;34:646–651. doi: 10.1038/nbt.3528.
47. Oldenburg K, Vo K, Michaelis S, Paddon C. Recombination-mediated PCR-directed plasmid construction in vivo in yeast. Nucleic Acids Research. 1997;25:451–452. doi: 10.1093/nar/25.2.451.
48. Pelet S, Rudolf F, Nadal-Ribelles M, de Nadal E, Posas F, Peter M. Transient activation of the HOG MAPK pathway regulates bimodal gene expression. Science. 2011;332(6030):732–735. doi: 10.1126/science.1198851.
49. Polstein L, Gersbach C. A light-inducible CRISPR-Cas9 system for controlling endogenous gene activation. Nature Chemical Biology. 2015;11:198–200. doi: 10.1038/nchembio.1753.
50. Qi LS, Larson MH, Gilbert LA, Doudna JA, Weissman JS, Arkin AP, Lim WA. Repurposing CRISPR as an RNA-guided platform for sequence-specific control of gene expression. Cell. 2013;152(5):1173–1183. doi: 10.1016/j.cell.2013.02.022.
51. Rose JC, Huang PS, Camp ND, Ye J, Leidal AM. A computationally engineered RAS rheostat reveals RAS-ERK signaling dynamics. Nature Chemical Biology. 2017;13:119–126. doi: 10.1038/nchembio.2244.
52. Rose J, Stephany J, Valente W, Trevillian B, Dang H, Bielas J, Maly D, Fowler D. Rapidly inducible Cas9 and DSB-ddPCR to probe editing kinetics. Nature Methods. 2017;14:891–896. doi: 10.1038/nmeth.4368.
53. Schirmaier F, Philippsen P. Identification of two genes coding for the translation elongation factor EF-1 alpha of S. cerevisiae. EMBO Journal. 1984;3(13):3311–3315. doi: 10.1002/j.1460-2075.1984.tb02295.x.
54. Schreiber-Agus N, Chin L, Chen K, Torres R, Rao G, Guida P, Skoultchi AI, DePinho RA. An amino-terminal domain of Mxi1 mediates anti-Myc oncogenic activity and interacts with a homolog of the yeast transcriptional repressor SIN3. Cell. 1995;80(5):777–786. doi: 10.1016/0092-8674(95)90356-9.
55. Senturk S, Shirole N, Nowak D, Corbo V, Pal D, Vaughan A, Tuveson D, Trotman L, Kinney J, Sordella R. Rapid and tunable method to temporally control gene editing based on conditional Cas9 stabilization. Nature Communications. 2017;8:14370. doi: 10.1038/ncomms14370.
56. Sheff M, Thorn K. Optimized cassettes for fluorescent protein tagging in Saccharomyces cerevisiae. Yeast. 2004;21:661–670. doi: 10.1002/yea.1130.
57. Siegel A, Baird M, Davidson M, Day R. Strengths and Weaknesses of Recently Engineered Red Fluorescent Proteins Evaluated in Live Cells Using Fluorescence Correlation Spectroscopy. International Journal of Molecular Sciences. 2013;14:20340–20358. doi: 10.3390/ijms141020340.
58. Smith JD, Suresh S, Schlecht U, Wu M, Wagih O, Peltz G, Davis RW, Steinmetz LM, Parts L, Onge RPS. Quantitative CRISPR interference screens in yeast identify chemical-genetic interactions and new rules for guide RNA design. Genome Biology. 2016;17:45. doi: 10.1186/s13059-016-0900-9.
59. Strickland D, Yao X, Gawlak G, Rosen MK, Gardner KH, Sosnick TR. Rationally improving LOV domain–based photoswitches. Nature Methods. 2010;7(8):623–626. doi: 10.1038/nmeth.1473.
60. Sweeney K, Moreno Morales N, Burmeister Z, Nimunkar A, McClean M. Easy calibration of the light plate apparatus for optogenetic experiments. MethodsX. 2019;6:1480–1488. doi: 10.1016/j.mex.2019.06.008.
61. Tang W, Hu J, Liu D. Aptazyme-embedded guide rnas enable ligand-responsive genome editing and transcriptional activation. Nature Communications. 2017;8:15939. doi: 10.1038/ncomms15939.
62. Vanegas K, Lehka B, Mortensen U. SWITCH: a dynamic CRISPR tool for genome engineering and metabolic pathway control for cell factory construction in Saccharomyces cerevisiae. Microbial Cell Factories. 2017 doi: 10.1186/s12934-017-0632-x.
63. Winston F, Dollard C, Ricupero-Havasse R. Construction of a set of convenient Saccharomyces cerevisiae strains that are isogenic to S288C. Yeast. 1995;11:53–55. doi: 10.1002/yea.320110107.
64. Zetsche B, Volz S, Zhang F. A split-Cas9 architecture for inducible genome editing and transcription modulation. Nature Biotechnology. 2015;33:139–142. doi: 10.1038/nbt.3149.
65. Zwietering M, Jongenburger I, Rombouts F, Van't Riet K. Modeling the bacterial growth curve. Applied and Environmental Microbiology. 1990;56(6):1875–1881.

Supplemental Information

Supplemental Methods

Details of Plasmid Construction by Recombination-Mediating Cloning

To create the different dCas9 and dCas9-Mxi1 repressor variants detailed in this study, we utilized recombination mediated cloning as previously described [5,15,18]. The construction for the plasmids listed in Supplemental Table S4 was done by recombining donor DNA amplified using appropriate oligos from the indicated donor plasmids into backbone plasmids cut with the indicated restriction enzymes. Details of the donor plasmids, oligos, and backbone vectors are in Supplemental Table S4.

Table S1: Details of Recombinational Cloning Scheme

Plasmid	Alias	Donor Plasmid	Oligos used for PCR	Backbone	RE Digestion
pMM397	Mxi-dCas9-mCherry-LINuS	pMM387	oMM1005 oMM1006 oMM1044-increased homology	pMM469	BglII
pMM399	dCas9-Mxi-mCherry-LINuS	pMM387 pMM386	oMM1008 oMM857 oMM1018 oMM1017	pMM396	XbaI & XmaI
pMM468	dCas9-LINuS	pMM386	oMM857 oMM858	pMM396	XbaI & XmaI
pMM469	dCas9-mCherry-LINuS	pMM386	oMM857 oMM859	pMM396	XbaI & XmaI
pMM470	dCas9-pKit-mCherry-LINuS	pMM386	oMM857 oMM711	pMM396	XbaI & XmaI
pMM471	dCas9-Snupn-mCherry-LINuS	pMM386	oMM857 oMM711	pMM398	XbaI & XmaI
pMM472	dCas9	pMM386	oMM1502 oMM857	pMM396	XbaI & XmaI
pMM473	gRNA Tefl	pMM388	oMM861 oMM860	pMM7	XhoI &SacI
pMM488	dCas9-Mxi	pMM387	oMM1503 oMM857	pMM396	XbaI & XmaI
pMM499	dCas9-mCherry-LINuS-Mxi	pMM387	oMM1009 oMM1010	pMM469	NotI

Details of Parts Plasmids Construction

To comply with the yTK format [14] parts must be domesticated by removal of BsmBI, BsaI and NotI restriction enzyme sites as described in the main text. Once domesticated, parts plasmids and multigene plasmids were constructed using the protocol described by Lee, *et al* [14]. Multipart plasmids were constructed using NEB Golden Gate Assembly. Primers used to create the parts in this study are listed in Supplemental Table S5. Plasmids used for construction of multipart plasmids are listed in Supplemental Table S6. Plasmids used for construction of multigene plasmids are listed in Supplemental Table S7.

Table S2: Parts Plasmid Construction

pMM	Desired Part/type	Template	PCR Oligo
pMM582	LINuS/4a	pMM396	oMM1083 oMM1084
pMM585	dCas9/3a	pMM814	oMM1079 oMM1081
pMM586	dCas9/3	pMM814	oMM1079 oMM1080
pMM587	dCas9/3b	pMM814	oMM1082 oMM1080
pMM725	LINuS-Mxi/4a	pMM499	oMM1153 oMM1221-adding stop codon oMM1083 oMM1222-adding stop codon
pMM727	Mxi/3	pMM387	oMM1089 oMM1093
pMM726	Mxi/3a	pMM387	oMM1089 oMM1094
pMM728	Mxi/3b	pMM387	oMM1090 oMM1093
pMM729	Mxi-dCas9/3	pMM814	oMM1089 oMM1080
pMM765	dCas9 NLS Stop/3	pMM386	oMM1079 oMM1650
pMM766	dCas9 NLS Stop/3b	pMM386	oMM1082 oMM1650
pMM767	dCas9 NLS/3	pMM386	oMM1079 oMM1651
pMM768	dCas9 NLS/3b	pMM386	oMM1082 oMM1651
pMM769	dCas NLS/3a	pMM386	oMM1079 oMM1652

Table S3: Cassette Plasmid Construction

pMM	Desired Plasmid	Part Plasmids
pMM0745	ConL1-Erg11 guide-ConR2-Leu2-CEN/ARS-KAN/ColE1	pMM755, pMM532, pMM537, pMM479, pMM524, pMM525
pMM0746	ConL1-Erg25 guide-ConR2-Leu2-CEN/ARS-KAN/ColE1	pMM756, pMM532, pMM537, pMM479, pMM524, pMM525
pMM0754	ConL1-TEF1 guide-ConR2-Leu2-CEN/ARS-KAN/ColE1	pMM764, pMM532, pMM537, pMM479, pMM524, pMM525
pMM0770	ConLS-pCCW12-dCas9-mRuby-tENO1-ConRE-Ura-Ura3'-Kan/ColE1-Ura5'	pMM489, pMM559, pMM767, pMM735, pMM733, pMM541, pMM734, pMM526, pMM481, pMM527
pMM0771	ConLS-dCas9-mRuby-LINuS-ConRE-Ura-Ura3'-Kan/ColE1-Ura5'	pMM489, pMM559, pMM585, pMM732, pMM582, pMM733, pMM541, pMM734, pMM526, pMM481, pMM527
pMM0776	ConLS-Spacer-ConR1-LEU2-CEN/ARS-ColE1-KanR	pMM489, pMM547,pMM491,pMM479,pMM524, pMM525
pMM0777	ConL1-Spacer-ConR2-Leu2-CEN/ARS-ColE1-KanR	pMM532, pMM547,pMM537,pMM479,pMM524, pMM525
pMM0778	ConL2-Spacer-ConRE-Leu2-CEN/ARS-ColE1-KanR	pMM533, pMM547,pMM541,pMM479,pMM524, pMM525
pMM0779	ConLS-pCCW12-	pMM489, pMM559, pMM586, pMM582, pMM733, pMM491, pMM734, pMM526, pMM481, pMM527

	dCas9-LINuS-tENO1-ConR1-URA3-Ura3'-ColE1-KanR-Ura5'	
pMM0780	ConLS-pCCW12-dCas9-mRuby-tENO1-ConR1-URA3-Ura3'-ColE1-KanR-Ura5'	pMM489, pMM559, pMM767, pMM735, pMM733, pMM491, pMM734, pMM526, pMM481, pMM527
pMM0781	ConLS-pCCW12-dCas9-mRuby-LINuS-tENO1-ConR1-URA3-Ura3'-ColE1-KanR-Ura5'	pMM489, pMM559, pMM585, pMM732, pMM582, pMM733, pMM491, pMM734, pMM526, pMM481, pMM527
pMM0782	ConLS-pCCW12-dCas9-mRuby-LINuS-Mxi1-tENO1-ConR1-URA3-Ura3'-ColE1-KanR-Ura5'	pMM489, pMM559, pMM585, pMM732 pMM725, pMM733, pMM491, pMM734, pMM526, pMM481, pMM527
pMM0783	ConLS-pCCW12-dCas9-Mxi1-mRuby-tENO1-ConR1-URA3-Ura3'-ColE1-KanR-Ura5'	pMM489, pMM559, pMM769, pMM728, pMM735 pMM733, pMM491, pMM734, pMM526, pMM481, pMM527
pMM0784	ConLS-pCCW12-dCas9-tENO1-ConR1-URA3-Ura3'-ColE1-KanR-Ura5'	pMM489, pMM559, pMM765, pMM542, pMM491, pMM734, pMM526, pMM481, pMM527
pMM0813	ConLS'-sfGFP-ConRE'-URA3-URA 3'homology-AmpR-ColE1-	pMM477, pMM490, pMM478, pMM734, pMM527, pMM744, pMM526

	URA 5' homology			

Table S4: Multigene Plasmid Construction

pMM	Desired Plasmid	Multipart Plasmids		
pMM0785	ConLS-pCCW12-dCas9-LINuS-tENO1-SCAR1-ptRNAPhe-tRNAPhe- HDV - sgERG11-SCAR2-Spacer-URA3-Ura3'-ColE1-AmpR-Ura5'	pMM0779, pMM0813	pMM0745,	pMM0778,
pMM0786	ConLS-pCCW12-dCas9-mRuby-tENO1-SCAR1-ptRNAPhe-tRNAPhe- HDV - sgERG11-SCAR2-Spacer-URA3-Ura3'-ColE1-AmpR-Ura5'	pMM0780, pMM0813	pMM0745,	pMM0778,
pMM0787	ConLS-pCCW12-dCas9-mRuby-LINuS-tENO1-SCAR1-ptRNAPhe- tRNAPhe- HDV - sgERG11 -SCAR2- Spacer- URA3-Ura3'- ColE1-AmpR-Ura5'	pMM0781, pMM0813	pMM0745,	pMM0778,
pMM0788	ConLS-pCCW12-dCas9-mRuby-LINuS-Mxi1-tENO1-SCAR1-ptRNAPhe- tRNAPhe- HDV - sgERG11- SCAR2- Spacer- URA3-Ura3'-ColE1-AmpR-Ura5'	pMM0782, pMM0813	pMM0745,	pMM0778,
pMM0789	ConLS-pCCW12-dCas9-Mxi1-mRuby-tENO1-SCAR1-ptRNAPhe- tRNAPhe- HDV - sgERG11- SCAR2- Spacer- URA3-Ura3'-ColE1-AmpR-Ura5'	pMM0783, pMM0813	pMM0745,	pMM0778,
pMM0790	ConLS-Spacer-SCAR1-ptRNAPhe- tRNAPhe- HDV-sgERG11- SCAR2- Spacer- URA3-Ura3'- ColE1- AmpR- Ura5'	pMM0776, pMM0813	pMM0745,	pMM0778,
pMM0791	ConLS-pCCW12-dCas9-tENO1-SCAR1-ptRNAPhe- tRNAPhe-HDV- sgERG11-SCAR2-Spacer-URA3-Ura3'-ColE1-AmpR-Ura5'	pMM0784, pMM0813	pMM0745,	pMM0778,
pMM0792	ConLS-pCCW12-dCas9-LINuS-tENO1-SCAR1-ptRNAPhe-	pMM0779, pMM0813	pMM0746,	pMM0778,

	tRNAPhe- HDV - sgERG25-SCAR2-Spacer-URA3-Ura3'-ColE1-AmpR-Ura5'			
pMM0793	ConLS-pCCW12-dCas9-mRuby-tENO1-SCAR1-ptRNAPhe-tRNAPhe- HDV - sgERG25-SCAR2-Spacer-URA3-Ura3'-ColE1-AmpR-Ura5'	pMM0780, pMM0813	pMM0746,	pMM0778,
pMM0794	ConLS-pCCW12-dCas9-mRuby-LINuS-tENO1-SCAR1-ptRNAPhe- tRNAPhe- HDV - sgERG25 -SCAR2- Spacer- URA3-Ura3'- ColE1-AmpR-Ura5'	pMM0781, pMM0813	pMM0746,	pMM0778,
pMM0795	ConLS-pCCW12-dCas9-mRuby-LINuS-Mxi1-tENO1-SCAR1-ptRNAPhe- tRNAPhe- HDV - sgERG25- SCAR2- Spacer- URA3-Ura3'-ColE1-AmpR-Ura5'	pMM0782, pMM0813	pMM0746,	pMM0778,
pMM0796	ConLS-pCCW12-dCas9-Mxi1-mRuby-tENO1-SCAR1-ptRNAPhe- tRNAPhe- HDV - sgERG25- SCAR2- Spacer- URA3-Ura3'-ColE1-AmpR-Ura5'	pMM0783, pMM0813	pMM0746,	pMM0778,
pMM0797	ConLS-Spacer-SCAR1-ptRNAPhe- tRNAPhe- HDV-sgERG25- SCAR2- Spacer- URA3-Ura3'- ColE1- AmpR- Ura5'	pMM0776, pMM0813	pMM0746,	pMM0778,
pMM0798	ConLS-pCCW12-dCas9-tENO1-SCAR1-ptRNAPhe- tRNAPhe-HDV- sgERG25-SCAR2-Spacer-URA3-Ura3'-ColE1-AmpR-Ura5'	pMM0784, pMM0813	pMM0746,	pMM0778,
pMM0799	ConLS-pCCW12-dCas9-LINuS-tENO1-SCAR1-ptRNAPhe-tRNAPhe- HDV - sgTEF1-SCAR2-Spacer-URA3-Ura3'-ColE1-AmpR-Ura5'	pMM0779, pMM0813	pMM0754,	pMM0778,
pMM0800	ConLS-pCCW12-dCas9-mRuby-tENO1-SCAR1-ptRNAPhe-tRNAPhe- HDV - sgTEF1-SCAR2-	pMM0780, pMM0813	pMM0754,	pMM0778,

	Spacer-URA3-Ura3'-ColE1-AmpR-Ura5'			
pMM0801	ConLS-pCCW12-dCas9-mRuby-LINuS-tENO1-SCAR1-ptRNAPhe- tRNAPhe- HDV -sgTEF1 -SCAR2- Spacer- URA3-Ura3'- ColE1-AmpR-Ura5'	pMM0781, pMM0813	pMM0754,	pMM0778,
pMM0802	ConLS-pCCW12-dCas9-mRuby-LINuS-Mxi1-tENO1-SCAR1-ptRNAPhe- tRNAPhe- HDV -sgTEF1- SCAR2- Spacer- URA3-Ura3'-ColE1-AmpR-Ura5'	pMM0782, pMM0813	pMM0754,	pMM0778,
pMM0803	ConLS-pCCW12-dCas9-Mxi1-mRuby-tENO1-SCAR1-ptRNAPhe- tRNAPhe- HDV -sgTEF1- SCAR2- Spacer- URA3-Ura3'-ColE1-AmpR-Ura5'	pMM0783, pMM0813	pMM0754,	pMM0778,
pMM0804	ConLS-Spacer-SCAR1-ptRNAPhe- tRNAPhe- HDV-sgTEF1- SCAR2- Spacer- URA3-Ura3'- ColE1- AmpR- Ura5'	pMM0776, pMM0813	pMM0754,	pMM0778,
pMM0805	ConLS-pCCW12-dCas9-tENO1-SCAR1-ptRNAPhe- tRNAPhe-HDV- sgTEF1-SCAR2-Spacer-URA3-Ura3'-ColE1-AmpR-Ura5'	pMM0784, pMM0813	pMM0754,	pMM0778,
pMM0806	ConLS-pCCW12-dCas9-LINuS-tENO1-SCAR1-Spacer-SCAR2-Spacer-URA3-Ura3'-ColE1-AmpR-Ura5'	pMM0779, pMM0813	pMM0777,	pMM0778,
pMM0807	ConLS-pCCW12-dCas9-mRuby-tENO1-SCAR1-Spacer-SCAR2-Spacer-URA3-Ura3'-ColE1-AmpR-Ura5'	pMM0780, pMM0813	pMM0777,	pMM0778,
pMM0808	ConLS-pCCW12-dCas9-mRuby-LINuS-tENO1-SCAR1-Spacer-SCAR2- Spacer- URA3- Ura3'-ColE1- AmpR- Ura5'	pMM0781, pMM0813	pMM0777,	pMM0778,

pMM0809	ConLS-pCCW12-dCas9-mRuby-LINuS-Mxi1-tENO1-SCAR1-Spacer- SCAR2- Spacer- URA3-Ura3'-ColE1-AmpR-Ura5'	pMM0782, pMM0813	pMM0777,	pMM0778,
pMM0810	ConLS-pCCW12-dCas9-Mxi1-mRuby-tENO1-SCAR1-Spacer-SCAR2- Spacer- URA3- Ura3'-ColE1- AmpR- Ura5'	pMM0783, pMM0813	pMM0777,	pMM0778,
pMM0811	ConLS-Spacer-SCAR1-Spacer-SCAR2- Spacer- URA3- Ura3'-ColE1- AmpR- Ura5'	pMM0776, pMM0813	pMM0777,	pMM0778,
pMM0812	ConLS-pCCW12-dCas9-tENO1-SCAR1-Spacer-SCAR2-Spacer-URA3-Ura3'-ColE1-AmpR-Ura5'	pMM0784, pMM0813	pMM0777,	pMM0778,

Supplemental Table S5. sgRNA oligos

pMM	sgRNA	Oligo
pMM755	sgERG11 ColE1-CamR Part234	oMM1722 oMM1723
pMM756	sgERG25 ColE1-CamR Part234	oMM1724 oMM1725
pMM764	sgTEF1 ColE1-CamR Part234	oMM1740 oMM1741

Supplemental Figures

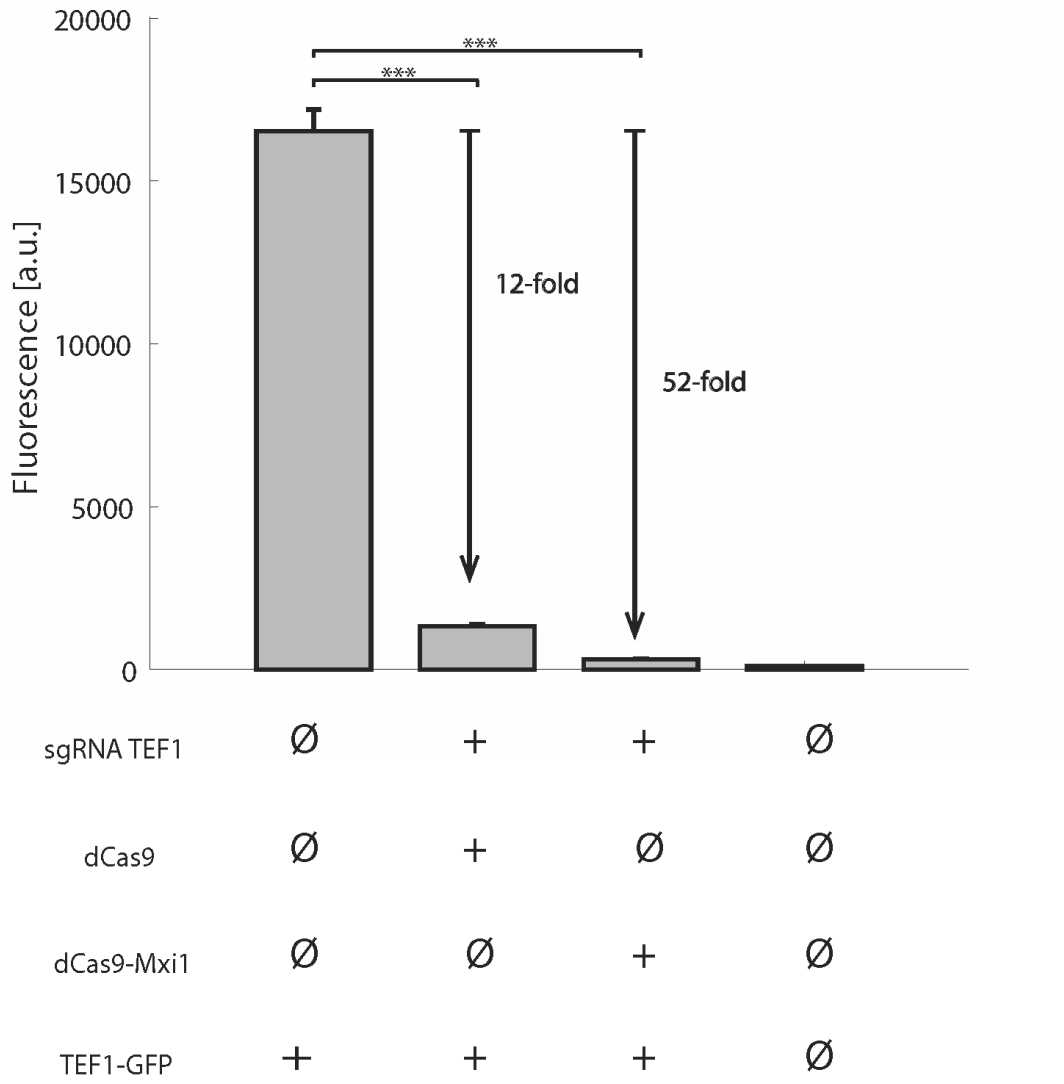

Supplemental Figure 1. Yeast strains with and without appropriate combinations of dCas9 or dCas9-Mxi1 and sgTEF1 guide RNA were compared for repression of Tef1-GFP based on fluorescence. Co-transformation of dCas9 and sgTEF1 results in 12-fold repression of median population fluorescence (n=3; p-value<0.0005, Welch's t-test) while co-transformation of dCas9-Mxi1 and sgTEF1 results in 52-fold repression (n=3, p-value<0.005, Welch's t-test). A non-fluorescent strain is shown for comparison. The levels of repression we see in our reporter strain are consistent with previously published results [3]. Both dCas9 and dCas9-Mxi1 contain the SV40 nuclear localization signal leading to constitutive nuclear localization [9].

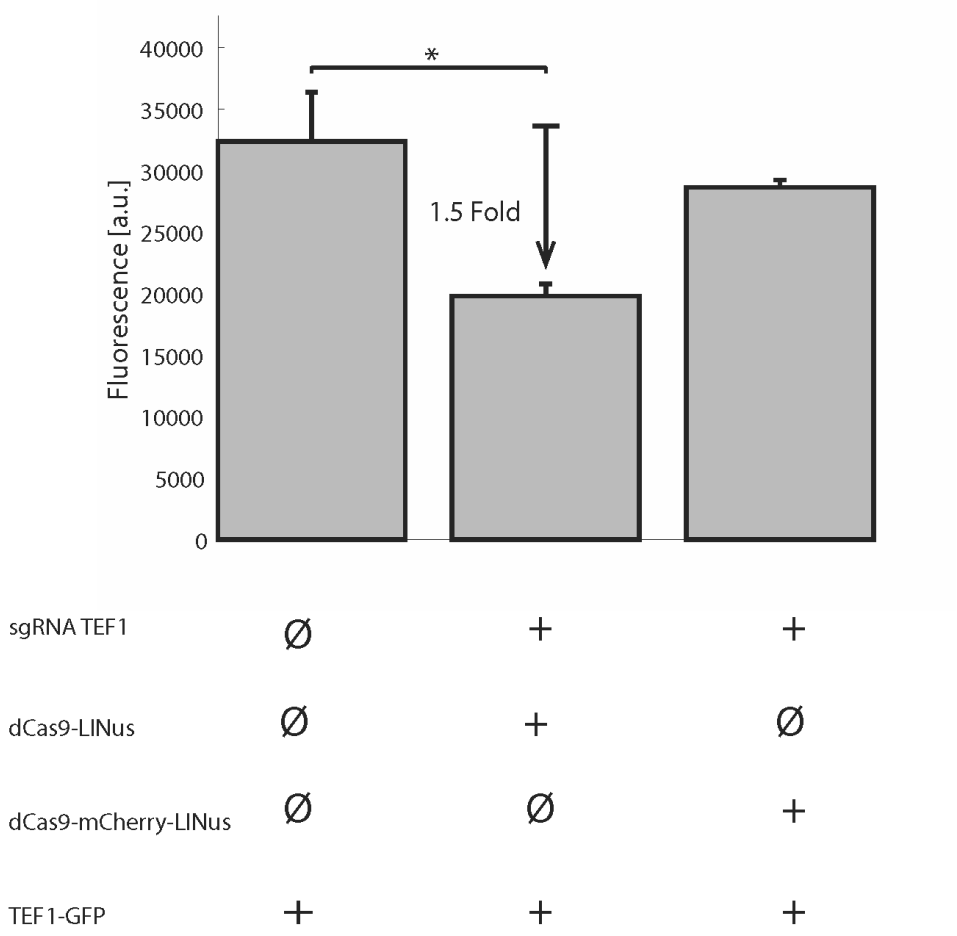

Supplemental Figure 2. Yeast strain yMM1385 (Tef1-GFP) was grown for up to 12 hours in the Light Plate Apparatus with either 0μW/cm^2 or 100μW/cm^2 light. While there is some decrease in Tef1-GFP over the course of the experiment (most likely due to changes in growth rate as the culture begins to reach stationary phase) there is no difference between the light and dark samples.

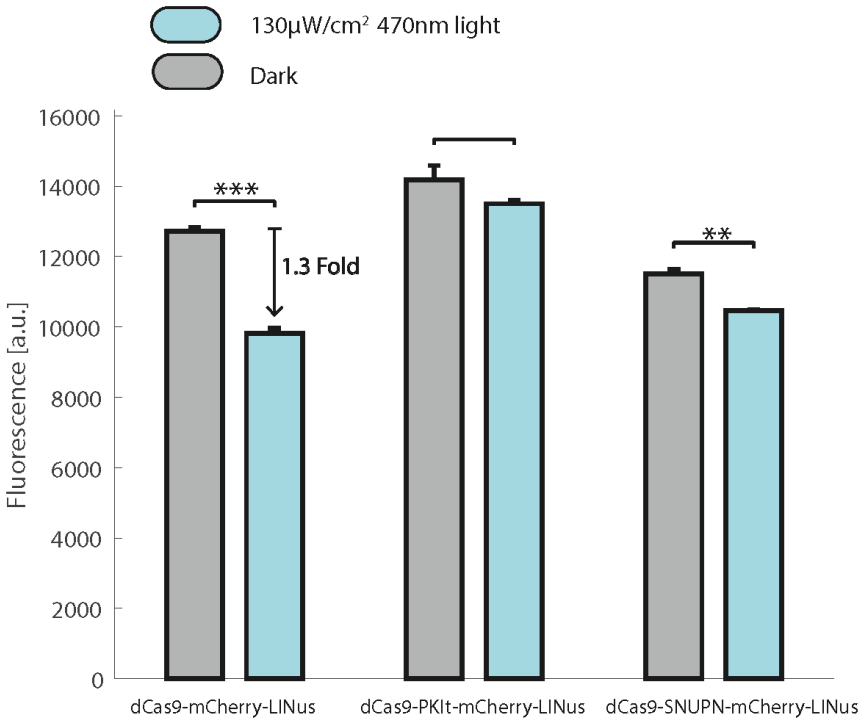

Supplemental Figure 3. Yeast strains with and without appropriate combinations of the dCas9-LINuS and dCas9-mCherry-LINuS constructs and sgTEF1 guide were compared for basal (no light) repression. Co-transformation of dCas9-LINuS and sgTEF1 guide results in a small, but significant, 1.5-fold repression even in the dark (n=3; p-value<0.05, Welch's t-test). We therefore pursued used of the dCas9-mCherry-LINuS construct.

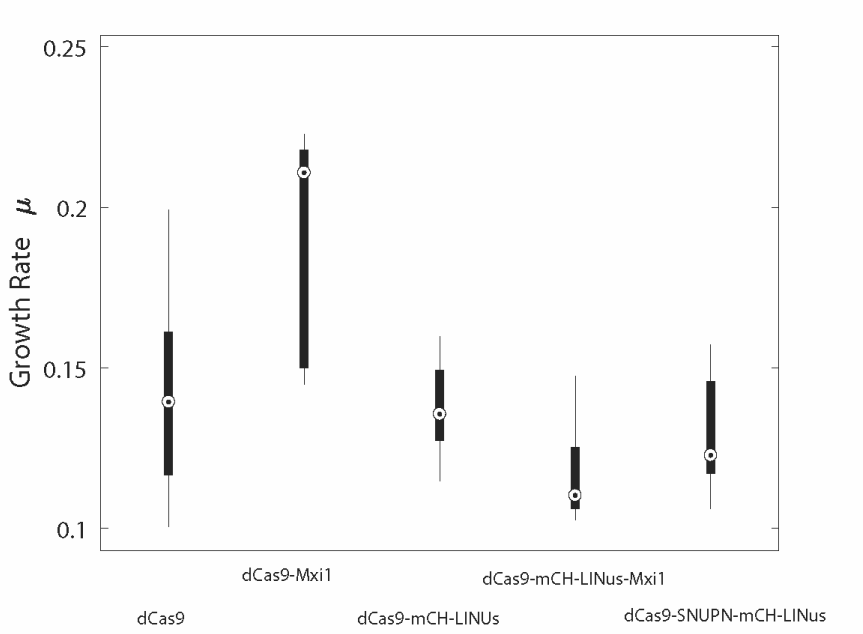

Supplemental Figure 4. Addition of nuclear export signals (NES) to create dCas9-PKIt-mCherry-LINuS and dCas9-SNUPN-mCherry-LINuS did not result in additional light-inducible repression. The dCas9-mCherry-LINuS construct achieves the greatest repression (1.3-fold; n=3; p-value<0.00005, Welch's t-test) while dCas9-PKIt-mCherry-LINuS did not show significant light-induced repression. The dCas9-SNUPN-mCherry-LINuS construct did show significant repression (n=3; p-value<0.005, Welch's t-test), but at a lower fold-change than dCas9-mCherry-LINuS (1.1-fold).

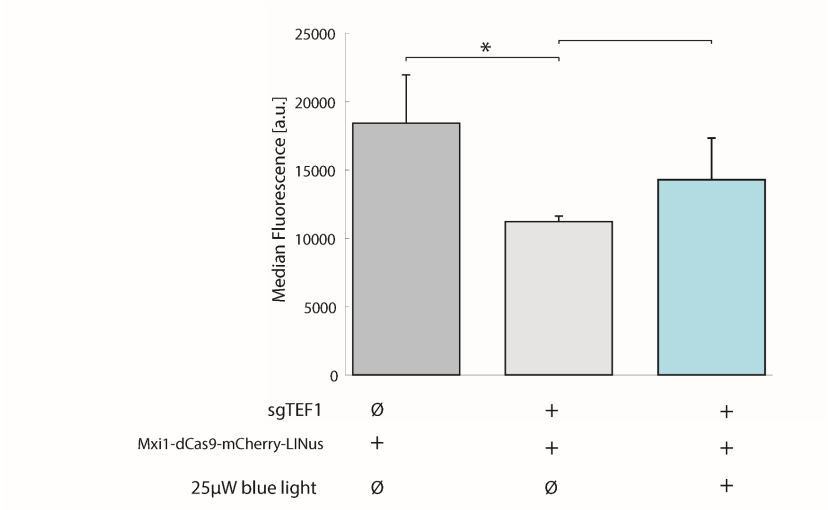

Supplemental Figure 5. Growth curves of strains transformed with dCas9, dCas9-Mxi1, dCas9-mCherry-LINuS, dCas9-mCherry-LINuS-Mxi1, or dCas9-SNUPN-mCherry-LINuS and the sgTEF1 guide grown in the dark. **(a)** Growth rate, μ, of strains transformed with dCas9, dCas9-mCherry-LINuS, dCas9-mCherry-LINuS-Mxi1, or dCas9-SNUPN-mCherry-LINuS and the sgTEF1 guide grown in the dark were obtained by fitting OD_{600} values to the Gompertz equation [8]. Strains containing dCas9-Mxi1 grew too slowly to be fit with the Gompertz equation. **(b)** Constitutive repression of Tef1-GFP expression by dCas9-Mxi1 increases growth rate variability between replicates and significantly reduces the growth rate.

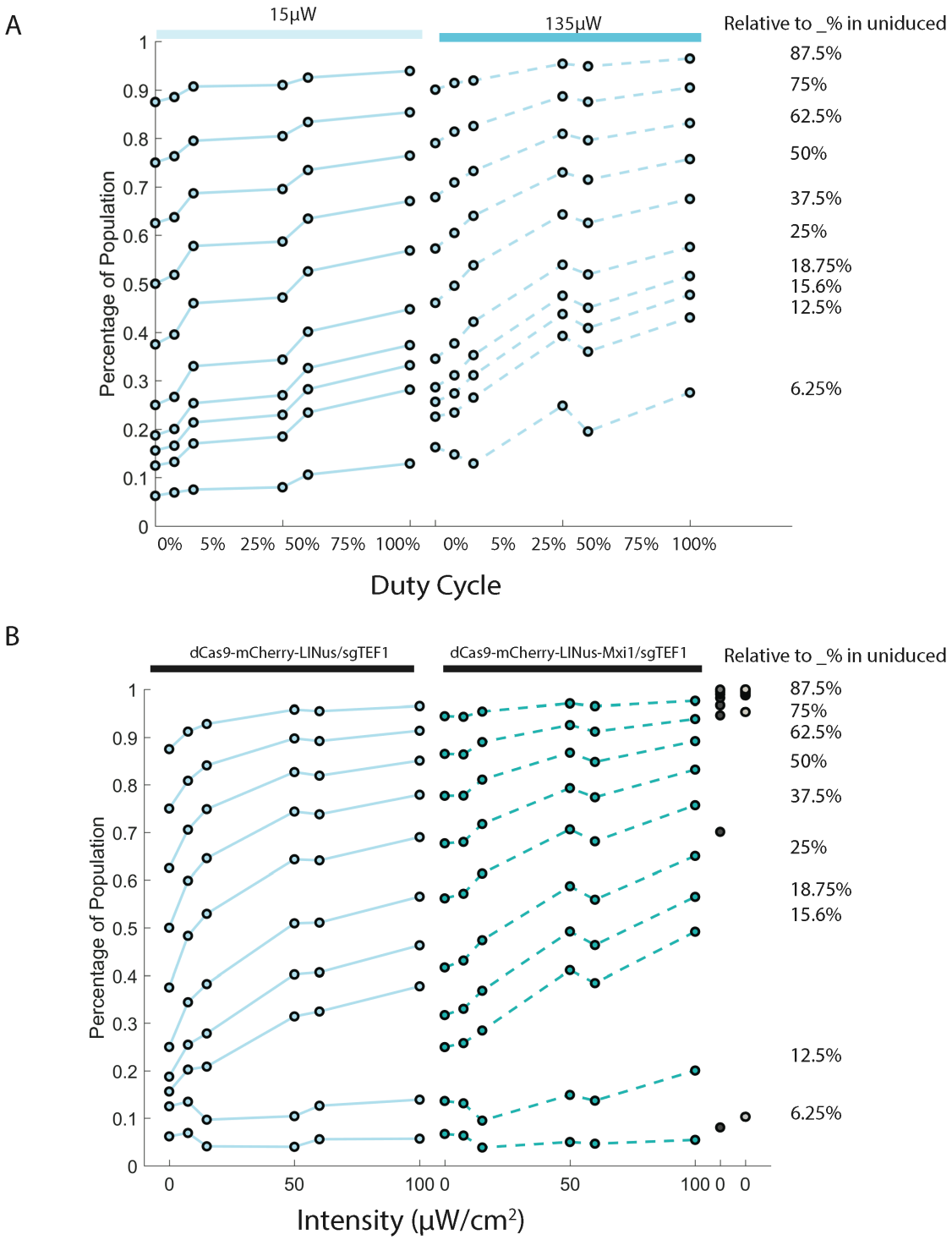

Supplemental Figure 6. Strains transformed with the Mxi1-dCas9-mCherry-LINuS construct and the sgTEF1 guide show a small increase in basal repression (1.6-fold, p-value<0.05, Welch's t-test) relative to the no-guide control. No additional repression occurs when strains are exposed to 25µW/cm^2 blue-light, indicating that this fusion protein does not function as a light-inducible repressor.

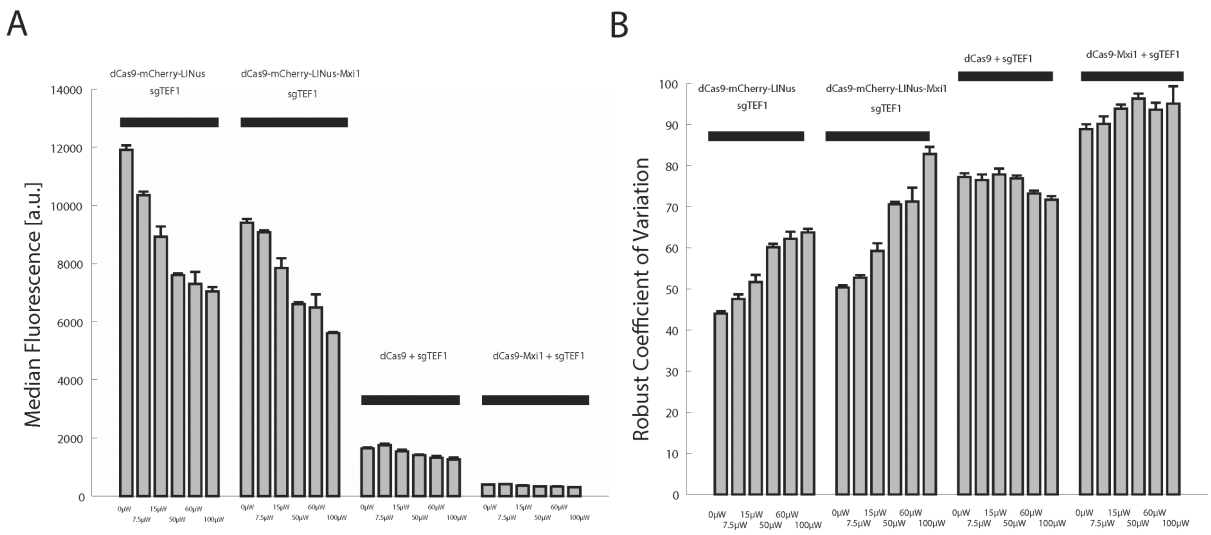

Supplemental Figure 7. The fraction of each population relative to the same percentile in the uninduced population is shown for **(a)** changing duty cycle at 15µW/ cm^2 and 135µW/ cm^2 or **(b)** increasing intensity for dCas9-mCherry-LINuS and dCas9-mCherry-LINuS-Mxi1. Constructs dCas9 and dCas9-Mxi1 with guide sgTEF1 are shown as controls. Moving up the plots the relative percentage of cells in a given sample corresponding to the labelled percentile in the uninduced population are shown. So, for example, the fraction of low inducers defined as the 25^{th}-percentile in the uninduced sample, increases from 25% to over 50% as dCas9-mCherry-LINuS and dCas9-mCherry-LINuS-Mxi1 are exposed to increasing light intensities.

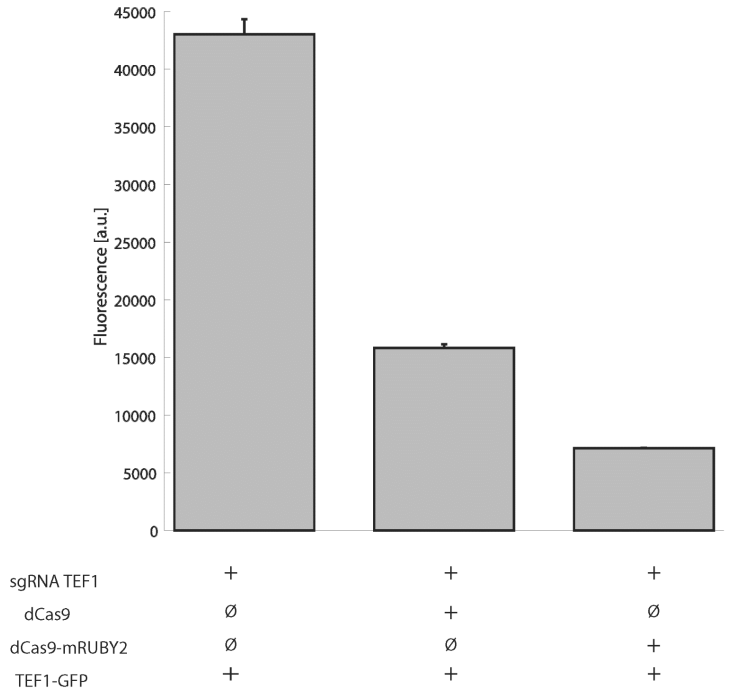

Supplemental Figure 8. Light intensity increases repression and expression variability in strains carrying the dCas9-mCherry-LINuS and dCas9-mCherry-LINuS-Mxi1 repressor. Light does not affect repression or variability in the dCas9 and dCas9-Mxi1 controls. **(a)** Strains carrying dCas9-mCherry-LINuS, dCas9-mCherry-LINuS-Mxi1, dCas9, or dCas9-Mxi1 and the sgTEF1 guide RNA were exposed to increasing light intensity. Light intensity increases repression in both the dCas9-mCherry-LINuS repressor and the dCas9-mCherry-LINuS-Mxi repressor, consistent with previous results. Light does not affect the dCas9 and dCas-Mxi1 controls. Error bars represent 95% confidence intervals on the average of the median fluorescence from n=3 biological replicates. **(b)** The coefficient of variation also increases with increasing light intensity for dCas9-mCherry-LINuS and dCas9-mCherry-LINuS-Mxi1. Error bars represent 95% confidence intervals on the average coefficient of variation for n=3 biological replicates. Light was measured in $\mu W/cm^2$.

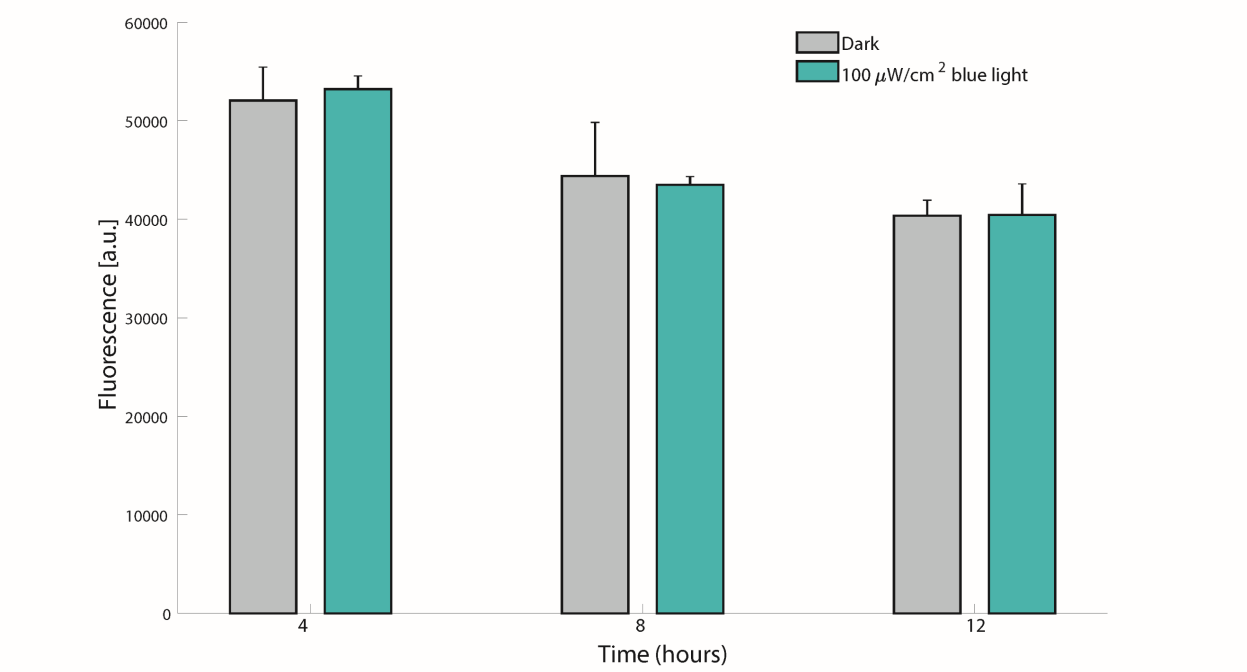

Supplemental Figure 9. C-terminal tagging of dCas9 does not inhibit its repressive ability, but rather seems to enhance it. Yeast strains carrying constitutively nuclear dCas9-NLS and dCas9-NLS-mRUBY2 demonstrate that dCas9-NLS-mRUBY2 confers greater repression of TEF1-GFP, perhaps due to increased steric hinderance. Error bars represent 95% confidence intervals for the median expression level of n=3 biological replicates.

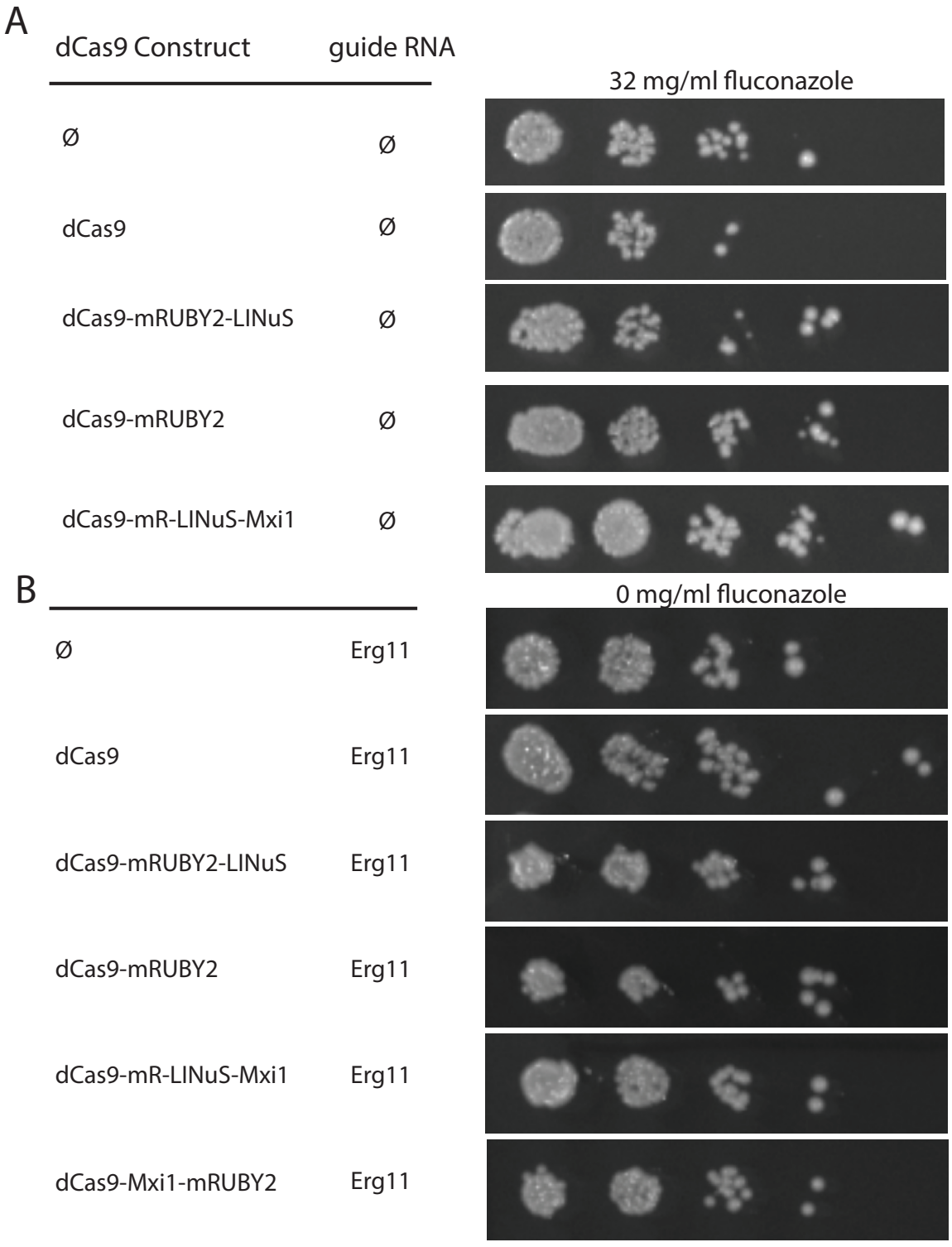

Supplemental Figure 10. We confirmed that the repressors themselves do not confer a growth defect on fluconazole, nor do they confer a growth defect without fluconazole. (**a**) Strains containing the same repressor constructs as in Figure 11 without the presence of the *ERG11* guide RNA do not cause a growth defect on 32 mg/ml fluconazole. (**b**) The repressors and the *ERG11*

gRNA do not cause a growth defect when grown on normal yeast media without the presence of fluconazole.

Strains, plasmids and other materials

Table S5: Yeast Strains

Strain	Alias	Genotype	Source
yMM84	BY4742	MAT alpha his3Δ1 leu2Δ0 lys2Δ0 MET15 ura3Δ0	Brachmann, et al 1998 [3]
yMM920	Nhp6a-iRFP	MAT alpha his3Δ1 leu2Δ0 lys2Δ0 MET15 ura3Δ0 Nhp6a-iRFP::caURA3	*McClean Lab*
yMM1032	FY auxotroph	FY Matα ura3Δ0 his3Δ200 leu2Δ0 lys2-1280 trp1Δ63 HAP1+	*McClean Lab*
yMM1384	TEF1-mCherry	FY Matα ura3Δ0 his3Δ200 leu2Δ0 lys2-1280 trp1Δ63 HAP1+ TEF1-mCherry-hphMX	*This study*
yMM1385	TEF1-GFP	FY Matα ura3Δ0 his3Δ200 leu2Δ0 lys2-1280 trp1Δ63 HAP1+ TEF1-GFP-KanMX	*This study*
yMM1442	Nhp6a-iRFP	MAT alpha his3Δ1 leu2Δ0 lys2Δ0 MET15 ura3Δ0 Nhp6a-iRFP	*McClean Lab*
yMM1502	Nhp6a-iRFPdCas9-mRuby	MAT alpha his3Δ1 leu2Δ0 lys2Δ0 MET15 ura3Δ0::pCCW12-dCas9-mRuby-tENO1-scURA3 Nhp6a-iRFP	*This study*
yMM1503	Nhp6a-iRFP dCas9-mRuby-LINuS	MAT alpha his3Δ1 leu2Δ0 lys2Δ0 MET15 ura3Δ0::pCCW12-dCas9-mRuby-LINuS-tENO1- scURA3 Nhp6a-iRFP	*This study*
yMM1504	TEF1-GFP dCas9-LINuS TEF1 sgRNA	FY Matα ura3Δ0::pCCW12-dCas9-LINuS-tENO1-Scar1-tRNA Phe promoter- tRNA Phe-HDV ribozyme- TEF1 sequence- gRNA scaffold-tSNR52- Scar2- Spacer- scURA3 his3Δ200 leu2Δ0 lys2-1280 trp1Δ63 HAP1+ TEF1-GFP-KanMX	*This study*
yMM1505	TEF1-GFP dCas9-mRuby TEF1 sgRNA	FY Matα ura3Δ0::pCCW12-dCas9-mRuby-tENO1-Scar1-tRNA Phe promoter- tRNA Phe-HDV ribozyme- TEF1 sequence- gRNA scaffold-tSNR52- Scar2- Spacer- scURA3 his3Δ200 leu2Δ0 lys2-1280 trp1Δ63 HAP1+ TEF1-GFP-KanMX	*This study*
yMM1506	TEF1-GFP dCas9-mRuby-LINuS TEF1 sgRNA	FY Matα ura3Δ0::pCCW12-dCas9-mRuby-LINuS-tENO1-Scar1-tRNA Phe promoter- tRNA Phe- HDV ribozyme- TEF1 sequence- gRNA scaffold- tSNR52- Scar2- Spacer- scURA3 his3Δ200 leu2Δ0 lys2-1280 trp1Δ63 HAP1+ TEF1-GFP-KanMX	*This study*
yMM1507	TEF1-GFP dCas9-mRuby-LINuS-Mxi1	FY Matα ura3Δ0::pCCW12- dCas9-mRuby-LINuS-Mxi1-tENO1-Scar1-tRNA Phe promoter-tRNA Phe- HDV ribozyme- TEF1 sequence-gRNA scaffold- tSNR52- Scar2- Spacer-	*This study*

	TEF1 sgRNA	scURA3 his3Δ200 leu2Δ0 lys2-1280 trp1Δ63 HAP1+ TEF1-GFP-KanMX	
yMM1508	TEF1-GFP dCas9-Mxi1-mRuby TEF1 sgRNA	FY Matα ura3Δ0::pCCW12- dCas9- Mxi1- mRuby- tENO1- Scar1- tRNA Phe promoter- tRNA Phe- HDV ribozyme- TEF1 sequence- gRNA scaffold- tSNR52- Scar2- Spacer- scURA3 his3Δ200 leu2Δ0 lys2-1280 trp1Δ63 HAP1+ TEF1-GFP-KanMX	*This study*
yMM1509	TEF1-GFP Spacer TEF1 sgRNA	FY Matα ura3Δ0::Spacer-Scar1-tRNA Phe promoter- tRNA Phe- HDV ribozyme- TEF1 sequence- gRNA scaffold- tSNR52- Scar2- Spacer- scURA3 his3Δ200 leu2Δ0 lys2-1280 trp1Δ63 HAP1+ TEF1-GFP-KanMX	*This study*
yMM1510	TEF1-GFP dCas9 TEF1 sgRNA	FY Matα ura3Δ0::pCCW12-dCas9-tENO1-Scar1-tRNA Phe promoter- tRNA Phe- HDV ribozyme- TEF1 sequence- gRNA scaffold- tSNR52- Scar2- Spacer- scURA3 his3Δ200 leu2Δ0 lys2-1280 trp1Δ63 HAP1+ TEF1-GFP-KanMX	*This study*
yMM1511	TEF1-GFP dCas9-LINuS	FY Matα ura3Δ0::pCCW12-dCas9-LINuS-tENO1-Scar1-spacer- Scar2- Spacer- scURA3 his3Δ200 leu2Δ0 lys2-1280 trp1Δ63 HAP1+ TEF1-GFP-KanMX	*This study*
yMM1512	TEF1-GFP dCas9-mRuby	FY Matα ura3Δ0::pCCW12-dCas9-mRuby-tENO1-Scar1-spacer Scar2- Spacer- scURA3 his3Δ200 leu2Δ0 lys2-1280 trp1Δ63 HAP1+ TEF1-GFP-KanMX	*This study*
yMM1513	TEF1-GFP dCas9-mRuby-LINuS	FY Matα ura3Δ0::pCCW12-dCas9-mRuby-LINuS-tENO1-Scar1-spacer- Scar2- Spacer- scURA3 his3Δ200 leu2Δ0 lys2-1280 trp1Δ63 HAP1+ TEF1-GFP-KanMX	*This study*
yMM1514	TEF1-GFP dCas9-mRuby-LINuS-Mxi1	FY Matα ura3Δ0::pCCW12- dCas9-mRuby-LINuS-Mxi1-tENO1-Scar1-spacer- Scar2- Spacer- scURA3 his3Δ200 leu2Δ0 lys2-1280 trp1Δ63 HAP1+ TEF1-GFP-KanMX	*This study*
yMM1515	TEF1-GFP dCas9-Mxi1-mRuby	FY Matα ura3Δ0::pCCW12- dCas9- Mxi1- mRuby- tENO1- Scar1- spacer- Scar2- Spacer- scURA3 his3Δ200 leu2Δ0 lys2-1280 trp1Δ63 HAP1+ TEF1-GFP-KanMX	*This study*
yMM1516	TEF1-GFP Spacer	FY Matα ura3Δ0::Spacer-Scar1-spacer Scar2- Spacer- scURA3 his3Δ200 leu2Δ0 lys2-1280 trp1Δ63 HAP1+ TEF1-GFP-KanMX	*This study*
yMM1517	TEF1-GFP dCas9	FY Matα ura3Δ0::pCCW12-dCas9-tENO1-Scar1-spacer- Scar2- Spacer- scURA3 his3Δ200	*This study*

		leu2Δ0 lys2-1280 trp1Δ63 HAP1+ TEF1-GFP-KanMX	
yMM1518	Nhp6a-iRFP dCas9-LINuS sgERG11	MAT alpha his3Δ1 leu2Δ0 lys2Δ0 MET15 ura3Δ0::pCCW12-dCas9-LINuS-tENO1-Scar1-tRNA Phe promoter- tRNA Phe- HDV ribozyme-ERG11 sequence- gRNA scaffold- tSNR52-Scar2- Spacer- scURA3 Nhp6a-iRFP	*This study*
yMM1519	Nhp6a-iRFP dCas9-mRuby sgERG11	MAT alpha his3Δ1 leu2Δ0 lys2Δ0 MET15 ura3Δ0::pCCW12-dCas9-mRuby-tENO1--Scar1-tRNA Phe promoter- tRNA Phe- HDV ribozyme- ERG11 sequence- gRNA scaffold-tSNR52- Scar2- Spacer- scURA3 Nhp6a-iRFP	*This study*
yMM1520	Nhp6a-iRFP dCas9-mRuby-LINuS sgERG11	MAT alpha his3Δ1 leu2Δ0 lys2Δ0 MET15 ura3Δ0::pCCW12-dCas9-mRuby-LINuS-tENO1-Scar1-tRNA Phe promoter- tRNA Phe-HDV ribozyme- ERG11 sequence- gRNA scaffold- tSNR52- Scar2- Spacer- scURA3 Nhp6a-iRFP	*This study*
yMM1521	Nhp6a-iRFP dCas9-mRuby-LINuS-Mxi1 sgERG11	MAT alpha his3Δ1 leu2Δ0 lys2Δ0 MET15 ura3Δ0::pCCW12-dCas9-mRuby-LINuS-Mxi1-tENO1-Scar1-tRNA Phe promoter- tRNA Phe-HDV ribozyme- ERG11 sequence- gRNA scaffold- tSNR52- Scar2- Spacer- scURA3 Nhp6a-iRFP	*This study*
yMM1522	Nhp6a-iRFP dCas9-Mxi1-mRuby sgERG11	MAT alpha his3Δ1 leu2Δ0 lys2Δ0 MET15 ura3Δ0::pCCW12-dCas9-Mxi1-mRuby-tENO1-Scar1-tRNA Phe promoter- tRNA Phe- HDV ribozyme- ERG11 sequence- gRNA scaffold-tSNR52- Scar2- Spacer- scURA3 Nhp6a-iRFP	*This study*
yMM1523	Nhp6a-iRFP Spacer sgERG11	MAT alpha his3Δ1 leu2Δ0 lys2Δ0 MET15 ura3Δ0::Spacer-Scar1-tRNA Phe promoter-tRNA Phe- HDV ribozyme- ERG11 sequence-gRNA scaffold- tSNR52- Scar2- Spacer-scURA3 Nhp6a-iRFP	*This study*
yMM1524	Nhp6a-iRFP dCas9 sgERG11	MAT alpha his3Δ1 leu2Δ0 lys2Δ0 MET15 ura3Δ0::pCCW12-dCas9-tENO1-Scar1-tRNA Phe promoter- tRNA Phe- HDV ribozyme-ERG11 sequence- gRNA scaffold- tSNR52-Scar2- Spacer- scURA3 Nhp6a-iRFP	*This study*
yMM1525	Nhp6a-iRFP dCas9-LINuS sgERG25	MAT alpha his3Δ1 leu2Δ0 lys2Δ0 MET15 ura3Δ0::pCCW12-dCas9-LINuS-tENO1-Scar1-tRNA Phe promoter- tRNA Phe- HDV ribozyme-ERG25 sequence- gRNA scaffold- tSNR52-Scar2- Spacer- scURA3 Nhp6a-iRFP	*This study*
yMM1526	Nhp6a-iRFP	MAT alpha his3Δ1 leu2Δ0 lys2Δ0 MET15 ura3Δ0::pCCW12-dCas9-mRuby-tENO1-Scar1-	*This study*

	dCas9-mRuby sgERG25	tRNA Phe promoter- tRNA Phe- HDV ribozyme- ERG25 sequence- gRNA scaffold- tSNR52- Scar2- Spacer- scURA3 Nhp6a-iRFP	
yMM1527	Nhp6a-iRFP dCas9-mRuby-LINuS sgERG25	MAT alpha his3Δ1 leu2Δ0 lys2Δ0 MET15 ura3Δ0::pCCW12-dCas9-mRuby-LINuS-tENO1-Scar1-tRNA Phe promoter- tRNA Phe- HDV ribozyme- ERG25 sequence- gRNA scaffold- tSNR52- Scar2- Spacer- scURA3 Nhp6a-iRFP	*This study*
yMM1528	Nhp6a-iRFP dCas9-mRuby-LINuS-Mxi1 sgERG25	MAT alpha his3Δ1 leu2Δ0 lys2Δ0 MET15 ura3Δ0::pCCW12-dCas9-mRuby-LINuS-Mxi1-tENO1-Scar1-tRNA Phe promoter- tRNA Phe- HDV ribozyme- ERG25 sequence- gRNA scaffold- tSNR52- Scar2- Spacer- scURA3 Nhp6a-iRFP	*This study*
yMM1529	Nhp6a-iRFP dCas9-Mxi1-mRuby sgERG25	MAT alpha his3Δ1 leu2Δ0 lys2Δ0 MET15 ura3Δ0::pCCW12-dCas9-Mxi-mRuby-tENO1-Scar1-ptRNAPhe- tRNAPhe- HDV ribozyme- ERG25 sequence- gRNA scaffold- tSNR52- Scar2- Spacer- scURA3 Nhp6a-iRFP	*This study*
yMM1530	Nhp6a-iRFP Spacer sgERG25	MAT alpha his3Δ1 leu2Δ0 lys2Δ0 MET15 ura3Δ0::Spacer-Scar1-tRNA Phe promoter- tRNA Phe- HDV ribozyme- ERG25 sequence- gRNA scaffold- tSNR52- Scar2- Spacer- scURA3 Nhp6a-iRFP	*This study*
yMM1531	Nhp6a-iRFP dCas9 sgERG25	MAT alpha his3Δ1 leu2Δ0 lys2Δ0 MET15 ura3Δ0::pCCW12-dCas9-tENO1-Scar1-tRNA Phe promoter- tRNA Phe- HDV ribozyme- ERG25 sequence- gRNA scaffold- tSNR52- Scar2- Spacer- scURA3 Nhp6a-iRFP	*This study*
yMM1532	Nhp6a-iRFP dCas9-LINuS	MAT alpha his3Δ1 leu2Δ0 lys2Δ0 MET15 ura3Δ0::pCCW12-dCas9-LINuS-tENO1-Scar1-spacer- Scar2- Spacer- scURA3 Nhp6a-iRFP	*This study*
yMM1533	Nhp6a-iRFP dCas9-mRuby	MAT alpha his3Δ1 leu2Δ0 lys2Δ0 MET15 ura3Δ0::pCCW12-dCas9-mRuby-tENO1-Scar1-spacer- Scar2- Spacer- scURA3 Nhp6a-iRFP	*This study*
yMM1534	Nhp6a-iRFP dCas9-mRuby-LINuS	MAT alpha his3Δ1 leu2Δ0 lys2Δ0 MET15 ura3Δ0::pCCW12-dCas9-mRuby-LINuS-tENO1-Scar1-spacer- Scar2- Spacer- scURA3 Nhp6a-iRFP	*This study*
yMM1535	Nhp6a-iRFP dCas9-mRuby-LINuS-Mxi1	MAT alpha his3Δ1 leu2Δ0 lys2Δ0 MET15 ura3Δ0::pCCW12-dCas9-mRuby-LINuS-Mxi1-tENO1-Scar1-spacer- Scar2- Spacer- scURA3 Nhp6a-iRFP	*This study*

yMM1536	Nhp6a-iRFP dCas9-Mxi1-mRuby	MAT alpha his3Δ1 leu2Δ0 lys2Δ0 MET15 ura3Δ0::pCCW12-dCas9-Mxi-mRuby-tENO1-Scar1-spacer- Scar2- Spacer- scURA3 Nhp6a-iRFP	*This study*
yMM1537	Nhp6a-iRFP Spacer	MAT alpha his3Δ1 leu2Δ0 lys2Δ0 MET15 ura3Δ0::Spacer-Scar1-spacer Scar2- Spacer-scURA3 Nhp6a-iRFP	*This study*
yMM1538	Nhp6a-iRFP dCas9	MAT alpha his3Δ1 leu2Δ0 lys2Δ0 MET15 ura3Δ0::pCCW12-dCas9-tENO1-Scar1-spacer-Scar2- Spacer- scURA3 Nhp6a-iRFP	*This study*

Table S6: Plasmids

Plasmid	Description	Alias & Source
pMM0007	LEU2 CEN/ARS Amp^R	pRS415; Sikorski and Heiter, 1989 [21]
pMM0008	URA3 CEN/ARS Amp^R	pRS416; Sikorski and Heiter, 1989 [21]
pMM0018	GFP KanMX Amp^R	pKT127; Sheff and Thorn, 2004 [20]
pMM0145	mCherry HpHMX Amp^R	*McClean Lab*
pMM0386	pTDH3-dCas9 LEU2 CEN/ARS Amp^R	AddGene ID46920; Gilbert, *et al* 2013 [9]
pMM0387	pTDH3-dCas9-Mxi1 LEU2 CEN/ARS Amp^R	AddGene ID46921; Gilbert, *et al* 2013 [9]
pMM0388	pSNR52-sgTEF1	AddGene ID46922; Gilbert, *et al* 2013 [9]
pMM0396	pTEF1-ccdb-LINuS-pKITNES-mCherry URA3 CEN/ARS Amp^R	*This study*
pMM0397	pTDH3-Mxi-dCas9-mCherry-LINuS URA3 CEN/ARS Amp^R	*This study*
pMM0398	pTEF1-ccdb-LINuS-SNUPNNES-mCherry URA3 CEN/ARS Amp^R	*This study*
pMM0399	pTDH3-dCas9-Mxi-mCherry-LINuS URA3 CEN/ARS Amp^R	*This study*
pMM0469	pTDH3-dCas9-mCherry-LINuS URA3 CEN/ARS Amp^R	*This study*
pMM0470	pTDH3-dCas9-pKit-mCherry-LINuS URA3 CEN/ARS Amp^R	*This study*
pMM0471	pTDH3-dCas9-Snupn-mCherry-LINuS URA3 CEN/ARS Amp^R	*This study*

pMM0472	pTDH3-dCas9 URA3 CEN/ARS Amp^R	*This study*
pMM0473	pSNR52-sgTEF1 LEU2 CEN/ARS Amp^R	*This study*
pMM0479	LEU2	*Lee, et al 2015* [14]
pMM0481	KanR ColE1	*Lee, et al 2015*
pMM0488	pTDH3-dCas9-Mxi1 URA3 CEN/ARS Amp^R	*This study*
pMM0489	ConLS	*Lee, et al 2015*
pMM0491	ConR1	*Lee, et al 2015*
pMM0499	pTDH3-dCas9-mCherry-LINuS-Mxi URA3 CEN/ARS Amp^R	*This study*
pMM0524	CEN6/ARS4	*Lee, et al 2015*
pMM0525	KanR-RFP	*Lee, et al 2015*
pMM0526	URA3 3' Homology	*Lee, et al 2015*
pMM0527	URA3 5' Homology	*Lee, et al 2015*
pMM0532	ConL1	*Lee, et al 2015*
pMM0533	ConL2	*Lee, et al 2015*
pMM0537	ConR2	*Lee, et al 2015*
pMM0541	ConRE	*Lee, et al 2015*
pMM0542	tENO1 (Type 4)	*Lee, et al 2015*
pMM0547	Spacer	*Lee, et al 2015*
pMM0559	pCCW12	*Lee, et al 2015*
pMM0567	iRFP-caURA3	*Hansen, et al 2013* [11]
pMM0582	LINuS ColE1-CamR Part4a	*This study*
pMM0585	dCas9 ColE1-CamR Part 3a	*This study*
pMM0586	dCas9 ColE1-CamR Part 3	*This study*
pMM0587	dCas9 ColE1-CamR Part3b	*This study*
pMM0725	LINuS-Mxi1 ColE1-CamR Part4a	*This study*
pMM0726	Mxi1 ColE1-CamR Part 3a	*This study*
pMM0727	Mxi1 ColE1-CamR Part 3	*This study*
pMM0728	Mxi1 ColE1-CamR Part 3b	*This study*
pMM0729	Mxi1-dCas9 ColE1-CamR Part 3	*This study*
pMM0732	mRUBY2 (Type 3b part)	*Lee, et al 2015*
pMM0733	tENO1 (Type 4b)	*Lee, et al 2015*
pMM0734	URA3	*Lee, et al 2015*
pMM0735	mRUBY2 (4a part)	*Lee, et al 2015*
pMM0736	sgRNA Dropout-ColE1-CamR	*Lee, et al 2015*
pMM0744	AMP-ColE1-RFP	*Lee, et al 2015*
pMM0745	ConL1-Erg11 guide-ConR2-Leu2-CEN/ARS-KAN/ColE1	*This study*
pMM0746	ConL1-Erg25 guide-ConR2-Leu2-CEN/ARS-KAN/ColE1	*This study*
pMM0754	ConL1-TEF1 guide-ConR2-Leu2-CEN/ARS-KAN/ColE1	*This study*
pMM0755	sgERG11 ColE1-CamR Part234	*This study*
pMM0756	sgERG25 ColE1-CamR Part234	*This study*
pMM0764	sgTEF1 ColE1-CamR Part234	*This study*
pMM0765	dCas9 NLS StopColE1-CamR Part 3	*This study*
pMM0766	dCas9 NLS StopColE1-CamR Part 3b	*This study*
pMM0767	dCas9 NLS ColE1-CamR Part 3	*This study*

pMM0768	dCas9 NLS ColE1-CamR Part 3b	*This study*
pMM0769	dCas9 NLS ColE1-CamR Part 3a	*This study*
pMM0770	ConLS-pCCW12-dCas9-mRuby-tENO1-ConRE-Ura3-Ura3'-ColE1-KanR-Ura5'	*This study*
pMM0771	ConLS-pCCW12-dCas9-mRuby-LINuS-tENO1-ConRE-Ura3-Ura3'-ColE1-KanR-Ura5'	*This study*
pMM0776	ConLS-Spacer-ConR1-Leu2-CEN/ARS-ColE1-KanR	*This study*
pMM0777	ConL1-Spacer-ConR2-Leu2-CEN/ARS-ColE1-KanR	*This study*
pMM0778	ConL2-Spacer-ConRE-Leu2-CEN/ARS-ColE1-KanR	*This study*
pMM0779	ConLS-pCCW12-dCas9-LINuS-tENO1-ConR1-URA3-Ura3'-ColE1-KanR-Ura5'	*This study*
pMM0780	ConLS-pCCW12-dCas9-mRuby-tENO1-ConR1-URA3-Ura3'-ColE1-KanR-Ura5'	*This study*
pMM0781	ConLS-pCCW12-dCas9-mRuby-LINuS-tENO1-ConR1-URA3-Ura3'-ColE1-KanR-Ura5'	*This study*
pMM0782	ConLS-pCCW12-dCas9-mRuby-LINuS-Mxi1-tENO1-ConR1-URA3-Ura3'-ColE1-KanR-Ura5'	*This study*
pMM0783	ConLS-pCCW12-dCas9-Mxi1-mRuby-tENO1-ConR1-URA3-Ura3'-ColE1-KanR-Ura5'	*This study*
pMM0784	ConLS-pCCW12-dCas9-tENO1-ConR1-URA3-Ura3'-ColE1-KanR-Ura5'	*This study*
pMM0785	ConLS-pCCW12-dCas9-LINuS-tENO1-SCAR1-ptRNAPhe- tRNAPhe- HDV - sgERG11-SCAR2-Spacer-URA3-Ura3'-ColE1-AmpR-Ura5'	*This study*
pMM0786	ConLS-pCCW12-dCas9-mRuby-tENO1-SCAR1-ptRNAPhe- tRNAPhe- HDV - sgERG11-SCAR2-Spacer-URA3-Ura3'-ColE1-AmpR-Ura5'	*This study*
pMM0787	ConLS-pCCW12-dCas9-mRuby-LINuS-tENO1-SCAR1-ptRNAPhe- tRNAPhe- HDV - sgERG11 -SCAR2- Spacer-URA3- Ura3'- ColE1-AmpR-Ura5'	*This study*
pMM0788	ConLS-pCCW12-dCas9-mRuby-LINuS-Mxi1-tENO1-SCAR1-ptRNAPhe- tRNAPhe- HDV - sgERG11- SCAR2-Spacer- URA3-Ura3'-ColE1-AmpR-Ura5'	*This study*
pMM0789	ConLS-pCCW12-dCas9-Mxi1-mRuby-tENO1-SCAR1-ptRNAPhe- tRNAPhe- HDV - sgERG11- SCAR2- Spacer-URA3- Ura3'-ColE1-AmpR-Ura5'	*This study*
pMM0790	ConLS-Spacer-SCAR1-ptRNAPhe- tRNAPhe- HDV-sgERG11- SCAR2- Spacer- URA3- Ura3'- ColE1- AmpR-Ura5'	*This study*
pMM0791	ConLS-pCCW12-dCas9-tENO1-SCAR1-ptRNAPhe-tRNAPhe- HDV- sgERG11-SCAR2-Spacer-URA3-Ura3'-ColE1-AmpR-Ura5'	*This study*
pMM0792	ConLS-pCCW12-dCas9-LINuS-tENO1-SCAR1-ptRNAPhe- tRNAPhe- HDV - sgERG25-SCAR2-Spacer-URA3-Ura3'-ColE1-AmpR-Ura5'	*This study*

pMM0793	ConLS-pCCW12-dCas9-mRuby-tENO1-SCAR1-ptRNAPhe- tRNAPhe- HDV - sgERG25-SCAR2-Spacer-URA3-Ura3'-ColE1-AmpR-Ura5'	*This study*
pMM0794	ConLS-pCCW12-dCas9-mRuby-LINuS-tENO1-SCAR1-ptRNAPhe- tRNAPhe- HDV - sgERG25 -SCAR2- Spacer-URA3- Ura3'- ColE1-AmpR-Ura5'	*This study*
pMM0795	ConLS-pCCW12-dCas9-mRuby-LINuS-Mxi1-tENO1-SCAR1-ptRNAPhe- tRNAPhe- HDV - sgERG25- SCAR2-Spacer- URA3-Ura3'-ColE1-AmpR-Ura5'	*This study*
pMM0796	ConLS-pCCW12-dCas9-Mxi1-mRuby-tENO1-SCAR1-ptRNAPhe- tRNAPhe- HDV - sgERG25- SCAR2- Spacer-URA3- Ura3'-ColE1-AmpR-Ura5'	*This study*
pMM0797	ConLS-Spacer-SCAR1-ptRNAPhe- tRNAPhe- HDV-sgERG25- SCAR2- Spacer- URA3- Ura3'- ColE1- AmpR-Ura5'	*This study*
pMM0798	ConLS-pCCW12-dCas9-tENO1-SCAR1-ptRNAPhe-tRNAPhe- HDV- sgERG25-SCAR2-Spacer-URA3-Ura3'-ColE1-AmpR-Ura5'	*This study*
pMM0799	ConLS-pCCW12-dCas9-LINuS-tENO1-SCAR1-ptRNAPhe- tRNAPhe- HDV - sgTEF1-SCAR2-Spacer-URA3-Ura3'-ColE1-AmpR-Ura5'	*This study*
pMM0800	ConLS-pCCW12-dCas9-mRuby-tENO1-SCAR1-ptRNAPhe- tRNAPhe- HDV - sgTEF1-SCAR2-Spacer-URA3-Ura3'-ColE1-AmpR-Ura5'	*This study*
pMM0801	ConLS-pCCW12-dCas9-mRuby-LINuS-tENO1-SCAR1-ptRNAPhe- tRNAPhe- HDV - sgTEF1 -SCAR2- Spacer-URA3- Ura3'- ColE1-AmpR-Ura5'	*This study*
pMM0802	ConLS-pCCW12-dCas9-mRuby-LINuS-Mxi1-tENO1-SCAR1-ptRNAPhe- tRNAPhe- HDV - sgTEF1- SCAR2-Spacer- URA3-Ura3'-ColE1-AmpR-Ura5'	*This study*
pMM0803	ConLS-pCCW12-dCas9-Mxi1-mRuby-tENO1-SCAR1-ptRNAPhe- tRNAPhe- HDV - sgTEF1- SCAR2- Spacer-URA3- Ura3'-ColE1-AmpR-Ura5'	*This study*
pMM0804	ConLS-Spacer-SCAR1-ptRNAPhe- tRNAPhe- HDV-sgTEF1- SCAR2- Spacer- URA3- Ura3'- ColE1- AmpR-Ura5'	*This study*
pMM0805	ConLS-pCCW12-dCas9-tENO1-SCAR1-ptRNAPhe-tRNAPhe- HDV- sgTEF1-SCAR2-Spacer-URA3-Ura3'-ColE1-AmpR-Ura5'	*This study*
pMM0806	ConLS-pCCW12-dCas9-LINuS-tENO1-SCAR1-Spacer-SCAR2-Spacer-URA3-Ura3'-ColE1-AmpR-Ura5'	*This study*
pMM0807	ConLS-pCCW12-dCas9-mRuby-tENO1-SCAR1-Spacer-SCAR2-Spacer-URA3-Ura3'-ColE1-AmpR-Ura5'	*This study*
pMM0808	ConLS-pCCW12-dCas9-mRuby-LINuS-tENO1-SCAR1-Spacer-SCAR2- Spacer- URA3- Ura3'- ColE1- AmpR-Ura5'	*This study*

pMM0809	ConLS-pCCW12-dCas9-mRuby-LINuS-Mxi1-tENO1-SCAR1-Spacer- SCAR2- Spacer- URA3-Ura3'-ColE1-AmpR-Ura5'	*This study*
pMM0810	ConLS-pCCW12-dCas9-Mxi1-mRuby-tENO1-SCAR1-Spacer- SCAR2- Spacer- URA3- Ura3'- ColE1- AmpR-Ura5'	*This study*
pMM0811	ConLS-Spacer-SCAR1-Spacer- SCAR2- Spacer- URA3-Ura3'- ColE1- AmpR- Ura5'	*This study*
pMM0812	ConLS-pCCW12-dCas9-tENO1-SCAR1-Spacer-SCAR2-Spacer-URA3-Ura3'-ColE1-AmpR-Ura5'	*This study*
pMM0813	ConLS'-sfGFP-ConRE'-URA3-URA 3'homology-AmpR-ColE1-URA 5' homology	*This study*
pMM0814	pTDH3-dCas9 LEU2 CEN/ARS Amp^R (Domesticated by BsaI site removal)	*This study*

Table S7: Oligonucleotides

Oligo	Function	Sequence	Source
oMM689	Tag TEF1	CGCTAAGGTTACCAAGGCTGCTCAAAAG GCTGCTAAGAAAGGTCGACGGATCCCCG GG	*This study*
oMM690	Tag TEF1	CGCTAAGGTTACCAAGGCTGCTCAAAAG GCTGCTAAGAAAGGTGACGGTGCTGGTT TA	*This study*
oMM691	Tag TEF1	ATATAAAAGATATGCAACTAGAAAAGTC TTATCAATCTCC TCGATGAATTCGAGCTCG	*This study*
oMM0711	AMP for d cas9-pKit/Snupn-mcherry-LINuS	ACTTCCACCTGAACCTCCAGATCCACCGC TAGCACTGGCagctccctcatcccctccga	*This study*
oMM0857	AMP for dcas9-(pKit/Snupn/Mxi1)-(mcherry)-LINuS	gcgcaattaaccctcactaaagggaacaaaagctggagct TCATTATCAATACTGCCATT	*This study*
oMM0858	AMP for dCas9-LINuS	TCTTCTCAATACGTTCAAGTGTAGTAGCC AAGGATCCTGCagctccctcatcccctccga	*This study*
oMM0859	AMP for dCas9-mCherry-LINuS	tgatgatggccatgttatcctcctcgcccttgctcaccatagctccctc atcccctccga	*This study*
oMM0860	AMP for gRNA Tef1	gcgccattcgccattcaggc	*This study*

oMM0861	AMP for gRNA Tef1	tttacactttatgcttccgg	*This study*
oMM1005	AMP for Mxi1-dCas9-mCherry-LINuS	GATCTgatatGGATCGAATTAGATCTCGCCACCAGCGGCGGCAGCATGGAACG	*This study*
oMM1006	AMP for Mxi1-dCas9-mCherry-LINuS	TAGTCCCGATGGCCAGTCCGATAGAATACTTCTTGTCCATGCCGCCAAGCTTGGAGCCTCTGGGAGAGGGCATGCT	*This study*
oMM1008	AMP for dCas9-Mxi1-mCherry-LINuS	tgatgatggccatgttatcctcctcgcccttgctcaccatgctGCCTCTGGGAGAGGGCATGCT	*This study*
oMM1009	AMP for dCas9-mCherry-LINuS-Mxi1	aactgcagaagagattgccaaaaagaagagaaaggtcGGCGGCAGCGGCGGCGGCAGCGGCAGCGGCGGCAGCATGGAACG	*This study*
oMM1010	AMP for dCas9-mCherry-LINuS-Mxi1	gtgacataactaattacatgactcgagctgcagcggccgcGCCTCTGGGAGAGGGCATGCT	*This study*
oMM1017	AMP for dCas9-Mxi1-mCherry-LINuS	gctactagatgaactactggacgtagagctactagatgaactagctccctcatcccctccga	*This study*
oMM1018	Amp for dCas9-Mxi1-mCherry-LINuS	AgttcatctagtagctctacgtccagtagttcatctagtagcAGCGGCGGCAGCATGGAACG	*This study*
oMM1044	Homology for Mxi1-dCas9-mCherry-LINuS	AATTCGATCCatatcAGATCTTTTGTTTGTTTATGTGTGTTTATTCGAAACTAAGTTCTT	*This study*
oMM1079	Amp for dCas9/NLS/Stop Part 3/3a	GCATCGTCTCATCGGTCTCATATGGACAAGAAGTATTCTAT	*This study*
oMM1080	Amp for dCas9 Part 3/3b	ATGCCGTCTCAGGTCTCAGGATCCagctccctcatcccctccga	*This study*
oMM1081	Amp for dCas9 Part 3a	ATGCCGTCTCAGGTCTCAAGAACCagctccctcatcccctccga	*This study*
oMM1082	Amp for dCas9/NLS/Stop Part 3b	GCATCGTCTCATCGGTCTCATTCTGACAAGAAGTATTCTATCGG	*This study*
oMM1083	Amp for LINuS Part 4a	GCATCGTCTCATCGGTCTCAATCCttggctactacacttgaacg	*This study*

oMM1084	Amp for LINuS and LINuS-Mxi1 Part 4a	ATGCCGTCTCAGGTCTCAGCCActcgagttagaccctttctcttctttt	*This study*
oMM1089	Amp for Mxi1 Part 3/3a	GCATCGTCTCATCGGTCTCATATGGAACGTGTGAGAATGAT	*This study*
oMM1090	Amp for Mxi1 Part 3b	GCATCGTCTCATCGGTCTCATTCTGAACGTGTGAGAATGAT	*This study*
oMM1093	Amp for Mxi1 Part 3/3b	ATGCCGTCTCAGGTCTCAGGATCCTCTGGGAGAGGGCATGCTAG	*This study*
oMM1094	Amp for Mxi1 Part 3a	ATGCCGTCTCAGGTCTCAAGAACCTCTGGGAGAGGGCATGCTAG	*This study*
oMM1122	Amp for removing BsaI site	TGATTCAGGGgaaACCGCTGAAG	*This study*
oMM1123	Amp for removing BsaI site	AAGAGGAGAGCTCCGATCAG	*This study*
oMM1153	Amp for LINuS-Mxi1	ATGCCGTCTCAGGTCTCAGCCAcctctgggagagggcatgctag	*This study*
oMM1202	Amp iRFP w/NHP6A homology	AATTAAATCACACAGACAAAAACGCGGGGAGGAAGTATCCcagtatagcgaccagcattc	*This study*
oMM1205	Amp iRFP w/NHP6A homology	GAATCCGAAAAGGAGTTATATAACGCCACTTTGGCTggtgacggtgctggtttaattaac	*This study*
oMM1221	Amp for LINuS-Mxi1	agttaTCTGGGAGAGGGCATGCT	*This study*
oMM1222	Amp for LINuS-Mxi1	cgagTGGCTGAGACCAGACCAATAAAAAAC	*This study*
oMM1650	Amp for dCas9 NLS Stop Part3/3b	ATGCCGTCTCAGGTCTCAGGATCCCTAGGATCCGGAACTACCTA	*This study*
oMM1651	Amp for dCas9 NLS Part3/3b	ATGCCGTCTCAGGTCTCAGGATCCGGATCCGGAACTACCTA	*This study*
oMM1652	Amp for dCas9 NLS Part 3a	ATGCCGTCTCAGGTCTCAAGAACCGGATCCGGAACTACCTA	*This study*
oMM1722	Anneal for sgERG11	gactttTATATAATGAATACACATGG	*This study*
oMM1723	Anneal for sgERG11	aaacCCATGTGTATTCATTATATAaa	*This study*
oMM1724	Anneal for sgERG25	gactttATATAGAAGTATGCATACAC	*This study*
oMM1725	Anneal for sgERG25	aaacGTGTATGCATACTTCTATATaa	*This study*

oMM1740	Anneal for sgTEF1	gactttTTGATATTTAAGTTAATAAA	*This study*
oMM1741	Anneal for sgTEF1	aaacTTTATTAACTTAAATATCAAaa	*This study*

Supplemental References

1. Amberg, D., Burke, D., & Strathern, J. (2005). *Methods in yeast genetics : a Cold Spring Harbor Laboratory course manual.* Cold Spring Harbor, N.Y. : Cold Spring Harbor Laboratory Press.
2. Andersen, E. (2011, 7 8). tPCR-Directed In Vivo Plasmid Construction Using Homologous Recombination in Baker's Yeast. (O. V., & R. M., Eds.) *Molecular Methods for Evolutionary Genetics. Methods in Molecular Biology , 772*, pp. 409-421.
3. Brachmann, C., Davies, A., Cost, G., Caputo, E., Li, J., Heiter, P., & Boeke, J. (1998). Designer deletion strains derived from Saccharomyces cerevisiae S288C: a useful set of strains and plasmids for PCR-mediated gene disruption and other applications. *Yeast, 14*, 115-132.
4. Carter, Z., & Delneri, D. (2010). New generation of loxP-mutated deletion cassettes for the genetic manipulation of yeast natural isolates. *Yeast, 27*, 765-775.
5. Dexter, J., Xu, P., Gunawardena, J., & McClean, M. (2015). Robust network structure of the Sln1-Ypd1-Ssk1 three-component phospho-relay prevents unintended activation of the HOG MAPK pathway in Saccharomyces cerevisiae. *BMC Systems Biology, 9*(1), 17.
6. Gerhardt, K. P., Olson, E. J., Castillo-Hair, S. M., Hartsough, L., Landry, B. P., Ekness, F., . . . Suh, J. (2016). An open-hardware platform for optogenetics and photobiology. *Scientific Reports, 6*, 35363.
7. Gerhardt, K., Olson, E., Castillo-Hair, S., Hartsough, L., Landry, B., Ekness, F., . . . Tabor, J. (2016). An open-hardware platform for optogenetics and photobiology. *Scientific Reports, 6*(35363).
8. Gietz, R., & Schiestl, R. (2007). High-efficiency yeast transformation using the LiAc/SS carrier DNA/PEG method. *Nature Protocols, 2*, 31-34.
9. Gilbert, L. A., Larson, M. H., Morsut, L., Liu, Z., Brar, G. A., Torres, S. E., . . . Weissman, J. S. (2013). CRISPR-mediated modular RNA-guided regulation of transcription in eukaryotes. *Cell, 154*(2), 442-451.
10. Gueldener, U., Heinisch, J., Koehler, G., Voss, D., & Hegemann, J. (2002). A second set of loxP marker cassettes for Cre-mediated multiple gene knockouts in budding yeast. *Nucleic acids research, 30*(6).
11. Hansen, A., & O'Shea, E. (2013). Promoter decoding of transcription factor dynamics involves a trade-off between noise and control of gene expression. *Molecular Systems Biology, 9*(704).
12. Harju, S., Fedosyuk, H., & Peterson, K. (2004). Rapid isolation of yeast genomic DNA: Bust n' Grab. *BMC Biotechnology, 4*(8).
13. *IRIS*. (n.d.). Retrieved from http://taborlab.github.io/Iris/.
14. Lee, M. E., Deloache, W., Cervantes, D., & Dueber, J. (2015). A highly characterized yeast toolkit for modular, multipart assembly. *ACS Synthetic Biology, 4*(9), 975-986.
15. Ma, H., Kunes, S., Schatz, P., & Botstein, D. (1987). Plasmid construction by homologous recombination in yeast. *Gene, 58*, 201–216.
16. McIsaac, R., Oakes, B., Wang, X., Dummit, K., Botstein, D., & Noyes, M. (2012). Synthetic gene expression perturbation systems with rapid, tunable single-gene specificity in yeast. *Nucleic Acids Research, 23*, 2993-3008.
17. McIsaac, R., Silverman, S., McClean, M., Gibney, P., Macinskas, J., Hickman, M., . . . Botstein, a. D. (2011). Fast-acting and nearly gratuitous induction of gene expression and protein depletion in Saccharomyces cerevisiae. *Molecular Biology of the Cell, 22*, 4447-4459.
18. Oldenburg, K., Vo, K., Michaelis, S., & Paddon, C. (1997). Recombination-mediated PCR-directed plasmid construction in vivo in yeast. *Nucleic Acids Research, 25*, 451–452.
19. Sambrook, J., & Russell, D. (2006). The Inoue Method for Preparation and Transformation of Competent E. Coli: "Ultra-competent" cells. *CSH Protocols*(1).
20. Sheff, M., & Thorn, K. (2004). Optimized cassettes for fluorescent protein tagging in Saccharomyces cerevisiae. *Yeast, 21*, 661-670.
21. Sikorski, R., & Heiter, P. (1989). A system of shuttle vectors and yeast host strains designed for efficient manipulation of {DNA} in Saccharomyces cerevisiae. *Genetics, 122*(1), 19-27.

Chapter 3: A yeast optogenetic toolkit (yOTK) for gene expression control in *Saccharomyces cerevisiae*

Contents of this chapter are published:

An-Adirekkun JM, Stewart CJ, Geller SH, Patel MT, Melendez J, Oakes BL, Noyes MB, McClean MN. A yeast optogenetic toolkit (yOTK) for gene expression control in *Saccharomyces cerevisiae*. Biotechnol Bioeng. 2020 Mar;117(3):886-893. doi: 10.1002/bit.27234. Epub 2019 Dec 18. PMID: 31788779; PMCID: PMC7015765.

Jidapas (My) An-adirekkun, Cameron J. Stewart, Stephanie H. Geller, Michael T. Patel, Justin Melendez, Benjamin L. Oakes, and Marcus B. Noyes created plasmids. Jidapas (My) An-adirekkun, and Stephanie H. Geller completed flow cytometry and growth assays. Stephanie H. Geller and Megan N. McClean analyzed the data. Jidapas (My) An-adirekkun, Stephanie H. Geller, and Megan McClean wrote the manuscript. All authors approved final version.

Abstract

Optogenetic tools for controlling gene expression are ideal for tuning synthetic biological networks due to the exquisite spatiotemporal control available with light. Here we develop an optogenetic system for gene expression control integrated with an existing yeast toolkit allowing for rapid, modular assembly of light-controlled circuits in the important chassis organism *Saccharomyces cerevisiae*. We reconstitute activity of a split synthetic zinc-finger transcription factor (TF) using light-induced dimerization mediated by the proteins CRY2 and CIB1. We optimize function of this split TF and demonstrate the utility of the toolkit workflow by assembling cassettes expressing the TF activation domain and DNA-binding domain at different levels. Utilizing this TF and a synthetic promoter we demonstrate that light-intensity and duty-cycle can be used to modulate gene expression over the range currently available from natural yeast promoters. This work allows for rapid generation and prototyping of optogenetic circuits to control gene expression in *S. cerevisiae*.

Introduction and Results

The budding yeast *S. cerevisiae* is an important chassis organism for synthetic biology and metabolic engineering [1]. These disciplines integrate biological parts (e.g. coding sequences, promoters) into biological circuits with novel cellular function. This process has become more routine in *S. cerevisiae* due to the creation of large libraries of well-characterized parts [2]. However, the inner workings of the cell continue to make the function and performance of engineered biological circuits unpredictable. Engineering efforts benefit greatly from the ability to tune the concentration of individual components to test and adjust circuit function. Additionally, tunability can allow circuits to be temporally and spatially adjusted to match dynamic constraints, such as the external environment or bioprocess phase [3].

Optogenetic approaches offer a potential solution for flexible tuning. Optogenetics take advantage of light-sensitive genetically encoded proteins to actuate processes inside of the cell in a light-dependent manner. Light is a powerful actuator as it is inexpensive, easily controlled in time and space, and *S. cerevisiae* contains no known native photoreceptors [4]. The ability to rapidly add and remove light from cell culture or spatially target specific cells makes it particularly advantageous for applications that require spatiotemporal precision such as dynamic stimulation or real-time feedback control of cellular processes [5]–[12]. To continue expanding the utility of optogenetics in *S. cerevisiae*, here we report the construction and optimization of a light-activated transcription factor and associated components for use with an existing toolkit of yeast parts [13]. Addition of these optogenetic components to the toolkit allows for rapid and modular assembly of light-controlled circuits to tune gene expression dynamically and over the range defined by native yeast constitutive promoters.

We took advantage of the naturally occurring Arabidopsis cryptochrome CRY2 and binding partner CIB1 to reconstitute the activity of a split transcription factor in a blue light-dependent manner. The feasibility of this approach was previously demonstrated by fusing CRY2 to the scGAL4 DNA-binding domain and CIB1 to the scGAL4 activation domain [14]. The GAL4 protein is a native *S. cerevisiae* transcription factor and using the GAL4 DNA-binding domain (DBD) to create synthetic transcription factors leads to crosstalk with native GAL4-inducible promoters [15]. To avoid this crosstalk orthogonal DNA-binding domains from natural sources, such as those from bacterial TFs, could be used to replace the GAL4DBD as has been successfully demonstrated using the LexA DNA-binding domain [16]. We chose to replace the GAL4DBD with a Cys_2-His_2 zinc finger (ZF) DNA-binding domain due to ZFs modularity and potential for engineered sequence specificity [17]. We used the three-finger DNA-binding domain from the Zif268 mouse transcription factor which specifies a 9-bp sequence that occurs infrequently (<20 instances) in the *S. cerevisiae* genome. This domain has been shown to be a powerful, orthogonal DNA-binding domain for generating chemically-inducible transcription factors in *S. cerevisiae* [15]. We fused the Zif268-DBD to the N-terminus of the CRY2 protein (ZDBD-CRY2) and the viral VP16 activation domain to CIB1 (VP16AD-CIB1) (Figure 12A). To create a promoter responsive to our artificial transcription factor, we removed the native GAL4 binding sites and integrated variable numbers and orientations of the Zif268 binding site (5'-GCG TGG GCG-3') into the scGAL1 promoter (Supplemental Figure 1, 2). Utilizing a promoter with three binding sites for the Zif268 DNA-binding domain (pZF(3BS)) upstream of yEVenus and plasmids containing ZDBD-CRY2 and GAL4AD-CIB1 constructs we showed that the ZDBD-CRY2 based system induced gene expression in response to blue light as well as the original GAL4DBD-CRY2 system (Figure 1B) [14]. Consistent with previous reports the GAL4DBD-CRY2PHR construct

containing only the CRY2 photolyase homology region (PHR) showed a stronger light-induced fold change as well as higher background gene expression. This background expression was greatly reduced in the ZDBD-CRY2PHR transcription factor. We verified that the native *S. cerevisiae* GAL machinery does not exhibit crosstalk with the pZF(3BS) promoter and that ZDBD-CRY2 did not activate expression from the scpGAL1 promoter (Supplemental Figure 3). We arrived at our final ZDBD-CRY2PHR construct and pZF(3BS) promoter by testing different design considerations (i.e. linkers, nuclear localization signals, binding site number) as detailed in the Supplemental Material (Supplemental Figures 2-5).

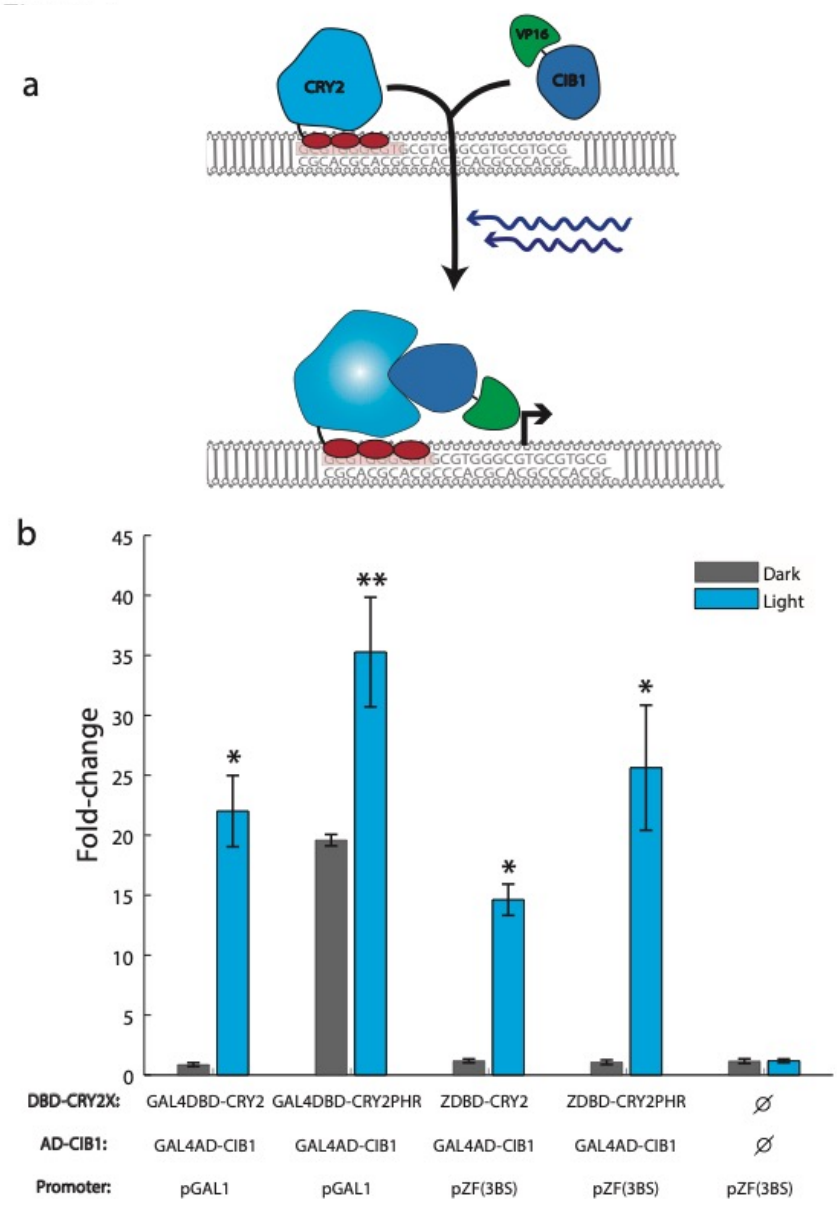

Figure 1. DBD-CRY2 AD-CIB1 optogenetic system

A. Schematic of the ZDBD-CRY2 and VP16AD-CIB1 optogenetic system. In response to blue light, CRY2 undergoes a conformational change that allows CIB1 to bind CRY2. This recruits the activation domain to a promoter containing Zif268 binding sites (GCG-TGG-GCG). B. Yeast cells were transformed with the following DBD-CRY2 or DBD-CRY2PHR, AD-CIB1, and reporter plasmids: GAL4DBD-CRY2/GAL4AD-CIB1/pGAL1-yEVenus, GAL4DBD-CRY2PHR/GAL4AD-CIB1/pGAL1-yEVenus, ZDBD-CRY2/GAL4AD-CIB1/pZF(3BS)-

yEVenus, or ZDBD-CRY2PHR/GAL4AD-CIB1/pZF(3BS)-yEVenus. The control sample contains pZF(3BS)-yEVenus and empty vector controls only. Cultures were grown for 12 hours in 15 μW/cm2 470nm blue light. No light controls were grown in identical conditions without illumination. Induction at T=12 hours is displayed as fold-change relative to the same sample at T=0 hours. Data is presented as the average ±SEM. Samples indicated with a * ($p<0.05$) or ** ($p<0.0.1$) were significantly induced at T=12 hours relative to T=0 hours (Welch's t-test). ANOVA followed by Tukey's-HSD indicated that the GAL4DBD split transcription factors do not induce significantly better that the ZDBD transcription factors ($F(3,8)=5.4$, $p=0.0252$, Groups: GAL4DBD-CRY2/GAL4AD-CIB1-ab, GAL4DBD-CRY2PHR/GAL4AD-CIB1-b, ZDBD-CRY2/GAL4AD-CIB1-a, and ZDBD-CRY2PHR/GAL4AD-CIB1/pZF(3BS)-ab).

In order to allow for rapid assembly of light controlled circuits, we domesticated our optogenetic components to interface with an existing yeast toolkit [13]. This toolkit contains highly characterized yeast components (i.e. promoters, terminators) categorized as "types" based on their function and location in the completed circuit (e.g. promoter types, coding sequence types) (Figure 2). Using a Golden Gate based MoClo (modular cloning) method parts can be rapidly assembled into single or multigene cassettes and integrated into the yeast genome. To domesticate our optogenetic components we removed the restriction enzyme sites (BsaI, BsmBI, NotI) used in the MoClo assembly scheme [13]. Our ZDBD-CRY2PHR and VP16AD-CIB1 components became coding sequence ("Type 3") parts and the pZF(3BS) promoter became a promoter ("Type 2") part. All parts created in this study that are compatible with the MoClo scheme are shown in Supplemental Figure 6. Using the MoClo scheme with our optogenetic parts and additional parts from the yeast toolkit allows for rapid assembly of multigene integration vectors containing all the necessary components for light-induced expression of a gene of interest.

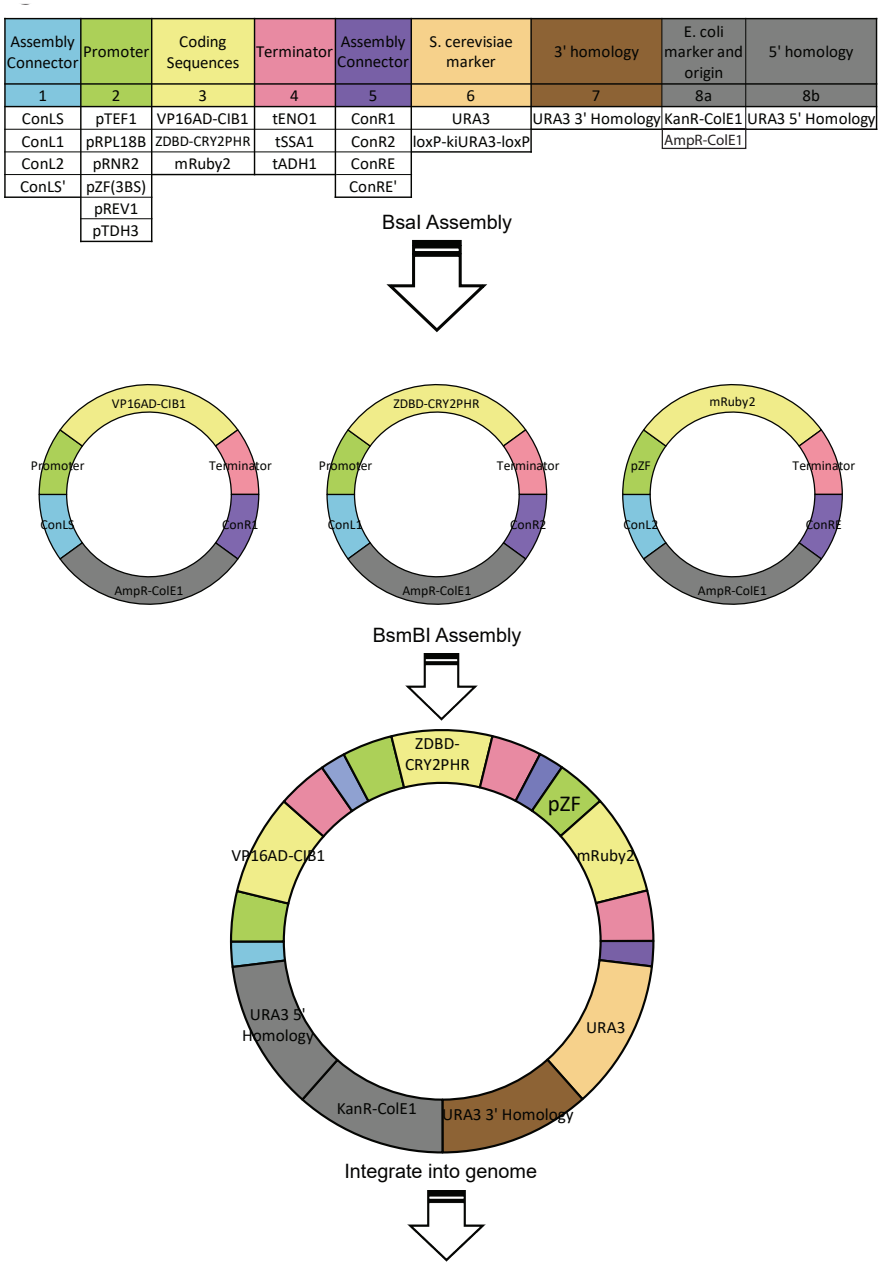

Figure 2. Circuit construction using the Yeast Toolkit scheme.

Part plasmids contain unique upstream and downstream BsaI-generated overhangs to assemble into the appropriate position in "cassette" plasmids. Cassette plasmids are fully functional transcriptional units that are further assembled into multigene plasmids using BsmBI assembly

and appropriate Assembly Connectors. This figure utilizes the color scheme and organization from Lee, *et al* (2015) to illustrate how the new optogenetic components integrate with an existing yeast toolkit [13].

We demonstrated the utility of the toolkit workflow (Figure 2) by using it to optimize our synthetic split TF. We reasoned that the concentration and ratio of the two TF components, the DNA-binding component (ZDBD-CRY2PHR) and the activation component (VP16AD-CIB1), might be important for circuit function. We generated nine different optogenetic constructs with the two components under low (L), medium (M), and high (H) strength yeast promoters. To test gene expression control, we took advantage of the red fluorescent protein mRuby2 already in the toolkit, which has an excitation spectrum further from the blue light used to excite CRY2 than yEVenus, and generated pZF(3BS)-mRuby2 reporters. We found that expression of VP16AD-CIB1 under a high strength promoter (pTDH3) and DBD-CRY2PHR under a medium strength promoter (pRPL18B) gave us maximal expression from pZF (3BS) (Figure 3A). However, this ZDBD-CRY2PHR$_{medium}$/VP16AD-CIB1$_{high}$ strain exhibited a growth defect. Indeed, all strains highly expressing the VP16AD-CIB1 construct exhibited a growth defect (Supplemental Figure 7). The ZDBD-CRY2PHR$_{medium}$/VP16AD-CIB1$_{medium}$ strain on the other hand, with both components under the control of pRPL18B, exhibited expression from pZF(3BS) equivalent to a medium strength yeast promoter without exhibiting growth defects (Figure 3B). Maximal expression was reached after approximately 6 hours (Supplemental Figure 8), which is comparable to commonly used yeast induction systems [18]. The dosage of the ZDBD-CRY2PHR and VP16AD-CIB1 components also affected the basal (dark) induction (Figure 3B). Our results tempt us to hypothesize that too little absolute DBD component (ZDBD-CRY2PHR) reduces function due to a lack of promoter occupancy, while too much ZDBD-CRY2PHR relative to the activation domain component (VP16AD-CIB1) reduces function by decreasing the probability that a ZDBD-

CRY2PHR bound at pZF(3BS) is also bound to VP16AD-CIB1. This leads to maximal fold induction along the diagonal as seen in Figure 3a. This was a crude dialing of protein concentration but suggests that one way to further optimize a split TF system would be by carefully titrating the total and relative dosage of each component, a knob not available in single-component and homogeneous two-component optogenetic systems [7], [14], [16], [19]–[21]. It is worth noting that the variability between biological replicates decreased when the ZDBD-PHR2/VP16AD-CIB1/pZF(3BS) components were chromosomally integrated using the toolkit (Figure 3b) rather than maintained on episomal plasmids (Figure 1b). This is consistent with known variability caused by plasmid copy number [13] and demonstrates that the ability to easily integrate optogenetic components into the chromosome is a further advantage of the toolkit format.

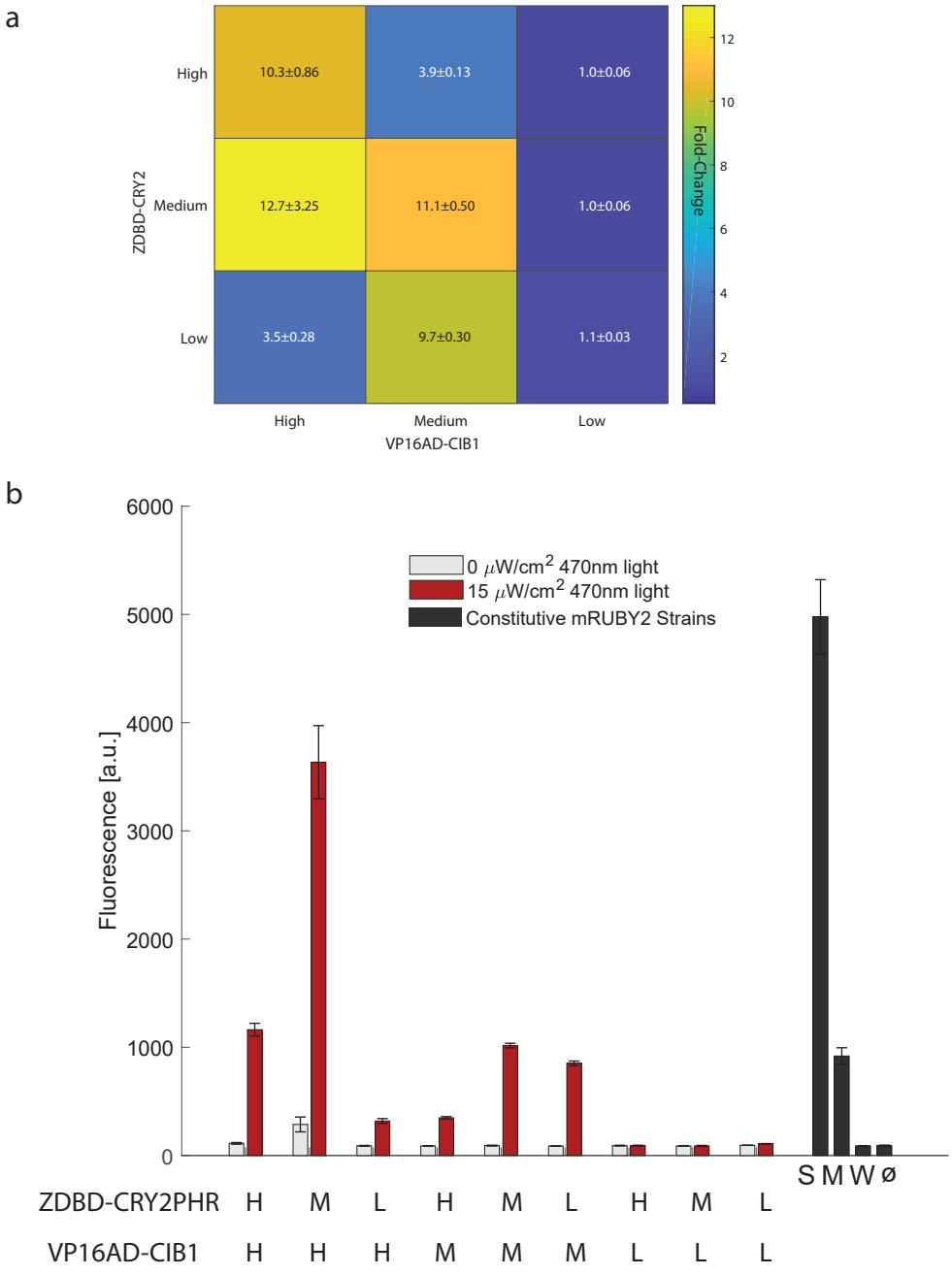

Figure 3. Optimization of the split transcription factor

A. Fold-induction in gene expression in response to 17 hours of 470nm 15μW/cm^2 blue-light from the pZF(3BS)-mRuby2 reporter was measured in nine strains expressing different ratios of the DNA-binding domain (ZDBD-CRY2PHR) and the activation domain (VP16AD-CIB1)

under High (pTEF1), Medium (pRPL18B), or Low (pRNR2) strength promoters to create ZDBD-CRY2$_{high/med/low}$/VP16AD-CIB1$_{high/med/low}$ strains. Data is presented as mean±SEM. A one-way ANOVA ($F(8,45)=30.04$, $p=1.35X10^{-15}$), followed by Tukey's-HSD shows that the fold-changes are significantly different with the following groups (ZDBD-CRY2$_{high/med/low}$/VP16AD-CIB1$_{high/med/low}$): M/H-a; H/H, M/M, M/L-b; H/L, M/H-c; L/H, L/M, L/L-d. B. Raw fluorescence data for strains shown in A.. Gene expression was compared to yeast strains expressing mRuby2 under constitutive promoters of different strengths (Strong-pTDH3, Medium-pRPL18B, Weak-pREV1). All constructs except those with the Low activation domain show very significant induction in the light ($p<0.0001$, Welch's t-test). ANOVA followed by Tukey's HSD ($F(12,65)=248$, $p=2.21\times10^{-49}$) shows that the following promoters or split TF combinations are significantly different: pTDH3 alone, M/H alone, the group containing H/H, M/M, L/M, pRPL18B, and the group containing L/H and H/M. All other lowly expressing promoters including the weak constitutive pREV1 promoter belong to the same group.

One of the advantages of light as an inducer is the ability to tune its intensity and duty cycle in cultures of cells. We examined our ability to tune output from the ZDBD-CRY2PHR$_{medium}$/VP16AD-CIB1$_{medium}$ strain as a function of light intensity. We found that we could tune output from the ZDBD-CRY2PHR$_{medium}$/VP16AD-CIB1$_{medium}$ system up to 15μW/cm^2 of light, at which point output from the system saturated (Figure 4A). We also measured output from the ZDBD-CRY2PHR$_{medium}$/VP16AD-CIB1$_{medium}$ strain as a function of duty cycle. We varied light at 15μW/cm^2 from a duty cycle of 5% (1min on/19 min off) to 100% (constant light). Gene expression output increased as a function of duty cycle. Utilizing either the ZDBD-CRY2PHR$_{medium}$/VP16AD-CIB1$_{medium}$ or ZDBD-CRY2PHR$_{medium}$/VP16AD-CIB1$_{high}$ strain we could achieve gene expression outputs equivalent to the weakest and strongest promoters in the Lee, *et al* yeast toolkit (Supplemental Figure 9). Thus, by putting the expression of a circuit component under the control of pZF (3BS) and using light chemostats or programmable

LED plates [22], [23] one could continuously and dynamically tune component concentration and monitor its effect on circuit function. To allow this optogenetic machinery to be easily integrated into a yeast strain of interest we created a yeast marker ("Type 6") part containing KlURA3 flanked by loxP sites to allow for marker recycling. We created a pre-assembled integration vector (Supplemental Figure 6) and used it to integrate ZDBD-CRY2PHR$_{medium}$/VP16AD-CIB1$_{medium}$ and pZF(3BS)-mRuby2. We verified that integration of ZDBD-CRY2PHR$_{medium}$/VP16AD-CIB1$_{medium}$ with the KlURA3 marker, followed by subsequent Cre-recombinase mediated excision of the marker, did not affect light-induced expression of mRuby2 (Supplemental Figure 10).

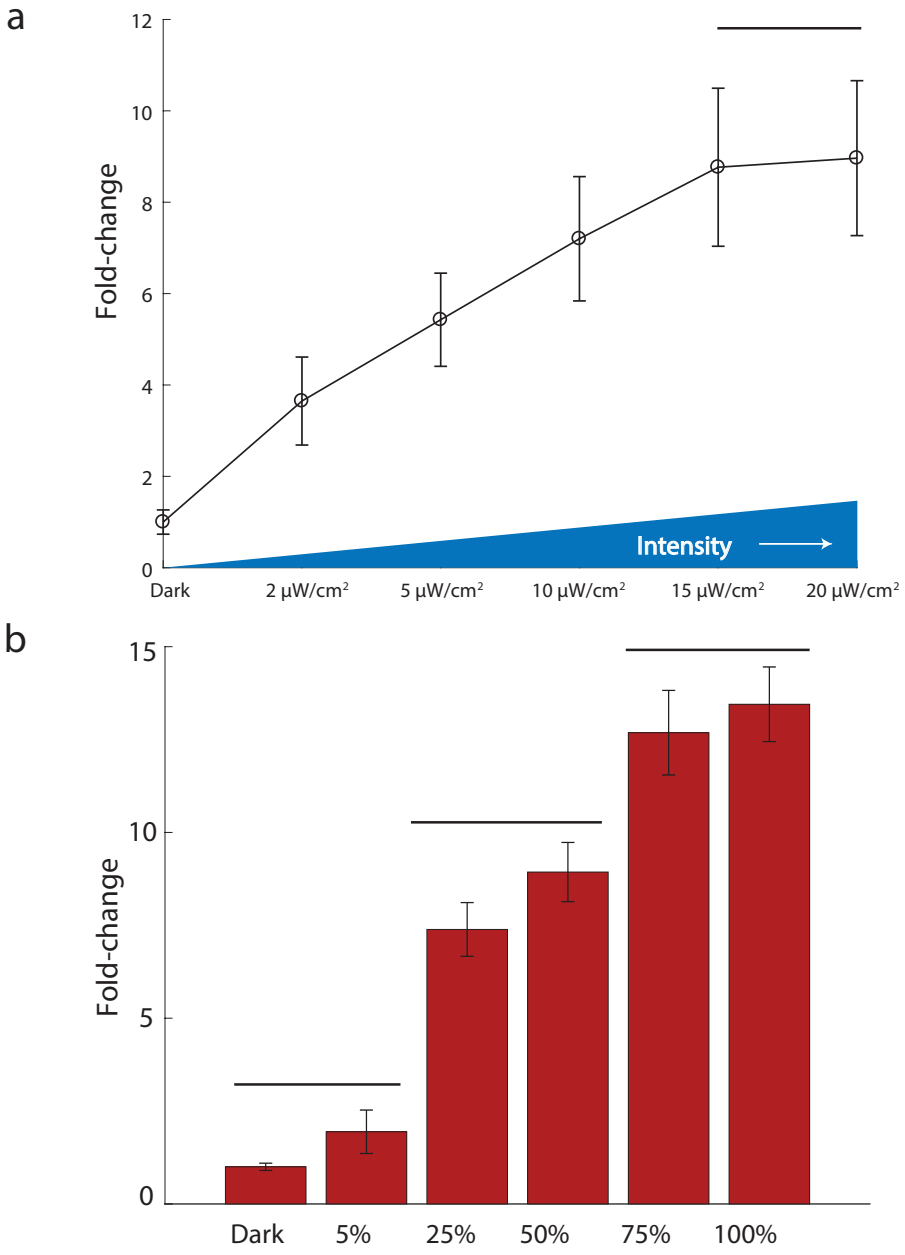

Figure 4. Tuning of gene expression

A. Gene expression in the ZDBD-CRY2PHR$_{medium}$/VP16AD-CIB1$_{medium}$ optogenetic strain is tunable as a function of blue-light intensity. Strains were induced for 17 hours at the indicated intensity of 470nm light. ANOVA followed by Tukey's-HSD shows that the expression at each light intensity is significantly different except for 15µW/cm^2 and 20µW/cm^2, which are in the same

group ($F(5,12)=209.93$, p-value=3.01×10^{-11}). B. Gene expression in the ZDBD-$CRY2PHR_{medium}$/VP16AD-$CIB1_{medium}$ optogenetic strain is tunable as a function of light duty cycle. Strains were induced with 20-minute periods with the indicated duty-cycle of 470nm blue light at 15μW/cm^2. Fluorescence was measured as fold-change relative to the dark control. Bars distinguish significantly different groups determined by one-way ANOVA followed by Tukey's HSD ($F(5,12)=325$, $p=2.2\times10^{-12}$).

Optogenetic approaches for controlling natural and synthetic biological networks are garnering attention as the toolkit expands and more powerful applications are demonstrated [8]–[10], [19], [22]. Here we report an orthogonal light-inducible transcriptional activator for gene expression control in *S. cerevisiae*. We have engineered this transcription factor to be compatible with an existing yeast toolkit which allows circuits for light-controlled gene expression to be assembled, integrated into the yeast genome, and tested in less than two weeks. We utilized this rapid prototyping to optimize the ratio and concentration of the two halves of our split transcription factor for maximal light-inducible gene expression with minimal growth defects. Both light intensity and duty cycle can be used to tune output from this gene expression system. We anticipate that this expansion of the yeast toolkit will be very useful to the community, as it will allow for rapid assembly of synthetic circuits with one or more components that can be dynamically tuned with light. This will allow for circuit optimization as well as real-time light-based control of circuit output.

Materials and Methods

Strains and Culture Methods

Yeast strains used in this study are shown in Supplemental Table 1. Yeast strains were grown in standard yeast media, as described in the Supporting Information. Yeast transformation was accomplished using standard lithium-acetate transformation [24]. Primers used for validating integrations are listed in Supplemental Table 2. *Escherichia coli* strain DH5α was used for all transformation and plasmid maintenance in this study. *E. coli* were grown on standard media as described in the Supporting Information with appropriate antibiotics to select for and maintain plasmids.

Blue light induction

Blue-light induction was accomplished by either (1) illuminating cultures grown in glass culture tubes on a roller drum or (2) in a Light Plate Apparatus (LPA).[23] Light intensity was measured and validated using a standard photodiode power sensor and power meter (Thorlabs #S120VC, Thorlabs #PM100D). The LPA was calibrated as described in Sweeney, *et al* [25] so that consistent light doses could be delivered between LPAs and between experiments.

Flow Cytometry

Gene expression in response to blue light was assayed using fluorescent reporters and flow cytometry. Flow cytometry was performed on either a BD Biosciences LRSII Flow Cytometer (488nm laser and 505LP dichroic filter) or an Attune NxT Flow Cytometer (ThermoFisher Scientific) with 561nm excitation laser and 620/15nm filter cube. For assaying mRuby2 fluorescence on the Attune, the voltages of the flow cytometer were calibrated using rainbow beads

so that the medians of FSS, SSC, and mRuby2 fluorescence of the rainbow beads were within 10% difference. The flow cytometry data was then analyzed using FlowJo software. All samples were prepared for flow cytometry by diluting yeast cell culture 1:3 into ice-cold PBS + 0.1% Tween-20. Samples were kept on ice or at 4°C until being analyzed. Samples run on the LPA were measured without sonication. Samples grown in glass culture tubes were sonicated with 10 bursts of 0.5 seconds each once diluted in PBS and prior to flow cytometry.

Construction and Optimization of the DBD-CRY2/AD-CIB1 Optogenetic Split Transcription Factor

Various plasmids were created and tested to determine an optimal DBD-CRY2/AD-CIB1 system (Supplemental Table 3, Supplemental Methods). Function of these plasmid combinations was tested by assaying for blue-light induced gene expression in glass culture tubes or LPAs as outlined above.

Domestication for the Yeast Toolkit

The parts added to the Yeast Toolkit) [13] are shown in Supplemental Figure 6. Domestication of parts for the Yeast Toolkit [13] requires removal of BsaI, BsmBI, and NotI restriction sites. This was accomplished using the Q5 site-directed mutagenesis kit (New England Biolabs E0554S) and appropriate primers as indicated in Supplemental Table 2 to introduce a synonymous mutation to remove the undesirable restriction enzyme site. Domestication was verified by Sanger sequencing. Domesticated parts were inserted into the part-plasmid backbone (yTK001) as described in Lee, *et al* using primers in Supplemental Table 2.

Golden Gate Assembly of Cassette and Multigene Plasmids

Cassette plasmids (consisting of transcriptional units, i.e. promoter-coding sequence-terminator) and multigene plasmids (consisting of multiple transcriptional units linked together through assembly connectors with appropriate homology to integrate into the yeast genome) were assembled using BsaI assembly or BsmBI assembly as outlined in Lee, *et al* [13]. Details and small adjustments are outlined in the Supplemental Methods.

Recycling of loxP-flanked markers

In order to allow for marker recycling utilizing the Cre-loxP system we created a loxP-KlURA3-loxP part plasmid (pMM0519). Cre-mediated recombination to recycle the KlURA3 marker was accomplished by adapting the Cre recombinase-mediated excision protocol from Carter and Delneri [26].

Statistical Analysis

All statistical analysis was carried out as described using Matlab (Mathworks, Natick, MA).

References

[1] K. Buchholz and J. Collins, "The roots-a short history of industrial microbiology and biotechnology," Appl. Microbiol. Biotechnol., vol. 97, no. 9, pp. 3747–3762, May 2013.

[2] B. Chen et al., "Synthetic biology toolkits and applications in Saccharomyces cerevisiae," Biotechnol. Adv., vol. 36, no. 7, pp. 1870–1881, Nov. 2018.

[3] T. D. Scott, K. Sweeney, and M. N. McClean, "Biological signal generators: integrating synthetic biology tools and in silico control," Curr. Opin. Syst. Biol., vol. 14, pp. 58–65, Apr. 2019.

[4] F. Salinas, V. Rojas, V. Delgado, E. Agosin, and L. F. Larrondo, "Optogenetic switches for light-controlled gene expression in yeast," Appl. Microbiol. Biotechnol., vol. 101, no. 7, pp. 2629–2640, Apr. 2017.

[5] A. Milias-Argeitis, M. Rullan, S. K. Aoki, P. Buchmann, and M. Khammash, "Automated optogenetic feedback control for precise and robust regulation of gene expression and cell growth," Nat. Commun., vol. 7, Aug. 2016.

[6] J. E. Toettcher, D. Gong, W. A. Lim, and O. D. Weiner, "Light-based feedback for controlling intracellular signaling dynamics," Nat. Methods, vol. 8, no. 10, pp. 837-U99, Oct. 2011.

[7] D. Benzinger and M. Khammash, “Pulsatile inputs achieve tunable attenuation of gene expression variability and graded multi-gene regulation,” Nat. Commun., vol. 9, Aug. 2018.

[8] P. Harrigan, H. D. Madhani, and H. El-Samad, “Real-Time Genetic Compensation Defines the Dynamic Demands of Feedback Control,” Cell, vol. 175, no. 3, p. 877+, Oct. 2018.

[9] A. H. Ng et al., “Modular and tunable biological feedback control using a de novo protein switch,” Nature, vol. 572, no. 7768, p. 265+, Aug. 2019.

[10] M. Rullan, D. Benzinger, G. W. Schmidt, A. Milias-Argeitis, and M. Khammash, “An Optogenetic Platform for Real-Time, Single-Cell Interrogation of Stochastic Transcriptional Regulation,” Mol. Cell, vol. 70, no. 4, p. 745+, May 2018.

[11] J.-B. Lugagne and M. J. Dunlop, “Cell-machine interfaces for characterizing gene regulatory network dynamics.,” Curr. Opin. Syst. Biol., vol. 14, pp. 1–8, Apr. 2019.

[12] S. M. Castillo-Hair, O. A. Igoshin, and J. J. Tabor, “How to train your microbe: methods for dynamically characterizing gene networks,” Curr. Opin. Microbiol., vol. 24, pp. 113–123, Apr. 2015.

[13] M. E. Lee, W. C. DeLoache, B. Cervantes, and J. E. Dueber, “A Highly Characterized Yeast Toolkit for Modular, Multipart Assembly,” ACS Synthetic Biology, 2015. [Online]. Available: http://pubs.acs.org/doi/pdf/10.1021/sb500366v. [Accessed: 29-Sep-2015].

[14] M. J. Kennedy, R. M. Hughes, L. A. Peteya, J. W. Schwartz, M. D. Ehlers, and C. L. Tucker, “Rapid blue-light-mediated induction of protein interactions in living cells,” Nat. Methods, vol. 7, no. 12, pp. 973-U48, Dec. 2010.

[15] R. S. McIsaac, B. L. Oakes, X. Wang, K. A. Dummit, D. Botstein, and M. B. Noyes, “Synthetic gene expression perturbation systems with rapid, tunable, single-gene specificity in yeast,” Nucleic Acids Res., vol. 41, no. 4, Feb. 2013.

[16] R. M. Hughes, S. Bolger, H. Tapadia, and C. L. Tucker, “Light-mediated control of DNA transcription in yeast,” METHODS, vol. 58, no. 4, pp. 385–391, Dec. 2012.

[17] A. S. Khalil et al., “A Synthetic Biology Framework for Programming Eukaryotic Transcription Functions,” Cell, vol. 150, no. 3, pp. 647–658, Aug. 2012.

[18] R. S. McIsaac et al., “Fast-acting and nearly gratuitous induction of gene expression and protein depletion in Saccharomyces cerevisiae,” Mol. Biol. Cell, vol. 22, no. 22, pp. 4447–4459, Nov. 2011.

[19] E. M. Zhao et al., “Optogenetic regulation of engineered cellular metabolism for microbial chemical production,” Nature, vol. 555, no. 7698, p. 683+, Mar. 2018.

[20] X. Xu et al., “A Single-Component Optogenetic System Allows Stringent Switch of Gene Expression in Yeast Cells,” ACS Synth. Biol., vol. 7, no. 9, pp. 2045–2053, Sep. 2018.

[21] F. Salinas, V. Rojas, V. Delgado, J. Lopez, E. Agosin, and L. F. Larrondo, “Fungal Light-Oxygen-Voltage Domains for Optogenetic Control of Gene Expression and Flocculation in Yeast,” MBio, vol. 9, no. 4, 2018.

[22] J. Melendez, M. Patel, B. L. Oakes, P. Xu, P. Morton, and M. N. McClean, “Real-time optogenetic control of intracellular protein concentration in microbial cell cultures,” Integr. Biol., vol. 6, no. 3, p. 366, Mar. 2014.

[23] K. P. Gerhardt et al., “An open-hardware platform for optogenetics and photobiology,” Sci. Rep., vol. 6, Nov. 2016.

[24] R. D. Gietz and R. H. Schiestl, “High-efficiency yeast transformation using the LiAc/SS carrier DNA/PEG method,” Nat. Protoc., vol. 2, no. 1, pp. 31–34, 2007.

[25] K. Sweeney, N. M. Morales, Z. Burmeister, A. J. Nimunkar, and M. N. McClean, "Easy calibration of the Light Plate Apparatus for optogenetic experiments," METHODSX, vol. 6, pp. 1480–1488, 2019.

[26] Z. Carter and D. Delneri, "New generation of loxP-mutated deletion cassettes for the genetic manipulation of yeast natural isolates," YEAST, vol. 27, no. 9, pp. 765–775, Sep. 2010.

Supplemental Information

Strains and Culture Media

Yeast strains and growth media

Yeast strains are shown in **Supplemental Table 1.** For light induction experiments followed by fluorescence assays, yeast were grown in either Synthetic Complete media (6.7 g/L Yeast Nitrogen Base without amino acids-DOT Scientific, 2% v/v glucose, 1% v/v KS amino acid supplement without appropriate amino acids) or Low Fluorescence Media (LFM) (1.7 g/L Yeast Nitrogen Base without ammonium sulfate, amino acids, folic acid, riboflavin-MP Biomedicals 4030-512, 5 g/L Ammonium sulfate-MP Biomedicals 808211, 1% v/v KS supplement, 2% v/v glucose-Fisher Scientific). Non-integrating plasmids were maintained by growing yeast in media lacking the appropriate amino acids required for plasmid selection.

Yeast Transformation

Yeast were transformed using standard lithium-acetate transformation [1]. For integrating plasmids, the integration was validated using either colony PCR or, when colony PCR proved difficult, by PCR of genomic DNA. Genomic DNA was extracted using the Bust n' Grab protocol [2]. Primers used for validating integrations are listed in **Supplemental Table 2**. All transformants were checked for the petite phenotype by growth on YEP-glycerol (1% w/v Bacto-yeast extract-BD Biosciences 212750, 2% w/v Bacto-peptone-BD Biosciences 211677, 3% [v/v] glycerol-

Fisher Bioreagents BP229-1, 2% w/v Bacto-agar-BD Biosciences #214030) [3]. Only strains deemed respiration competent by growth on YEP-glycerol were used for subsequent analysis.

Bacterial strains and growth media

Escherichia coli strain DH5α was used for all transformation and plasmid maintenance in this study. *E. coli* were made chemically competent following either the Inoue method [4] or using the Zymo Research Mix & Go! Protocol (Zymo Research T3002). *E. coli* were grown on LB agar (10% w/v Bacto-Tryptone, 5% w/v Bacto Yeast Extract, 5% w/v NaCl, 15% w/v Bacto Agar) or LB liquid media (10% w/v Bacto-Tryptone, 5% w/v Bacto Yeast Extract, 5% w/v NaCl). Appropriate antibiotics were used to select for and maintain plasmids. Antibiotic concentrations used in this study were as follows: LB+CARB agar 100 μg/mL carbenicillin, LB+CARB liquid media 50 μg/mL carbenicillin, 25μg/ml chloramphenicol, 50μg/ml kanamycin.

Blue light induction

For blue light induction on a roller drum, biological replicates were selected from single yeast colonies and grown in Synthetic Complete media (lacking appropriate amino acids to maintain plasmid selection) at 30°C in the dark to mid-log. Each culture was then split and half of the culture was placed on the outside lane of a roller drum at room temperature in a glass culture tube. The other half of the culture was put in a test tube wrapped in foil on the inner lane of the roller drum. Three LEDs outputting 460nm blue light (Sparkfun COM-08718) were placed at the three, nine, and twelve o'clock positions of the roller drum and turned on at T=0 (~25 $\mu W/cm^2$). At each

timepoint, 500µL of culture was sampled into ice-cold PBS + 0.1% Tween and immediately placed at 4°C until being analyzed by flow cytometry.

For blue light induction in the Light Plate Apparatus, yeast were grown overnight (12-16 hours) in 1ml of Low Fluorescence Media or Synthetic Complete in each well of the 24-well plate (Artic White, AWLS-303008) in the Light Plate Apparatus, in a light-proof coffin shaker at 30°C with constant shaking (250RPM). One glass microbead (Fisher Scientific 11-312A 3mm or 11-312B 4mm) was added to each well of the plate to increase aeration. The plate was covered with a Breathe-Easy® sealing membrane. After overnight growth, cultures were diluted to either OD_{600}=0.01 in a new 24-well plate and grown for 4-5hrs before light induction or OD_{600} = 0.2 and grown in a new 24-well plate on the LPA with immediate light induction for the time indicated at the indicated light intensity. Timepoints were taken by transferring 50 µL of culture from each well to a 96-well plate containing 150 µL of PBS+0.1% Tween-20 in each well.

The LPA is programmable, such that the timing, intensity, and duration of illumination in each well can be controlled [5]. For the duty cycle experiment, the LPA was programmed to alternate between light on and light off with the following programs: turn on for 1 min, off for 19 min; on for 5 min, off for 15 min; on for 10 min, off for 10 min; on for 15 min, off for 5 min.

Construction and Optimization of the ZDBD-CRY2/AD-CIB1 Optogenetic Split Transcription Factor

To compare ZDBD-CRY2/AD-CIB1 combinations, yeast strain yMM1146 (Matα trp1Δ63 leu2Δ1 ura3-52) was cotransformed with appropriate plasmid combinations (ZDBD-CRY2/AD-

CIB1/Reporter plasmid) as outlined in detail below using standard lithium acetate transformation [1]. Transformants were selected on and cultured in SC media with appropriate amino acids left out (SC-ura-leu-trp) for plasmid maintenance. Various plasmids were created and tested to determine an optimal ZDBD-CRY2/AD-CIB1 system (**Supplemental Table 3,** see below). Function of these plasmid combinations was tested by assaying for blue-light induced gene expression in glass culture tubes as outlined above.

Plasmid Construction

VP16AD-CIB1

The VP16AD-CIB1 plasmid (pMM0281) was created using yeast homologous recombination [6]. The VP16 activation domain from the GEV artificial transcription factor [7] was amplified from yMM1008 genomic DNA using oMM0400/0401. The pMM0159 plasmid was cut with KpnI, which digests the plasmid between the existing SV40NLS and the GAL4AD. The PCR product containing VP16AD and the digested plasmid were co-transformed into yMM83 [1] (Mat a his3Δ1 leu2Δ0 LYS2 met15Δ0 ura3Δ0) and positive transformants that repaired the lesion in the plasmid with the VP16AD activation domain (replacing the GAL4AD) were selected for growth on SC-Leu media. Plasmids were prepped from yeast and verified by sequencing.

ZDBD-CRY2 with different linkers between Zif268DBD and CRY2

The original ZDBD-CRY2 plasmids (pMM0282, pMM0283, pMM0284) were made by molecular cloning and assembly into the pRS414 vector (pMM0006 CEN TRP1) [2]. The ADH1 promoter

from pMM0160 was amplified using oMM0456/0457 and cloned between the NgoMIV and NotI sites in pRS414. The FLAG(3X)-NLS-Zif268 cassette was amplified from plasmid pMN8-FLAG(3x)-NLS-Zif-Nuclease (a gift from the Noyes lab) using oMM0458 and oMM0407, 0408 or 0409 (to achieve different linker lengths between Zif268 and CRY2) and cloned between the NotI and NheI sites. The CRY2-tADH1 region from pMM0160 was amplified using oMM0383/oMM0384 and cloned between the NheI and SacI restriction sites. The three linkers between the Zif268 DBD (ZDBD) and CRY2 are Linker 3 (ASF), Linker 4 (PASF) and Linker 10 (GGGSGGGASF).

pZF promoters

The binding site reporter plasmids (pMM0285-pMM0290) were made using the engineered pGAL1 promoter from McIsaac, *et al* [8]. This GAL1 promoter was engineered to have XbaI and NotI sites on either side of the three native GAL4 (5'-CGG-N $_{11}$ -CCG-3') binding sites. This promoter was cloned into pMM0008 (pRS416 [9]) using NheI and XmaI sites. The fluorescent protein yEVenus from pMM0223 (pKT90 [10]) was cloned between the XmaI and AscI sites using oMM0421/0423. To replace the GAL4 binding sites with binding sites for the Zif268 zinc-finger DNA-binding domain (GCGTGGGCG), pMM0301 was digested with XbaI and NotI, and the oligo pairs oMM0413-0420, oMM0481-0486 were annealed and ligated into the pMM0301 backbone. Plasmid pMM0301 is the original GAL1 promoter from McIsaac, *et al* [8] in front of yEVenus. The pZF(1BS) promoter contains 1 Zif268 DBD binding site. The pZF(2BS) promoter contains three Zif268 DBD binding sites, but two of the sites overlap. The pZF(3BS) promoter contains three Zif268 DBD binding sites separated by an 'A'. The ZF(3BS*) promoter is identical to pZF(3BS) except that the binding sites are now separated by an 'T'. This creates the appropriate

cross-strand contact for Zif268 as outlined in [3]. The pZF(4BS*) promoter has four binding sites with the appropriate cross-strand contact. The pZF(3BSopp) is the same as pZF(3BS) but with the Zif268 DBD binding sites reversed on the opposite strand.

ZDBD-CRY2 with different Nuclear Localization Signals (NLS)

Plasmids pMM0313 and pMM0314 utilizing the SV40NLS and the H2BNLS respectively were made by digesting out the FLAG(3X)-SV40NLS tag in pMM0284 between KpnI and NotI and annealing and ligating in either the oMM0566/0567 or the oMM0568/0569 oligonucleotide pairs to reinsert a lone SV40NLS-linker or H2B NLS-linker.

Control Plasmid

Plasmids pMM0315 (GAL4AD scLEU2 CEN) and pMM0316 (GAL4BD scTRP1 CEN) were constructed by yeast homologous recombination to remove the CIB1 and CRY2 open reading frames, while preserving GAL4AD and GAL4BD, from pMM0159 and pMM0160, respectively. Plasmid pMM0159 was digested with ClaI and transformed with the annealed oligonucleotide pair oMM0547/0548. Positive transformants were selected on SC-LEU, plasmids were recovered from the yeast and verified by sequencing, resulting in pMM0315. Plasmid pMM0160 was digested with SalI and transformed with the annealed oligonucleotide pair oMM0549/0550. Positive transformants were selected on SC-Trp, plasmids were recovered from the yeast and verified by sequencing, resulting in pMM0316.

ZDBD-CRY2 without N-terminal FLAG (3x)

Plasmids pMM0317 (SV40NLS-ZCRY2 (L3) scTRP1) and pMM0320 (SV40NLS-ZCRY2PHR scTRP1) were created by using yeast homologous recombination to remove the FLAG(3X) tag in pMM0284 and using yeast homologous recombination to truncate CRY2. Plasmid pMM0317 was constructed by cutting pMM0284 with NotI and co-transforming this cut plasmid with annealed and extended oMM0551/0552 into yMM83. Positive transformants were selected on SC-Trp, purified from yeast, and verified by sequencing. Plasmid pMM0320 was constructed by digesting pMM0284 with both SalI and NotI and transforming this digested plasmid with annealed and extended oMM0551/0552 as well as oMM0562/0563.

Domestication for the YTK

The parts added to the Yeast Toolkit [11] are shown in **Supplemental Figure 6.** Domestication of parts for the Yeast Toolkit [11] requires removal of BsaI, BsmBI, and NotI restriction sites. This was accomplished using the Q5 site-directed mutagenesis kit (New England Biolabs E0554S) and appropriate primers as indicated in **Supplemental Table 2** to introduce a synonymous mutation to remove the undesirable restriction enzyme site**.** Domestication was verified by Sanger sequencing. Domesticated parts were inserted into the part-plasmid backbone (yTK001) as described in Lee, *et al* using primers in **Supplemental Table 2.**

Golden Gate Assembly of Cassette and Multigene Plasmids

Cassette plasmids (consisting of transcriptional units, *i.e.* promoter-coding sequence-terminator) and multigene plasmids (consisting of multiple transcriptional units linked together through assembly connectors with appropriate homology to integrate into the yeast genome) were assembled using BsaI assembly or BsmBI assembly as outlined in Lee, *et al* [11].

NEB Golden Gate assembly mix (E1600) was used for BsaI assembly. The 10 μL Golden Gate reaction mixture consisted of 1 μL of NEB Golden Gate Buffer (10x), 0.5 μL NEB Golden Gate assembly mix, 20 fmol of each plasmid, and water. We found that using commercially available NEB Golden Gate assembly mixture, as opposed to using BsaI, T7 Ligase, and T4 Ligase buffer, increases the reaction efficiency greatly. For BsmBI assembly, the protocol was adapted from Lee, *et al* [11] and each 10 μL BsmBI reaction mixture consisted of 0.5 μL BsmBI, 0.5 μL T7 Ligase, 1 μL T4 Ligase buffer, 20 fmol of each plasmid, and water.

The thermocycler program was adapted from Lee, *et al* (2015) [11] and consisted of 20-30 cycles of digestion and ligation (2 min at 37-42°C; 5 min at 16°C) followed by a final digestion (55-60 °C) and a heat inactivation step (80°C for 10-20 min). For final cassettes with internal BsaI cut sites (i.e., integration vectors), the reaction was ended with ligation, and final digestion and inactivation steps were omitted.

5 μL of reaction mixture was then transformed into DH5α competent *E. coli* and plated on LB plates with appropriate antibiotics. Plasmids were then extracted, digested with BsmBI or NotI-HF as a first-pass test, and sequenced with appropriate primers for final verification. For both BsaI and BsmBI assemblies, the efficiencies were found to be at least 50%. However, final cassettes with internal BsaI cut sites have notably lower assembly efficiency.

Construction of the ZDBD-CRY2PHR/VP16AD-CIB1 Dosage Strains

To understand how the dosage and ratio of the DNA-binding domain (ZDBD-CRY2PHR) and activation domain (VP16AD-CIB1) components of the optogenetic system affected function, we constructed nine strains with different ratios of ZDBD-CRY2 and VP16AD-CIB1. These strains are yMM1458-1466 and have the genotypes shown in **Supplemental Table 1.** To construct these strains, we made multigene cassettes containing pPROMOTER-VP16AD-CIB1-tTerminator-pPROMOTER-ZDBD-CRY2PHR-tTerminator-pZF(3BS)-mRUBY2 (pMM0637-pMM0645) designed to integrate at the scURA3 locus. These multigene cassettes were made using BsmBI Golden Gate assembly (as described above) and cassette plasmids containing the ZDBD-CRY2, VP16AD-CIB1, and pZF(3BS)-mRUBY2 elements with appropriate assembly connectors (pMM0620- pMM0624, pMM0628- pMM0629). As benchmarks for mRUBY2 expression we also made multigene plasmids containing pCONSTITUTIVE-mRUBY2 instead of the pZF(3BS)-mRUBY2 (pMM0625- pMM0627) and integrated them into yMM1146 to create yMM1472-1480. As a no fluorescence control we created a multigene plasmid with a spacer in place of pZF(3BS)-mRUBY2 (pMM0619) and integrated this into yMM1146 to create the no-fluorescence controls yMM1473 and yMM1477.

Growth Assays

Yeast colonies were inoculated in 1 mL of LFM or SC-URA in a 24-well plate (Corning #3370) and grown for 24hrs in a light-proof coffin shaker at 30°C with shaking (250rpm). One glass bead was added to each well and the plate was covered with a Breathe-Easy® sealing membrane (Sigma-Aldrich) to minimize evaporation. On the next day, the culture was diluted in 1 mL of LFM to OD_{600} = 0.2 in a 24 well plate with cover (with no glass beads added). The OD_{600} of the culture was measured every 15 min for 18 hours using the TECAN plate reader (Tecan Infinite

M1000). Cells were grown for 18 hours with continuous double orbital shaking (120 rpm) and OD_{600} readings taken every 15 minutes. Four readings were taken for each well for every time point. Growth rate μ was determined for the culture in each well by fitting the log-transformed OD_{600} readings to a linear model ($\log(y)=\log(A_0)+ \mu * t$. The doubling time is calculated as $\ln(2)/\mu$. Fitting was done using the non-linear least squares method in Matlab (Mathworks, Natick, MA). Only fits with $r^2 > 0.9$ were considered.

Recycling of loxP-flanked markers

In order to allow for marker recycling utilizing the Cre-loxP system we created a loxP-KlURA3-loxP part plasmid (pMM0519). The loxP-KlURA3-loxP cassette was amplified from pMM0326 (pUG72; Gueldener, *et al* 2002) using oMM0991/0992 and assembled into the part entry vector (pYTK001/pMM0452) using a BsmBI Golden Gate reaction. This part was further assembled into a multigene cassette designed for integration at the scURA3 locus (pMM0617). This cassette plasmid contains 3'- and 5'- homology to the scURA3 locus flanking loxP-KlURA3-loxP. The Type234 GFP dropout is flanked by the special assembly connectors conLS' and conRE'. This pre-assembled integration vector allows additional cassettes flanked by assembly connectors to be assembled into this vector using a BsmBI Golden Gate reaction.

We used a BsmBI Golden Gate reaction with cassette plasmids pMM0617, pMM0621 (pRPL18B-VP16AD-CIB1), pMM0623 (pRPL18B-ZDBDCRY2PHR), and pMM0624 (pZF(3BS)-mRuby2) to generate pMM0647 (pRPL18B-VP16AD-CIB1-tENO1 pRPL18B-ZDBDCRY2PHR-tSSA1 pZF(3BS)-mRuby2-tADH1 loxP-KlURA3-loxP scURA3 3' homology-KanR-ColE1-scURA3 5' homology). This multigene cassette plasmid was linearized with NotI and transformed into

yMM1146 using a standard lithium acetate protocol [1]. Positive transformants were selected on SC-URA and verified by colony PCR and sequencing. This generated yeast strain yMM1468. Yeast strain yMM1468 is identical to the ZDBD-CRY2$_{medium}$/VP16AD-CIB1$_{medium}$ strain yMM1462 except that yMM1468 has the KlURA3 marker flanked by loxP sites instead of the standard scURA3 marker. Cre-mediated recombination to recycle the KlURA3 marker was accomplished by adapting the CRE recombinase-mediated excision protocol from Carter and Delneri [12]. yMM1468 was transformed with 0.25-0.5 µg of pMM0296 (pSH65, pGAL1-CRE Bleo^R). These transformants were plated onto YPD and then replica plated onto selective media (YPD +10µg/ml phleomycin (InvivoGen)) after overnight growth. To express CRE and induce recombination phleomycin resistant colonies were selected and grown overnight in 3ml of YP-Raffinose (1% w/v yeast extract (BD Biosciences), 2% w/v Bacto-peptone (BD Biosciences), and 2% w/v raffinose (Becton Dickinson 217410)). The following day, cells were harvested by centrifuging at 3750 rpm for 5 minutes, washed in sterile miliQ water, and resuspended in 10ml of YP-Galactose (1% w/v yeast extract (BD Biosciences), 2% w/v Bacto-peptone (BD Biosciences), 2% w/v galactose (BD Biosciences 216310)) at an OD_{600} of 0.3. These cultures were incubated at 30°C with shaking for 2-3 hours. This culture was then diluted and plated on YPD and then replica plated onto SC-5FOA (25% w/v g Bacto-Agar, 6.72% w/v YNB, 1% v/v mL 20x KS supplement without URA, 2% v/v glucose, 10 mL 5-Fluoroorotic Acid (Zymo Research), 50 mg uracil (MP Biomedicals 103204). 5FOA resistant colonies were checked for excision of the KlURA3 marker using colony PCR. Transformants with KlURA3 excised were grown in liquid YPD to saturation twice and then plated on YPD for ~100 colonies per plate. These were replica plated onto YPD + 10µg/ml phleomycin. Phleomycin sensitive colonies (colonies that had lost the plasmid pMM0296) were reconfirmed by colony PCR to have loxed out KlURA3. This generated

yMM1472 (Matα trp1Δ63 leu2Δ1 ura3::pRPL18B-VP16AD-CIB1-tENO1-pRPL18B-ZCRY2PHR-pZF(3BS)-mRuby2-loxPScar).

To test that neither the loxP-KlURA3-loxP marker nor removal of the KlURA3 affected the function of ZDBD-CRY2PHR or VP16AD-CIB1 we compared mRuby2 induction in yMM1462, yMM1468, and yMM1472. These strains were grown overnight in low fluorescence media and then diluted back to OD_{600} 0.01 in the LPA in the morning. Cultures were run in triplicate in the LPA at 15μW/cm^2 blue light overnight (16 hours). Fluorescence was assessed by flow cytometry. As seen in **Supplemental Figure 10,** all three strains induce at comparable levels.

Supplemental Figures

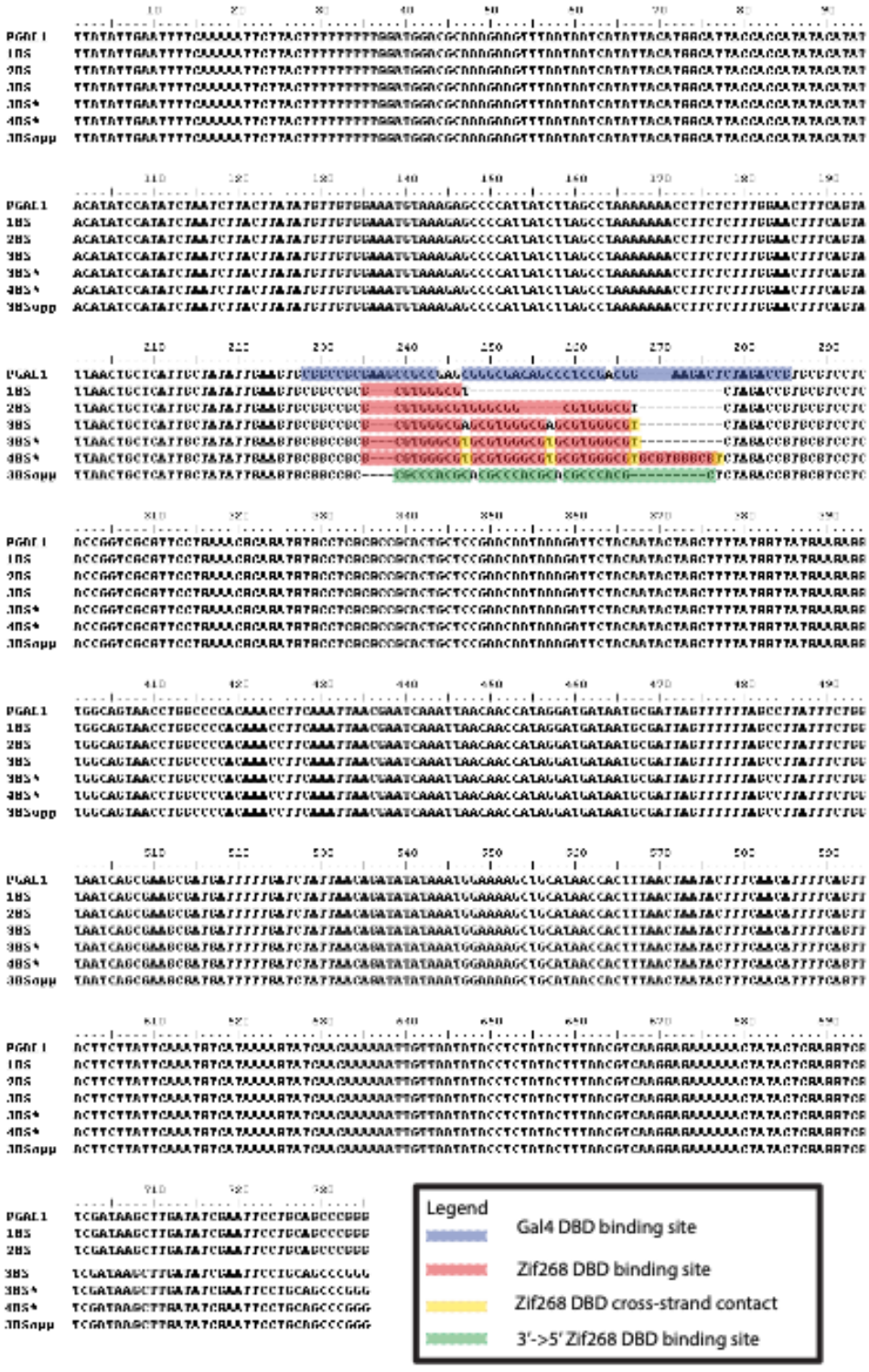

Supplemental Figure 1. pZF Promoter Sequences. Sequence of the scpGAL1 promoter compared with the synthetic promoters containing variable numbers and orientations of binding

sites for the Zif268DBD. The motif recognized by the GAL4 DNA binding domain is 5'- CGG-N_{11}-CCG-3' (highlighted in blue) while the motif recognized by the zinc finger DNA binding domain (Zif268) is GCGTGGGCG (highlighted in red, reverse compliment in green). Cross-strand contacts for the Zif268 zinc fingers are highlighted in yellow.

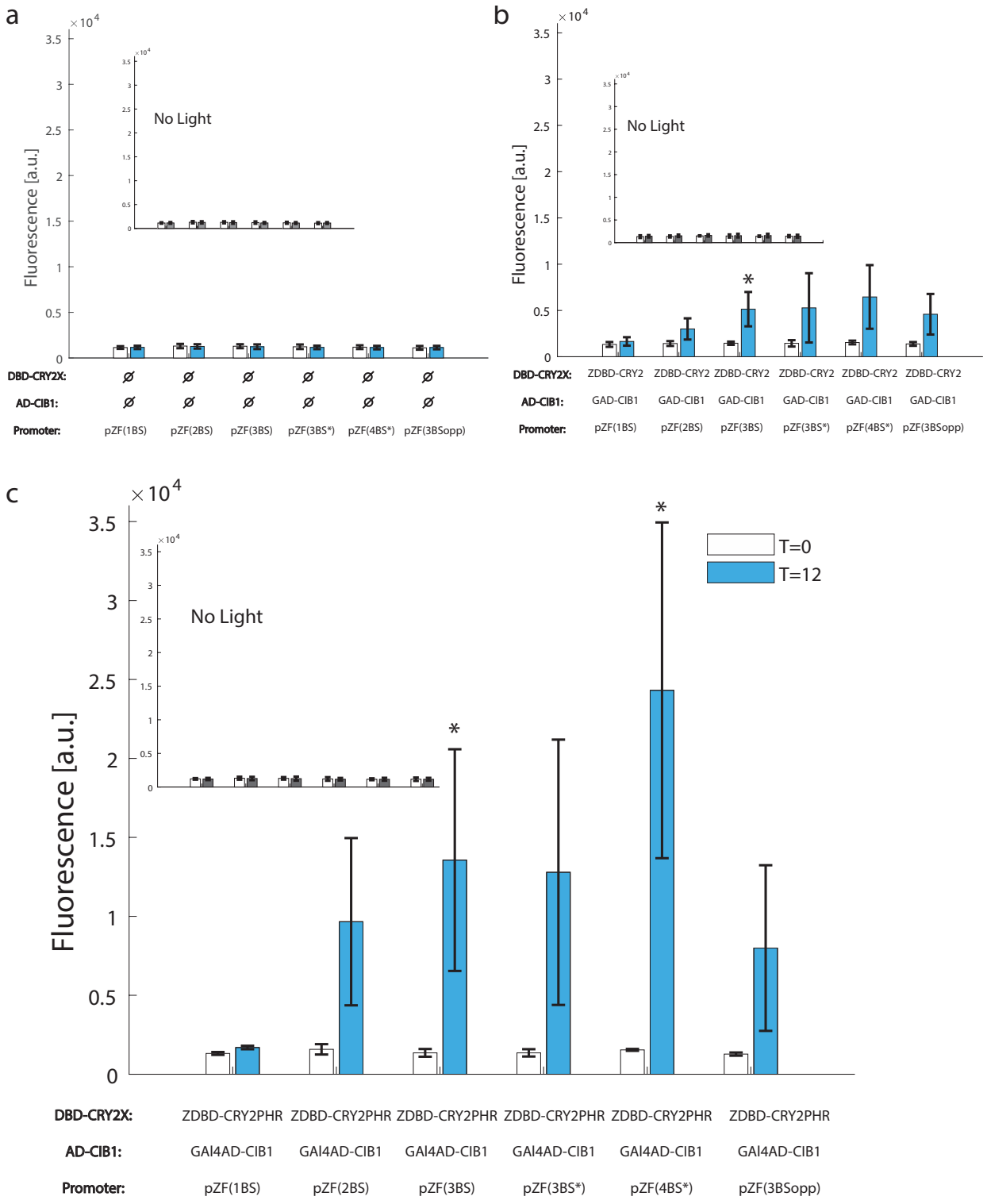

Supplemental Figure 2. pZF Promoters. Comparison of the synthetic pZF(XBS) promoters. **(a)** Strain yMM1146 (Mat α trp1Δ63 leu2Δ1 ura3-52) was co-transformed with the pZF(XBS)-yEVenus reporter plasmids (pMM0285-pMM0290) and empty vector controls (pMM0316 and

pMM0315). There is no significant induction of the pZF(XBS)-yEVenus promoters after 12 hours of growth in 15μW/cm^2 470nm blue light ($p>0.05$ all samples, light vs dark, Welch's t-test). **(b)** Strain yMM1146 (Mat α trp1Δ63 leu2Δ1 ura3-52) was co-transformed with the pZF(XBS)-yEVenus reporter plasmids (pMM0285-pMM0290) and the ZDBD-CRY2 (pMM0317)/GAL4AD-CIB1 (pMM0159) split transcription factor. The pZF(3BS)-yEVenus reporter was significantly induced by 12 hours of growth in blue light ($p<0.03$, light vs dark, Welch's t-test) while the pZF(4BS*)-yEVenus and pZF(3BSopp) were close to significantly induced ($p<0.07$, light vs dark, Welch's t-test). **(c)** Strain yMM1146 (Mat α trp1Δ63 leu2Δ1 ura3-52) was co-transformed with the pZF(XBS)-yEVenus reporter plasmids (pMM0285-pMM0290) and the ZDBD-CRY2PHR (pMM0320)/GAL4AD-CIB1 (pMM0159) split transcription factor. The pZF(3BS) and pZF(4BS*)-yEVenus reporters induced significantly ($p<0.04$, light vs dark, Welch's t-test) after 12 hours of growth in 15μW/cm^2 470nm blue light. An analysis of variance ($F(47,96)=0.77$, $p=0.8443$) indicated that none of the pZF(XBS) promoters were distinguishable in the dark before or after growth for 12 hours, indicating that there is minimal background induction due to culture saturation for the pZF(XBS) promoters. Both the pZF(3BS) and pZF(4BS*) promoters were used for further testing (nuclear localization signals and linkers, **Supp Fig3** and **Supp Fig 4**). Since the pZF(3BS) promoter reliably induced when paired with the ZDBD-CRY2 or ZDBD-CRY2PHR DNA-binding components it was chosen for use in the toolkit.

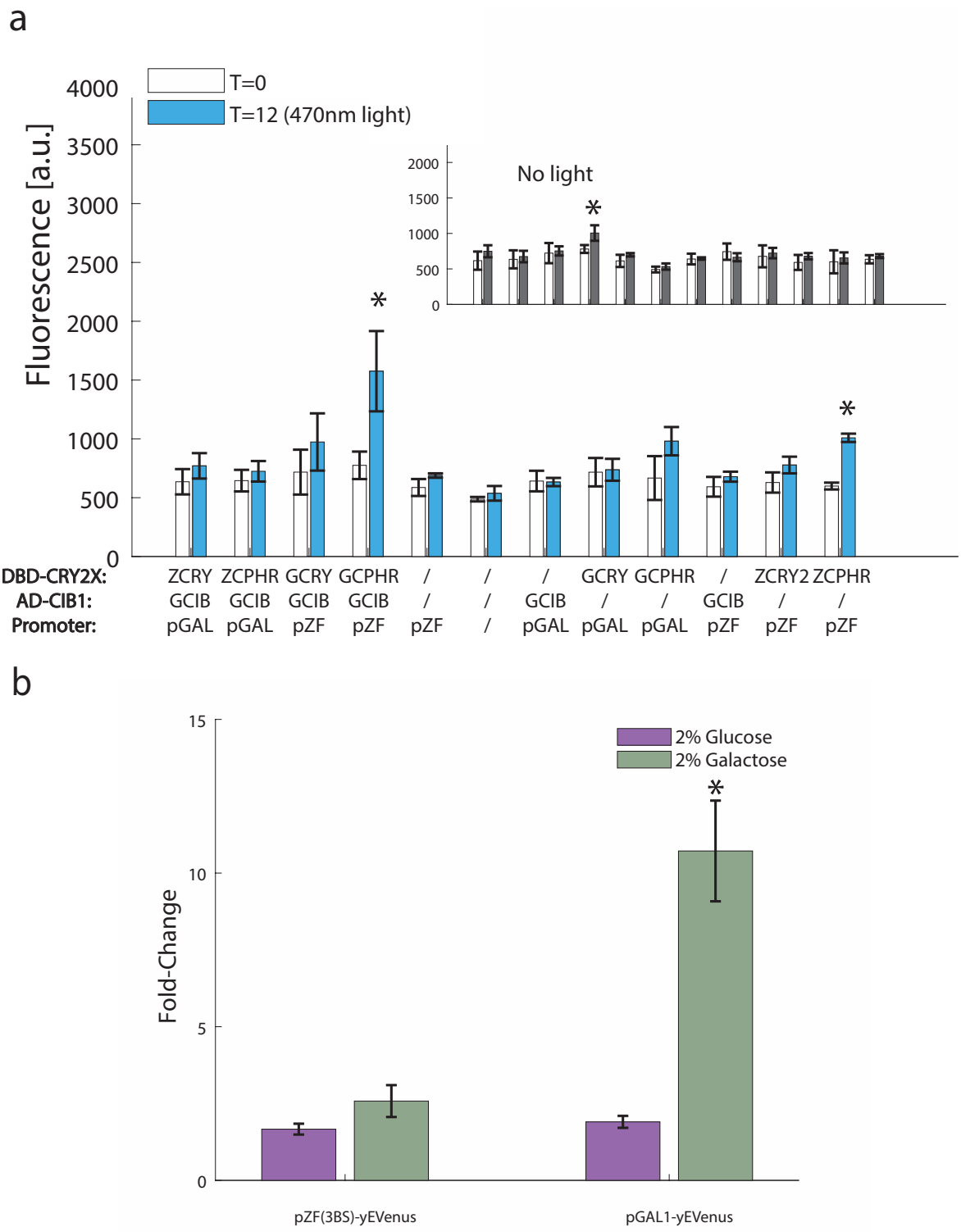

Supplemental Figure 3. Crosstalk. (a) Strain yMM1146 was transformed with the indicated constructs and exposed to 470nm blue light for 12 hours at 15μW/cm^2. After twelve hours of growth in the light and in the dark, the strain carrying GAL4DBD-CRY2PHR/GAL4AD-CIB1/pZF(3BS) shows a weak (less than 2-fold) but significant induction ($p<0.03$, Wilcox's t-

test). In the light, the strain carrying the ZDBD-CRY2PHR and pZF(3BS) reporter without an activation domain displays a weak (less than 2-fold) but significant induction ($p<0.001$, Wilcox's t-test). We also see weak (not statistically significant, $p=0.082$) induction in the GAL4DBD-CRY2PHR/pGAL1 sample. We interpret these results to suggest that the CRY2PHR protein has weak activation domain function that may increase in response to light. For clarity in the figure, protein names have been abbreviated as follows: ZDBD-CRY2 is ZCRY2; ZDBD-CRY2PH is ZCPHR; GAL4DBD-CRY2 is GCRY2; GAL4DBD-CRY2PHR is GCPHR; GAL4AD-CIB1 is GCIB1; pZF(3BS)-yEVenus is pZF **(b)** To determine if the native *S. cerevisiae* galactose machinery could induce gene expression from the pZF(3BS) promoter we grew yeast strain yMM1146 with pZF(3BS)-yEVenus or pGAL1-yEVenus for 16 hours in either 2% glucose or 2% galactose as a carbon source. Only induction of the pGAL1-yEVenus reporter in galactose is significant (10-fold induction, $p=0.002$, Welch's t-test).

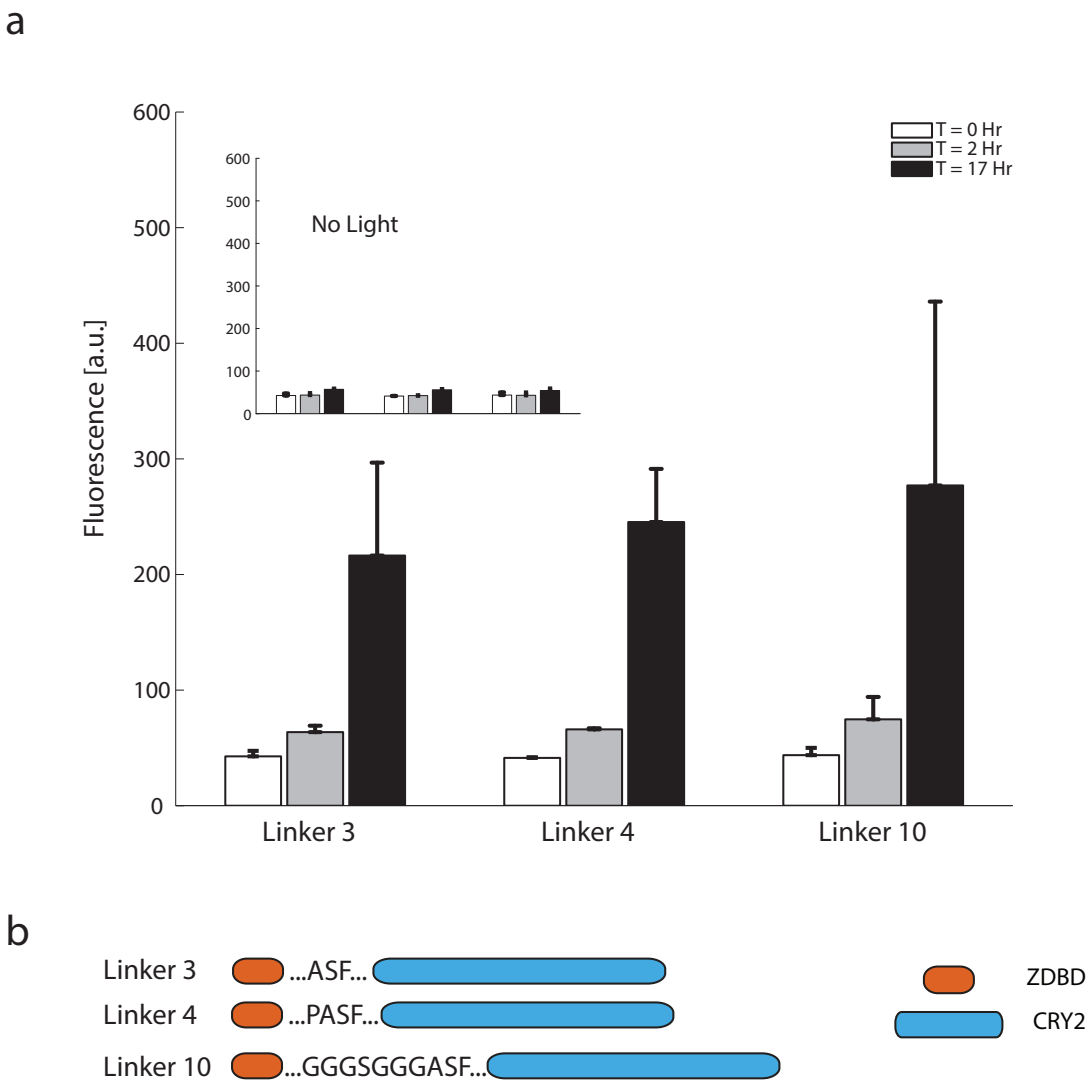

Supplemental Figure 4. Linkers. Quantification of the effect of linker length between Zif268DBD and the CRY2 protein. Strain yMM1146 (Mat alpha trp1Δ63 leu2Δ1 ura3-52) was co-transformed with the GAL4AD-CIB1 plasmid (pMM0159), the pZF(4BS*)-yEVenus plasmid (pMM0289) and ZDBD-CRY2 with three different linker lengths (pMM0282, pMM0283, pMM0284). In the different linkers, the amino acids between the Zif268 DNA-binding domain (ZDBD) and the CRY2 protein are Linker 3 (ASF), Linker 4 (PASF), and Linker 10 (GGGSGGGASF). Cells were grown to mid-log in SC-Ura-Leu-Trp before being exposed to 470nm blue-light for 17 hours as detailed in the **Methods.** Data is presented as average ±SEM. There is no statistical difference in induction between the three linker constructs (ANOVA, $F(2,6)=2.91$, $p=0.1305$).

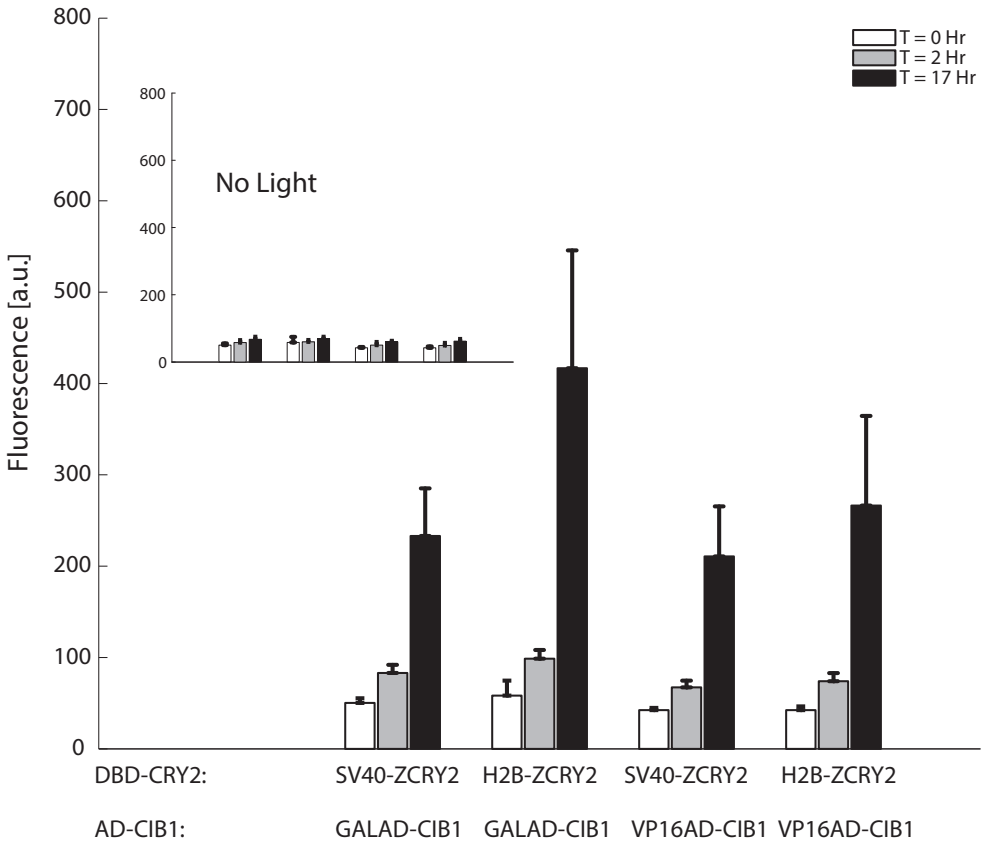

Supplemental Figure 5. Nuclear Localization Signal. We used two different nuclear localization signal (NLS) sequences to localize the ZDBD-CRY2 construct to the nucleus. The SV40 sequence (P K K K R K V) was taken from pMM0159 (GAL4AD-CIB1), while the H2B nuclear localization sequence (G K K R S K A K) is based on the *Saccharomyces cerevisiae* histone H2B sequence. Cells were transformed with the p4BS*-yEVenus reporter plasmid (pMM0289), pGAL4AD-CIB1 (pMM0159) or pVP16AD-CIB1 (pMM0281), and SV40NLS-ZDBD-CRY2 (pMM0313) or H2BNLSDBD-Z-CRY2 (pMM0314) and exposed to blue-light for 17 hours. The induction of yEVenus was measured using flow cytometry, as detailed in the **Methods.** Data is presented as average±SEM. There is no statistical difference in induction between the nuclear localization signals with either activation domain (ANOVA, $F(3,8)=3.21$, $p=0.0832$).

A

Assembly Connector 1	Promoter 2	Coding Sequences 3	Terminator 4	Assembly Connector 5	S. cerevisiae marker 6
ConLS	pTEF1	VP16AD-CIB1	tENO1	ConR1	URA3
ConL1	pRPL18B	ZDBD-CRY2PHR	tSSA1	ConR2	loxP-kiURA3-loxP
ConL2	pRNR2	ZDBD-CRY2	tADH1	ConRE	
ConLS'	pZF(3BS)	mRuby2		ConRE'	
	pREV1				
	pTDH3				

B

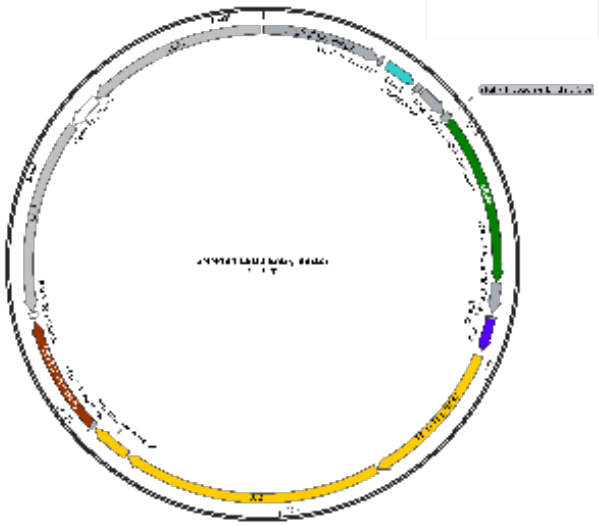

C

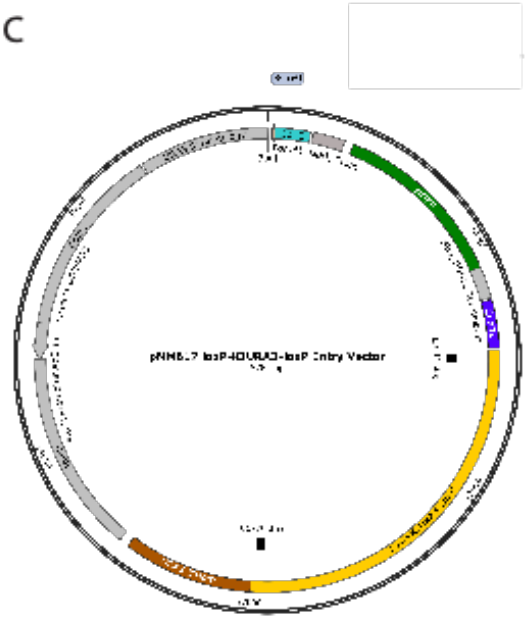

Supplemental Figure 6. Yeast Optogenetic Toolkit Parts. (a) Optogenetic parts created in this paper that integrate with the Lee, *et al* Yeast Toolkit [11] are highlighted and shown with additional Yeast Toolkit parts used in this paper. (**b**) A preassembled entry vector for integration at the LEU2 locus. A transcriptional unit (promoter, coding sequence, terminator) can be assembled into this vector replacing the BsaI-flanked GFP dropout. (**c**) A similar preassembled integration vector but using the loxP-KlURA3-loxP yeast selection marker. Once integrated, the KlURA3 selection marker can be removed by Cre-recombinase expression as detailed in the **Methods**.

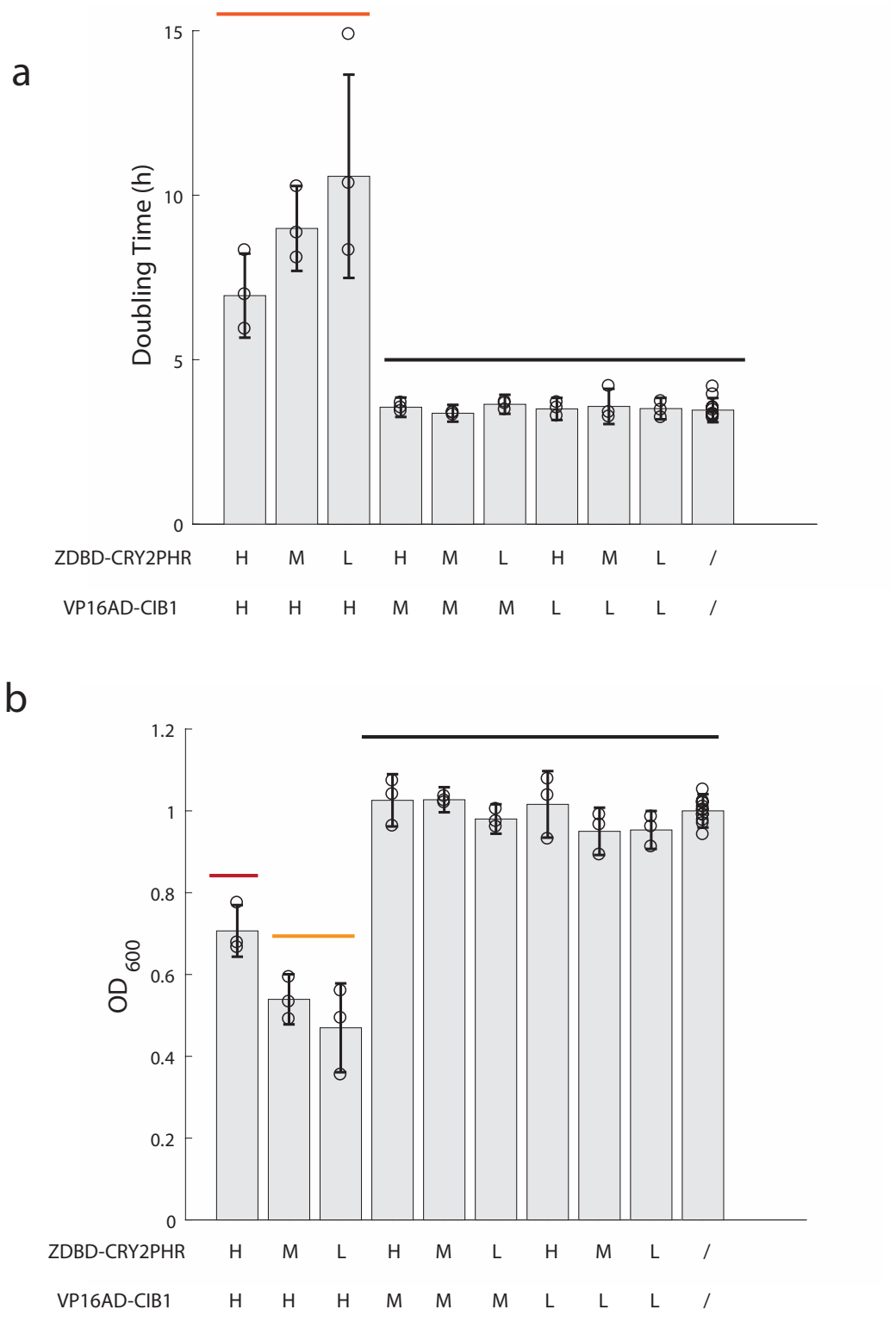

Supplemental Figure 7. Dosage Strains Growth. (a) Doubling time of the nine dosage strains (**Main Text, Figure 3**). Doubling time was calculated from the growth rate (μ h^{-1}) which was determined by fitting as described in the **Supplemental Methods.** Horizontal bars indicate

significantly different groups determined by one-way ANOVA followed by Tukey's HSD ($F(9,20)=56.38$, $p=2.98\times10^{-12}$) **(b)** The endpoint optical density (OD_{600}) for the same cultures as shown in **(a).** Bars indicate significantly different groups determined by one-way ANOVA followed by Tukey's-HSD ($F(9,20)=43.62$, $p=3.35\times10^{-11}$).

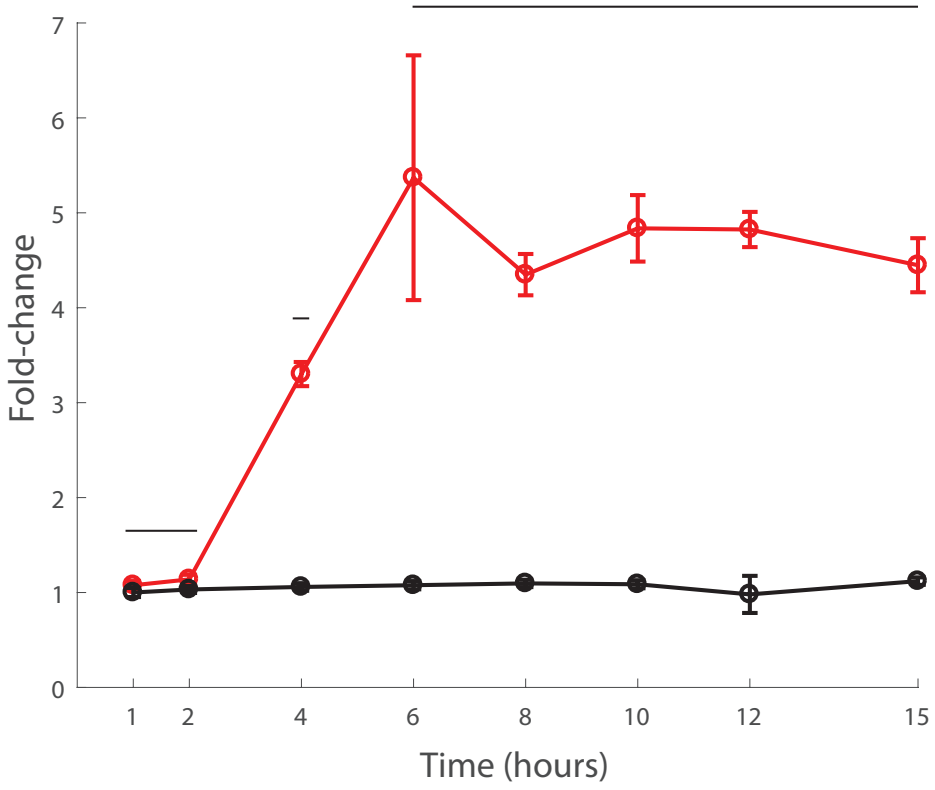

Supplemental Figure 8. Time course. Time course of gene expression in the ZDBD-$CRY2_{medium}$/VP16AD-$CIB1_{medium}$ strain compared in dark (black) and 15µW/cm^2 light (red). Time is in hours after turning on the light in the Light Plate Apparatus. Bars indicate significantly different groups determined by one-way ANOVA followed by Tukey's-HSD ($F(9,20)=37.46$, $p=9.32\times10^{-09}$).

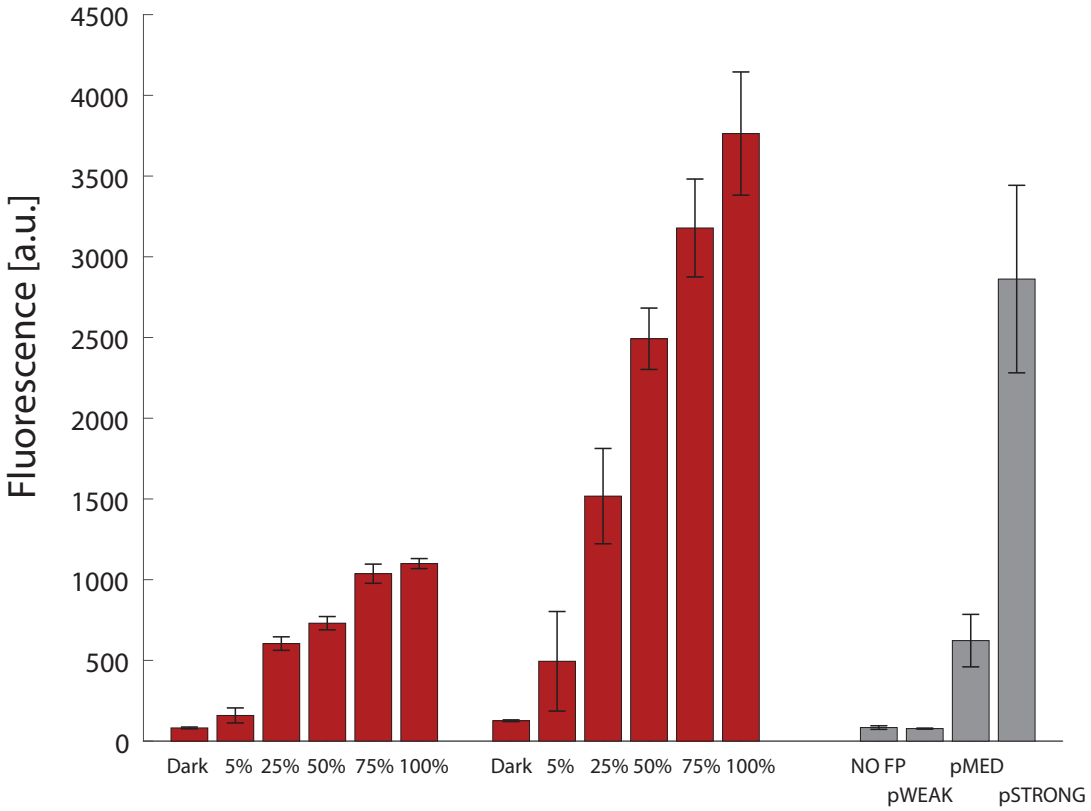

Supplemental Figure 9. Duty Cycle. Expression of mRUBY2 in the ZDBD-CRY2PHR$_{medium}$ /VP16AD-CIB1$_{medium}$ strain (left, same as **Figure 4**) compared to the ZDBD-CRY2PHR$_{medium}$/VP16AD-CIB1$_{high}$ strains (middle). Both strains show gene expression that is tunable by light duty cycle. Gray bars show expression in the constitutive promoters and no fluorescence control.

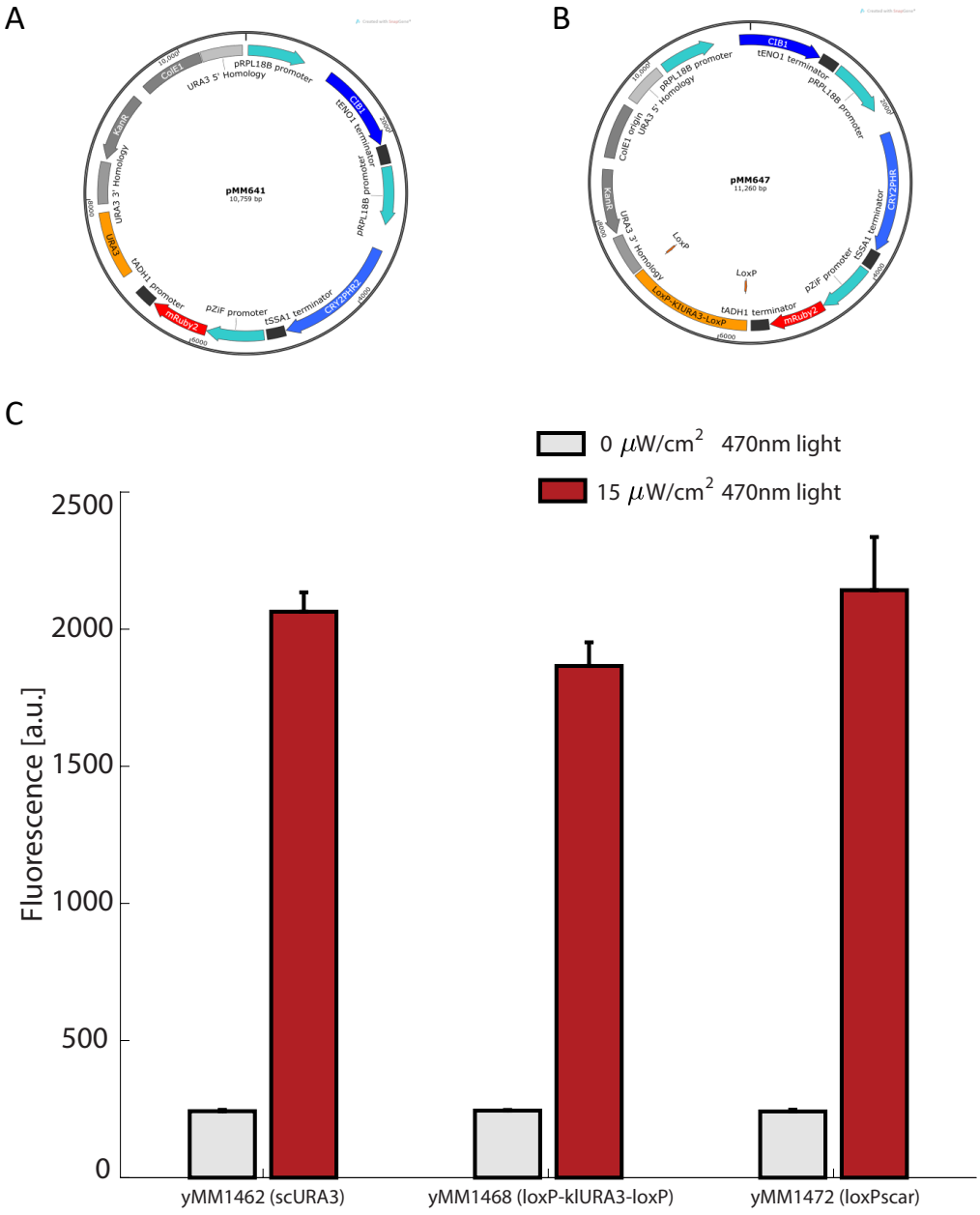

Supplemental Figure 10. Marker Recycling. Integration of the ZDBD-CRY2$_{medium}$/VP16AD-CIB1$_{medium}$ pZF(3BS)-mRUBY2 cassette using **(A)** pMM0641 (scURA3 selection marker) and **(B)** pMM0647 (KlURA3 selection marker) were compared for their ability to induce mRUBY2 expression in response to blue light. The choice of marker (yMM1462/scURA3 vs yMM1468/KlURA3) or recycling of the KlURA3 marker using CRE-recombinase expression (yMM1472) did not affect the optogenetic system as indicated by comparable mRuby2 fluorescence after growing the different strains in blue light (or dark) for 16 hours. Means of the

induced and uninduced populations were determined by fitting the flow cytometry data to a lognormal distribution. Error bars represent S.E.M.

Supplemental Tables

Additional details on yeast strains, oligos, and plasmids can be found in the **Supplemental Material.**

Supplemental Table 1: Yeast Strains

ID	Alias	Genotype	Description	Source/ Reference
yMM83	ySR32, BY4741	MATa his3Δ1 leu2Δ0 met15Δ0 ura3Δ0	Assembly strain	[13]
yMM1008	pGAL1-ARO80	(PGAL10+gal1)Δ::loxP gal4Δ::LEU2 HAP1 leu2Δ0::PACT1-GEV-NatMX KANMX-PGAL1-ARO80	Source of VP16AD from GEV	McClean Lab
yMM1146	DBY8750, KSY1284	Mat alpha trp1Δ63 leu2Δ1 ura3-52	Assembly and integration strain	Botstein lab
yMM1367	yMM1146_ pMM0364 @HO	Mat alpha trp1Δ63 leu2Δ1 ura3-52 HO::SV40NLS-VP16AD-CIB1 loxP-KlURA3-loxP SV40NLS-Zif268DBD-CRY2PHR	Strain with integrated optogenetic system, to allow for induction of GOI using KanMXREV-pZF promoter	This study
yMM1401	mRuby2 HIGH	Mat alpha trp1Δ63 leu2Δ1::LEU2-pTDH3-mRUBY2-tADH1 ura3-52 HO::S40NLS-VP16AD-CIB1 loxP-KlURA3-loxP SV40NLS-Zif268DBD-CRY2PHR	Benchmark for high mRuby2 expression (pTDH3)	This study
yMM1403	mRuby2 LOW	Mat alpha trp1Δ63 leu2Δ1::LEU2-pREV1-mRUBY2-tADH1 ura3-52 HO::S40NLS-VP16AD-CIB1 loxP-KlURA3-loxP SV40NLS-Zif268DBD-CRY2PHR	Benchmark for low mRuby2 expression (pREV1)	This study
yMM1444	mRuby2 MEDIUM	Mat alpha trp1Δ63 leu2Δ1::LEU2-pRPL18B-mRUBY2-tADH1 ura3-52 HO::S40NLS-VP16AD -CIB1 loxP-KlURA3-loxP SV40NLS-Zif268DBD-CRY2PHR	Benchmark for medium mRuby2 expression (pRPL18B)	This Study
yMM1458	yMA001	Matα trp1Δ63 leu2Δ1 ura3-52::pTEF1-SV40NLS-VP16AD-CIB1-tENO1-Scar1-pTEF1-SV40NLS-ZifDBDCRY2PHR-tSSA1-Scar2-pZF(3BS)-mRuby2-tADH1-ScarRE-scURA3	High/HighCIB1AD/ ZCRY2 expressing strain	This Study
yMM1459	yMA002	Matα trp1Δ63 leu2Δ1 ura3-52::pTEF1-SV40NLS-VP16AD-CIB1-tENO1-Scar1-pRPL18B-SV40NLS-ZifDBDCRY2PHR-tSSA1-Scar2-pZF(3BS)-mRuby2-tADH1-ScarRE-scURA3	High/Medium CIB1AD/ZCRY2 expressing strain	This Study
yMM1460	yMA003	Matα trp1Δ63 leu2Δ1 ura3-52::pTEF1-SV40NLS-VP16AD-CIB1-tENO1-Scar1-	High/Low CIB1AD/ZCRY2 expressing strain	This Study

		pRNR2-SV40NLS-ZifDBDCRY2PHR-tSSA1-Scar2-pZF(3BS)-mRuby2-tADH1-ScarRE-scURA3		
yMM1461	yMA004	Matα trp1Δ63 leu2Δ1 ura3-52::pRPL18B-SV40NLS-VP16AD-CIB1-tENO1-Scar1-pTEF1-SV40NLS-ZifDBDCRY2PHR-tSSA1-Scar2-pZF(3BS)-mRuby2-tADH1-ScarRE-scURA3	Medium/High CIB1AD/ZCRY2 expressing strain	This Study
yMM1462	yMA005	Matα trp1Δ63 leu2Δ1 ura3-52::pRPL18B-SV40NLS-VP16AD-CIB1-tENO1-Scar1-pRPL18B-SV40NLS-ZifDBDCRY2PHR-tSSA1-Scar2-pZF(3BS)-mRuby2-tADH1-ScarRE-scURA3	Medium/Medium CIB1AD/ZCRY2 expressing strain	This Study
yMM1463	yMA006	Matα trp1Δ63 leu2Δ1 ura3-52::pRPL18B-SV40NLS-VP16AD-CIB1-tENO1-Scar1-pRNR2-SV40NLS-ZifDBDCRY2PHR-tSSA1-Scar2-pZF(3BS)-mRuby2-tADH1-ScarRE-scURA3	Medium/Low CIB1AD/ZCRY2 expressing strain	This Study
yMM1464	yMA007	Matα trp1Δ63 leu2Δ1 ura3-52::pRNR2-SV40NLS-VP16AD-CIB1-tENO1-Scar1-pTEF1-SV40NLS-ZifDBDCRY2PHR-tSSA1-Scar2-pZF(3BS)-mRuby2-tADH1-ScarRE-scURA3	Low/High CIB1AD/ ZCRY2 expressing strain	This Study
yMM1465	yMA008	Matα trp1Δ63 leu2Δ1 ura3-52::pRNR2-SV40NLS-VP16AD-CIB1-tENO1-Scar1-pRPL18B-SV40NLS-ZifDBDCRY2PHR-tSSA1-Scar2-pZF(3BS)-mRuby2-tADH1-ScarRE-scURA3	Low/Medium CIB1AD/ZCRY2 expressing strain	This Study
yMM1466	yMA009	Matα trp1Δ63 leu2Δ1 ura3-52::pRNR2-SV40NLS-VP16AD-CIB1-tENO1-Scar1-pRNR2-SV40NLS-ZifDBDCRY2PHR-tSSA1-Scar2-pZF(3BS)-mRuby2-tADH1-ScarRE-scURA3	Low/Low CIB1AD/ZCRY2 expressing strain	This Study
yMM1467	yMA011	Matα trp1Δ63 leu2Δ1 ura3-52::pTEF1-SV40NLS-VP16AD-CIB1-tENO1-Scar1-pRPL18B-SV40NLS-ZifDBDCRY2PHR-tSSA1-Scar2-pZF(3BS)-mRuby2-tADH1-ScarRE-loxP-KlURA3-loxP	High/Medium CIB1AD/ZCRY2 expressing strain w/loxP-KlURA3	This Study
yMM1468	yMA014	Matα trp1Δ63 leu2Δ1 ura3-52::pRPL18B-SV40NLS-VP16AD-CIB1-tENO1-Scar1-pRPL18B-SV40NLS-ZifDBDCRY2PHR-tSSA1-Scar2-pZF(3BS)-mRuby2-tADH1-ScarRE-loxP-KlURA3-loxP	Medium/Medium CIB1AD/ZCRY2 expressing strain	This Study
yMM1472	yMA032	Matα trp1Δ63 leu2Δ1 ura3-52::pRPL18B-SV40NLS-VP16AD-CIB1-tENO1-Scar1-pRPL18B-SV40NLS-ZifDBDCRY2PHR-tSSA1-Scar2-pZF(3BS)-mRuby2-tADH1-ScarRE-loxPScar	Medium/Medium CIB1AD/ZCRY2 expressing strain	This Study
yMM1473	yMA037	Matα trp1Δ63 leu2Δ1 ura3-52::pTEF1-SV40NLS-VP16AD-CIB1-tENO1-Scar1-pRPL18B-SV40NLS-ZifDBDCRY2PHR-tSSA1-Scar2-spacer-ScarRE-scURA3	No fluorescence control for yMM1458	This Study
yMM1474	yMA038	Matα trp1Δ63 leu2Δ1 ura3-52::pTEF1-SV40NLS-VP16AD-CIB1-tENO1-Scar1-pRPL18B-SV40NLS-ZifDBDCRY2PHR-	Low mRuby2 fluorescence control for yMM1458	This Study

		tSSA1-Scar2-pREV1-mRUBY2-tADH1-ScarRE-scURA3		
yMM1475	yMA039	Matα trp1Δ63 leu2Δ1 ura3-52::pTEF1-SV40NLS- VP16AD-CIB1-tENO1-Scar1-pRPL18B-SV40NLS-ZifDBDCRY2PHR-tSSA1-Scar2-pRPL18B-mRUBY2-tADH1-ScarRE-scURA3	Medium mRuby2 fluorescence control for yMM1458	This Study
yMM1476	yMA040	Matα trp1Δ63 leu2Δ1 ura3-52::pTEF1-SV40NLS- VP16AD-CIB1-tENO1-Scar1-pRPL18B-SV40NLS-ZifDBDCRY2PHR-tSSA1-Scar2-pTDH3-mRUBY2-tADH1-ScarRE-scURA3	High mRuby2 fluorescence control for yMM1458	This Study
yMM1477	yMA041	Matα trp1Δ63 leu2Δ1 ura3-52::pRPL18B-SV40NLS- VP16AD-CIB1-tENO1-Scar1-pRPL18B-SV40NLS-ZifDBDCRY2PHR-tSSA1-Scar2-Spacer-ScarRE-scURA3	No fluorescence control for yMM1459	This Study
yMM1478	yMA042	Matα trp1Δ63 leu2Δ1 ura3-52::pRPL18B-SV40NLS- VP16AD-CIB1-tENO1-Scar1-pRPL18B-SV40NLS-ZifDBDCRY2PHR-tSSA1-Scar2-pREV1-mRUBY2-tADH1-ScarRE-scURA3	Low mRuby2 fluorescence control for yMM1459	This Study
yMM1479	yMA043	Matα trp1Δ63 leu2Δ1 ura3-52::pRPL18B-SV40NLS- VP16AD-CIB1-tENO1-Scar1-pRPL18B-SV40NLS-ZifDBDCRY2PHR-tSSA1-Scar2-pRPL18B-mRUBY2-tADH1-ScarRE-scURA3	Medium mRuby2 fluorescence control for yMM1459	This Study
yMM1480	yMA044	Matα trp1Δ63 leu2Δ1 ura3-52::pRPL18B-SV40NLS- VP16AD-CIB1-tENO1-Scar1-pRPL18B-SV40NLS-ZifDBDCRY2PHR-tSSA1-Scar2-pTDH3-mRUBY2-tADH1-ScarRE-scURA3	High mRuby2 fluorescence control for yMM1459	This Study

Supplemental Table 2: Primer used in this study

oMM	Alias	Sequence	Target	Purpose (Brief)
oMM0166	rev_pGal4AD-CIB1_check	aagtgaacttgcggggtttt	CIB1, CIB1N	Amplification /Sequencing
oMM0186	tADH1_rev	CCGGTAGAGGTGTGGTCAAT	tADH1	Sequencing
oMM0212	Forward_pGAL1	GTTTTCCCAGTCACGACGTT	pGAL1	Sequencing
oMM0214	Forward_pGAL1	ACGCTTAACTGCTCATTGCT	pGAL1	Sequencing
oMM0250	Lox_General_for	cgtacgctgcaggtcgac	loxP_KlURA3-loxP	Amplification
oMM0251	Lox_General_rev	cactatagggagaccggcag	loxP_KlURA3-loxP	Amplification
oMM0323	pRS415_for	cccagtcacgacgttgtaaaacg	pRS415	Sequencing
oMM0349	URA3_reverse	URA3	CCCTACACGTTCGCTATGCT	Sequencing
oMM0354	pADH1_forward	TCGTTGTTCCAGAGCTGATG	pADH1	Sequencing
oMM0383	CRY2_ZFBD_tem2_for	tgcggccgcaatacaatagctagcttcatgaagatggacaaaa	CRY2-tADH1	Cloning

oMM0384	CRY2_ZFBD_tem2_rev	ataagagctccatgccggtagaggtgt	CRY2-tADH1	Cloning
oMM0393	Seq_3	GTGAGCAGCTGCTGCTAATG	CRY2	Sequencing
oMM0399	For_Internal_CRY2	CAGTCTTGCTCGTTGGCATC	CRY2	Sequencing
oMM0400	For_GAL4AD_VP16AD_swap	tccaaaaaagaagagaaaggtcgaattgggtaccgccgccTCGGAGCTCCACTTAGACGG	GAL4AD,VP16	Yeast Recombinational Cloning
oMM0401	Rev_GAL4AD_VP16AD_swap	cgctagcttcggcgctcgccctatagtgagtcgtattaaaCCCACCGTACTCGTCAATTC	GAL4AD,VP16	Yeast Recombinational Cloning
oMM0402	GAL4AD_forward	GCGTATAACGCGTTTGGAAT	GAL4AD	Colony PCR, Sequencing
oMM0403	CIB1_reverse	CGGAAAGAACCATTTCAGGA	CIB1	Colony PCR, Sequencing
oMM0404	VP16AD_forward	TTTCGATCTGGACATGTTGG	VP16	Colony PCR, Sequencing
oMM0405	pADH1_seq	TTCCTTCATTCACGCACACT	pyADH1	Sequencing
oMM0407	Rev_ZFBD-CRY2 linker3	ataagctagcACCTGTATGGATTTTGGTATG	FLAG(3X)-NLS-Zif268DBD	Cloning
oMM0408	Rev_ZFBD-CRY2 linker4pro	ataagctagctggACCTGTATGGATTTTGGTATG	FLAG(3X)-NLS-Zif268DBD	Cloning
oMM0409	Rev_ZFBD-CRY2 linker10	ataagctagctccgccaccactgccacctccACCTGTATGGATTTTGGTATG	FLAG(3X)-NLS-Zif268DBD	Cloning
oMM0413	ZIF1_Top	ggccgcGCGTGGGCGt	Zif268 Binding Sites	Cloning of ZF BS
oMM0414	ZIF1_Bottom	ctagaCGCCCACGCgc	Zif268 Binding Sites	Cloning of ZF BS
oMM0415	Zif3_Top	ggccgcGCGTGGGCGAGCGTGGGCGAGCGTGGGCGt	Zif268 Binding Sites	Cloning of ZF BS
oMM0416	Zif3_Bottom	ctagaCGCCCACGCTCGCCCACGCTCGCCCACGCgc	Zif268 Binding Sites	Cloning of ZF BS
oMM0417	Zif3_overlap2_top	ggccgcGCGTGGGCGTGGGCGGCGTGGGCGt	Zif268 Binding Sites	Cloning of ZF BS
oMM0418	Zif3_overlap2_bottom	ctagaCGCCCACGCCGCCCACGCCCACGCgc	Zif268 Binding Sites	Cloning of ZF BS
oMM0419	Zif3_invert2_top	ggccgcGCGTGGGCGAGCGGGTGCGt	Zif268 Binding Sites	Cloning of ZF BS
oMM0420	Zif3_intert2_bottom	ctagaCGCACCCGCTCGCCCACGCgc	Zif268 Binding Sites	Cloning of ZF BS
oMM0421	XmaI-5'-Venus	ttatcccgggatgtctaaaggtgaagaattat	Venus	Cloning
oMM0423	AscI-3'-Venus	ataaggcgcgccCTAttatttgtacaattcatccatac	Venus	Cloning
oMM0456	ZCRY ADH 5p (NgoMIV)	ttatgccggcCAACTTCTTTTCTTTTTTTTTCT	pADH1	Cloning
oMM0457	ZCRY ADH3p (spacer-not1)	gcggccgcaggcttgcttcaagcttGGAGTTGATTGTATGCTTGG	pADH1	Cloning
oMM0458	NLS 5p (ADH spacer homology-NotI)	caagcctgcggccgcATGGATTACAAGGATGACGA	FLAG(3X)-NLS-Zif268DBD	Cloning
oMM0481	Zif 3corrected_top	ggccgcGCGTGGGCGTGCGTGGGCGTGCGTGGGCGt	Zif268 Binding Sites	Cloning of ZF BS
oMM0482	Zif 3corrected_bottom	ctagaCGCCCACGCACGCCCACGCACGCCCACGCgc	Zif268 Binding Sites	Cloning of ZF BS

oMM0483	Zif 4_top	ggccgcGCGTGGGCGTGCGTGGGCGTGCGTGGGCGTGCGTGGGCGt	Zif268 Binding Sites	Cloning of ZF BS
oMM0484	Zif 4_bottom	ctagaCGCCCACGCACGCCCACGCACGCCCACGCACGCCCACGCgc	Zif268 Binding Sites	Cloning of ZF BS
oMM0485	Zif opp3_top	ggccgcCGCCCACGCACGCCCACGCACGCCCACGCt	Zif268 Binding Sites	Cloning of ZF BS
oMM0486	Zif opp3_bottom	ctagaGCGTGGGCGTGCGTGGGCGTGCGTGGGCGgc	Zif268 Binding Sites	Cloning of ZF BS
oMM0535	ZCRY2_promswap_noATGmut_for	CTGCACAATATTTCAAGCTATACCAAGCATACAATCAACTATCTCATATACAATGGATTA	ZDBD-CRY2	Yeast Recombinational Cloning
oMM0536	ZCRY2_promswap_noATGmut_rev	ATCGTCCTTATAGTCCCCGGTCTTATCGTCGTCATCCTTGTAATCCATTGTATATGAGAT	ZDBD-CRY2	Yeast Recombinational Cloning
oMM0538	ZCRY2_promswap_insertPACI_for	CTGCACAATATTTCAAGCTATACCAAGCATACAATCAACTttaattaaATGGATTACAAG	ZDBD-CRY2	Yeast Recombinational Cloning
oMM0539	ZCRY2_promswap_insertPACI_rev	CATCATCGTCCTTATAGTCCCCGGTCTTATCGTCGTCATCCTTGTAATCCATTTAATTAA	ZDBD-CRY2	Yeast Recombinational Cloning
oMM0547	pMM0159_exCIB1_for	AGATCTTTAATACGACTCACTATAGGGCGAcatcgagctcgagctgcagatgaatcgtag	CIB1	Yeast Recombinational Cloning
oMM0548	pMM0159_exCIB1_rev	CTACGATTCATCTGCAGCTCGAGCTCGATGTCGCCCTATAGTGAGTCGTATTAAAGATCT	CIB1	Yeast Recombinational Cloning
oMM0549	pMM0160_exCRY2_for	AACAAAGGTCAAAGACAGTTGACTGTATCGggcaagtgcacaaacaatacttaaataaat	CRY2	Yeast Recombinational Cloning
oMM0550	pMM0160_exCRY2_rev	ATTTATTTAAGTATTGTTTGTGCACTTGCCCGATACAGTCAACTGTCTTTGACCTTTGTT	CRY2	Yeast Recombinational Cloning
oMM0551	SV40NLS_YRC_Forward	CTGCACAATATTTCAAGCTATACCAAGCATACAATCAACTATCTCATATACAATGGCCCC	Zif268DBD-CRY2	Yeast Recombinational Cloning
oMM0552	SV40NLS_YRC_Reverse	CCCCGTGAATACCAACCTTCCTCTTCTTCTTGGGGGCCATTGTATATGAGAT	Zif268DBD-CRY2	Yeast Recombinational Cloning
oMM0553	SV40NLS_cterm_YRC_Forward	TTACTACAAGTTTGGGAAAAAATGGTTGCAAAGCCCCCAAGAAGAAGAGGAAGGTTGTGA	CRY2, SV40NLS	Yeast Recombinational Cloning
oMM0554	SV40NLS_cterm_YRC_Reverse	TTATTTAATAATAAAAATCATAAATCATAAGAAATTCGCCTCACAACCTTCCTCTTCTTC	CRY2, SV40NLS	Yeast Recombinational Cloning
oMM0562	CRY2->CRY2PHR_forward_YRC	TTCAAGAACCCGTGAAGCACAGATCATGATCGGAGCAGCAgcccgggtcgacctgcagcc	CRY2, CRY2PHR	Yeast Recombinational Cloning
oMM0563	CRY2->CRY2PHR_reverse_YRC	AAAAATCATAAATCATAAGAAATTCGCCCGGAATTAGCTTGGCTGCAGGTCGACCCGGGC	CRY2, CRY2PHR	Yeast Recombinational Cloning
oMM0564	CRY2->CRY2PHR-SV40NLS_forward_YRC	GAACCCGTGAAGCACAGATCATGATCGGAGCAGCAGCCCCCAAGAAGAAGAGGAAGGTTG	CRY2, CRY2PHR	Yeast Recombinational Cloning
oMM0565	CRY2->CRY2PHR-SV40NLS_reverse_YRC	AAAAATCATAAATCATAAGAAATTCGCCCGGAATTAGCTTCAACCTTCCTCTTCTTCTTG	CRY2, CRY2PHR	Yeast Recombinational Cloning
oMM0566	SV40_NoFlag_NotI_KpnI_forward	ggccgcATGGCtCCCAAGAAGAAGAGGAAGGTTGGTATTCACGGGggtac	SV40	Cloning
oMM0567	SV40_NoFlag_NotI_KpnI_reverse	cCCCGTGAATACCAACCTTCCTCTTCTTCTTGGGaGCCATgc	SV40	Cloning

oMM0568	Histone 2B NLS w/GlyPro Linker 4x_NotI_KpnI_forward	ggccgcATGGGTAAGAAGAGATCTAAGGCTAAGGGACCAGGTCCTGGACCAGGACCTGGCGGAGGCggtac	H2B NLS	Cloning
oMM0569	Histone 2B NLS w/GlyPro Linker 4x_NotI_KpnI_reverse	cGCCTCCGCCAGGTCCTGGTCCAGGACCTGGTCCCTTAGCCTTAGATCTCTTCTTACCCATgc	H2B NLS	Cloning
oMM0684	KlURA3_rev	KlURA3	GAATCAGCGCTCCCCATTAA	Sequencing
oMM0776	pZF Part Forward	GCATCGTCTCATCGGTCTCAAACGcgaggcaagctaaacagat	pZF	Cloning
oMM0870	Gene_plasmid_for	CGGATGACACGAACTCACGA	ConE	Sequencing
oMM0871	Gene_plasmid_rev	GGTTCCGGCTGTCTTGCTTA	ConS	Sequencing
oMM0991	loxP-KlURA3_for	GCATCGTCTCATCGGTCTCATACAGCAGGTCGACAACCCTTA	loxP-KlURA3-loxP	Cloning
oMM0992	loxP-KlURA3_rev	ATGCCGTCTCAGGTCTCAACTCAGTGGATCTGATATCACCTAATAA	loxP-KlURA3-loxP	Cloning
oMM1003	SV40NLS'_ZiF_CRY2PHR forward	GCATCGTCTCATCGGTCTCATATGgcccccaagaagaagaggaa	SV40NLS-Zif268DBD-CRY2PHR	Cloning
oMM1039	pZiF_Rev	ATGCCGTCTCAGGTCTCACATAgtaccatatagttttttctccttgac	pZF	Cloning
oMM1065	pZiF_F	TTGAAGTGCGcgCGCGCGTGGG	pZF(3BS)	Site-directed mutagenesis
oMM1066	pZiF_R	TATAGCAATGAGCAGTTAAGCG	pZF(3BS)	Site-directed mutagenesis
oMM1067	pCIB1_F	TGTACGGTGActCGACGGTGGAAG	CIB1	Site-directed mutagenesis
oMM1068	pCIB1_R	TCATCGGAAGATTCAAAC	CIB1	Site-directed mutagenesis
oMM1069	pCRY2_1_F	GTTTAGAAGActCCTAAGGATTGAGGATAATC	CRY2PHR	Site-directed mutagenesis
oMM1070	pCRY2_1_R	CAAACTATAGTCTTTTTGTCC	CRY2PHR	Site-directed mutagenesis
oMM1071	pCRY2_2_F	TAGAGCTTGGagTCCAGGATGG	CRY2PHR	Site-directed mutagenesis
oMM1072	pCRY2_2_R	GTTAACAACGCATTGCTC	CRY2PHR	Site-directed mutagenesis
oMM1073	CRY2_REV	ATGCCGTCTCAGGTCTCAGGATCCtttgcaaccatttttcccaaac	CRY2	Cloning
oMM1074	CRY2PHR_REV	ATGCCGTCTCAGGTCTCAGGATCCCCGGGCtgctgctccgatcatgat	SV40NLS-Zif268DBD-CRY2PHR	Cloning
oMM1124	pMM0281_mutate_for	TGTACGGTGAaACGACGGTGG	CIB1	Site-directed mutagenesis
oMM1125	pMM0281_mutate_rev	TCATCGGAAGATTCAAACCGGC	CIB1	Site-directed mutagenesis
oMM1126	pMM0515_mutate_for	GTTTAGAAGAgatCTAAGGATTGAGGATAATCC	CRY2	Site-directed mutagenesis
oMM1127	pMM0515_mutate_rev	CAAACTATAGTCTTTTTGTCC	CRY2	Site-directed mutagenesis
oMM1137	pMM0491_rev	TCACAGGCTTAGGTGGATCT	ConR1	Sequencing
oMM1138	pMM0532_Rev	CATGATGACCGCACTGACTG	ConL1	Sequencing
oMM1141	pMM0537_rev	CGGATCACCGTACTATGTGTGA	ConR2	Sequencing

oMM1142	pMM0533_fwd	ACAGGAGCAAGCGCGATAGG	ConL2	Sequencing
oMM1146	pMM0534_fwd	ATGCCGATGCACGCTCATAT	ConL3	Sequencing
oMM1149	pMM0539_rev	GTTAGCCTGCCTCGATTTCA	ConR4	Sequencing
oMM1150	pMM0535_fwd	GATGACGTAACACCGAGCCA	ConL4	Sequencing
oMM1174	tENO1_for	cgcgtgtatccgcccgc	tENO1	Sequencing
oMM1175	tSSA1_for	gccaattggtgcggcaattg	tSSA1	Sequencing
oMM1176	scURA3_rev	ggactaggatgagtagcagcacgttcc	scURA3	Sequencing
oMM1177	scURA3_5'	gtggctgtggtttcagggtccat	scURA3	Sequencing
oMM1220	tADH1_forward	TGCAAATCGCTCCCCATT	tADH1	Sequencing

Supplemental Table 3: Plasmids used in this study

ID	Alias	Gene(s) or Insert Name	Yeast Marker	Bacterial Resistance	Source/ Reference
pMM0006	pRS414	TRP1 CEN6 ARS4	TRP1	Ampicillin	Sikorski and Heiter, 1989
pMM0008	pRS416	URA3 CEN6 ARS4	URA3	Ampicillin	Sikorski and Heiter, 1989
pMM0159	pGal4AD-CIB1	pscADH1-GAL4AD-CIB1-tscADH1	LEU2	Ampicillin	AddGene #28245; Kennedy, et al 2010
pMM0160	pGal4BD-CRY2	pscADH1-GAL4BD-CRY2-tscADH1	TRP1	Kanamycin	AddGene #28243; Kennedy, et al 2010
pMM0162	bSR97	His3 Pfus1-yEVenus pSTL1-dsRED	HIS3	Ampicillin	Ramanathan Lab, Unpublished
pMM0223	pKT90	pFA6a–link–yEVenus–SpHIS5	SpHIS5	Ampicillin	Sheff, MA and KT Thorn 2004 Yeast
pMM0281	SV40NLS-VP16AD-CIB1	pscADH1-SV40NLS-VP16AD-CIB1-tscADH1	LEU2	Ampcillin	Melendez, et al 2014
pMM0282	pFLAG(3X)-NLS-ZIF268DBD-CRY2 (L10) TRP1	pscADH1-FLAG(3X)-NLS-ZIF268DBD-CRY2 (L10)-tscADH1 TRP1	TRP1	Ampcillin	This study
pMM0283	pFLAG(3X)-NLS-ZIF268DBD-CRY2 (L4) TRP1	pscADH1-FLAG(3X)-NLS-ZIF268DBD-CRY2 (L4)-tscADH1 TRP1	TRP1	Ampcillin	This study
pMM0284	FLAG(3X)-NLS-ZIF268DBD-CRY2 (L3)	pscADH1-pFLAG(3X)-NLS-ZIF268DBD-CRY2 (L3)-tscADH1 TRP1	TRP1	Ampcillin	This study
pMM0285	pZF(1BS)	pZF(1BS)-yEVenus	URA3	Ampcillin	This study
pMM0286	pZF(2BS)	pZF(2BS)-yEVenus	URA3	Ampcillin	This study
pMM0287	pZF(3BS)	pZF(3BS)-yEVenus	URA3	Ampcillin	This study

pMM0288	pZF(3BS*)	pZF(3BS*)-yEVenus	URA3	Ampcillin	This study
pMM0289	pZF(4BS*)	pZF(4BS*)-yEVenus	URA3	Ampcillin	This study
pMM0290	pZF(3BSopp)	pZF(3BSopp)-yEVenus	URA3	Ampcillin	This study
pMM0296	pSH65	pGAL1-CRE PheloR	PHLEO	Ampicillin	Botstein Lab; Gueldener, et al 2002
pMM0301	pGAL1-VENUS	pGAL1-yEVenus CEN scURA3	URA3	Ampicillin	This study
pMM0305	pADH1(native)-FLAG(3X)-Zif268DBD-CRY2	pADH1(native)-FLAG(3X)-Zif268DBD-CRY2 TRP1 CEN	TRP1	Ampicillin	This study
pMM0306	pADH1_PacI-FLAG(3X)-Zif268DBD-CRY2	pADH1_PacI-FLAG(3X)-Zif268DBD-CRY2 TRP1 CEN	TRP1	Ampicillin	This study
pMM0313	SV40NLS-Zif268DBD-CRY2 (L3)	pscADH1-SV40NLS-Zif268DBD-CRY2 (L3)-tADH1 TRP CEN	TRP1	Ampicillin	This study
pMM0314	H2BNLS-Zif268DBD-CRY2 (L3)	pscADH1-H2BNLS-Zif268DBD-CRY2 (L3)-tADH1 TRP CEN	TRP1	Ampicillin	This study
pMM0315	pGal4AD	GAL4AD	LEU2	Ampicillin	This study
pMM0316	pGal4BD	GAL4BD	TRP1	Kanamycin	This study
pMM0317	NLS-ZIF268DBD-CRY2 (L3)	pscADH-SV40NLS-Zif268DBD-CRY2 (L3)-tscADH1 scTRP1	TRP1	Ampicillin	This study
pMM0318	FLAG(3X)-SV40NLS-Zif-ZCRY2-SV40NLS	pscADH-FLAG(3X)-SV40NLS-Zif268DBD-CRY2-SV40NLS-tscADH1 scTRP1	TRP1	Ampicillin	This study
pMM0319	FLAG(3X)-SV40NLS-Zif-ZCRYPHR	pscADH-FLAG(3X)-SV40NLS-Zif-ZCRYPHR(L3)-tscADH1 scTRP1	TRP1	Ampicillin	This study
pMM0320	SV40NLS-Zif268DBD-CRY2PHR	pscADH1-SV40NLS-ZIF268DBD-CRY2PHR (L3)-tscADH1 TRP1	TRP1	Ampicillin	This Study
pMM0321	FLAG(3X)-Zif268DBD-CRY2PHR-SV40NLS	pscADH-FLAG(3X)-SV40NLS-Zif-ZCRY2PHR-SV40NLS-tscADH1 scTRP1	TRP1	Ampicillin	This Study
pMM0326	pUG72	loxP-KlURA3-loxP	NA	Ampicillin	Gueldener, *et al* 2002 [14]
pMM0452	pYTK001	None	NA	Chloramphenicol	AddGene #65108; Lee, et al 2015
pMM0453	pYTK009	pscTDH3	NA	Chloramphenicol	AddGene #65116; Lee, et al 2015
pMM0454	pYTK017	pscRPL18B	NA	Chloramphenicol	AddGene #65214; Lee, et al 2015
pMM0455	pYTK027	pscREV1	NA	Chloramphenicol	AddGene #65134; Lee, et al 2015
pMM0456	pYTK034	mRUBY2	NA	Chloramphenicol	AddGene #65141; Lee, et al 2015

pMM0457	pYTK053	tADH1	NA	Chloramphenicol	AddGene #65160; Lee, et al 2015
pMM0458	pYTK096	5' URA3 homology-ConLS'-GFP dropout-ConRE' URA3 URA3 3'-homology KanR-ColE1	scURA3	Kanamycin	Addgene #65203; Lee, et al 2015
pMM0477	pYTK008	ConLS'	NA	Chloramphenicol	Addgene #65115; Lee et al 2015
pMM0478	pYTK073	ConRE'	NA	Chloramphenicol	Addgene #65180; Lee, et al 2015
pMM0479	pYTK075	LEU2	LEU2	Chloramphenicol	AddGene #65182; Lee, et al 2015
pMM0480	pYTK087	LEU2 3' homology	NA	Chloramphenicol	AddGene #65194; Lee, et al 2015
pMM0481	pYTK090	KanR-ColE1 mRFP1	NA	Kanamycin	AddGene #65197; Lee, et al 2015
pMM0482	pYTK093	LEU2 5' homology	NA	Chloramphenicol	AddGene #65200; Lee et al 2015
pMM0489	pYTK002	ConLS	NA	Chloramphenicol	AddGene #65109; Lee, et al 2015
pMM0490	pYTK047	sfGFP dropout	NA	Chloramphenicol	AddGene #65154; Lee, et al 2015
pMM0491	pYTK067	ConR1	NA	Chloramphenicol	AddGene #65174; Lee, et al 2015
pMM0494	yOTK_LEU2entry	LEU2 5' homology-ConLS-sfGFP dropout-ConR1-LEU2 3' homology	LEU2	Kanamycin	This study
pMM0495	pTDH3-mRUBY2	LEU2 5' homology-ConLS-pTDH3-mRUBY2-tADH1-ConR1-LEU2 3' homology	LEU2	Kanamycin	This study
pMM0496	pRPL18B-mRUBY2	LEU2 5' homology-ConLS-pRPL18B-mRUBY2-tADH1-ConR1-LEU2 3' homology	LEU2	Kanamycin	This study
pMM0497	pREV1-mRUBY2	LEU2 5' homology-ConLS-pREV1-mRUBY2-tADH1-ConR1-LEU2 3' homology	LEU2	Kanamycin	This study
pMM0515	NLS-ZIF268DBD-CRY2 (L3)	SV40NLS-Zif268DBD-CRY2 (L3) CEN scTRP1	TRP1	Ampicillin	This study
pMM0518	pZF(3BS)-Venus	KanMXrev-pZF(3BS)-Venus	KanMX	Ampicillin	This study
pMM0519	loxP-KlURA3-loxP	loxP-KlURA3-loxP	KlURA3	Chloramphenicol	This study

pMM0520	CIB1VP16	SV40NLS-VP16AD-CIB1 LEU2 2µ	LEU2	Ampicillin	This study
pMM0521	NLS-ZIF268DBD-CRY2 (L3)	SV40NLS-Zif268DBD-CRY2 (L3) scTRP1	TRP1	Ampicillin	This study
pMM0522	pYTK013	pTEF1	NA	Chloramphenicol	Addgene #65120; Lee, et al 2015
pMM0526	pYTK086	*URA3* 3' Homology	NA	Chloramphenicol	AddGene #65193; Lee, et al 2015
pMM0527	pYTK092	*URA3* 5' Homology	NA	Chloramphenicol	AddGene #65199; Lee, et al 2015
pMM0528	pZF(3BS)	pZF(3BS)	NA	Chloramphenicol	This study
pMM0529	SV40NLS-ZiF268-CRY2	SV40NLS-ZiF268DBD-CRY2	NA	Chloramphenicol	This study
pMM0530	SV40NLS-ZiF268-CRY2PHR	SV40NLS-ZiF268DBD-CRY2PHR	NA	Chloramphenicol	This study
pMM0531	SV40NLS-VP16-CIB1	SV40NLS-VP16AD-CIB1	NA	Chloramphenicol	This study
pMM0532	pYTK003	ConL1	NA	Chloramphenicol	AddGene #65110; Lee, et al 2015
pMM0533	pYTK004	ConL2	NA	Chloramphenicol	Addgene #65111; Lee, et al 2015
pMM0537	pYTK068	ConR2	NA	Chloramphenicol	Addgene #65175; Lee, et al 2015
pMM0541	pYTK072	ConRE	NA	Chloramphenicol	Addgene #65179; Lee, et al 2015
pMM0542	pYTK051	tENO1	NA	Chloramphenicol	Addgene #65158; Lee, et al 2015
pMM0543	pYTK052	tSSA1	NA	Chloramphenicol	Addgene #65159; Lee, et al 2015
pMM0547	pYTK048	Spacer	NA	Chloramphenicol	Addgene Plasmid #65155; Lee, et al 2015
pMM0553	pZF(3BS)-mRUBY2 @ LEU2	Leu2 5' homology-pZF(3BS)-mRuby2-tADH1-Con1-LEU2-Leu2 3' homology	LEU2	Kanamycin	This study
pMM0554	pTDH3-VP16AD-CIB1 @ LEU2	Leu2 5' homology-pTDH3-SV40NLS-VP16AD-CIB1-tADH1-Con1-LEU2-Leu2 3' homology	LEU2	Kanamycin	This study

pMM0556	pYTK095	sfGFP AmpR-ColE1	NA	Ampicillin	AddGene #65202; Lee, et al 2015
pMM0557	pTDH3-ZCRY2 @ LEU2	Ura3 3' homology-pTDH3-SV40NLS-ZiF268-CRY2-tADH1-URA3-Ura3 5' homology	URA3	Kanamycin	This study
pMM0558	pTHD3-ZCRY2PHR2 @ LEU2	Ura3 3' homology-pTDH3-SV40NLS-ZiF268-CRY2PHR-tADH1-URA3-Ura3 5' homology	URA3	Kanamycin	This study
pMM0562	pYTK023	pscRNR2	NA	Chloramphenicol	Addgene #65130; Lee, et al 2015
pMM0617	pCS0010, A, loxP entry vector	KanR-ColE1 URA 5' homology-ConLS'-sfGFP dropout-ConRE'-loxP-KlURA3-loxP-URA3 5' homology	KlURA3	Kanamycin	This study
pMM0619	pCS0012, C, C3F spacer, background fluorescence control	ConL2-Spacer-ConRE-AmpR-Col-E1	NA	Ampicillin	This study
pMM0620	pCS0013, D, C1_pTEF1_CIB1	ConLS_pTEF1-SV40NLS-VP16AD-CIB1-tENO1-ConR1 AmpR Col-E1	NA	Ampicillin	This study
pMM0621	pCS0014, E, C1_pRPL18B_CIB1	ConLS_pRPL18B-SV40NLS-VP16AD-CIB1-tENO1-ConR1 AmpR Col-E1	NA	Ampicillin	This study
pMM0622	pCS0015, F, C2_pTEF1_CRY2PHR	ConL1-pTEF1-SV40NLS-ZiF268DBD-CRY2PHR-tSSA1-ConR2 AmpR-ColE1	NA	Ampicillin	This study
pMM0623	pCS0016, G, C2_pRPL18B_CRY2phr	ConL1-pRPL18B-SV40NLS-ZiF268DBD-CRY2PHR-tSSA1-ConR2 AmpR-ColE1	NA	Ampicillin	This study
pMM0624	pCS0017, H, C3F_pZiF_mRuby2	ConL2-pZF(3BS)-mRUBY2-tADH1-ConRE AmpR-ColE1	NA	Ampicillin	This study
pMM0625	pCS0018, I, C3F_pREV1_mRuby2	ConL2-pREV1-mRUBY2-tADH1-ConRE AmpR-ColE1	NA	Ampicillin	This study
pMM0626	pCS0019, J, C3F_pRPL18B_mRuby2	ConL2-pRPL18B-mRUBY2-tADH1-ConRE AmpR-ColE1	NA	Ampicillin	This study
pMM0627	pCS0020, K, C3F_pTDH3_mRuby2	ConL2-pTDH3-mRUBY2-tADH1-ConRE AmpR-ColE1	NA	Ampicillin	This study
pMM0628	pCS0021, L, C1_pRNR2_CIB1	ConLS_pRNR2-SV40NLS-VP16AD-CIB1-tENO1-ConR1 AmpR Col-E1	NA	Ampicillin	This study
pMM0629	pCS0022, M, C2_pRNR2_CRY2PHR	ConL1-pRNR2-SV40NLS-ZiF268DBD-CRY2PHR-tSSA1-ConR2 AmpR-ColE1	NA	Ampicillin	This study
pMM0637	pCS0030, C1_pTEF1-CIB1 C2_pTEF1-CRY2PHR C3F_pZIF-mRuby2	5' URA3 homology-pTEF1-SV40NLS-VP16AD-CIB1-tENO1-pTEF1-SV40NLS-ZiF268DBD-CRY2PHR-tSSA1-pZF(3BS)-mRUBY2-tADH1-URA3 URA3 3'-homology KanR-ColE1	scURA3	Kanamycin	This study
pMM0638	pCS0031, C1_pTEF1-CIB1 C2_pRPL18B-CRY2PHR C3F_pZIF-mRuby2	5' URA3 homology-pTEF1-SV40NLS-VP16AD-CIB1-tENO1-pRPL18B-SV40NLS-ZiF268DBD-CRY2PHR-tSSA1-pZF(3BS)-mRUBY2-tADH1-URA3 URA3 3'-homology KanR-ColE1	scURA3	Kanamycin	This study
pMM0639	pCS0032, C1_pTEF1-CIB1 C2_pRNR2-	5' URA3 homology-pTEF1-SV40NLS-VP16AD-CIB1-tENO1-pRNR2-SV40NLS-ZiF268DBD-CRY2PHR-	scURA3	Kanamycin	This study

	CRY2PHR2 C3F_pZIF-mRuby2	tSSA1-pZF(3BS)-mRUBY2-tADH1-URA3 URA3 3'-homology KanR-ColE1			
pMM0640	pCS0033, C1_pRPL18B-CIB1 C2_pTEF1-CRY2PHR C3F_pZIF-mRuby2	5' URA3 homology-pRPL18B-SV40NLS-VP16AD-CIB1-tENO1-pTEF1-SV40NLS-ZiF268DBD-CRY2PHR-tSSA1-pZF(3BS)-mRUBY2-tADH1-URA3 URA3 3'-homology KanR-ColE1	scURA3	Kanamycin	This study
pMM0641	pCS0034, C1_pRPL18B-CIB1 C2_pRPL18B-CRY2PHR C3F_pZIF-mRuby2	5' URA3 homology-pRPL18B-SV40NLS-VP16-CIB1-tENO1-pRPL18B-SV40NLS-ZiF268DBD-CRY2PHR-tSSA1-pZF(3BS)-mRUBY2-tADH1-URA3 URA3 3'-homology KanR-ColE1	scURA3	Kanamycin	This study
pMM0642	pCS0035, C1_pRPL18B-CIB1 C2_pRNR2-CRY2PHR2 C3F_pZIF-mRuby2	5' URA3 homology-pRPL18B-SV40NLS-VP16AD-CIB1-tENO1-pRNR2-SV40NLS-ZiF268DBD-CRY2PHR-tSSA1-pZF(3BS)-mRUBY2-tADH1-URA3 URA3 3'-homology KanR-ColE1	scURA3	Kanamycin	This study
pMM0643	pCS0036, C1_pRNR2-CIB1 C2_pTEF1-CRY2PHR C3F_pZIF-mRuby2	5' URA3 homology-pRNR2-SV40NLS-VP16AD-CIB1-tENO1-pTEF1-SV40NLS-ZiF268DBD-CRY2PHR-tSSA1-pZF(3BS)-mRUBY2-tADH1-URA3 URA3 3'-homology KanR-ColE1	scURA3	Kanamycin	This study
pMM0644	pCS0037, C1 pRNR2-CIB1 C2_pRPL18B-CRY2PHR C3F_pZIF-mRuby2	5' URA3 homology-pRNR2-SV40NLS-VP16AD-CIB1-tENO1-pRPL18B-SV40NLS-ZiF268DBD-CRY2PHR-tSSA1-pZF(3BS)-mRUBY2-tADH1-URA3 URA3 3'-homology KanR-ColE1	scURA3	Kanamycin	This study
pMM0645	pCS0038, C1_pRNR2-CIB1 C2_pRNR2-CRY2-PHR2 C3F_pZIF-mRuby2	5' URA3 homology-pRNR2-SV40NLS-VP16-CIB1-tENO1-pRNR2-SV40NLS-ZiF268DBD-CRY2PHR-tSSA1-pZF(3BS)-mRUBY2-tADH1-URA3 URA3 3'-homology KanR-ColE1	scURA3	Kanamycin	This study
pMM0646	pCS0040, C1_pTEF1-CIB1 C2 pRPL18B-CRY2PHR C3F_pZIF-mRuby2	KanR-ColE1 URA 5' homology-pTEF1-SV40NLS-VP16AD-CIB1-tENO1--pRPL18B-SV40NLS-ZiF268DBD-CRY2PHR-tSSA1--pZF(3BS)-mRUBY2-tADH1--loxP-KlURA3-loxP-URA3 3' homology	KlURA3	Kanamycin	This study
pMM0647	pCS0043, C1_pRPL18B-CIB1 C2_pRPL18B-CRY2PHR C3F_pZIF-mRuby2	KanR-ColE1 URA 5' homology-pRPL18B-SV40NLS-VP16AD-CIB1-tENO1--pRPL18B-SV40NLS-ZiF268DBD-CRY2PHR-tSSA1--pZF(3BS)-mRUBY2-tADH1--loxP-KlURA3-loxP-URA3 3' homology	KlURA3	Kanamycin	This study
pMM0648	pCS0048, C1_pTEF1-CIB1 C2_pRPL18B-CRY2PHR C3F_spacer	5' URA3 homology-pTEF1-SV40NLS-VP16AD-CIB1-tENO1-pRPL18B-SV40NLS-ZiF268DBD-CRY2PHR-tSSA1-Spacer-URA3 URA3 3'-homology KanR-ColE1	scURA3	Kanamycin	This study
pMM0649	pCS0049, C1_pTEF1-CIB1 C2_pRPL18B-CRY2PHR C3F_pREV1-mRuby2	5' URA3 homology-pTEF1-SV40NLS-VP16AD-CIB1-tENO1-pRPL18B-SV40NLS-ZiF268DBD-CRY2PHR-tSSA1-pREV1-mRUBY2-tADH1-URA3 URA3 3'-homology KanR-ColE1	scURA3	Kanamycin	This study
pMM0650	pCS0050, C1 pTEF1-CIB1 C2_pRPL18B-CRY2PHR C3F_pRPL18B-mRuby2	5' URA3 homology-pTEF1-SV40NLS-VP16AD-CIB1-tENO1-pRPL18B-SV40NLS-ZiF268DBD-CRY2PHR-tSSA1-pRPL18B-mRUBY2-tADH1-URA3 URA3 3'-homology KanR-ColE1	scURA3	Kanamycin	This study
pMM0651	pCS0051, C1_pTEF1-CIB1 C2_pRPL18B-	5' URA3 homology-pTEF1-SV40NLS-VP16AD-CIB1-tENO1-pRPL18B-	scURA3	Kanamycin	This study

	CRY2PHR C3F_pTDH3-mRuby2	SV40NLS-ZiF268DBD-CRY2PHR-tSSA1-pTDH3-mRUBY2-tADH1-URA3 URA3 3'-homology KanR-ColE1			
pMM0652	pCS0052, C1_pRPL18B-CIB1 C2_pRPL18B-CRY2PHR C3F_spacer	5' URA3 homology-pRPL18B-SV40NLS-VP16AD-CIB1-tENO1-pRPL18B-SV40NLS-ZiF268DBD-CRY2PHR-tSSA1-Spacer-URA3 URA3 3'-homology KanR-ColE1	scURA3	Kanamycin	This study
pMM0653	pCS0053, C1_pRPL18B-CIB1 C2_pRPL18B-CRY2PHR C3F_pREV1-mRuby2	5' URA3 homology-pRPL18B-SV40NLS-VP16AD-CIB1-tENO1-pRPL18B-SV40NLS-ZiF268DBD-CRY2PHR-tSSA1-pREV1-mRUBY2-tADH1-URA3 URA3 3'-homology KanR-ColE1	scURA3	Kanamycin	This study
pMM0654	pCS0054, C1_pRPL18B-CIB1 C2_pRPL18B-CRY2PHR C3F_pRPL19B-mRuby2	5' URA3 homology-pRPL18B-SV40NLS-VP16AD-CIB1-tENO1-pRPL18B-SV40NLS-ZiF268DBD-CRY2PHR-tSSA1-pRPL18B-mRUBY2-tADH1-URA3 URA3 3'-homology KanR-ColE1	scURA3	Kanamycin	This study
pMM0655	pCS0055, C1_pRPL18B-CIB1 C2_pRPL18B-CRY2PHR C3F_pTDH3-mRuby2	5' URA3 homology-pRPL18B-SV40NLS-VP16AD-CIB1-tENO1-pRPL18B-SV40NLS-ZiF268DBD-CRY2PHR-tSSA1-pTDH3-mRUBY2-tADH1-URA3 URA3 3'-homology KanR-ColE1	scURA3	Kanamycin	This study
pMM0656	pCS0056	ConL1-pTEF1-SV40NLS-ZiF268DBD-CRY2-tSSA1-ConR2-ColE1-AmpR	NA	Ampicillin	This study
pMM0657	pCS0057	ConL1-pRPL18B-SV40NLS-ZiF268DBD-CRY2-tSSA1-ConR2-ColE1-AmpR	NA	Ampicillin	This study
pMM0658	pCS0058	ConL1-pRNR2-SV40NLS-ZiF268DBD-CRY2-tSSA1-ConR2-ColE1-AmpR	NA	Ampicillin	This study

Supplemental References

[1] R. Gietz and R. Schiestl, "High-efficiency yeast transformation using the LiAc/SS carrier DNA/PEG method," *Nature Protocols,* vol. 2, pp. 31-34, 2007.

[2] S. Harju, H. Fedosyuk and K. Peterson, "Rapid isolation of yeast genomic DNA: Bust n' Grab," *BMC Biotechnology,* vol. 4, no. 8, 2004.

[3] D. Amberg, D. Burke and J. Strathern, Methods in yeast genetics : a Cold Spring Harbor Laboratory course manual, Cold Spring Harbor, N.Y. : Cold Spring Harbor Laboratory Press, 2005.

[4] J. Sambrook and D. Russell, "The Inoue Method for Preparation and Transformation of Competent E. Coli: "Ultra-competent" cells," *CSH Protocols,* no. 1, 2006.

[5] K. Gerhardt, E. Olson, S. Castillo-Hair, L. Hartsough, B. Landry, F. Ekness, R. Yokoo, E. Gomez, P. Ramakrishnan, J. Suh, D. Savage and J. Tabor, "An open-hardware platform for optogenetics and photobiology," *Scientific Reports,* vol. 6, no. 35363, 2016.

[6] E. Andersen, "tPCR-Directed In Vivo Plasmid Construction Using Homologous Recombination in Baker's Yeast," *Molecular Methods for Evolutionary Genetics. Methods in Molecular Biology ,* vol. 772, pp. 409-421, 8 7 2011.

[7] R. McIsaac, S. Silverman, M. McClean, P. Gibney, J. Macinskas, M. Hickman, A. Petti and a. D. Botstein, "Fast-acting and nearly gratuitous induction of gene expression and protein depletion in Saccharomyces cerevisiae.," *Molecular Biology of the Cell,* vol. 22, pp. 4447-4459, 2011.

[8] R. McIsaac, B. Oakes, X. Wang, K. Dummit, D. Botstein and M. Noyes, "Synthetic gene expression perturbation systems with rapid, tunable single-gene specificity in yeast," *Nucleic Acids Research,* vol. 23, pp. 2993-3008, 2012.

[9] R. Sikorski and P. Heiter, "A system of shuttle vectors and yeast host strains designed for efficient manipulation of {DNA} in Saccharomyces cerevisiae," *Genetics,* vol. 122, no. 1, pp. 19-27, 1989.

[10] M. Sheff and K. Thorn, "Optimized cassettes for fluorescent protein tagging in Saccharomyces cerevisiae," *Yeast,* vol. 21, pp. 661-670, 2004.

[11] M. E. Lee, W. Deloache, D. Cervantes and J. Dueber, "A highly characterized yeast toolkit for modular, multipart assembly," *ACS Synthetic Biology,* vol. 4, no. 9, pp. 975-986, 2015.

[12] Z. Carter and D. Delneri, "New generation of loxP-mutated deletion cassettes for the genetic manipulation of yeast natural isolates," *Yeast,* vol. 27, pp. 765-775, 2010.

[13] C. Brachmann, A. Davies, G. Cost, E. Caputo, J. Li, P. Heiter and J. Boeke, "Designer deletion strains derived from Saccharomyces cerevisiae S288C: a useful set of strains and plasmids for PCR-mediated gene disruption and other applications," *Yeast,* vol. 14, pp. 115-132, 1998.

[14] U. Gueldener, J. Heinisch, G. Koehler, D. Voss and J. Hegemann, "A second set of loxP marker cassettes for Cre-mediated multiple gene knockouts in budding yeast," *Nucleic acids research,* vol. 30, no. 6, 2002.

[15] J. Dexter, P. Xu, J. Gunawardena and M. McClean, "Robust network structure of the Sln1-Ypd1-Ssk1 three-component phospho-relay prevents unintended activation of the HOG MAPK pathway in Saccharomyces cerevisiae," *BMC Systems Biology,* vol. 9, no. 1, p. 17, 2015.

[16] H. Ma, S. Kunes, P. Schatz and D. Botstein, "Plasmid construction by homologous recombination in yeast," *Gene,* vol. 58, p. 201–216, 1987.

[17] K. Oldenburg, K. Vo, S. Michaelis and C. Paddon, "Recombination-mediated PCR-directed plasmid construction in vivo in yeast.," *Nucleic Acids Research,* vol. 25, p. 451–452, 1997.

[18] L. A. Gilbert, M. H. Larson, L. Morsut, Z. Liu, G. A. Brar, S. E. Torres, N. Stern-Ginossar, O. Brandman, E. H. Whitehead, J. A. Doudna, W. A. Lim and J. S. Weissman, "CRISPR-mediated modular RNA-guided regulation of transcription in eukaryotes.," *Cell,* vol. 154, no. 2, pp. 442-451, 2013.

[19] M. Sheff and K. Thorn, "Optimized cassettes for fluorescent protein tagging in Saccharomyces cerevisiae," *Yeast,* vol. 21, pp. 661-670, 2004.

[20] A. Hansen and E. O'Shea, "Promoter decoding of transcription factor dynamics involves a trade-off between noise and control of gene expression," *Molecular Systems Biology,* vol. 9, no. 704, 2013.

[21] K. P. Gerhardt, E. J. Olson, S. M. Castillo-Hair, L. Hartsough, B. P. Landry, F. Ekness, R. Yokoo, E. J. Gomez, P. Ramakrishnan and J. Suh, "An open-hardware platform for optogenetics and photobiology," *Scientific Reports,* vol. 6, p. 35363, 2016.

[22] "IRIS," [Online]. Available: http://taborlab.github.io/Iris/..

Chapter 4: Development of a toolkit for rapid plasmid assembly for integration into *Candida albicans*

Stephanie H. Geller designed this research, created the plasmids with the help of Roberta Candela and Dhaval Ghone (graduate rotation students in the laboratory), performed flow cytometry experiments, analyzed the data, and wrote the chapter.

Abstract

Candida albicans is an opportunistic fungus that can cause deadly systemic infections in immunocompromised individuals. These infections often develop on medical devices such as catheters and pacemakers and can disseminate to other parts of the body to cause serious systemic infection. Dissemination or dispersion is the last stage of the biofilm lifecycle, making it quite difficult to study with static mutations, which can also disrupt biofilm development and dispersion. Gene induction systems are well suited for teasing out a gene's role in dispersion as gene induction can be timed to affect dispersion without disrupting biofilm development. Optogenetics—the use of genetically encoded, light-controlled effector proteins—allows spatial and temporal control of gene expression by simply turning on or off a light. However, optogenetic tools require optimization, for example, by tuning the expression levels of light-sensitive components or even determining which components to use. I therefore built upon an existing toolkit for *S. cerevisiae* by creating fluorescent markers, transcription factors, and homology arms with the aim of allowing optogenetic control in *C. albicans*. Additionally, I characterized the ability of *S. cerevisiae* promoters and terminators to express a fluorescent marker in *C. albicans*. Lastly, I characterized an orthogonal transcription factor with the Zif268 DNA binding domain and VP16 or VP64 activation domains in *C. albicans*.

Introduction

Candida albicans is an opportunistic fungus that has been known to cause systemic infection in immunocompromised individuals reaching a mortality rate up to 25% [1]. The *C. albicans* lifecycle begins when planktonic cells attach to a surface and begin developing a biofilm, which entails changes in gene expression and cell morphology. Once a biofilm has developed and matured, it starts releasing yeast form "dispersed" cells that disseminate infection [2][3]. Studying the process of dispersion is difficult using traditional genetic manipulations as knockout or over expression assays because static mutations also disrupt the preceding processes of biofilm initiation and development. Therefore, it may appear that dispersion is affected by a specific gene when the gene disrupts biofilm development. Inducible systems that allow timed perturbations of gene expression are more helpful in understanding which genes are directly linked to dispersion [4]. Optogenetic systems, which employ genetically encoded, light-sensitive effector proteins, enable the control of gene expression with light, which can be cheaper to administer than chemical inducers and can be easily controlled in space and time [5]. However, many optogenetic systems—like the two component systems previously used in *C. albicans*—need optimization to efficiently control gene expression [6]. In Chapter 3, I showed that the function of the CRY2/CIB1 optogenetic system in *S. cerevisiae* depended greatly on the relative expression of both CRY2 and CIB1. Optimizing such tools therefore requires the use of multiple promoters with different expression levels [7].

C. albicans is very efficient at using homologous recombination to repair or alter its genome [8]. This mechanism can be exploited integrate desired genes into the *C. albicans* genome. However, integrating multiple genes with similar sequences can lead to unwanted recombination events.

Therefore, it is useful to have well characterized systems that ensure stable integration into the genome. In addition, *C. albicans* belongs to a clade that translates a CTG codon as serine instead of the traditional leucine [12]. Therefore, genetic manipulation of *C. albicans* requires components with appropriate codon usage.

In Chapters 2 and 3, I described a toolkit for building optogenetic tools in *S. cerevisiae*. Having used the toolkit to quickly engineer and optimize optogenetic tools, it was evident that a similar toolkit would be useful in *C. albicans*. In fact, commonly used tools for genetic engineering in *S. cerevisiae* such as well characterized promoters and terminators, origins of replication, and synthetic transcription factors are lacking in *C. albicans*. Although *C. albicans* is mostly studied for its pathogenic properties, such tools would allow fast and easy assembly of genes for integration. Lee *et al* [7] developed a modular cloning (MoClo) toolkit for the modular assembly of plasmids with unique promoters, terminators, coding sequences, selections markers, and homology arms creation. The toolkit allows the rapid assembly of many plasmid variants, which can be linearized for genomic integration by simple restriction enzyme digest. Additionally, individual components of the toolkit can for appropriate codon usage in different species. Lastly, storing the resulting plasmids in *E. coli* is a simple and effective way to maintain the constructs for integration into different strains over time.

Here I describe a toolkit for *C. albicans* featuring promoters, fluorescent markers, DNA binding domains, activation domains, homology arms, and the optogenetic proteins CRY2 and CIB1. This toolkit enables the rapid assembly and integration of proteins under different strength promoters and terminators to the *NEUT5L* safe haven locus [9] and facilitates genetic engineering in *Candida*

by providing well-characterized, modular components. I used the toolkit to develop an optogenetic gene induction system for investigating dispersion. Lastly, I characterized an orthogonal transcription factor for use in *C. albicans*, which features the Zif268 DNA binding domain and VP16 or VP64 activation domains.

Results

Integrating tools for *C. albicans* into a toolkit

I began by integrating *Candida*-optimized components into the MoClo toolkit. This involved making "part" plasmids by amplifying desired DNA sequences with appropriate overhangs and integrating the amplified DNA into an entry vector provided by Lee, *et al* (2015) using golden gate assembly [7]. I created part plasmids with a variety of promoters, fluorescent markers, transcription factors, and homology (Fig.2). From there, I created cassette plasmids by combining different combinations of parts into BsaI golden gate assemblies. If only one genetic construct must be integrated, this cassette can then be digested with NotI and transformed into yeast. If multiple constructs must be integrated, then multiple cassettes can be combined into a multi-gene cassette plasmid via BsmBI Golden Gate assembly. The multi-gene cassette plasmids can then be digested with NotI and integrated into the genome. A benefit of integrating these components into a toolkit is that these plasmids are then stored in *E. coli* for use in the future.

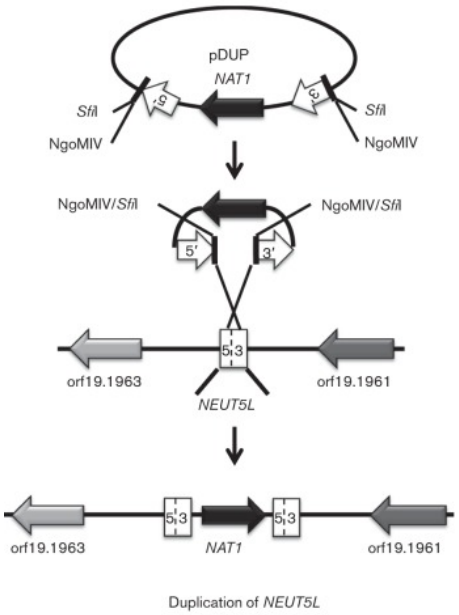

Figure 1. Maps of the shuttle vectors for integration into the *C. albicans* NEUT5L locus. This figure is taken from Gerami-Nejad, *et al* (2013) [9] and illustrates the integration technique used in the toolkit described in this paper. Here, pDUP has the 3' homology arm followed by the gene of interest and the 5' homology arm. When this plasmid is digested and transformed into Candida, it duplicates the NEUT5L locus and integrates the gene of interest in the opposite direction of the surrounding genes.

I selected homology arms based on the pDUP plasmid, so that cassettes that are linearized by digestion and transformed into *Candida* cause the duplication of the *NEUT5L* locus and the integration of the gene of interest between the duplicated *NEUT5L* sites (Fig1) [9]. Using this method, the gene of interest is integrated in the opposite orientation of surrounding genes. This method was selected to reduce the negative effects of having multiple genes in tandem when using multi-gene cassettes [10], [11].

I included the herpes virus activation domains VP16 and VP64 in the toolkit to test their efficiency in *Candida* [12], [13]. VP64 has been shown be the stronger activation domain in other species as it consists of four repeated VP16 activation, but this has not been confirmed in *C. albicans* [14]. I

also included the Zif268 and LexA DNA binding domains in the toolkit to test their function in *C. albicans*. Zif268 is a mouse zinc finger DBD that was adapted to work in *S. cerevisiae* as an orthogonal TF with minimal off target binding. (Chapter 3 Fig 1) BLAST revealed that there are only 9 perfect Zif268 binding sites in the *Candida albicans* SC5314 genome, , versus 11 sites in the *S. cerevisiae* genome [15]. In *S. cerevisiae*, Zif268 can be paired with a synthetic promoter (pZIF) built by replacing the Gal4 binding domains in the GAL4 promoter with Zif268 binding domains. (Chapter 3) I also added the light responsive proteins CRY2 and CIB1 to the toolkit for building optogenetic tools in *C. albicans* [16]. Lastly, I added the fluorescent proteins mCherry and mScarlet to the toolkit to function as reporters and allow the characterization of promoter, terminator, and transcription factor strengths.

Assembly Connector	Promoter	Coding Sequences		Terminator	Assembly Connector	C. albicans marker	3' homology	E. coli Marker and origin	5' homology
1	2	3		4	5	6	7	8a	8b
ConLS	pACT1	mCherry		tENO1	ConR1	NatR	Neut5L 5'	AmpR-ColE1	Neut5L 3'
ConL1	pCCW12	mScarlet		tENO2	ConR2				
ConL2	pENO1	Zif268-VP64		tPGK1	ConRE				
	pHHF1	Zif268-VP16		tSSA1					
	pPAB1	Spacer		tTDH1					
	pPGK1	3a	3b						
	pPOP6	NLS-LexA	CRY2						
	pPSP2	NLS-zif268	CIB1						
	pRET2	NLS-VP64							
	pREV1								
	pRNR1								
	pRNR2								
	pRPL18B								
	pTDH3								
	pTEF1								
	pTEF2								
	pZif								
	pLexA								

E. coli marker and origin
678
AmpR-ColE1

Figure 2. Parts in the *C. albicans* toolkit. Green text indicates that I added the part specifically for *C. albicans*. Additional parts were already present in the yeast toolkit or the yeast optogenetic toolkit [7], [17].

Testing *S. cerevisiae* promoter and terminator functions in *C. albicans*

I next tested how different promoters performed when integrated at the *NEUT5L* locus of *C. albicans* (Fig.3). The original toolkit contained constitutive promoters selected to achieve a wide range of expression levels in *S. cerevisiae*. While *S. cerevisiae* promoters are not widely used in *C. albicans*, it is not unprecedented [18] and the *S. cerevisiae CYC1* promoter has been used as a base promoter for a tetracycline inducible system in *C. albicans* [4],[19]. I also added the *C. albicans* promoters pENO1 and pACT1 to the toolkit, as they are commonly used in overexpression studies. I characterized how each of these promoters performed in *C. albicans* by using them to control the expression of mCherry. The promoters were able to achieve a wide range of expression levels, though none were as strong as the *C. albicans* promoters pACT1 and pENO1 (Fig. 3).

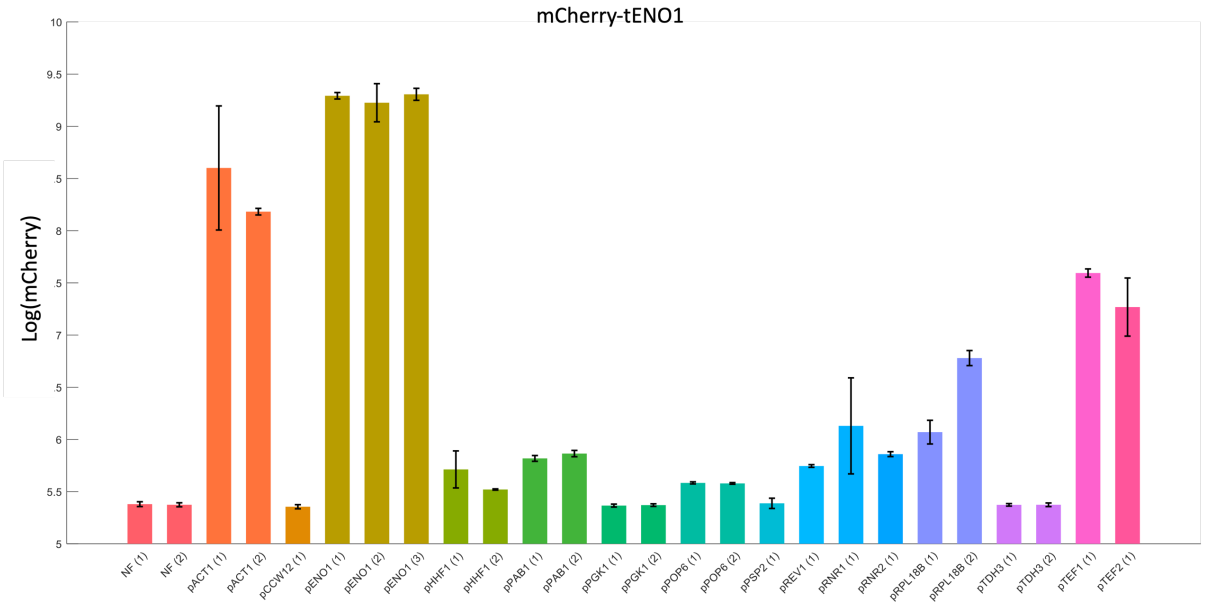

Figure 3. Promoter activity in *C. albicans*. Each promoter construct drove the expression of mCherry and was integrated at the *NEUT5L* locus. The promoters pACT1 and pENO1 were from *C. albicans* while all others were from *S. cerevisiae*. NF indicates a non-fluorescent cassette. Error

bars represent the standard deviation of 3 technical replicates and numbers following the promoters indicate biological replicates.

I next tested how the terminators in the existing toolkit functioned in *C. albicans* (Fig 4). *S. cerevisiae* terminators, such as tCYC1, are commonly used *C. albicans* [20], [21]. To do this, I constructed cassettes with the *C. albicans* promoters pENO1 or pACT1, mCherry, and each of the terminators from the existing toolkit. All terminators tested resulted in similar mCherry expression levels. This is consistent with the results of Lee, *et al*, who chose these terminators for their toolkit because they have similar expression levels in *S. cerevisiae*. [7]

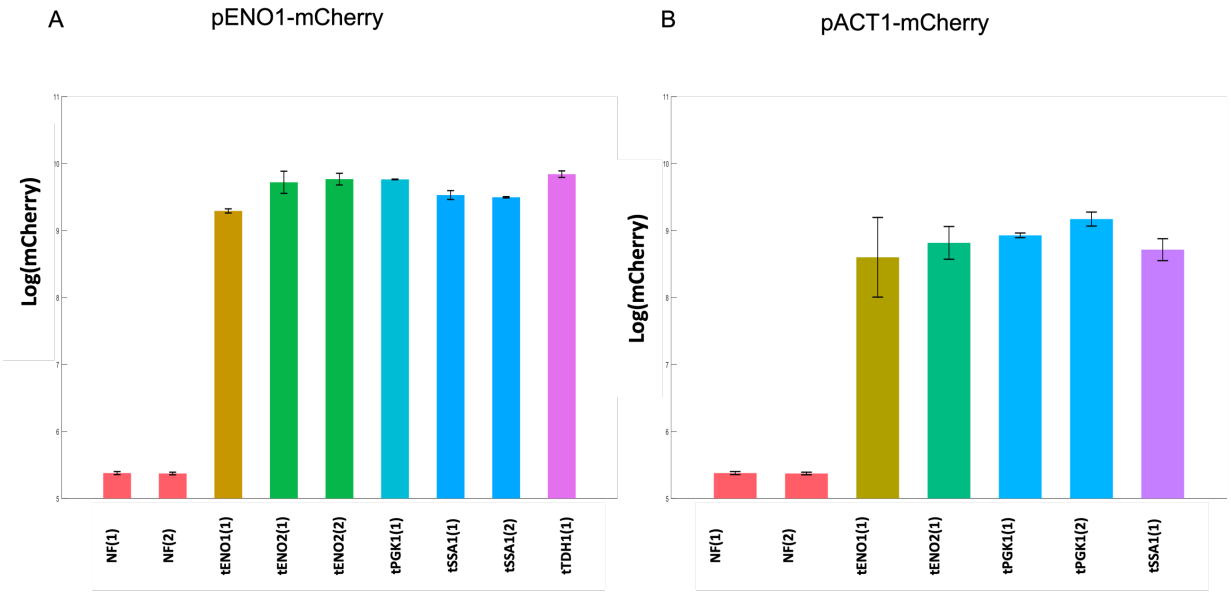

Figure 4. Terminator activity in *C. albicans.* *S. cerevisiae* terminators are used to help halt transcription of A) pACT1-mCherry or B) pENO1-mCherry in *C. albicans*. NF indicates a non-fluorescent cassette is integrated into the genome. Error bars represent the standard deviation of 3 technical replicates. Numbers following the promoters indicate biological replicates.

Developing an optogenetic tool to control gene expression in response to light

Having characterized a variety of promoters and terminators in *C. albicans*, I next used them to build an optogenetic tool based on the light sensitive proteins CRY2 and CIB1. Much like my previous work in *S. cerevisiae*, I fused a Zif268 or LexA DNA binding domain to CRY2 and a VP16 or VP64 activation domain to CIB1. In response to light, CRY2 undergoes a conformational change that allows it to bind CIB1 and recruit the activation domain to the promoter of a gene of interest. We know from previous work that the ratio of CRY2 to CIB1 is crucial for optimal expression of a gene of interest, in this case a fluorescent marker (Chapter 3). Based on my promoter screen in *C. albicans* (Fig 2), I selected high and medium strength promoters to drive the expression of CRY2 and CIB1. I started with pTEF1 and pRPL18B but did not observe light-inducible reporter expression. I hypothesized that the light sensitive components of our optogenetic system were not expressed strongly enough, as low, and medium strength promoters did not allow light inducible reporter expression in *S. cerevisiae* (Chapter 3). I therefore switched to using pENO1 as a high strength promoter and pACT1 as medium strength promoter. I created cassettes with both CRY2 and CIB1 at high expression, CRY2 at high expression and CIB1 at medium expression, CIB1 at high expression and CRY2 at medium expression, and both CRY2 and CIB1 at medium expression. For comparison, I also built constitutive expression controls with mScarlet under the control of pTEF1, pRPL18B, pENO1, and pACT1.

None of the optogenetic constructs tested caused light induced fluorescent reporter expression greater than a no fluorescence control (Fig 5). I also noticed that constitutively expressed fluorescent markers were not as bright as might be expected from the literature when the highly expressed CRY2 and CIB1 components were integrated upstream [22]. In contrast, additional controls with only spacers upstream of the fluorescent reporter had significantly higher expression

than the no fluorescent controls. This suggests that having genes in cis results in decreased expression in *C. albicans*. This “transcriptional interference” has been observed in many species but has been mostly studied in *S. cerevisiae* and *E. coli* [10], [11].

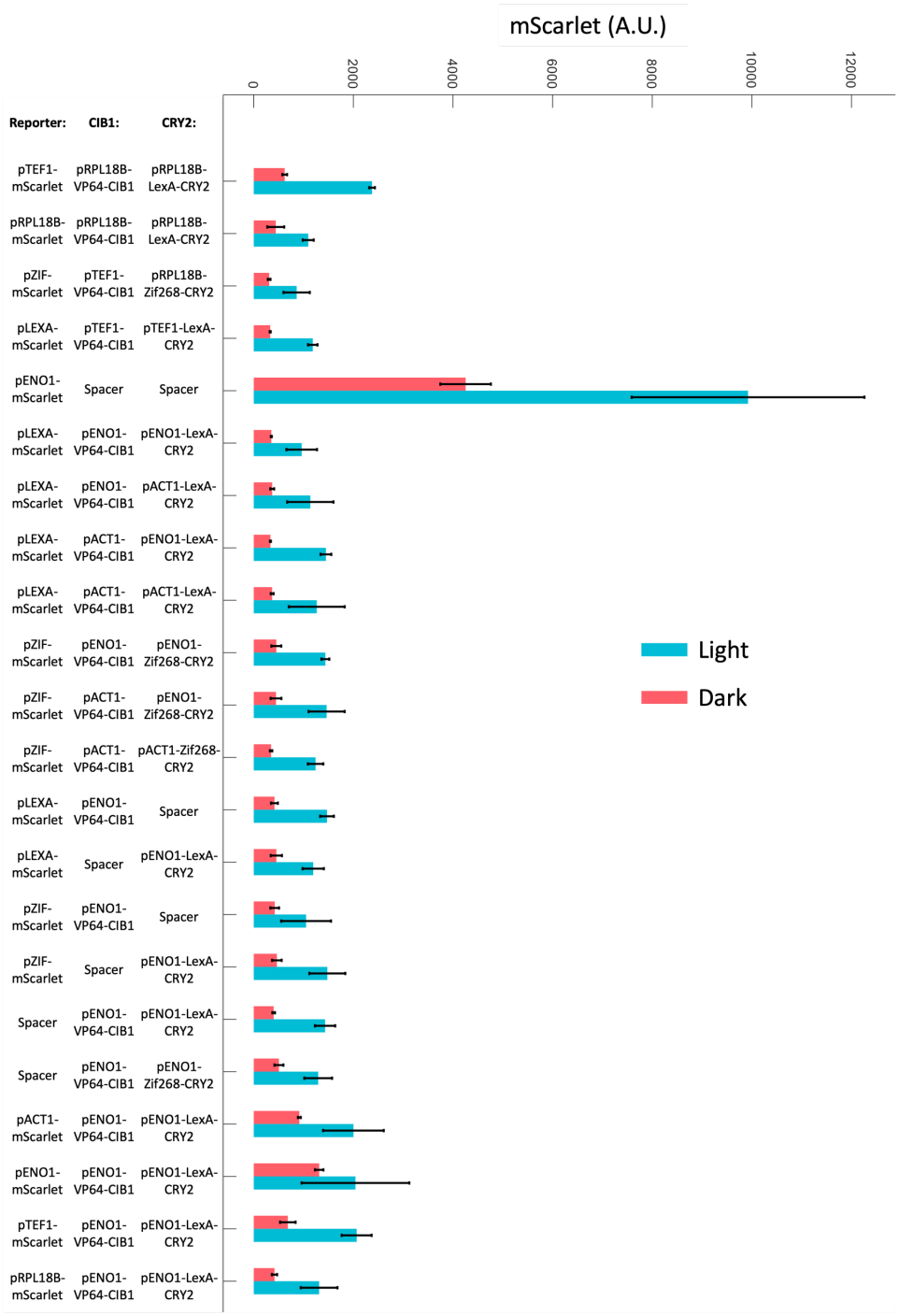

Figure 5. mScarlet expression of the CRY2-CIB1 optogenetic tool. Strains were grown in LFM + ClonNat (200µg/mL) and exposed to 405 µW/cm^2 blue light for 4 hours using an optoplate. Data is the average of 3 technical replicates. Error bars indicate standard deviation of the three technical replicates.

I also observed that all strains were more fluorescent when exposed to light. I therefore looked at size difference between the light and dark samples by comparing forward scatter (FSCA) and side scatter (SSCA) measurements from flow cytometry (Fig 6). FSCA is proportional to the diameter of the cell while SSCA is proportional to the granularity of the cell [23]. The FSCA measurements suggested that cells exposed to light were on average smaller than cells grown in the dark. In contrast, there were few distinct differences in granularity between the light and dark conditions.

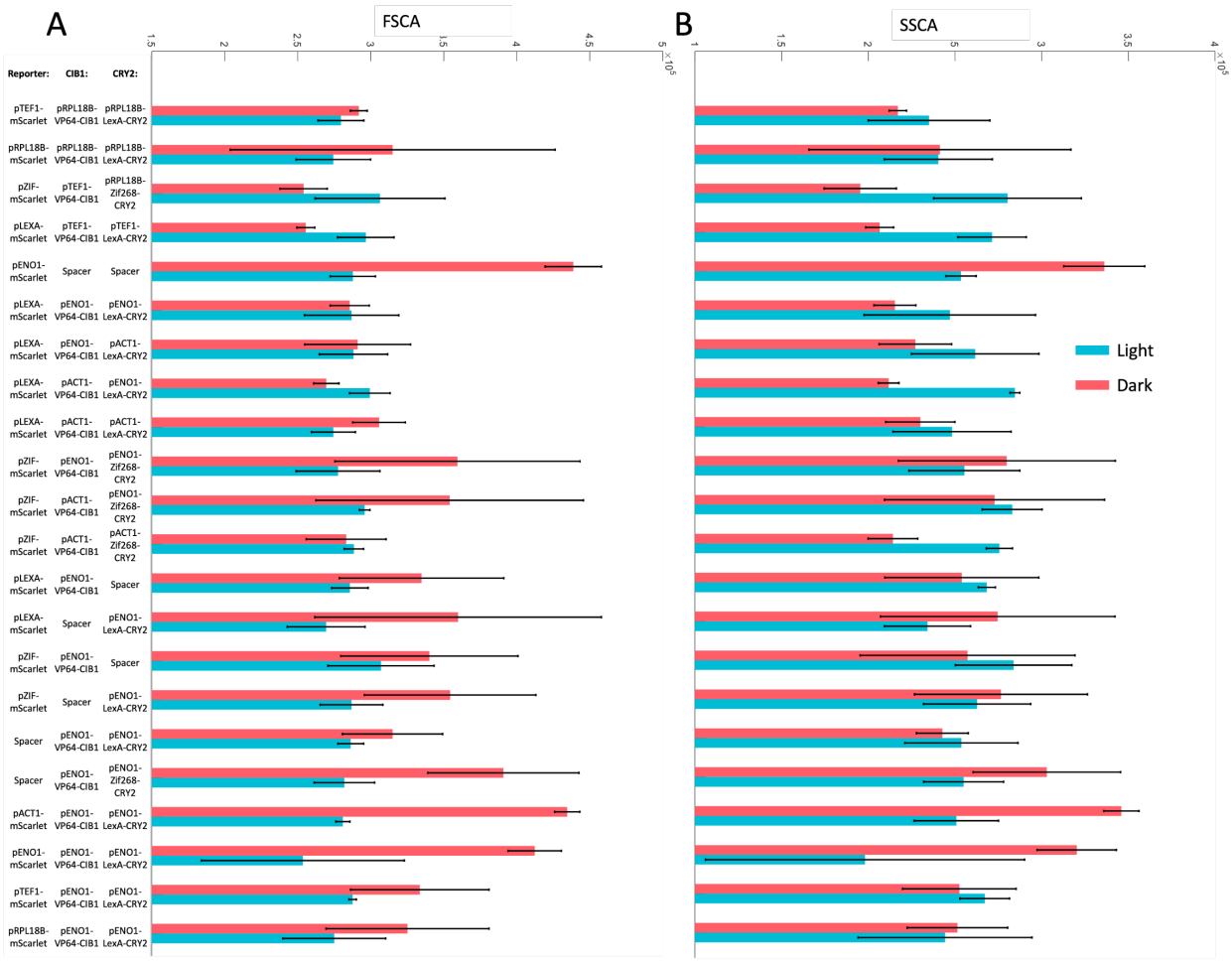

Figure 6. Determining the size of the cells using the FSCA (A) and SSCA(B) reading from flow cytometry. Data is the average of 3 technical replicates. Error bars indicate standard deviation of the three technical replicates.

Knowing that the cell size may differ between light and dark samples, I next normalized fluorescence by cell size (Fig 7). However, light samples still fluoresced more strongly than dark samples, when correcting for differences in cell size. This suggests that light causes the cells to fluorescence in the measured wavelength (585nm), even in strains lacking any fluorescent marker. Light samples were also brighter in the GFP channel (530nm), though no strain had any green fluorescent marker (Data not shown). This suggests that light, like other stresses, may cause cells to autofluorescence [24]–[26].

When comparing size-corrected dark samples, I also noticed that strains with constitutively expressed mScarlet showed significantly stronger expression than a no fluorescence control, except pRPL18B-mScarlet. While I did not test pRPL18B-mScarlet with upstream spacers in this experiment, when I tested pRPL18B-mCherry (Fig 2) I saw significant expression of mCherry compared to the no fluorescent control, again indicating that transcriptional interference is likely causing a decrease in gene expression.

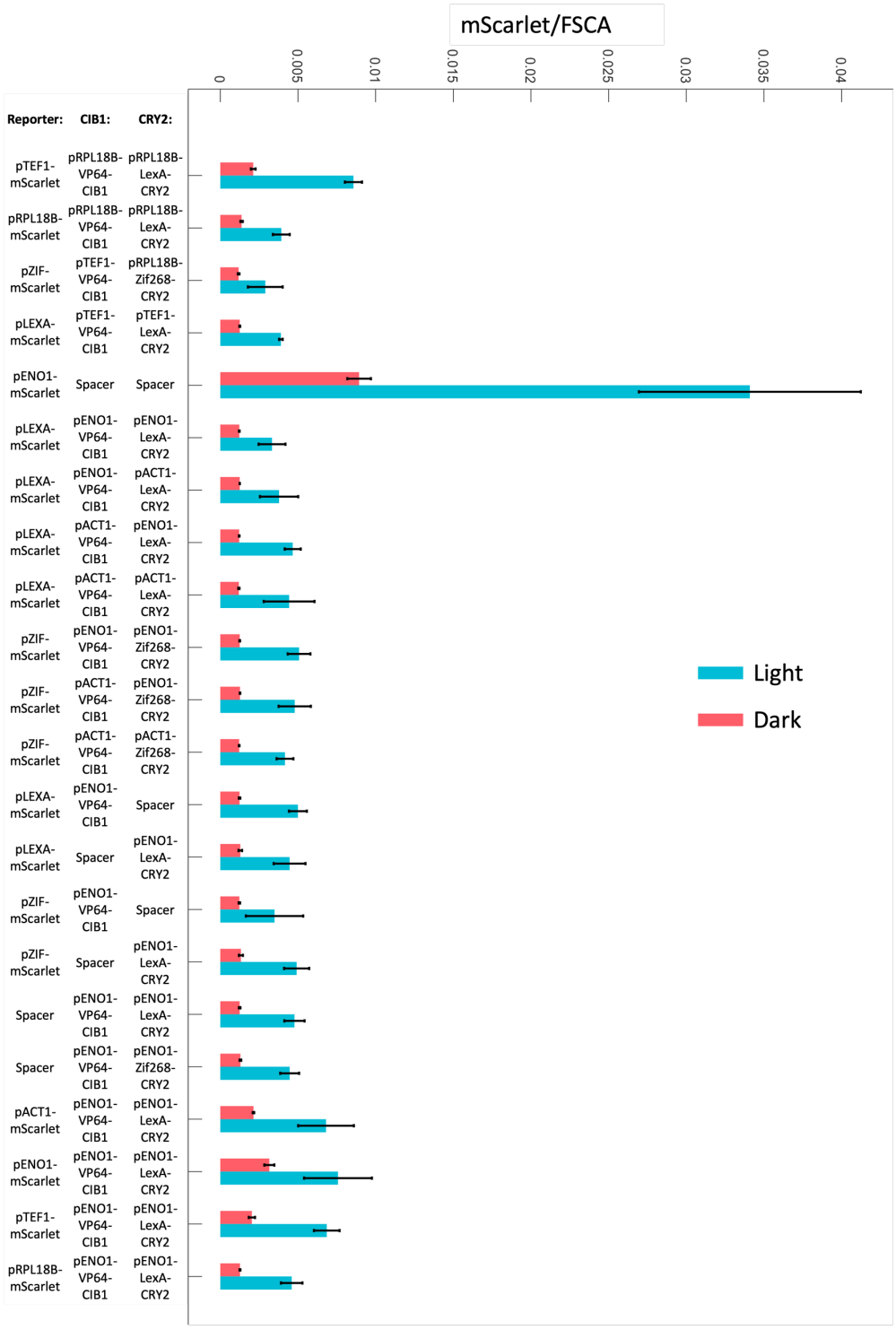

Figure 7. Expression of mScarlet normalized to cell size. Data represent mean and standard deviation of three technical replicates.

Testing TFZIFs ability to activate expression of fluorescent marker mCherry

Since my Zif268-based optogenetic tool did not measurably induce the expression of a fluorescent reporter in *C. albicans*, I decided to test another synthetic transcription factor with the Zif268 DBD, one without optogenetic components. I built a *C. albicans* optimized transcription factor ("TFZIF") featuring a Zif268 DBD, a constitutive nuclear localization signal, and a transcriptional activation domain. I also incorporated a reporter—which featured mCherry expressed under the constitutive promoter pACT1—into the same multi-gene cassette with varying spacer configurations to test for transcriptional interference. No TFZIF construct measurably induced the mCherry reporter compared to controls (Fig 8). However, my reporter constructs were not affected by transcriptional interference because the spacer placement between my two reporters were not significantly different ($p=0.9828$). This indicates that having TFZIF directly in front of the fluorescent reporter does not cause a downregulation of the fluorescent reporter.

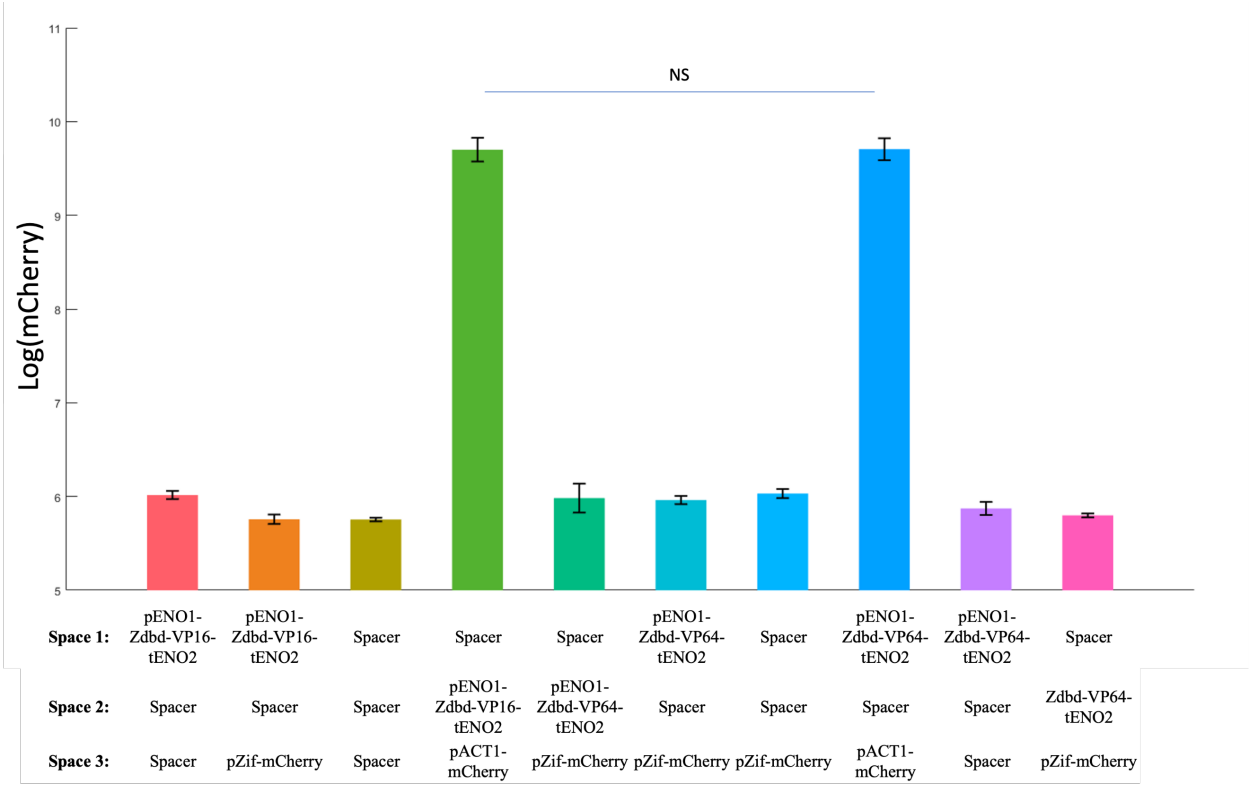

Figure 8. Testing the ability of the synthetic to drive mCherry expression. TFZIF was placed either directly in front of a fluorescent marker, or with a spacer between TFZIF and the fluorescent marker. Data represent mean and standard deviation of three technical replicates. NS indicates $p>0.05$.

Conclusions

The toolkit described in this chapter allows the rapid, modular assembly of plasmids for integration in *C. albicans*. Using this toolkit, I found that multiple *S. cerevisiae* promoters are functional in *C. albicans.* While not as strong as the *C. albicans* promoters pACT1 and pENO1, the *S. cerevisiae* promoters offer a range of expression strengths, which is critical for applications such as the development of optogenetic tools. I found that a variety of terminators that drive comparable levels in *S. cerevisiae* also drive comparable expression levels in *C. albicans*. However, due to limitations in the ability to integrate the fluorescent marker into the *C. albicans* genome, three biological

replicates were not achieved for every promoter and terminator construct. Additional replicates should be constructed to further confirm these results.

I used the toolkit to construct a CRY2/CIB1-based gene induction tool in *C. albicans* that's like existing optogenetic systems in *S. cerevisiae*. However, this tool did not measurably drive reporter expression in response to light. There are several approaches which may fix this problem. First, I used CRY2 because it was previously used in *C. albicans* [16]. However, a truncated version of CRY2, CRY2PHR, is more effective at activating gene expression in *S. cerevisiae* and this may also be the case in *C. albicans* [27]. Lastly, transcriptional interference may strongly affect the expression of genes integrated with the toolkit and this should be considered when adding tools with multiple components to the *C. albicans* genome. For example, Silva, *et al* (2019) exploited the fact that *C. albicans* is a diploid organism by splitting the components of their optogenetic tool across both *NEUT5L* loci [16]. Overall, further work is needed to create a functional optogenetic gene induction system in *C. albicans*.

I also determined that TFZIF does not induce mCherry expression from the synthetic promoter pZIF. While I did not confirm that TFZIF itself was expressed, I have successfully used the pENO1 promoter to express fluorescent markers. Expression of TFZIF could be confirmed by adding a fluorescent marker to it or by using qPCR or a Western blot. Since they may affect gene expression, additional linker configurations between the DBD and AD of TFZIF should also be tested [28], [29]. Binding assays could also be used to determine if Zif686 binds the pZIF promoter in *C. albicans* as effectively as it does in *S. cerevisiae* [30], [31]. A binding affinity assay would have to be done to determine binding in *C. albicans* is different than other organisms. Lastly, the

transactivation domains VP16 vs VP64 should be tested with additional, functional DBDS to compare their efficacy in *C. albicans*. Having well characterized, modular transcription factor components would be useful for tool development in *C. albicans*.

Methods

Strain Growth

All yeast strains are listed below. The background strain for the promoter, terminator, and optogenetic strains is SC5314 (cMM0001) while the background strain for testing ZIF268 and AD is RM1000#2 (cMM0002). Strains are grown in YPD supplemented with uridine (80ug/ml) and if appropriate ClonNat (200ug/ml). Strains are stored in 15% glycerol stocks in the -80°C freezer.

Table 1. *C. albicans* strain table

ID	Genotype	Description	Source
cMM001	Wildtype	Wildtype	Noble, *et al* 2015 Eukaryotic Cell
cMM0046	*ura3::imm434/ura3::imm434 iro1/iro1::imm434 his1::hisG/his1::hisG NEUT5L::pEno1-zdbd-vp16-tEno2-Spacer-Spacer-NatR*	RM1000#2 + pMM1391	This Study
cMM0047	*ura3::imm434/ura3::imm434 iro1/iro1::imm434 his1::hisG/his1::hisG NEUT5L::pEno1-zdbd-vp16-tEno2-Spacer-pZF(3BS)-mCherry-tTDH1-NatR*	RM1000#2 + pMM1398	This Study
cMM0048	*ura3::imm434/ura3::imm434 iro1/iro1::imm434 his1::hisG/his1::hisG NEUT5L::Spacer-Spacer-Spacer-NatR*	RM1000#2 + pMM1389	This Study
cMM0049	*ura3::imm434/ura3::imm434 iro1/iro1::imm434 his1::hisG/his1::hisG NEUT5L::Spacer-pEno1-zdbd-vp16-tEno2-pZF(3BS)-mCherry-tTDH1-NatR*	RM1000#2 + pMM1406	This Study
cMM0050	*ura3::imm434/ura3::imm434 iro1/iro1::imm434 his1::hisG/his1::hisG NEUT5L::pEno1-zdbd-vp16-tEno2-Spacer-pZF(3BS)-mCherry-tTDH1-NatR*	RM1000#2 + pMM1398	This Study
cMM0051	*ura3::imm434/ura3::imm434 iro1/iro1::imm434 his1::hisG/his1::hisG NEUT5L::pEno1-zdbd-vp64-tEno2-Spacer-pZF(3BS)-mCherry-tTDH1-NatR*	RM1000#2 + pMM1394	This Study
cMM0052	*ura3::imm434/ura3::imm434 iro1/iro1::imm434 his1::hisG/his1::hisG NEUT5L::Spacer-Spacer-pZF(3BS)-mCherry-tTDH1-NatR*	RM1000#2 + pMM1402	This Study
cMM0053	*ura3::imm434/ura3::imm434 iro1/iro1::imm434 his1::hisG/his1::hisG NEUT5L::pEno1-zdbd-vp64-tEno2-Spacer-pAct1-mCherry-tTDH1-NatR*	RM1000#2 + pMM1405	This Study
cMM0054	*ura3::imm434/ura3::imm434 iro1/iro1::imm434 his1::hisG/his1::hisG NEUT5L::pEno1-zdbd-vp64-tEno2-Spacer-Spacer-NatR*	RM1000#2 + pMM1390	This Study
cMM0055	*ura3::imm434/ura3::imm434 iro1/iro1::imm434 his1::hisG/his1::hisG NEUT5L::Spacer-pEno1-zdbd-vp64-tEno2-pZF(3BS)-mCherry-tTDH1-NatR*	RM1000#2 + pMM1395	This Study

cMM0056	*NEUT5L::pHHF1-mCherry-tENO1-NatR*	SC5314 and pMM1115	This Study
cMM0057	*NEUT5L::pPAB1-mCherry-tENO1-NatR*	SC5314 and pMM1116	This Study
cMM0058	*NEUT5L::pRET2-mCherry-tENO1-NatR*	SC5314 and pMM1117	This Study
cMM0059	*NEUT5L::pRNR1-mCherry-tENO1-NatR*	SC5314 and pMM1118	This Study
cMM0060	*NEUT5L::pPOP6-mCherry-tENO1-NatR*	SC5314 and pMM1119	This Study
cMM0061	*NEUT5L::pPSP2-mCherry-tENO1-NatR*	SC5314 and pMM1120	This Study
cMM0062	*NEUT5L::pREV1-mCherry-tENO1-NatR*	SC5314 and pMM1121	This Study
cMM0063	*NEUT5L::pCCW12-mCherry-tENO1-NatR*	SC5314 and pMM1122	This Study
cMM0064	*NEUT5L::pPGK1-mCherry-tENO1-NatR*	SC5314 and pMM1123	This Study
cMM0065	*NEUT5L::pTEF2-mCherry-tENO1-NatR*	SC5314 and pMM1124	This Study
cMM0066	*NEUT5L::pTEF1-mCherry-tENO1-NatR*	SC5314 and pMM1125	This Study
cMM0067	*NEUT5L::pRPL18B-mCherry-tENO1-NatR*	SC5314 and pMM1126	This Study
cMM0068	*NEUT5L::pRNR2-mCherry-tENO1-NatR*	SC5314 and pMM1127	This Study
cMM0069	*NEUT5L::pTDH3-mCherry-tENO1-NatR*	SC5314 and pMM1128	This Study
cMM0070	*NEUT5L::SPACER-NatR*	SC5314 and pMM1129	This Study
cMM0071	*NEUT5L::pACT1-mCherry-tENO1-NatR*	SC5314 and pMM1130	This Study
cMM0072	*NEUT5L::pENO1-mCherry-tENO1-NatR*	SC5314 and pMM1131	This Study
cMM0073	*NEUT5L::pENO1-mCherry-tssa1-NatR*	SC5314 and pMM1274	This Study
cMM0074	*NEUT5L::pENO1-mCherry-tpgk1-NatR*	SC5314 and pMM1275	This Study
cMM0075	*NEUT5L::pENO1-mCherry-teno2-NatR*	SC5314 and pMM1276	This Study
cMM0076	*NEUT5L::pENO1-mCherry-ttdh1-NatR*	SC5314 and pMM1277	This Study
cMM0077	*NEUT5L::pACT1-mCherry-tssa1-NatR*	SC5314 and pMM1278	This Study
cMM0078	*NEUT5L::pACT1-mCherry-tpgk1-NatR*	SC5314 and pMM1279	This Study
cMM0079	*NEUT5L::pACT1-mCherry-teno2-NatR*	SC5314 and pMM1280	This Study
cMM0080	*Neut5L::pEno1-LexA-Cry2-pEno1-VP64-Cib1-pLexa-mScarlet-Neut5-Kan-Nat-Neut5*	SC5314 and pMM1297	This Study
cMM0081	*Neut5L::pAct1-LexA-Cry2-pEno1-VP64-Cib1-pLexa-mScarlet-Neut5-Kan-Nat-Neut5*	SC5314 and pMM1298	This Study
cMM0082	*Neut5L::pEno1-LexA-Cry2-pAct1-VP64-Cib1-pLexa-mScarlet-Neut5-Kan-Nat-Neut5*	SC5314 and pMM1299	This Study
cMM0083	*Neut5L::pAct1-LexA-Cry2-pAct1-VP64-Cib1-pLexa-mScarlet-Neut5-Kan-Nat-Neut5*	SC5314 and pMM1300	This Study
cMM0084	*Neut5L::pEno1-zDBD-Cry2-pEno1-VP64-Cib1-pZif-mScarlet-Neut5-Kan-Nat-Neut5*	SC5314 and pMM1301	This Study
cMM0085	*Neut5L::pAct1-zDBD-Cry2-pEno1-VP64-Cib1-pZif-mScarlet-Neut5-Kan-Nat-Neut5*	SC5314 and pMM1302	This Study
cMM0086	*Neut5L::pEno1-zDBD-Cry2-pAct1-VP64-Cib1-pZif-mScarlet-Neut5-Kan-Nat-Neut5*	SC5314 and pMM1303	This Study
cMM0087	*Neut5L::pAct1-zDBD-Cry2-pAct1-VP64-Cib1-pZif-mScarlet-Neut5-Kan-Nat-Neut5*	SC5314 and pMM1304	This Study
cMM0088	*Neut5L::Spacer-pEno1-VP64-Cib1-pLexa-mScarlet-Neut5-Kan-Nat-Neut5*	SC5314 and pMM1305	This Study

cMM0089	*Neut5L::pEno1-LexA-Cry2-Spacer-pLexa-mScarlet-Neut5-Kan-Nat-Neut5*	SC5314 and pMM1306	This Study
cMM0090	*Neut5L::Spacer-pEno1-VP64-Cib1-pZif-mScarlet-Neut5-Kan-Nat-Neut5*	SC5314 and pMM1307	This Study
cMM0091	*Neut5L::pEno1-LexA-Cry2-Spacer-pZif-mScarlet-Neut5-Kan-Nat-Neut5*	SC5314 and pMM1308	This Study
cMM0092	*Neut5L::pEno1-LexA-Cry2-pEno1-VP64-Cib1-Spacer-Neut5-Kan-Nat-Neut5*	SC5314 and pMM1309	This Study
cMM0093	*Neut5L::pEno1-zDBD-Cry2-pEno1-VP64-Cib1-Spacer-Neut5-Kan-Nat-Neut5*	SC5314 and pMM1310	This Study
cMM0094	*Neut5L::pEno1-LexA-Cry2-pEno1-VP64-Cib1-pAct1-mScarletNeut5-Kan-Nat-Neut5*	SC5314 and pMM1311	This Study
cMM0095	*Neut5L::pEno1-LexA-Cry2-pEno1-VP64-Cib1-pEno1-mScarletNeut5-Kan-Nat-Neut5*	SC5314 and pMM1312	This Study
cMM0096	*Neut5L::pEno1-LexA-Cry2-pEno1-VP64-Cib1-pTef1(sc)-mScarletNeut5-Kan-Nat-Neut5*	SC5314 and pMM1313	This Study
cMM0097	*Neut5L::pEno1-LexA-Cry2-pEno1-VP64-Cib1-pRPL18B(sc)-mScarletNeut5-Kan-Nat-Neut5*	SC5314 and pMM1314	This Study
cMM0098	*Neut5L::pRPL18B-LexA-Cry2-pERPL18B-VP64-Cib1-pTef1(sc)-mScarlet-Neut5-Kan-Nat-Neut5*	SC5314 and pMM1412	This Study
cMM0099	*Neut5L::pRPL18B-LexA-Cry2-pERPL18B-VP64-Cib1-pRPL18B-mScarlet-Neut5-Kan-Nat-Neut5*	SC5314 and pMM1413	This Study
cMM0100	*Neut5L::pRPL18B-zDBD-Cry2-pTEF1-VP64-Cib1-pZif-mScarlet-Neut5-Kan-Nat-Neut5*	SC5314 and pMM1414	This Study
cMM0101	*Neut5L::pTEF1-LexA-Cry2-pTEF1-VP64-Cib1-pLexa-mScarlet-Neut5-Kan-Nat-Neut5*	SC5314 and pMM1415	This Study
cMM0102	*Neut5L::Spacer-Spacer-pEno1-mScarletNeut5-Kan-Nat-Neut5*	SC5314 and pMM1416	This Study

Table 2. Plasmid table

ID	Gene(s) or Insert	Source
pMM0453	ColE1-CamR-pTDH3	Lee *et al* (2015)
pMM0454	ColE1-CamR-pRPL18B	Lee *et al* (2015)
pMM0455	ColE1-CamR-pREV1	Lee *et al* (2015)
pMM0489	ColE1-CamR-ConLS	Lee *et al* (2015)
pMM0491	ColE1-CamR-ConR1	Lee *et al* (2015)
pMM0522	ColE1-CamR-pTEF1	Lee *et al* (2015)
pMM0528	ColE1-CamR-pZF(3BS)	Lee *et al* (2015)
pMM0532	ColE1-CamR-ConL1	Lee *et al* (2015)
pMM0533	ColE1-CamR-ConL2	Lee *et al* (2015)
pMM0537	ColE1-CamR-ConR1	Lee *et al* (2015)
pMM0541	ColE1-CamR-ConRE	Lee *et al* (2015)
pMM0542	ColE1-CamR-tENO1	Lee *et al* (2015)
pMM0543	ColE1-CamR-tSSA1	Lee *et al* (2015)
pMM0544	ColE1-CamR-tPGK1	Lee *et al* (2015)

pMM0545	ColE1-CamR-tENO2	Lee *et al* (2015)
pMM0546	ColE1-CamR-tTDH1	Lee *et al* (2015)
pMM0547	ColE1-CamR-Spacer	Lee *et al* (2015)
pMM0556	ColE1-AmpR-sfGFP dropout	Lee *et al* (2015)
pMM0559	ColE1-CamR-pCCW12	Lee *et al* (2015)
pMM0560	ColE1-CamR-pPGK1	Lee *et al* (2015)
pMM0561	ColE1-CamR-pTEF2	Lee *et al* (2015)
pMM0562	ColE1-CamR-pRNR2	Lee *et al* (2015)
pMM0580	pDup3	Gerami-Nejad *et al* (2013)
pMM0607	AHB102	Nobile *et al* (2012)
pMM0676	pADH99	Nguyen *et al* (2017)
pMM0744	ColE1-AMP-RFP	Lee *et al* (2015)
pMM0894	ColE1-CamR-Neut5L 3' homology arm	This Study
pMM0895	ColE1-CamR-Neut5L 5' homology arm	This Study
pMM0897	ColE1-CamR-mCherry	This Study
pMM0898	ColE1-CamR-NatR	Lee *et al* (2015)
pMM1104	ColE1-CamR-pHHF1	Lee *et al* (2015)
pMM1106	ColE1-CamR-pPAB1	Lee *et al* (2015)
pMM1107	ColE1-CamR-pRET2	Lee *et al* (2015)
pMM1108	ColE1-CamR-pRNR1	Lee *et al* (2015)
pMM1110	ColE1-CamR-pPOP6	Lee *et al* (2015)
pMM1112	ColE1-CamR-pPSP2	Lee *et al* (2015)
pMM1113	ColE1-CamR-pACT1	This Study
pMM1114	ColE1-CamR-pENO1	This Study
pMM1115	ColE1-AmpR-Neut5-pHHF1-mCherry-tENO1-NatR-Neut5	This Study
pMM1116	ColE1-AmpR-Neut5-pPAB1-mCherry-tENO1-NatR-Neut5	This Study
pMM1117	ColE1-AmpR-Neut5-pRET2-mCherry-tENO1-NatR-Neut5	This Study
pMM1118	ColE1-AmpR-Neut5-pRNR1-mCherry-tENO1-NatR-Neut5	This Study
pMM1119	ColE1-AmpR-Neut5-pPOP6-mCherry-tENO1-NatR-Neut5	This Study
pMM1120	ColE1-AmpR-Neut5-pPSP2-mCherry-tENO1-NatR-Neut5	This Study
pMM1121	ColE1-AmpR-Neut5-pREV1-mCherry-tENO1-NatR-Neut5	This Study
pMM1122	ColE1-AmpR-Neut5-pCCW12-mCherry-tENO1-NatR-Neut5	This Study
pMM1123	ColE1-AmpR-Neut5-pPGK1-mCherry-tENO1-NatR-Neut5	This Study
pMM1124	ColE1-AmpR-Neut5-pTEF2-mCherry-tENO1-NatR-Neut5	This Study
pMM1125	ColE1-AmpR-Neut5-pTEF1-mCherry-tENO1-NatR-Neut5	This Study
pMM1126	ColE1-AmpR-Neut5-pRPL18B-mCherry-tENO1-NatR-Neut5	This Study
pMM1127	ColE1-AmpR-Neut5-pRNR2-mCherry-tENO1-NatR-Neut5	This Study
pMM1128	ColE1-AmpR-Neut5-pTDH3-mCherry-tENO1-NatR-Neut5	This Study

pMM1129	ColE1-AmpR-Neut5-SPACER-NatR-Neut5	This Study
pMM1130	ColE1-AmpR-Neut5-pACT1-mCherry-tENO1-NatR-Neut5	This Study
pMM1131	ColE1-AmpR-Neut5-pENO1-mCherry-tENO1-NatR-Neut5	This Study
pMM1149	ColE1-KanR-Neut5-GFP dropout-NatR-Neut5	This Study
pMM1274	ColE1-AmpR-Neut5-pENO1-mCherry-tssa1-NatR-Neut5	This Study
pMM1275	ColE1-AmpR-Neut5-pENO1-mCherry-tpgk1-NatR-Neut5	This Study
pMM1276	ColE1-AmpR-Neut5-pENO1-mCherry-teno2-NatR-Neut5	This Study
pMM1277	ColE1-AmpR-Neut5-pENO1-mCherry-ttdh1-NatR-Neut5	This Study
pMM1278	ColE1-AmpR-Neut5-pACT1-mCherry-tssa1-NatR-Neut5	This Study
pMM1279	ColE1-AmpR-Neut5-pACT1-mCherry-tpgk1-NatR-Neut5	This Study
pMM1280	ColE1-AmpR-Neut5-pACT1-mCherry-teno2-NatR-Neut5	This Study
pMM1366	NLS-zDBD-VP16	This Study
pMM1367	NLS-zDBD-VP64	This Study
pMM1368	NLS-LexA-VP16	This Study
pMM1369	NLS-LexA-VP64	This Study
pMM1370	pLexA w/ one LexA binding site	This Study
pMM1371	pEno1-zDBD-VP64-tEno2	This Study
pMM1372	pEno1-zDBD-VP64-tEno2	This Study
pMM1373	pEno1-LexA-VP64-tEno2	This Study
pMM1374	pEno1-LexA-VP64-tEno2	This Study
pMM1375	pEno1-zDBD-VP16-tEno2	This Study
pMM1376	pEno1-zDBD-VP16-tEno2	This Study
pMM1377	pEno1-LexA-VP16-tEno2	This Study
pMM1378	pEno1-LexA-VP16-tEno2	This Study
pMM1379	pZif-mCherry-tTdh1	This Study
pMM1380	pLexA-mCherry-tTdh1	This Study
pMM1381	pAct1-mCherry-tTdh1	This Study
pMM1382	p5xOPlexA	This Study
bMM1389	Spacer-Spacer-Spacer-Nat	This Study
bMM1390	pEno1-zdbd-vp64-tEno2-Spacer-Spacer-Nat	This Study
bMM1391	pEno1-zdbd-vp16-tEno2-Spacer-Spacer-Nat	This Study
bMM1394	pEno1-zdbd-vp64-tEno2-Spacer-pZif-mCherry-tTDH1-Nat	This Study
bMM1395	Spacer-pEno1-zdbd-vp64-tEno2-pZif-mCherry-tTDH1-Nat	This Study
bMM1398	pEno1-zdbd-vp16-tEno2-Spacer-pZif-mCherry-tTDH1-Nat	This Study
bMM1399	Spacer-pEno1-zdbd-vp16-tEno2-pZif-mCherry-tTDH1-Nat	This Study
bMM1402	Spacer-Spacer-pZif-mCherry-tTDH1-Nat	This Study
bMM1405	pEno1-zdbd-vp64-tEno2-Spacer-pAct1-mCherry-tTDH1-Nat	This Study
bMM1406	Spacer-pEno1-zdbd-vp64-tEno2-pAct1-mCherry-tTDH1-Nat	This Study

pMM1132	ColE1-CamR-CRY2	This Study
pMM1133	ColE1-CamR-CIB1	This Study
pMM1134	ColE1-CamR-LexA	This Study
pMM1135	ColE1-CamR-VP64	This Study
pMM1136	ColE1-CamR-zDBD	This Study
pMM1137	ColE1-CamR-pLexA	This Study
pMM1138	ColE1-CamR-mScarlet (*Candida* optimized)	This Study
pMM1140	conls-pRPL18b-lexa-cry2-teno1-conr1-(amp-cole1)	This Study
pMM1142	conls-pRPL18b-zDBD-cry2-teno1-conr1-(amp-cole1)	This Study
pMM1139	conls-ptef1-lexa-cry2-teno1-conr1-(amp-cole1)-	This Study
pMM1143	conl1-ptef1-vp64-cib1-teno1-conr2-(amp-cole1)	This Study
pMM1144	conl1-pRPL18B-vp64-cib1-teno1-conr2-(amp-cole1)	This Study
pMM1145	conl2-plexA-mscarlet-teno2-conre-ampcole1	This Study
pMM1146	conl2-ptef1-mscarlet-teno2-conre-ampcole1	This Study
pMM1147	conl2-rpl18b-mscarlet-teno2-conre-ampcole1	This Study
pMM1148	conl2-pzif-mscarlet-teno2-conre-ampcole1	This Study
pMM1281	1.conls-pACT1-lexa-cry2-teno1-conr1-(amp-cole1)-	This Study
pMM1282	2.conls-pENO1-lexa-cry2-teno1-conr1-(amp-cole1)	This Study
pMM1283	3.conls-pACT1-zDBD-cry2-teno1-conr1-(amp-cole1)	This Study
pMM1284	4.conls-pENO1-zDBD-cry2-teno1-conr1-(amp-cole1)	This Study
pMM1285	5.conl1-pACT1-vp64-cib1-ttdh1-conr2-(amp-cole1)	This Study
pMM1286	6.conl1-pENO1-vp64-cib1-ttdh1-conr2-(amp-cole1)	This Study
pMM1287	8.conl2-pACT1-mscarlet-teno2-conre-ampcole1	This Study
pMM1288	9.conl2-pENO1-mscarlet-teno2-conre-ampcole1	This Study
pMM1297	pEno1-LexA-Cry2-pEno1-VP64-Cib1-pLexa-mScarlet-Neut5-Kan-Nat-Neut5	This Study
pMM1298	pAct1-LexA-Cry2-pEno1-VP64-Cib1-pLexa-mScarlet-Neut5-Kan-Nat-Neut5	This Study
pMM1299	pEno1-LexA-Cry2-pAct1-VP64-Cib1-pLexa-mScarlet-Neut5-Kan-Nat-Neut5	This Study
pMM1300	pAct1-LexA-Cry2-pAct1-VP64-Cib1-pLexa-mScarlet-Neut5-Kan-Nat-Neut5	This Study
pMM1301	pEno1-zDBD-Cry2-pEno1-VP64-Cib1-pZif-mScarlet-Neut5-Kan-Nat-Neut5	This Study
pMM1302	pAct1-zDBD-Cry2-pEno1-VP64-Cib1-pZif-mScarlet-Neut5-Kan-Nat-Neut5	This Study
pMM1303	pEno1-zDBD-Cry2-pAct1-VP64-Cib1-pZif-mScarlet-Neut5-Kan-Nat-Neut5	This Study

pMM1304	pAct1-zDBD-Cry2-pAct1-VP64-Cib1-pZif-mScarlet-Neut5-Kan-Nat-Neut5	This Study
pMM1305	Spacer-pEno1-VP64-Cib1-pLexa-mScarlet-Neut5-Kan-Nat-Neut5	This Study
pMM1306	pEno1-LexA-Cry2-Spacer-pLexa-mScarlet-Neut5-Kan-Nat-Neut5	This Study
pMM1307	Spacer-pEno1-VP64-Cib1-pZif-mScarlet-Neut5-Kan-Nat-Neut5	This Study
pMM1308	pEno1-LexA-Cry2-Spacer-pZif-mScarlet-Neut5-Kan-Nat-Neut5	This Study
pMM1309	pEno1-LexA-Cry2-pEno1-VP64-Cib1-Spacer-Neut5-Kan-Nat-Neut5	This Study
pMM1310	pEno1-zDBD-Cry2-pEno1-VP64-Cib1-Spacer-Neut5-Kan-Nat-Neut5	This Study
pMM1311	pEno1-LexA-Cry2-pEno1-VP64-Cib1-pAct1-mScarletNeut5-Kan-Nat-Neut5	This Study
pMM1312	pEno1-LexA-Cry2-pEno1-VP64-Cib1-pEno1-mScarletNeut5-Kan-Nat-Neut5	This Study
pMM1313	pEno1-LexA-Cry2-pEno1-VP64-Cib1-pTef1(sc)-mScarletNeut5-Kan-Nat-Neut5	This Study
pMM1314	pEno1-LexA-Cry2-pEno1-VP64-Cib1-pRPL18B(sc)-mScarletNeut5-Kan-Nat-Neut5	This Study
pMM1412	pRPL18B-LexA-Cry2-pERPL18B-VP64-Cib1-pTef1(sc)-mScarlet-Neut5-Kan-Nat-Neut5	This Study
pMM1413	pRPL18B-LexA-Cry2-pERPL18B-VP64-Cib1-pRPL18B-mScarlet-Neut5-Kan-Nat-Neut5	This Study
pMM1414	pRPL18B-zDBD-Cry2-pTEF1-VP64-Cib1-pZif-mScarlet-Neut5-Kan-Nat-Neut5	This Study
pMM1415	pTEF1-LexA-Cry2-pTEF1-VP64-Cib1-pLexa-mScarlet-Neut5-Kan-Nat-Neut5	This Study
pMM1416	Spacer-Spacer-pEno1-mScarletNeut5-Kan-Nat-Neut5	This Study

Table 3. Oligo table

oMM	**Sequence**
oMM1970	GCATCGTCTCATCGGTCTCACAATaggccttaaacaagtggtatt
oMM1971	ATGCCGTCTCAGGTCTCAAGGGactgaattctacatcgaacaa
oMM1972	GCATCGTCTCATCGGTCTCAGAGTgggggggccgtaattgtaga
oMM1973	ATGCCGTCTCAGGTCTCATCGGctaggcctggaaggacgatga
oMM1976	GCATCGTCTCATCGGTCTCATatggtttctaagggtgaaga

oMM1977	ATGCCGTCTCAGGTCTCAGGATCCttacttgtacaattcatcca
oMM2182	GCATCGTCTCATCGGTCTCAaacgacagctaacaattacacaaaaa
oMM2183	ATGCCGTCTCAGGTCTCAcatacccgggttgtaatattcctg
oMM2184	GCATCGTCTCATCGGTCTCAaacgcgtcaaaactagagaataat
oMM2185	ATGCCGTCTCAGGTCTCAcatatttgaatgattatatttttt
oMM2107	GCATCGTCTCATCGGTCTCATatgccgaaaaagaaacgcaaa
oMM2108	ATGCCGTCTCAGGTCTCAAGAACCtagcatatctagat
oMM2109	GCATCGTCTCATCGGTCTCA/aacgggccgcaataatatat
oMM2110	ATGCCGTCTCAGGTCTCA/CATAGATCTtatagaagtat
oMM2186	GCATCGTCTCATCGGTCTCAT/atgccgaaaaagaaacgcaaagttggtagtcgcccatatgcttgccctgt
oMM2187	ATGCCGTCTCAGGTCTCAAGAACCatggattttggtatgcctct

Table 4. Plasmid Construction

pMM0894	oMM1970 andoMM1971 were used to amplify pMM580.This was then put in a golden gate with pMM452.
pMM0895	oMM1972 andoMM1973 were used to amplify pMM580.This was then put in a golden gate with pMM452.
pMM0897	oMM1976 andoMM1977 were used to amplify pMM607.This was then put in a golden gate with pMM452.
pMM1113	oMM2184 and oMM2185 were used to amplify pMM607.This was then put in a golden gate with pMM452.
pMM1114	oMM2182 and oMM2183 were used to amplify pMM676. This was then put in a golden gate with pMM452.
pMM1115	pMM894,pMM489,pMM1104,pMM897,pMM542,pMM491,pMM898, pMM895,pMM744 Golden Gated together
pMM1116	pMM894,pMM489,pMM1106,pMM897,pMM542,pMM491,pMM898, pMM895,pMM744 Golden Gated together
pMM1117	pMM894,pMM489,pMM1107,pMM897,pMM542,pMM491,pMM898, pMM895,pMM744 Golden Gated together
pMM1118	pMM894,pMM489,pMM1108,pMM897,pMM542,pMM491,pMM898, pMM895,pMM744 Golden Gated together
pMM1119	pMM894,pMM489,pMM1110,pMM897,pMM542,pMM491,pMM898, pMM895,pMM744 Golden Gated together
pMM1120	pMM894,pMM489,pMM1112,pMM897,pMM542,pMM491,pMM898, pMM895,pMM744 Golden Gated together
pMM1121	pMM894,pMM489,pMM455,pMM897,pMM542,pMM491,pMM898, pMM895,pMM744 Golden Gated together
pMM1122	pMM894,pMM489,pMM559,pMM897,pMM542,pMM491,pMM898, pMM895,pMM744 Golden Gated together
pMM1123	pMM894,pMM489,pMM560,pMM897,pMM542,pMM491,pMM898, pMM895,pMM744 Golden Gated together
pMM1124	pMM894,pMM489,pMM561,pMM897,pMM542,pMM491,pMM898, pMM895,pMM744 Golden Gated together
pMM1125	pMM894,pMM489,pMM522,pMM897,pMM542,pMM491,pMM898, pMM895,pMM744 Golden Gated together
pMM1126	pMM894,pMM489,pMM454,pMM897,pMM542,pMM491,pMM898, pMM895,pMM744 Golden Gated together
pMM1127	pMM894,pMM489,pMM562,pMM897,pMM542,pMM491,pMM898, pMM895,pMM744 Golden Gated together
pMM1128	pMM894,pMM489,pMM453,pMM897,pMM542,pMM491,pMM898, pMM895,pMM744 Golden Gated together
pMM1129	pMM894,pMM489,pMM457,pMM491,pMM898, pMM895,pMM744 Golden Gated together
pMM1130	pMM894,pMM489,pMM1113,pMM897,pMM542,pMM491,pMM898, pMM895,pMM744 Golden Gated together
pMM1131	pMM894,pMM489,pMM1114,pMM897,pMM542,pMM491,pMM898, pMM895,pMM744 Golden Gated together
pMM1149	pMM477,pMM490,pMM478,pMM898,pMM894,pMM481,pMM895 Golden Gated togeher
pMM1274	pMM894,pMM489,pMM1114,pMM897,pMM543,pMM491,pMM898, pMM895,pMM744 Golden Gated together
pMM1275	pMM894,pMM489,pMM1114,pMM897,pMM544,pMM491,pMM898, pMM895,pMM744 Golden Gated together

pMM1276	pMM894,pMM489,pMM1114,pMM897,pMM545,pMM491,pMM898, pMM895,pMM744 Golden Gated together
pMM1277	pMM894,pMM489,pMM1114,pMM897,pMM546,pMM491,pMM898, pMM895,pMM744 Golden Gated together
pMM1278	pMM894,pMM489,pMM1113,pMM897,pMM543,pMM491,pMM898, pMM895,pMM744 Golden Gated together
pMM1279	pMM894,pMM489,pMM1113,pMM897,pMM544,pMM491,pMM898, pMM895,pMM744 Golden Gated together
pMM1280	pMM894,pMM489,pMM1113,pMM897,pMM545,pMM491,pMM898, pMM895,pMM744 Golden Gated together
pMM1366	gMM0061 Golden Gate with 451
pMM1367	gMM0062 Golden Gate with 451
pMM1368	gMM0063 Golden Gate with 451
pMM1369	gMM0064 Golden Gate with 451
pMM1371	pMM489,1114,1367,545,491,556 golden gated together with BsaI
pMM1372	pMM532,1114,1367,545,537,556 golden gated together with BsaI
pMM1375	pMM489,1114,1366,545,491,556 golden gated together with BsaI
pMM1376	pMM532,1114,1366,545,537,556 golden gated together with BsaI
pMM1379	pMM533,528,897,546,541,556 golden gated together with BsaI
pMM1381	pMM533,1113,897,546,541,556 golden gated together with BsaI
bMM1389	pMM 822,823,619,1149 golden gated together with BSMBI
bMM1390	pMM 1371,823,619,1149 golden gated together with BSMBI
bMM1391	pMM 1375,823,619,1149 golden gated together with BSMBI
bMM1394	pMM 1371,823,1379,1149 golden gated together with BSMBI
bMM1395	pMM 1372,822,1379,1149 golden gated together with BSMBI
bMM1398	pMM 1375,823,1379,1149 golden gated together with BSMBI
bMM1399	pMM 1376,822,1379,1149 golden gated together with BSMBI
bMM1402	pMM 822,823,1379,1149 golden gated together with BSMBI
bMM1405	pMM 1371,823,1381,1149 golden gated together with BSMBI
bMM1406	pMM 1372,823,1381,1149 golden gated together with BSMBI
pMM1132	gMM0045 golden gate with pMM452
pMM1133	gMM0030 golden gate with pMM452
pMM1134	gMM0029 golden gate with pMM452
pMM1135	oMM2107 and oMM2108 to amplify VP64 from pMM390
pMM1136	oMM2186 and oMM2187 to amplify ZIF268 from pMM317
pMM1137	oMM2109 and oMM2110 to amplify pLexA from pMM907
pMM1138	gMM0037 golden gate with pMM452
pMM1140	pMM556,pMM489,pMM454,pMM1134,pMM1132,pMM542,and pMM491 golden gated together
pMM1142	pMM556,pMM489,pMM454,pMM1136,pMM1132,pMM542,and pMM491 golden gated together
pMM1139	pMM556,pMM489,pMM522,pMM1134,pMM1132,pMM542,and pMM491 golden gated together
pMM1143	pMM556,pMM532,pMM522,pMM1135,pMM1133,pMM542,and pMM537 golden gated together
pMM1144	pMM556,pMM532,pMM454,pMM1135,pMM1133,pMM542,and pMM537 golden gated together
pMM1145	pMM556,pMM533,pMM1137,pMM1138,pMM545,and pMM541 golden gated together

pMM1146	pMM556,pMM533,pMM522,pMM1138,pMM545,and pMM541 golden gated together
pMM1147	pMM556,pMM533,pMM454,pMM1138,pMM545,and pMM541 golden gated together
pMM1148	pMM556,pMM533,pMM528,pMM1138,pMM545,and pMM541 golden gated together
pMM1281	pMM556,pMM489,pMM1113,pMM1134,pMM1132,pMM542,and pMM491 golden gated together
pMM1282	pMM556,pMM489,pMM1114,pMM1134,pMM1132,pMM542,and pMM491 golden gated together
pMM1283	pMM556,pMM489,pMM1113,pMM1136,pMM1132,pMM542,and pMM491 golden gated together
pMM1284	pMM556,pMM489,pMM1114,pMM1136,pMM1132,pMM542,and pMM491 golden gated together
pMM1285	pMM556,pMM532,pMM1113,pMM1135,pMM1133,pMM542,and pMM537 golden gated together
pMM1286	pMM556,pMM532,pMM1114,pMM1135,pMM1133,pMM542,and pMM537 golden gated together
pMM1287	pMM556,pMM533,pMM1113,pMM1138,pMM545,and pMM541 golden gated together
pMM1288	pMM556,pMM533,pMM1114,pMM1138,pMM545,and pMM541 golden gated together
pMM1297	pMM1149,pMM1282,pMM1286,pMM1145 golden gated together
pMM1298	pMM1149,pMM1281,pMM1286,pMM1145 golden gated together
pMM1299	pMM1149,pMM1282,pMM1285,pMM1145 golden gated together
pMM1300	pMM1149,pMM1281,pMM1285,pMM1145 golden gated together
pMM1301	pMM1149,pMM1284,pMM1286,pMM1148 golden gated together
pMM1302	pMM1149,pMM1283,pMM1286,pMM1148 golden gated together
pMM1303	pMM1149,pMM1284,pMM1285,pMM1148 golden gated together
pMM1304	pMM1149,pMM1283,pMM1285,pMM1148 golden gated together
pMM1305	pMM1149,pMM822,pMM1286,pMM1145 golden gated together
pMM1306	pMM1149,pMM1282,pMM823,pMM1145 golden gated together
pMM1307	pMM1149,pMM822,pMM1286,pMM1148 golden gated together
pMM1308	pMM1149,pMM1282,pMM823,pMM1148 golden gated together
pMM1309	pMM1149,pMM1282,pMM1286,pMM619 golden gated together
pMM1310	pMM1149,pMM1284,pMM1286,pMM619golden gated together
pMM1311	pMM1149,pMM1282,pMM1286,pMM1287 golden gated together
pMM1312	pMM1149,pMM1282,pMM1286,pMM1288 golden gated together
pMM1313	pMM1149,pMM1282,pMM1286,pMM1146 golden gated together
pMM1314	pMM1149,pMM1282,pMM1286,pMM1147 golden gated together
pMM1412	pMM1149,pMM1140, pMM1144, pMM1146 golden gated together
pMM1413	pMM1149,pMM1140, pMM1144, pMM1147 golden gated together
pMM1414	pMM1149, pMM1142,pMM1143,pMM1148 golden gated together
pMM1415	pMM1149, pMM1139, pMM1143, pMM1145 golden gated together
pMM1416	pMM1149,pMM822,pMM823,pMM1288 golden gated together

Golden Gate Assembly

Plasmids and how they were constructed are listed above. Plasmids were constructed using either BsmB1 or Bsa1 Golden Gate assembly. Briefly, 20fmol of each plasmid was combined with 1µL of Golden Gate enzyme, 2µL of T4 ligase buffer, and water to 20µL. The thermocycler program was adapted from Lee, *et al* (2015) and included 30 cycles of digestion and ligation (5 min at 37(BsmBI) or 42(BsaI)°C; 5 min at 16°C) followed by a final digestion (60 °C for 10min) and a heat inactivation step (80°C for 10min). For cassettes where BsmBI assembly is needed the final ligation and heat inactivation steps were omitted. 2-5µL of the assembly mix was then transformed into DH5α competent *E. coli* and plated on LB plates with appropriate antibiotics. Plasmids were then extracted, digested with an appropriate enzyme as a first-pass test, and sequenced with appropriate primers for final verification.

Candida Transformations

Transformations were done using a LiAc protocol as described in [9]. Briefly, strains are grown overnight shaking in YPD + Uri at 30ºC. Then 500µL of cells are added to 50mL of YPD and grown shaking for ~4 hrs at 30 ºC. During this time 1-3 µg of plasmid is digested with Not1(.5µL enzyme, 2.5µL 3.1 buffer, 1-3µg plasmid, and water to 25µL) at 37ºC. After 4 hours cells are spun down at 3000rpm for 3 min and supernatant is discarded. 10ml of water is added and the spin is repeated. 500µL of TeLiAc (0.5ml 10X TE pH7.5, 0.5ml 1M LiAc, 4ml ddH20) is added and 100µL is added to each transformation along with 20-50mg of single stranded salmon sperm, and the digested plasmid. Transformation reactions incubate at 30ºC for 30 minutes before 700µL of PLATE (0.5ml10X TE pH7.5, 0.5ml 1M LiAc, 4ml 50% PEG) is added. Then transformations incubate at 30ºC overnight (16-20hrs). After overnight incubation, transformation reactions are heat shocked at 44ºC for 15 min before they are spun down at 3000rpm for 30sec. Cells are washed

with 1xPBS, 1ml YPD is added, and cells are incubated at 30 for ~4hrs before being plated on YPD+Nat (200µg/ml). Transformants are checked using colony or gDNA PCR using OneTaq master mix and primers appropriate to check integration at both ends.

Flow cytometry for Promotor and Terminator data

Strains were grown up overnight in LFM+Nat. They were then diluted 1:100 and grown for 5 hours. Cells were then diluted 1:4 in PBS+Tween and taken to flow cytometry. They were measured using the Attune Flow cytometer at the UW-Madison Carbone Cancer Center. Data was analyzed using a custom MATLAB script.

Flow cytometry for Optogenetic tools

Cells were grown overnight to saturation in the dark in a 96-well plate in LFM+ClonNat (200 µg/mL). The 96-well plates were covered with a Breath-Easy (USA Scientific) film to prevent evaporation but allow oxygen exchange. They were then diluted 1:20 and grown for 4 hours in the dark. The log phase cells were then diluted 1:2 and grown up for an additional 4 hours in either 405 µW/cm^2 light or dark. Blue light was delivered using an optoplate [32]–[34]. They were diluted 1:4 into 1xPBS + 0.1% Tween 20 and taken for flow cytometry on the Attune flow cytometer at the UW-Madison Carbone Cancer Center. Data was analyzed using a custom MATLAB script.

Flow cytometry for pZif

Cells were grown overnight to saturation in the dark in a 96-well plate in LFM+ClonNat (200 µg/mL). The 96-well plates were covered with a Breath-Easy (USA Scientific) film to prevent

evaporation but allow oxygen exchange. They were then diluted 1:20 and grown for 5hrs to reach log phase. Cells were then diluted 1:4 in PBS+Tween and taken to flow cytometry. They were measured using the Attune Flow cytometer at the UW-Madison Carbone Cancer Center. Data was analyzed using a custom MATLAB script.

References

[1] E. Rayens and K. A. Norris, "Prevalence and Healthcare Burden of Fungal Infections in the United States, 2018," *Open Forum Infect. Dis.*, vol. 9, no. 1, Jan. 2022.

[2] M. Gulati and C. J. Nobile, "Candida albicans biofilms: development, regulation, and molecular mechanisms.," *Microbes Infect.*, vol. 18, no. 5, pp. 310–21, May 2016.

[3] P. Uppuluri *et al.*, "Dispersion as an important step in the Candida albicans biofilm developmental cycle.," *PLoS Pathog.*, vol. 6, no. 3, p. e1000828, Mar. 2010.

[4] T. Roemer *et al.*, "Large-scale essential gene identification in Candida albicans and applications to antifungal drug discovery," *Mol. Microbiol.*, vol. 50, no. 1, pp. 167–181, Oct. 2003.

[5] E. M. Zhao, M. A. Lalwani, J. M. Chen, P. Orillac, J. E. Toettcher, and J. L. Avalos, "Optogenetic Amplification Circuits for Light-Induced Metabolic Control," *ACS Synth. Biol.*, vol. 10, no. 5, pp. 1143–1154, May 2021.

[6] P. M. Silva, C. Puerner, A. Seminara, M. Bassilana, and R. A. Arkowitz, "Secretory Vesicle Clustering in Fungal Filamentous Cells Does Not Require Directional Growth," 2019.

[7] M. E. Lee, W. C. DeLoache, B. Cervantes, and J. E. Dueber, "A Highly Characterized Yeast Toolkit for Modular, Multipart Assembly," *ACS Synthetic Biology*, 2015. [Online]. Available: http://pubs.acs.org/doi/pdf/10.1021/sb500366v. [Accessed: 29-Sep-2015].

[8] T. Ciudad *et al.*, "Homologous recombination in Candida albicans: role of CaRad52p in DNA repair, integration of linear DNA fragments and telomere length," *Mol. Microbiol.*, vol. 53, no. 4, pp. 1177–1194, Aug. 2004.

[9] M. Gerami-Nejad, L. F. Zacchi, M. McClellan, K. Matter, and J. Berman, "Shuttle vectors for facile gap repair cloning and integration into a neutral locus in Candida albicans.," *Microbiology*, vol. 159, no. Pt 3, pp. 565–579, Mar. 2013.

[10] A. C. Palmer, J. Barry Egan, and K. E. Shearwin, "Transcriptional interference by RNA polymerase pausing and dislodgement of transcription factors," *Transcription*, vol. 2, no. 1, p. 9, 2011.

[11] K. E. Shearwin, B. P. Callen, and J. B. Egan, "Transcriptional interference – a crash course," *Trends Genet.*, vol. 21, no. 6, p. 339, Jun. 2005.

[12] B. Stynen, P. van Dijck, and H. Tournu, "A CUG codon adapted two-hybrid system for the pathogenic fungus Candida albicans," *Nucleic Acids Res.*, vol. 38, no. 19, p. e184, Oct. 2010.

[13] E. Román, I. Coman, D. Prieto, R. Alonso-Monge, and J. Pla, "Implementation of a CRISPR-Based System for Gene Regulation in Candida albicans.," *mSphere*, vol. 4, no. 1, pp. e00001-19, Feb. 2019.

[14] R. R. Beerli, D. J. Segal, B. Dreier, and C. F. Barbas, "Toward controlling gene expression at will: Specific regulation of the erbB-2/HER-2 promoter by using polydactyl zinc finger proteins constructed from modular building blocks," *Proc. Natl. Acad. Sci. U. S. A.*, vol. 95, no. 25, p. 14628, Dec. 1998.

[15] N. C. for B. I. [1988] – [cited 2017 A. 06]. A. from: https://www. ncbi. nlm. nih. gov. National Center for Biotechnology Information (NCBI)[Internet]. Bethesda (MD): National Library of Medicine (US), "No Title." .

[16] P. M. Silva, C. Puerner, A. Seminara, M. Bassilana, and R. A. Arkowitz, "Secretory Vesicle Clustering in Fungal Filamentous Cells Does Not Require Directional Growth," *Cell Rep.*, vol. 28, no. 8, pp. 2231-2245.e5, Aug. 2019.

[17] J. (My) An-adirekkun *et al.*, "A yeast optogenetic toolkit (yOTK) for gene expression control in *Saccharomyces cerevisiae*," *Biotechnol. Bioeng.*, vol. 117, no. 3, pp. 886–893, Mar. 2020.

[18] D. H. Purohit, “Tec1 and Ste12 transcription factors play a role in adaptation to low pH stress and biolm formation in the human opportunistic fungal pathogen Candida glabrata,” 2022.
[19] S. E. Eckert and F. A. Mühlschlegel, “Promoter regulation in Candida albicans and related species,” *FEMS Yeast Res.*, vol. 9, no. 1, pp. 2–15, Feb. 2009.
[20] G. Tripathi, C. Wiltshire, S. Macaskill, H. Tournu, S. Budge, and A. J. P. Brown, “Gcn4 co-ordinates morphogenetic and metabolic responses to amino acid starvation in Candida albicans,” *EMBO J.*, vol. 21, no. 20, pp. 5448–5456, Oct. 2002.
[21] C. J. Barelle, C. L. Manson, D. M. MacCallum, F. C. Odds, N. A. R. Gow, and A. J. P. Brown, “GFP as a quantitative reporter of gene regulation in Candida albicans,” *Yeast*, vol. 21, no. 4, pp. 333–340, Mar. 2004.
[22] C. Frazer, A. D. Hernday, and R. J. Bennett, “Monitoring Phenotypic Switching in Candida albicans and the Use of Next-Gen Fluorescence Reporters,” *Curr. Protoc. Microbiol.*, vol. 53, no. 1, p. e76, Jun. 2019.
[23] B. Attractors *et al.*, “Introduction to Flow Cytometry: A Learning Guide,” 2002.
[24] J. Surre, C. Saint-Ruf, V. Collin, S. Orenga, M. Ramjeet, and I. Matic, “Strong increase in the autofluorescence of cells signals struggle for survival,” *Sci. Reports 2018 81*, vol. 8, no. 1, pp. 1–14, Aug. 2018.
[25] R. Maslanka, M. Kwolek-Mirek, and R. Zadrag-Tecza, “Autofluorescence of yeast *Saccharomyces cerevisiae* cells caused by glucose metabolism products and its methodological implications,” *J. Microbiol. Methods*, vol. 146, pp. 55–60, Mar. 2018.
[26] M. Monici, “Cell and tissue autofluorescence research and diagnostic applications,” *Biotechnol. Annu. Rev.*, vol. 11, no. SUPPL., pp. 227–256, Jan. 2005.
[27] M. J. Kennedy, R. M. Hughes, L. A. Peteya, J. W. Schwartz, M. D. Ehlers, and C. L. Tucker, “Rapid blue light induction of protein interactions in living cells,” *Nat. Methods*, vol. 7, no. 12, p. 973, Dec. 2010.
[28] A. Gräwe and V. Stein, “Linker Engineering in the Context of Synthetic Protein Switches and Sensors,” *Trends Biotechnol.*, vol. 39, no. 7, pp. 731–744, Jul. 2021.
[29] X. Chen, J. L. Zaro, and W. C. Shen, “Fusion Protein Linkers: Property, Design and Functionality,” *Adv. Drug Deliv. Rev.*, vol. 65, no. 10, p. 1357, Oct. 2013.
[30] M. Elrod-Erickson, M. A. Rould, L. Nekludova, and C. O. Pabo, “Zif268 protein-DNA complex refined at 1.6 Å: A model system for understanding zinc finger-DNA interactions,” *Structure*, 1996.
[31] M. Elrod-Erickson and C. O. Pabo, “Binding Studies with Mutants of Zif268: CONTRIBUTION OF INDIVIDUAL SIDE CHAINS TO BINDING AFFINITY AND SPECIFICITY IN THE Zif268 ZINC FINGER-DNA COMPLEX,” *J. Biol. Chem.*, vol. 274, no. 27, pp. 19281–19285, Jul. 1999.
[32] L. J. Bugaj and W. A. Lim, “High-throughput multicolor optogenetics in microwell plates,” *Nat. Protoc.*, vol. 14, no. 7, pp. 2205–2228, Jul. 2019.
[33] O. S. Thomas, M. Hörner, and W. Weber, “A graphical user interface to design high-throughput optogenetic experiments with the optoPlate-96,” *Nat. Protoc. 2020 159*, vol. 15, no. 9, pp. 2785–2787, Jul. 2020.
[34] E. O. S. Grødem, K. Sweeney, and M. N. McClean, “Automated calibration of optoPlate LEDs to reduce light dose variation in optogenetic experiments,” *Biotechniques*, vol. 69, no. 4, p. 313, Oct. 2020.

Chapter 5: Exploring under-oil microfluidics to develop a dispersion assay for *C. albicans*

Portions of this chapter were published:

Li C, Hite Z, Warrick JW, Li J, Geller SH, Trantow VG, McClean MN, Beebe DJ. Under oil open-channel microfluidics empowered by exclusive liquid repellency. Sci Adv. 2020 Apr 17;6(16):eaay9919. doi: 10.1126/sciadv.aay9919. PMID: 32494607; PMCID: PMC7164933.

Stephanie H Geller designed the research shown in Figure 2. Chao Li designed the remaining research. Chao Li, Zachary Hite, and Jiayi Li performed the experiments for Figures 1a, 3, and 4. Stephanie H Geller performed the experiments in Figure 1b and 2. Chao Li , Zachary Hite, Jiayi Li, and Stephanie H Geller performed the experiments for Figure 5. Chao Li, Jay W. Warrick, Zachary Hite, and Stephanie H Geller analyzed the raw data and prepared data visualization. All authors wrote the manuscript and revised it. Stephanie H. Geller wrote the chapter.

Abstract

The assays that are currently available for studying dispersion are limited in the ability to screen large libraries while visualizing biofilm development and collecting dispersed and biofilm cells. Additionally, the only assay that has the possibility to visualize biofilm growth in a high throughput manner, the 96-well microwell plate, does not allow for the addition of flow through the biofilm, which mimics physiological conditions that may be present in the body. Underoil open microfluidics have all the characteristics desired for a comprehensive dispersion assay since biofilm growth can for visualized using microscopy, cells can be collected for downstream analysis, passive or active flow can be added through the biofilm during development, and numerous strains can be screened at once. Here we describe an underoil microfluidic assay using double exclusive liquid repellency (ELR) to study biofilm development and dispersion. Visual comparison between strains grown in the standard 96-well assay and the underoil microfluidic assay show similar growth and dispersion phenotypes, confirmed through use of XTT (2,3-Bis-(2-Methoxy-4-Nitro-5-Sulfophenyl)-2H-Tetrazolium-5-Carboxanilide) and manual scoring. We then describe underoil channels that can add flow through a biofilm during or after biofilm development. We can temporally add passive flow to our assay using valves. Valves create changes in pressure in the channel that result in flow through the channel that is great enough to move dispersed cells. Lastly, we outline the characteristics of under oil channels compared to the current assays available.

Introduction

Candida albicans is an opportunistic pathogen that can cause severe infections in immunocompromised individuals and those with medical devices implanted with mortality rate reaching up to 25% [1]. Infections are almost always caused by biofilms developing on a surface such as a medical device and causing damage to a host tissue [2]. Biofilms form when yeast cells adhere to a surface and initiate biofilm formation through a change to hyphal growth. The biofilm will continue developing until it reaches maturation. During development and maturation, biofilm cells will bud and release yeast form "dispersed" cells. These cells will leave and seed additional downstream biofilms. Compared to biofilm development and virulence, there is less known about the environmental and genetic factors in the process of dispersion. This is at least partially due to insufficient tools for studying dispersion. Current tools cannot easily screen large mutant libraries in a biologically relevant environment.

The current assays available are the macro-flow assay, the micro-flow assay and a 96-well microplate assay [3]–[6]. The macro-flow assay involves biofilms growing on silicone sheet in a conical tube, where fresh media is constantly being flowed over the biofilm. Dispersed cells are collected in the flow through located under the conical. While this assay is the gold standard measuring dispersion directly, it fails to provide visualization of the biofilm which is critical when screening mutant libraries where biofilm growth is not characterized. This is because dispersed cells bud from hyphal cells, therefore characterization of biofilm development is needed. Additionally, it would be difficult for this assay to accommodate-high throughput screening of libraries due to the space required to run multiple replicates. The micro-flow assay works in a microfluidic device where media with cells is transported with tubing from a flask to a slide and

back to the flask for the first 2 hours of the experiment. Some cells will attach to the slide surface and begin biofilm development. After the first 2 hours fresh media will flow over the biofilm and dispersion can be visualized through the slide. While this assay allows for visualization of biofilm development, due to the nature of constant flow, this assay will not be suitable for adhesion mutants. Additionally, the cells cannot be removed from this assay for downstream analysis. Lastly, the microplate assay develops biofilm in a 96-well microplate by seeding cells in each well and letting them adhere for 6 hours. The media is then removed, and fresh media is added. After an allotted amount of time, usually 24 to 48 hours, the supernatant is removed and quantified as dispersed cells. XTT, which is a metabolic assay, is usually added to quantify the metabolic output of the cells, which is used as a proxy for cell count [7]. XTT is metabolized by *C. albicans* through a redox reaction that results in a colored formazan that can be measured using a plate reader at OD495. This assay cannot accommodate flow through the biofilm but does allow for visualization of biofilm growth and enough wells to contain a high throughput screen.

Open microfluidics has been defined as a microfluidic system with at least one solid boundary confining the fluid removed, exposing the fluid either to air (i.e., single liquid phase) or a second fluid (i.e., multiliquid phase) [8]–[12]. In single liquid–phase open microfluidics, fluid is directly exposed to air, which makes the systems susceptible to evaporation and airborne contamination through the liquid/air interface. Many open microfluidic systems use an oil overlay (i.e., under oil) [13], [14] to prevent detrimental fluid loss via evaporation and sample contamination. Important advantages of open microfluidics compared to closed microfluidics include accessibility, air bubble elimination, decreased biofouling and ease of use. Closed microfluidics are vulnerable to biofouling by *C. albicans* since it is known to bind to many types of surfaces [15], [16]. The liquid-

air or liquid-liquid interface above and surrounding the fluid provides direct physical access to the fluid of interest, and the oil overlay prevents contamination of the sample [10]. In addition, without the need to bond to another surface, open microfluidic devices are generally easy to make and easy to use.

Here we describe using an underoil open microfluidic system for studying dispersion. Due to its characteristics of open accessibility for additional or removal of cells or media, its ability to sit on a microscope for visualizing biofilm development, the ability to create channels that allow flow through a biofilm during development, and the ability to create multiple channels or droplets to accommodate a large screen, this assay would be able to fill the needs that other assays lack. We also can create droplets that allow for static growth much like that of a 96-well plate assay.

Results

Underoil droplets recapitulate the biofilm lifecycle

Underoil microfluidic assays are crafted using double exclusive liquid repellency (ELR), which results in one surface having two different surface chemistries to create patterns with clear boundaries [17], [18]. This is produced by first oxygen plasma treating a glass slide and vapor depositing PDMS silane to create a hydrophobic surface (Fig 1A). A mask is then applied to the glass slide and oxygen plasma treatment is repeated. The sections that are exposed to air will then become hydrophilic by oxidation from the plasma. The slide is then covered with oil and inoculated media can be placed on each droplet or in the channels (discussed later). We added 1000 cells of wildtype *C. albicans* SC5314 to 2μL RPMI + MOPS droplets and imaged biofilm growth every 30 min for 20 hours at 37ºC (Fig 1B). All stages of biofilm development were evident in the underoil droplets; planktonic cells at 0hrs, biofilm initiation at 3.5hrs, biofilm maturation at 7.5hrs,

and finally dispersion at 14.5hrs. We were not surprised that biofilms would grow in small volumes since we know from previous work in small droplets that *C. albicans* can grow biofilms in volumes as low as 50nL [19], [20].

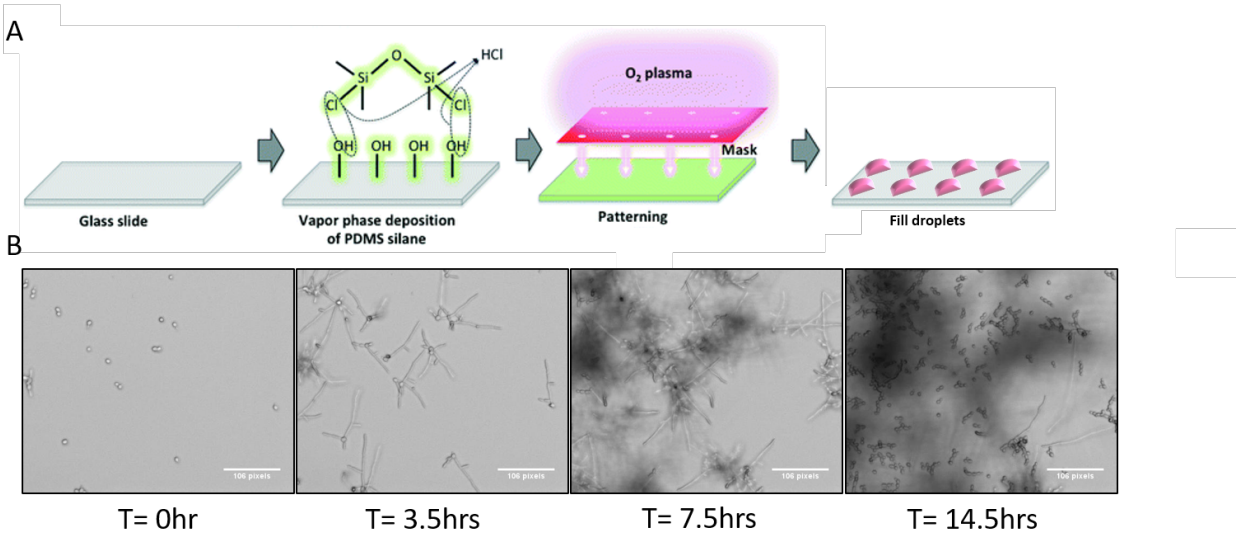

Figure 1. Stages of the biofilm lifecycle are present in underoil microfluidic droplets. A. Underoil microfluidics are built by starting with a glass slide or chambered glass coverslips, plasma treating the glass with oxygen plasma, and depositing PDMS silane through vapor deposition creating a hydrophobic surface. A mask with the microfluidic design is then put on the treated glass and plasma treatment is repeated, resulting in hydrophilic areas that were exposed to the oxygen plasma and hydrophobic areas that were covered by the mask. Oil is then overlayed on the glass and media with cells can be added directly to the microfluidic. This figure is adapted from Li, *et al* (2018) [17]. B. Wildtype SC5314 is able to show all stages of biofilm growth (adhesion, initiation, maturation, and dispersion) in underoil droplets.

Differences in dispersion apparent by XTT assays are also apparent in underoil assays

To determine if phenotypic differences in dispersion are detectable underoil we compared the XTT from a 96-well microplate assay and visual scoring from an underoil microfluidic droplet assay. We grew wildtype SC5314 strain (cMM1) and a clinical isolate (cMM11) that we know from the 96-well microplate assay, has less hyphae and greater dispersion than wildtype. We grew

them in both the 96-well microfluidic assay and the underoil microfluidic assay to compare growth. The 96-well microfluidic assay was seeded with $1x10^5$ cells in RPMI supplemented with MOPS and was grown for 22hrs at 37ºC with images taken every 30 minutes. After 22 hours the supernatant was removed and imaged. XTT was then added to the supernatant and biofilm and incubated for 1.25hrs at 37ºC with OD495 measurements taken every 15 minutes. The underoil microfluidic assay was seeded with $1x10^3$ cells in RPMI + MOPS and grown for 20 hours at 37ºC with images taken every 30 minutes. The images from the underoil microfluidic assay were then hand scored by 3 individuals to rate dispersion on a scale of deficient in dispersion(-), good at dispersion (+), or great at dispersion(++).

When comparing growth images of the wildtype strain in the 96-well microplate assay to the underoil microfluidic assay, there is hyphal growth in both assays which is indicated by the red arrows (Fig 2A, bottom two rows). Dispersion is visible in the underoil assay (Fig 2A, 12hrs) which is not achievable in the 96-well assay as the field of view gets too crowded to visualize individual cells by 5.4hrs of growth (Fig 2A). When looking at the clinical isolate (cMM11), the 96-well microplate assay there appears to be a dominance of pseudohyphal growth with some hyphal growth determined by eye and indicated by the red arrows (Fig 2A top row). However, in the underoil assay there appears to be a dominance of hyphal growth with some pseudohyphal growth. When comparing the dispersion from cMM11 and cMM1, both the images (Fig 2A), XTT measurements (Fig 2B), and manual scorers (Fig 2D) agree that cMM11 disperses more than cMM1. This indicates that the quantity of dispersion in the underoil assay is phenotypically similar of dispersion in the 96-well microplate. Though there is not statistical significance in the supernantant XTT readings, I predict that these differences may be biologically significant. Since

XTT was applied to both the biofilm and supernatant in the 96-well microplate assay, we were able to determine a "dispersive capacity" of each strain by dividing the supernatant XTT measurement by the biofilm XTT measurement. This calculates the amount of dispersion relative to the size of the biofilm. This is important since it can be hypothesized that a large biofilm will disperse more cells than a smaller biofilm, therefore normalizing by the size of the biofilm is important to determining if the strain is highly dispersive or not. Though not statistically significant, there is a shift in the mean of cMM11 when compared to cMM1 (Fig 2C).

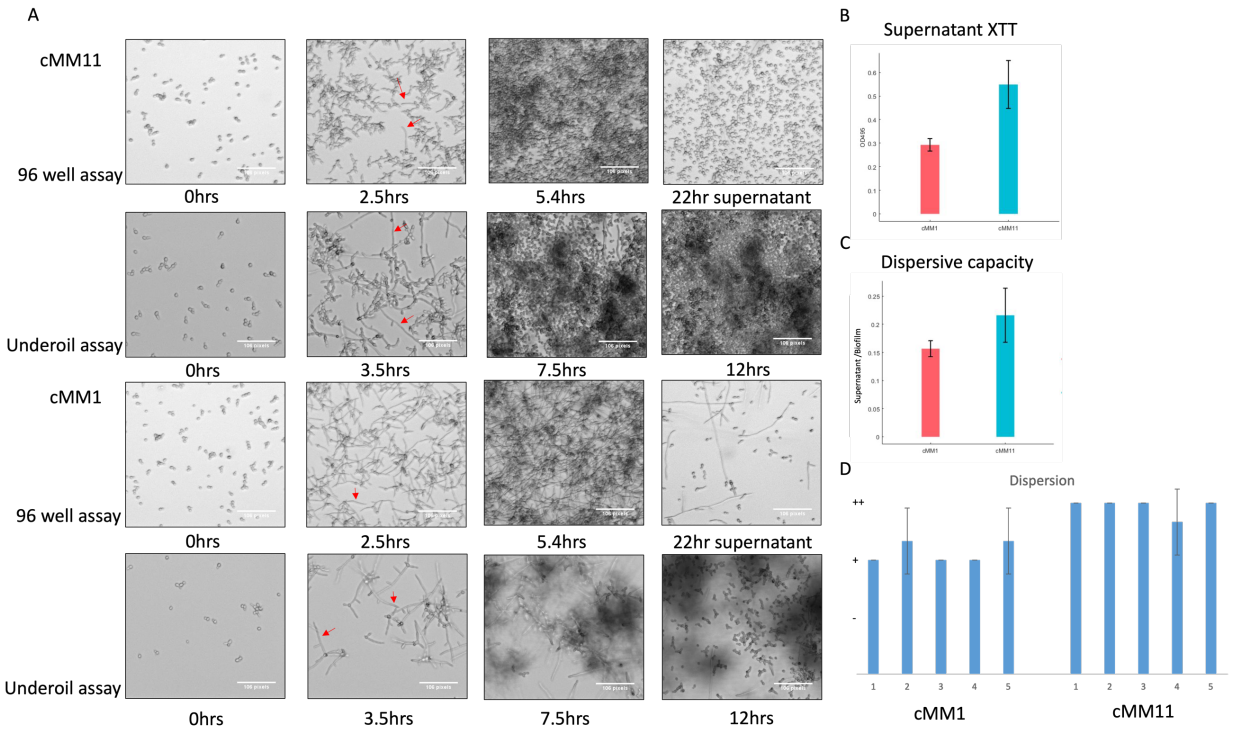

Figure 2. Comparing strains grown using the 96-well plate assay to strains grown in the underoil microfluidic assay. A. Two *C. albicans* strains are shown growing in either the 96-well biofilm assay or the microfluidic assay. Time lapse imaging was used to visualize the morphology of biofilm growth. The red arrows indicate hyphal growth is present in the samples. B. XTT was applied to the supernatant of cMM1 and cMM11 from the 96-well assay after imaging. Data represents the mean of 3 technical replicates after 1hr with XTT. Error bars indicate standard error of the mean C. Dispersive capacity of cMM1 and cMM11 was calculated by dividing the supernatant XTT by the biofilm XTT. Data represents the mean of 3 technical replicates and error

bars indicate standard error of the mean. D. Hand scoring of dispersion from the underoil microfluidic assay for cMM1 and cMM11. Labels 1-5 distinguish 5 replicate biofilms. Error bars are standard deviation of the 3 scorers.

We explored additional strains to determine if we could distinguish high dispersers in the underoil assay by manual scoring. We took 10 additional clinical isolates (JMI labs) and grew them in the 96-well assay and the underoil assay as done above (Fig S1). Using XTT we saw that there were differences in dispersion between the isolates, though not statistically significant (Fig S1A-B), however, this was not replicated in the manual scoring (Fig S1E). This indicates that while differences can be seen in the strains, our manual scoring tests were not able to distinguish those differences, likely due to limited scores available (if everything dispersed then there are only two options to choose, + or ++) and the inherent variability in human scoring. With the increasing ability of imaging processing and machine learning to distinguish cells and cell types in images, we think that image processing should be further investigated for distinguishing differences in dispersion.

Characterizing flow in an underoil microfluidic channel

The environment of a *C. albicans* infection such as a biofilm grown on a catheter is not static. There is consistently liquid flowing through the catheter and over the biofilm. So far, we have only used the microfluidic droplets for static growth of biofilms, much like that of the 96-well microplate assay. However, the underoil microfluidic assay can create channels for incorporating flow during biofilm development. Using inlets and outlets of different sizes creates Laplace pressure differentials that causes flow through the channel to the larger outlet where there is less resistance (Fig 3A). Dye was added to the inlet of a microfluidic channel after 2.5 hours we could see that the dye was delivered from the inlet to the outlet (Fig 3B). Changing the channel width

and length affected the flow of the dye to the outlet (Fig 3C). We determined that as the channel length and width increased, the flow rate to the outlet decreased as shown by less dye being delivered to the outlet. While it is predicted that this is due to increased resistance in the channel, causing flow rate to decrease, the physic in these microenvironments is not well understand [21]. We also observed that the flow rate did not seem to decrease over time as evident by the experimental data fitting directly over the linear fit line for the channels with a longer length (Fig 3C).

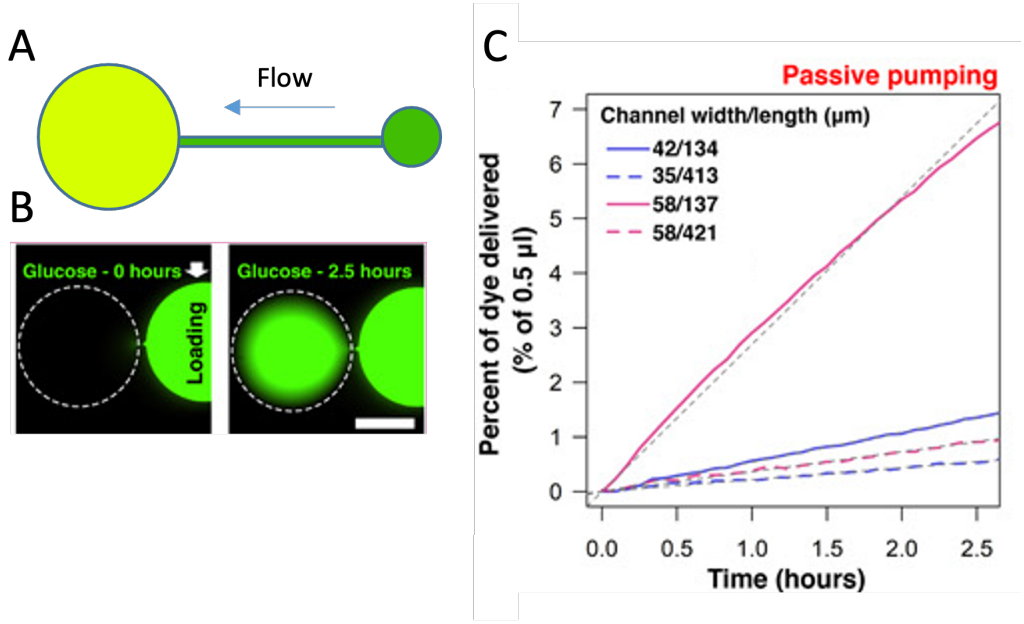

Figure 3. Channels incorporate flow in an underoil microfluidic. A. Passive flow is achieved in open channel microfluidics by different sized inlet and outlet, causing a Laplace pressure differential and flow to where there is the least surface tension, which is the larger outlet. B. Dye was added to the inlet of the microfluidic channel (58μm width/137 μm length) and images (485 nm/505 nm (excitation/emission)) were taken at 0hrs and 2.5hrs to evaluate passive flow through the channel. C. Percentage of dye delivered versus time by passive pumping from the microchannels. The fluorescence intensity (on the outlet spot) was converted to the percentage of volume delivered. The smaller dashed lines show the linear fitting. Images B and C were created by Chao Li and were taken from Li, *et al* (2020) [21].

We can also temporally control when flow is initiated in the channel by using an underoil valve (Fig 4). Valves can combine two portions of a channel when media is added to create a full channel that causes flow to the outlet port. The Pokeball valve is made of two horseshoes with a circle in the middle that connects the two sides of the channel (Fig 4A). Temporal control of flow is important because existing dispersion assays contains an adhesion step where cells are left to adhere to a surface for 2-6 hours before flow is added. Using the valve we are able to give the cells time to adhere to the slide before adding flow to the channel. Next, we tested the ability of the valve connection when the size of the horseshoes, distance between the horseshoes, or size of the inner circle changes when the channel size stays consistent (Fig4B). We noticed that when the size of the Pokeball increases the flow rate into the outlet also increases. Note that the spacing between the two horseshoes has a dominant influence on flow when it is small [21]. We also noticed that with these configurations, all the valves stably connected the channels for at least 14 hours, though we did not test if flow was still present at 14 hours.

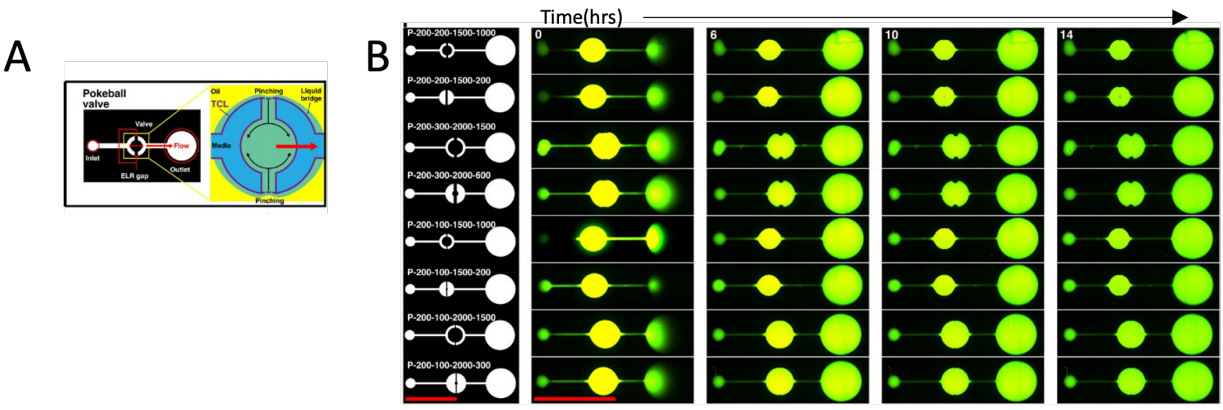

Figure 4. Valves allow for temporal control of flow through a channel. A. The Pokeball valve is made of two sides shaped like horseshoes that almost meet at the top and the bottom with a circle in the middle, much like the Pokeball coined by the Pokemon franchise. Adding media to the valve connects the two channel sides and causes flow to the outlet due to pressure differentials. B. Changing the configuration of the Pokeball by changing the distance of the sides from each other, the thickness of the horseshoes, and the size of the inner circle all change the flow rate to the outlet.

However, all configurations are stable for up to 14 hours. Images A and B were created by Chao Li and were taken from Li, *et al* (2020) [21].

Flow over biofilms result in movement of dispersed cells in an underoil microfluidic channel

Lastly, we investigated dispersion from a wildtype biofilm using a underoil microfluidic channel (Fig 5). Our channel consisted of an inlet port followed by a preculture channel area, a valve, the main channel with side channels for capturing cells, and an outlet port (Fig 5A). Wildtype *C. albicans* was seeded into the inlet port and grown for 4 hours to begin biofilm initiation. After 4 hours the inlet and preculture area contained mainly hyphal cells with a few remaining planktonic cells (Fig 5B). 3μL of fresh media was then added to the valve to connect the channels and some unadhered hyphae and planktonic cells flowed through the valve to either the main channel or the outlet port (Fig 5C). Next, media was then removed from the valve causing flow to be reversed back to the valve. Over the course of 18 hours, we see small clusters of hyphae begin to grow and release cells that travel through the channel to the valve (Fig 5D and E).

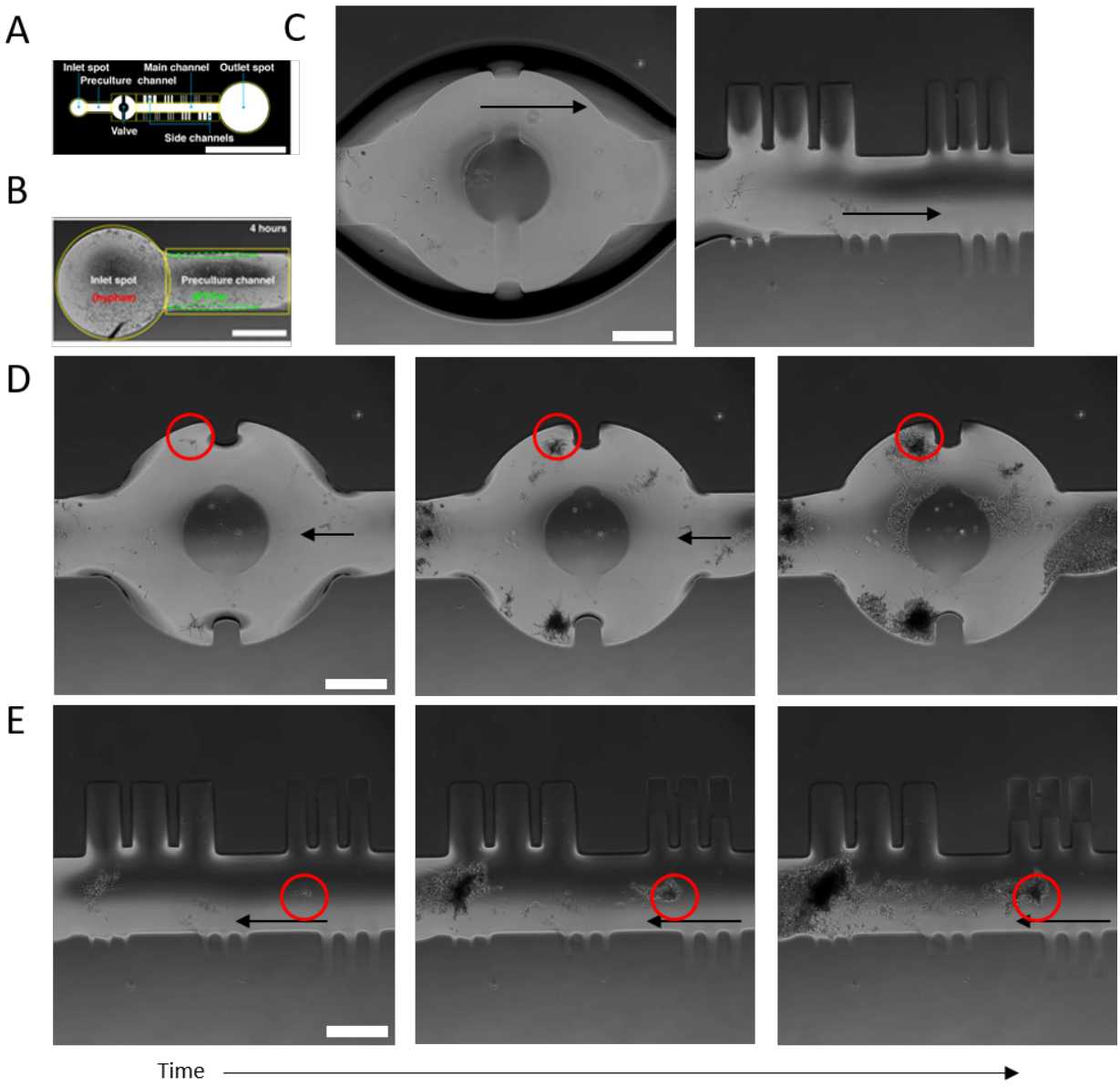

Figure 5. *C. albicans* disperses in the underoil microfluidic channel under flow environments. A. Schematic shows the components (in yellow boxes) and geometry of the microchannel. A straight channel with a set of side channels and a Pokeball valve (P-500-200-1500-600) to study dispersion events by separating dispersed cells from biofilm. Scale bar, 5 mm. B.Wild type (WT) *C. albicans* were seeded to the pre-culture channel at a density of 1000 cells/µL then incubated for 4hrs to grow into hyphae and initiate biofilm formation. The green circles on the side of the pre culture channel are indicating cells that have remained in yeast growth which the rest of the channel is in hyphal growth. Scale bar, 500 µm. C. A volume of media (RPMI 1640, 3µL) was added to

the valve to connect the microchannel and generate a bulk flow via passive pumping from left to right. Yeast and hyphal cells were flushed into the main channel and the valve. Scale bar, 500 μm. D. Some volume (~2.5μL) of the media was removed from the valve to reverse the direction of passive pumping or the flow (before, from left to right; after, from right to left). In time we see that the attached hyphal cells (circled in red) developed into second biofilms (and released dispersed cells to the flow in the main channel (left). Scale bar, 500 μm. E. In the main channel dispersion from biofilms (circled in red) can be seen over time after flow was reversed. Scale bar, 500 μm. Images are adapted from Li, *et al* (2020) [21].

Conclusions

Here we have described a new assay for dispersion that uses an open channel underoil microfluidic to visualize biofilm growth and dispersion. This assay allows for visualization of biofilm growth, flow through the biofilm, and the ability to collect the cells for downstream analysis while having the flexibility to have enough droplets to accommodate high throughput screening (Table 1). We have demonstrated that the underoil microfluidic droplets can screen 12 strains with 5 replicates per strain, resulting in 60 total droplets. This is equivalent to the number of strains that can be screened in a 96-well microplate when water is added to the outer wells to dampen the edge effects seen in microplates.

Assay	Visualize biofilm growth	Flow through biofilm	Ability to collect cells	Throughput
96-well	+	-	++	High
Underoil	++	++	+	High
Macro-flow	-	++	++	Medium
Micro-flow	++	++	-	Low

Table 1. The benefits of the underoil assay compared other dispersion assays.
++ indicates that this is easily possible, + indicates that this possible, and – indicates that this is not possible. High throughput is indicated by ability assay >30 strains at one time; medium throughput is indicated by the ability to screen >5 strains at onetime; low throughput indicated the ability to screen < 5 strains at one time.

We also identified that *C. albicans* can grow biofilms in the droplets and the channels. Scoring from the underoil droplets of a highly dispersive strain and a wildtype strain show that visually we can differentiate high dispersers from moderate dispersers. However, strains that lie between high dispersers and moderate dispersers were not able to be accurately identified using XTT in the 96-well assay or manual scoring in the underoil microfluidic assay. From this we can conclude that the underoil assay can recapitulate the dispersion phenotypes seen in the 96-well microplate assay for high and moderate dispersers evident by the XTT assay. However, without accurate quantification of the dispersion seen in the underoil microfluidic, we cannot determine if the underoil assay recapitulated the dispersion phenotype for all the strains. Scoring alternative identifiers of cell growth and dispersion such as the frame where dispersion begins or total biofilm

mass, may be helpful in distinguishing strains from each other. With the increasing ability of machine learning and image processing to identify cells and cell morphologies, images from underoil microfluidic assays may be able to be evaluated using these techniques and show greater differences between strains than we can by eye.

We described how flow can be added to the underoil microfluidic assay by using channels instead of droplets. When the inlet is smaller than the outlet this provides a pressure difference that results in media flowing to the outlet channel. This flow rate can be changed by altering the width and the length of the channel. We are also able to temporally control when flow is added to the system by using a valve. This allows for biofilms to grow in a static environment before flow is added. We also showed that the flow from changing pressure in the valve is enough to move dispersed cells through the channel. Eventually, this can lead to complete spatial separation of the biofilm and the dispersed cells.

While there is still a lot to learn about the biological environment of this tool, we believe this is a promising tool for screening large mutant libraries for extreme dispersion phenotypes. Without transcriptomic evidence we cannot confirm that the biofilms grown in the underoil microfluidic assay are comparable to the 96-well assay. However, similar morphologies throughout biofilm growth as seen in Figure 2 points to the assays producing comparable biofilms. We did observe that all strains tested produced large amounts of dispersed cells which may indicate the presence of a resource limitation that promotes dispersion. This should be investigated further by either RNA sequencing or changes in environment such as growth in nutrient dropout media. It has also been recently published that the oxygen state of the underoil environment can be changed by using

different oil overlays, specifically fluorinated oil, resulting in the absence of oxygen exchange through the oil [22]. This can soon create a hypoxic environment. Investigation into biofilm growth and dispersion in these environments would be interesting since many places that *C. albicans* infects are oxygen depleted such as the gut and the vagina [23], [24]. The versatility and flexibility of this tool makes it very useful for studying biofilm development and specifically dispersion.

Methods

Fabrication of PDMS-grafted glass

Premium microscope slide (Fisherfinest, 3″ × 1″ × 1 mm; Thermo Fisher Scientific, 12-544-1) or chambered coverglass (1 well, no. 1.5 borosilicate glass, 0.13 to 0.17 mm thick; Thermo Fisher Scientific, 155360) was treated first with O2 plasma (Diener Electronic Femto, Plasma Surface Technology) at 60 W for 3 min and then moved to a vacuum desiccator (Bel-Art F420220000, Thermo Fisher Scientific, 08-594-16B) for vapor phase deposition. PDMS-silane (1,3-dichlorotetramethylsiloxane; Gelest, SID3372.0) (about 10 μl per device) was vaporized under pumping for 3 min and then condensed onto glass substrate under vacuum at room temperature for 30 min. The PDMS-grafted surface was thoroughly rinsed with ethanol (anhydrous, 99.5%) and deionized (DI) water and then dried with nitrogen for use.

Fabrication of PDMS stamp

Photo mask was designed with Adobe Illustrator (Ai) and then sent to a service (Fineline Imaging) for printing. Standard photolithography was applied to make a master that contains all the microchannel features. A 4″ silicon wafer (University Wafer, ID 1116) was thoroughly cleaned and rinsed with acetone, isopropanol, and DI water and then dried with nitrogen before use. The wafer was baked on a hotplate (EchoTherm HP30, Torrey Pines Scientific) at 95°C for 30 min

before spin coating of a photoresist (SU-8 50, MicroChem, Y131269 1000 L 1GL). SU-8 was coated evenly onto the silicon wafer on a spin coater (Spincoater Model P6700, Specialty Coating Systems) with a speed setting (ramp to 500 rpm at 100 rpm/s and hold for 10 s, ramp to 2000 rpm at 300 rpm/s and hold for 30 s) that produces a thickness of about 50 μm. After prebaking on a hotplate at 65°C for 6 min, followed by 95°C of softbaking for 20 min, the photoresist layer hardened. Photo mask was placed on top of the silicon wafer and exposed to 365 nm of ultraviolet (OmniCure Series 1000) at 350 mJ/cm2 for about 30 min. To reduce stresses built up by traditional postexposure baking, the wafer was placed on a hotplate and ramped from room temperature to 95°C over approximately 5 min. Once the hotplate reached 95°C, it was turned off and allowed to cool down to room temperature. Uncross-linked SU-8 was washed off in propylene glycol monomethyl ether acetate (ReagentPlus, ≥99.5%; Sigma-Aldrich, 484431) on a shaker (SeaStar Digital Orbital Shaker) for 90 min to develop the features. The development was checked by rinsing the wafer with isopropanol, and a fully developed wafer showed no white residue, was washed with DI water, and was dried with nitrogen. Last, PDMS stamps were made by pouring a degassed (about 20 min using a vacuum desiccator) silicone precursor and curing agent mixture (SYLGARD 184, Silicone Elastomer Kit, Dow, 04019862) in 10:1 mass ratio onto the master and cured on a hotplate at 80°C for 4 hours. The PDMS stamps were stripped off with tweezers and punched with holes (Miltex Biopsy Punch with Plunger, Ted Pella, 15110) at the inlet and outlet of a microchannel for the following O2 plasma diffusion treatment.

Preparation of under oil open microchannels

The PDMS-grafted glass was masked by a punched PDMS stamp and then treated with O2 plasma at 60 W for 3 min. After surface patterning, the PDMS stamp was removed by tweezers and stored

in a clean space for reuse. The glass slides were held in a plate [Nunc four-well tray, polystyrene (PS), nontreated sterile, Thermo Fisher Scientific, 267061] and overlaid with oil (silicone oil, 5 cSt; Sigma-Aldrich, 317667). The chambered coverglass was directly overlaid with oil. Silicone oil is the "right" oil to give the extreme wettability (i.e., ELR) based on our previous work.[18] Tests on extraction of vital biomolecules (e.g., mRNA) from under oil and the quantitative polymerase chain reaction results in another previous work showed no obvious cargo loss during the processing [17]. The microchannels were filled with a media, Dulbecco's modified Eagle's medium (Thermo Fisher Scientific, 11960051) + 10% fetal bovine serum (Thermo Fisher Scientific, 10437010), by under oil sweep before use. The same media (unless otherwise specified) was used in preparation of all of the solution and suspension used in this study. An antistatic gun (Zerostat 3 Milty, EMS 60610) was used to generate perturbation during sweep and to facilitate the displacement of oil by media [17].

Measurement of the dimensions of underoil open microchannels

A reference curve was created from measuring a serially diluted 2-NBDG solution (from 20 to 0.1, 0.05, 0.02, 0.01, 0.005, and 0.002 mM in media) on a Nikon Eclipse Ti. The 2-NBDG solution was added to a set of under oil spots (2 mm in diameter) for 2 μl per spot, making a spherical cap-shaped microdroplet with a height of ~970 μm. Fluorescent images were taken using the 485-nm/525-nm (Ex/Em) channel (exposure time, 2 s) with no lookup table applied. The peak intensity in a small area (30 μm in diameter) close to the center of the microdroplets was measured in ImageJ (Set ROI–Measure–Analyze). Background intensity was measured using the same method and was subtracted from the peak intensity. The measured intensity was then converted to height equivalent to 2 mM 2-NBDG solution, which was used on the microchannels for profile analysis in the

following. (ii) The microchannels were prepared 5 mm in length with varying target widths (10, 25, 50, 100, and 200 μm) and spacings (50, 100, 200, and 500 μm). Fluorescent images were taken immediately after the microchannels were filled with the solution (i.e., 2 mM 2-NBDG solution) by under oil sweep. The profile was extracted and quantified in ImageJ (plot profile) with a region of interest (ROI) of 1750 μm (orthogonal to the channels) × 1900 μm (parallel to the channels). R/RStudio was used to find the peaks of the background subtracted profiles ('peakPick' package). Thresholding of the profiles was used to detect the edges of the channels. Width versus height was plotted and fit with the 'lm' function of R to estimate slopes and slope confidence intervals.

Double-ELR reversible valves. Microchannels (1 mm diameter inlet spot, 3 mm diameter outlet spot, 7 mm in length, and 500 μm or 200 μm in width) with three different types of valves (straight-channel, Bowman's capsule, and Pokeball) were prepared on PDMS-grafted glass slides. The microchannel between the valves with 2000 μm horseshoe patterns (Bowman's and Pokeball) and the outlet spot is 2 mm in length. For all other conditions, the microchannel is 3 mm in length. Formatting for valve labeling X-YYY-ZZZ-AAAA-CCC. X denotes the valve type (S = straight-channel, B = Bowman's capsule, P = Pokeball), YYY is the channel width, ZZZ is the size of the ELR gap (on straight-channel and Pokeball valves), AAAA is the size of horseshoe (on Bowman's capsule and Pokeball valves), and CCC is the size of the center spot (on Bowman's capsule and Pokeball valves). All the values are target dimensions in microns. (I) The 500 μm-wide microchannels were tested on a stereoscope (Olympus SZX12). Images and videos were collected with a CCD camera (Exo Labs Focus) connected to an iPad and samples were lit with a secondary light source (Dolan Jenner, Fiber-Lite Series 180). Each valve was loaded with 3 μL of a suspension containing fluorescent microbeads (1 μm in diameter, Interfacial Dynamics,

Fluorescent Nile Red CML Latex, 2-FN-1000) at a 1:50 dilution in media. The anti-static gun method was used to help distribute the microdrop on the valve. Video was recorded immediately after the valve was connected. Valves were used for multiple videos and therefore required washing with media between tests. Approximately 100 µL of media was dispensed on top of the microchannel and manually flushed and removed by pipet. (II) The 200 µm-wide microchannels were tested on a Nikon Eclipse Ti using time lapse (10 hr with 10 min intervals). 3 µL of 2-NBDG solution (2 mM in media) was placed on each valve. Time lapse was started immediately after all valves were connected and imaged using the 485 nm/525 nm (Ex/Em) channel (exposure time, 2 sec).

Spatiotemporal control on the dispersion of C. albicans

C. albicans SC5314 cells were grown overnight in a roller drum (250 rpm) at 37°C in yeast extract peptone dextrose (YPD) (1% yeast extract; BD), 2% peptone (BD), 2% dextrose (Thermo Fisher Scientific) supplemented with uridine (80 µg/ml; Acros Organics). To explore *Candida* life cycle checkpoints, two concentrations of the seeding cells (7000 cells/µl versus 70 cells/µl) were tested. The cell stock (vortexed) was added to a set of under oil spots (2 mm in diameter) for 2 µl per spot. Time lapse was taken on a Nikon Eclipse Ti using bright field for 18 hours with 5-min intervals. High-magnification images and z-stacks were recorded at 18 hours as the end point. For the dispersion test, the concentration of the cell stock for under oil seeding was 1000 cells/µl. The microchannel was prepared on a PDMS-grafted chambered coverglass. The device was then overlaid with oil, transferred to the on-stage incubator (37°C, 95% RH, 5% CO2) and filled with a media, RPMI 1640 (Gibco, Thermo Fisher Scientific, 11875093) by under oil sweep. One microliter of the cell stock (vortexed) was added to the inlet spot and the preculture channel and

then incubated for 4 hours with the valve disconnected. The primary biofilm was imaged using bright field on a Nikon Eclipse Ti at 4 hours. Then, 3 µl of RPMI 1640 was added to the valve to connect the preculture channel with the main channel, initiating movement of cells or hyphae from the primary biofilm to downstream into the main channel via bulk flow and passive pumping. After about 10 min, 2.5 µl of the volume at the valve was manually removed to reverse the direction of flow to stop further dispersion of the primary biofilm while maintaining a bulk flow (reversed) in the main channel. Time lapse was recorded at ×6 magnification from 4 to 45 hours with multiple locations, i.e., inlet spot and preculture channel, valve, left main channel and right main channel with side channels, and part of the outlet spot. Images were taken at 45 hours on a Nikon Eclipse Ti for end point using bright field. Last, the valve was disconnected by removing the volume along with the biomass (biofilm and cells) in the liquid bridge with pipet (and a 1- to 200-µl large orifice tip).

96-well microfluidic assay

Strains were grown overnight in YPD + uridine (80µg/mL) at 30ºC. Cells were then diluted to $1x10^6$ cells/mL in RPMI+MOPS. 100µL of diluted cells were put in a glass flat bottom 96-well microplate (Cellvis) with 100µL of RPMI+MOPS preloaded into the well. The microplate is then put in an 37ºC incubated box on the microscope (Nikon Eclipse Ti) and 10x magnification images are taken every 30 minutes for 22hrs. After 22 hours the supernatant is removed and added into unused wells in the 96-well plate. The supernatant is then imaged at 10x magnification and 100µL of XTT (90 µL XTT salt (0.5µg/µL), 10µL Phenazine methosulfate (0.32mg/mL)) is added to the biofilm and the supernatant. The microplate is then put in the Tecan Infinite M1000 plate reader

at 37ºC and OD495 readings were taken every 15 minutes for 1.25 hours. XTT analysis and image analysis was done using a custom Matlab script and ImageJ respectively.

Underoil microfluidic assay

Strains were grown overnight in YPD + uridine (80µg/mL) at 30ºC. Cells were then diluted to $1x10^6$ cells/mL in RPMI+MOPS. 1 µL of diluted cells were put in each droplet that had already been established with 1µL of fresh RPMI+MOPS. Slides were fabricated as described above. The underoil microfluidic slide is then put in an 37ºC incubated box on the microscope (Nikon Eclipse Ti) and 10x magnification images are taken every 30 minutes for 20hrs. Image analysis is done using ImageJ.

Table 2. Strain table

cMM	Strain	Source
cMM0001	SC5314	Noble, *et al* 2015 Eukaryotic Cell
cMM0011	Clinical Isolate 9817	Nett Lab
cMM0019	Clinical Isolate 1046484	Castanheira/JMI Labs
cMM0020	Clinical Isolate 1048706	Castanheira/JMI Labs
cMM0021	Clinical Isolate 1043914	Castanheira/JMI Labs
cMM0022	Clinical Isolate 1025998	Castanheira/JMI Labs
cMM0023	Clinical Isolate 1050032	Castanheira/JMI Labs
cMM0024	Clinical Isolate 1089716	Castanheira/JMI Labs
cMM0025	Clinical Isolate 1040838	Castanheira/JMI Labs
cMM0026	Clinical Isolate 1081202	Castanheira/JMI Labs

cMM0027	Clinical Isolate 1080518	Castanheira/JMI Labs
cMM0028	Clinical Isolate 1027877	Castanheira/JMI Labs

References

[1] E. Rayens and K. A. Norris, "Prevalence and Healthcare Burden of Fungal Infections in the United States, 2018," *Open Forum Infect. Dis.*, vol. 9, no. 1, Jan. 2022.

[2] P. Patricio, J. A. Paiva, and L. M. Borrego, "Immune Response in Bacterial and Candida Sepsis," *Eur. J. Microbiol. Immunol. (Bp).*, vol. 9, no. 4, p. 105, Dec. 2019.

[3] P. Uppuluri and J. L. Lopez-Ribot, "An easy and economical in vitro method for the formation of Candida albicans biofilms under continuous conditions of flow.," *Virulence*, vol. 1, no. 6, pp. 483–7, 2010.

[4] P. Uppuluri, A. K. Chaturvedi, and J. L. Lopez-Ribot, "Design of a simple model of Candida albicans biofilms formed under conditions of flow: development, architecture, and drug resistance," *Mycopathologia*, vol. 168, no. 3, pp. 101–109, 2009.

[5] A. McCall and M. Edgerton, "Real-Time Approach to Flow Cell Imaging of Candida albicans Biofilm Development.," *J. fungi (Basel, Switzerland)*, vol. 3, no. 1, Mar. 2017.

[6] M. B. Lohse, M. Gulati, A. V. Arevalo, A. Fishburn, A. D. Johnson, and C. J. Nobile, "Assessment and optimizations of Candida albicans in vitro biofilm assays 1," 2017.

[7] D. M. Kuhn, M. Balkis, J. Chandra, P. K. Mukherjee, and M. A. Ghannoum, "Uses and limitations of the XTT assay in studies of Candida growth and metabolism.," *J. Clin. Microbiol.*, vol. 41, no. 1, pp. 506–8, Jan. 2003.

[8] B. Zhao, J. S. Moore, and D. J. Beebe, "Surface-directed liquid flow inside microchannels," *Science (80-.).*, vol. 291, no. 5506, pp. 1023–1026, 2001.

[9] B. P. Casavant *et al.*, "Suspended microfluidics," *Proc. Natl. Acad. Sci. U. S. A.*, vol. 110, no. 25, pp. 10111–10116, 2013.

[10] G. V Kaigala, R. D. Lovchik, and E. Delamarche, "Microfluidics in the 'Open Space' for Performing Localized Chemistry on Biological Interfaces," *Angew. CHEMIE-INTERNATIONAL Ed.*, vol. 51, no. 45, pp. 11224–11240, 2012.

[11] E. K. Sackmann, A. L. Fulton, and D. J. Beebe, "The present and future role of microfluidics in biomedical research," *Nature*, vol. 507, no. 7491, pp. 181–189, 2014.

[12] J. Berthier, K. A. Brakke, and E. Berthier, "Open Microfluidics," *Open Microfluid.*, pp. 1–310, Jan. 2016.

[13] R. L. BRINSTER, "A METHOD FOR IN VITRO CULTIVATION OF MOUSE OVA FROM 2-CELL TO BLASTOCYST," *Exp. Cell Res.*, vol. 32, no. 1, pp. 205-+, 1963.

[14] J. C. Tae, E. Y. Kim, W. D. Lee, S. P. Park, and J. H. Lim, "Sterile filtered paraffin oil supports in vitro developmental competence in bovine embryos comparable to co-culture," *J. Assist. Reprod. Genet.*, vol. 23, no. 3, pp. 121–127, 2006.

[15] K. Lagree, H. H. Mon, A. P. Mitchell, and W. A. Ducker, "Impact of surface topography on biofilm formation by Candida albicans," *PLoS One*, vol. 13, no. 6, p. e0197925, Jun. 2018.

[16] S. A. Nikou *et al.*, "Candida albicans Interactions with Mucosal Surfaces during Health and Disease," *Pathogens*, vol. 8, no. 2, Jun. 2019.

[17] C. Li, J. Yu, P. Paine, D. S. Juang, S. M. Berry, and D. J. Beebe, "Double-exclusive liquid repellency (double-ELR): an enabling technology for rare phenotype analysis," *Lab Chip*, vol. 18, no. 18, pp. 2710–2719, Sep. 2018.

[18] C. Li *et al.*, "Exclusive Liquid Repellency: An Open Multi-Liquid-Phase Technology for Rare Cell Culture and Single-Cell Processing," *ACS Appl. Mater. Interfaces*, vol. 10, no. 20, pp. 17065–17070, May 2018.

[19] A. Srinivasan, P. Uppuluri, J. Lopez-Ribot, and A. K. Ramasubramanian, "Development of a High-Throughput Candida albicans Biofilm Chip," *PLoS One*, vol. 6, no. 4, p. e19036, Apr. 2011.

[20] A. Srinivasan, K. P. Leung, J. L. Lopez-Ribot, and A. K. Ramasubramanian, "High-Throughput Nano-Biofilm Microarray for Antifungal Drug Discovery," *MBio*, vol. 4, no. 4, Jun. 2013.

[21] C. Li *et al.*, "Under oil open-channel microfluidics empowered by exclusive liquid repellency," *Sci. Adv.*, vol. 6, no. 16, p. eaay9919, Apr. 2020.

[22] C. Li *et al.*, "Under-Oil Autonomously Regulated Oxygen Microenvironments: A Goldilocks Principle-

Based Approach for Microscale Cell Culture," *Adv. Sci.*, vol. 9, no. 10, p. 2104510, Apr. 2022.
[23] B. Ma, L. J. Forney, and J. Ravel, "The vaginal microbiome: rethinking health and diseases," *Annu. Rev. Microbiol.*, vol. 66, p. 371, Oct. 2012.
[24] E. S. Friedman *et al.*, "Microbes vs. chemistry in the origin of the anaerobic gut lumen," *Proc. Natl. Acad. Sci. U. S. A.*, vol. 115, no. 16, pp. 4170–4175, Apr. 2018.

Supplemental Figures

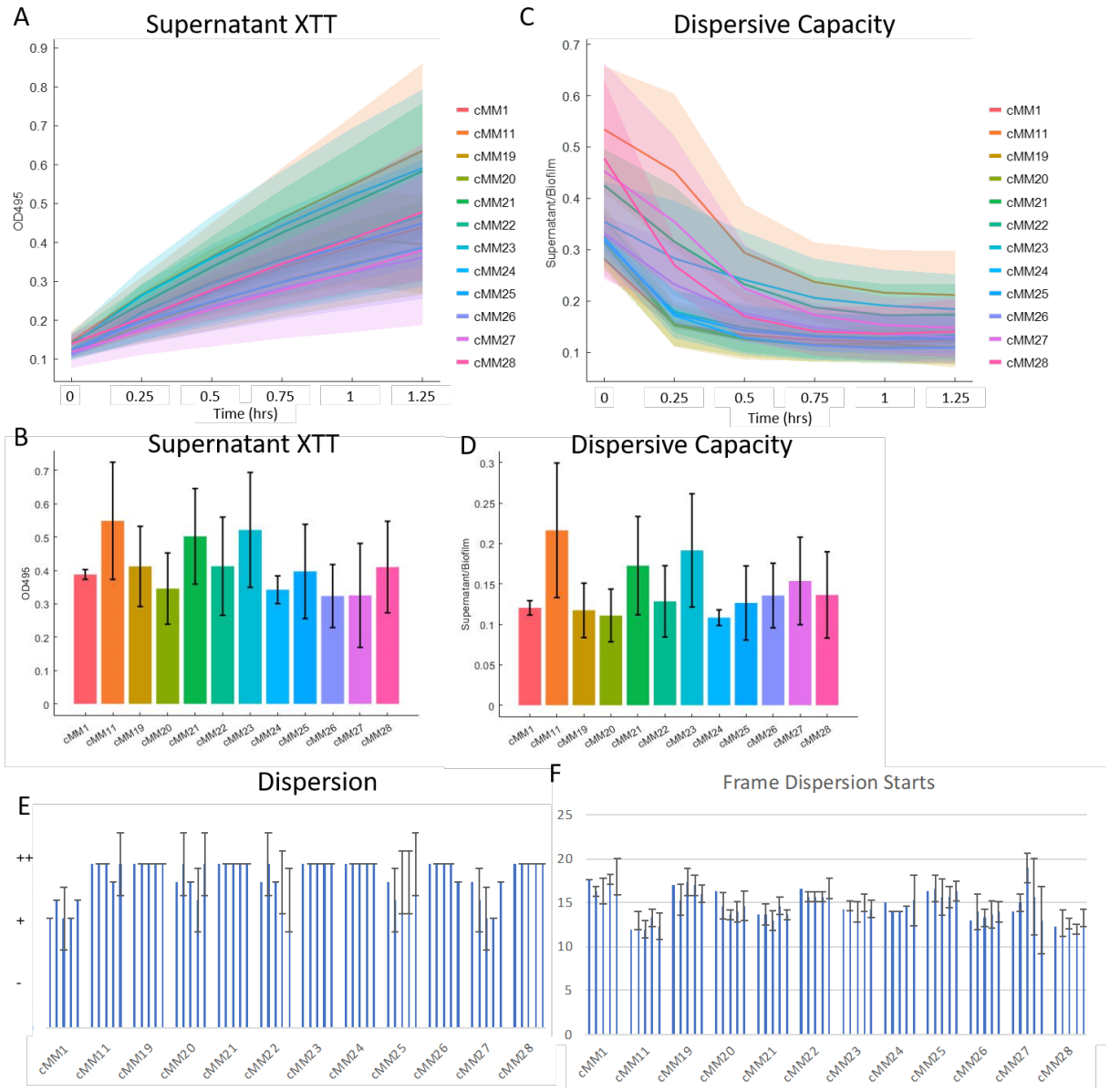

Figure S1. Comparing 10 clinical isolates using the 96-well microplate assay and the underoil microfluidic assay. A. XTT was applied to the supernatant of the strains from the 96-

well assay after imaging. Data was collected every 15 minutes for 1.25hrs after XTT was added. Data represents the mean of 3 technical replicates. Error bars indicate standard deviation B. Data from (A) at the 1hr reading. Data represents the mean of 3 technical replicates. Error bars indicate standard deviation. C. Dispersive capacity of the strains was calculated by dividing the supernatant XTT by the biofilm XTT for each time point. Data represents the mean of 3 technical replicates and error bars indicate standard deviation. D. Data from (C) at the 1hr time point. Data represents the mean of 3 technical replicates. Error bars indicate standard deviation. E. Hand scoring of dispersion from the underoil microfluidic assay for all samples. Each bar distinguishes a replicate biofilm. Error bars are standard deviation of the 3 scorers. F. Hand scoring of the frame dispersion start from the underoil microfluidic assay for all samples. Each bar distinguishes a replicate biofilm. Error bars are standard deviation of the 3 scorers.

Chapter 6: Measuring the dispersion of a *Candida albicans* transcription factor knockout library and measuring gene expression in highly dispersive strains

Stephanie H Geller designed this research, did the experimentation with the help of Eli Cytrynbaum and Lucas Voce, analyzed the data with the help of Kieran Sweeney, and wrote the chapter. Stephanie H Geller produced Figures 1-6. RNA sequencing was completed by the Biotechnology Center at UW-Madison. RNA sequencing data were analyzed by the Bioinformatics Resource Center at UW-Madison producing Figures 7-11.

Abstract

Candida albicans is an opportunistic pathogen that attaches to surfaces, such as implanted medical devices, and develops biofilms that can cause serious infections in immunocompromised individuals. The ability to dissemination or dispersion cells from these biofilms impacts the virulence of the infection. Previously it has been reported that dispersion is dependent on the environment such as nutrient availability and drug selection. However, little is known about dispersion on a transcriptomic level. Uppuluri, *et al* discovered 4 genes that are shown to affect dispersion: UME6, PES1, NRG1, and HSP90. Additionally, they completed RNA sequencing of dispersed cells, the biofilm, and age matched planktonic cells and found that dispersed cells show a different gene profile than biofilm or planktonic cells. To discover additional genes that influence the process of dispersion I screened a library of 165 transcription factor (TF) mutants for a dispersion phenotype that was significantly different than their wildtype parent strain. I discovered one mutant (rob1) that showed increased dispersion when compared to the parent strain while retaining the ability to grew hyphal cells and investigated it further using the underoil device that was introduced in Chapter 5. I then grew wildtype parent strain and *rob1Δ/Δ* biofilms to different time points for RNA sequencing to determine changes in gene expression over the biofilm lifecycle including dispersion. From RNA sequencing, I hypothesize that carbohydrate transport is important in the process of dispersion.

Introduction

Candida albicans is an opportunistic pathogen that causes severe infections in immunocompromised individuals and those with implanted medical devices [1], [2]. Biofilm development begins when planktonic cells adhere to a surface, such as a catheter, and begin biofilm initiation by changing their morphology to hyphal growth [3], [4]. Hyphae continue to replicate until the biofilm reaches maturation. The biofilm then creates yeast shaped lateral buds that will release from the biofilm and travel to a new location and develop new biofilms in a process called dispersion [5], [6]. The ability to disperse is an important aspect of how virulent a strain is since strains lacking dispersion are less virulent and dispersed cells are more virulent than planktonic cells [6], [7]. Due to insufficient tools, the process of dispersion has only been directly looked at in the last decade.

Our current knowledge of dispersion is limited. The process of dispersion is greatly affected by its environment; most notably is the abundance of carbon availability, and the pH of the environment [6]. Dispersed cells have been characterized to have increased drug resistance, and increased adherence to mammalian cells [6]. Additionally, dispersed cells have a unique gene expression when compared to a planktonic yeast cell and hyphal biofilm cells [8]. Dispersed cells have upregulated expression of genes relating to adhesion, transport, ribosome biogenesis and lipid metabolism when compared to biofilm cells, just to name a few [8]. Interestingly, dispersed cells have a carbon metabolism phenotype more like that of a planktonic cell than biofilm cells, however many other functions relating to ergosterol, methionine, and ribosome biosynthesis, resemble more closely to a biofilm cell. Dispersed cells are primed for infection with the upregulation of virulence genes such as host adhesion and invasion [8].

The only gene that has been directly linked to dispersion and no other function has been PES1 [6]–[8]. Overexpression of PES1 results in increased lateral budding while a knockdown using the TetR system decreases lateral budding. UME6, HSP90, and NRG1 have also been linked to dispersion, however it is known that these genes have other function in the cell such as cell stress response and hyphal development [6], [9], [10]. This indicates a need to find additional genes that are directly linked to dispersion.

Here I describe a screen of a transcription factor (TF) mutant library for increased dispersion phenotypes [11]. This library was built by Homann, *et al* and includes 165 homozygous TF mutant knockouts. This screen yielded one mutant (rob1Δ/ Δ) that was significantly more dispersive than its wildtype parent strain. Using our underoil microfluidic device, this mutant was visually confirmed to have a hyper dispersive phenotype (Chapter 5). I then completed RNA sequencing on biofilm development including dispersion for both the WT and *rob1Δ/Δ* mutant. Here, I report the results of my TF mutant library screen and subsequent RNA sequencing of the biofilm lifecycle for the wildtype parent strain and rob1Δ/ Δ.

Results

Using the 96-well microplate assay to screen 165 TF mutants for dispersion phenotypes

To discover additional genes that influence the process of dispersion, I screened the Homann, *et al* TF mutant library for an increase in dispersion [11]. This library is made up of 165 strains that have homozygous deletions of the TF of interest, with many strains having two biological replicates to ensure phenotypes that are seen are not due to any unlinked mutations that occurred

during the knockout. For my screen, I chose to use a 96-well microplate assay because it can screen multiple strains at once, making it more optimal for a large library screen over the gold standard macro-flow assay. However, to better utilize the 96-well microplate assay, biofilm growth and dispersion were imaged to visualize cell morphologies in these life stages. Outer wells of the 96-well microplate were filled with water to dampen any edge affects that may occur, resulting in six 96-well microplates to test every mutant strain in the library. Each plate contained three control strains to account for day-to-day variability; wildtype (WT) which is the wildtype parent strain SN152, SN152's parent strain SC5314 (cmm1), and a clinical isolate that is more dispersive than cmm1 (cmm11) (Chapter 5). Strains were inoculated into a 96-well flat bottom microplate and grown overnight in YPD supplemented with uridine (Fig 1). OD600 readings of the overnight culture were taken on a plate reader. The Tecan Fluent liquid handling robot was then used to dilute all the samples to 0.1 OD600. Plates were then imaged every 30 minutes for 6hrs in an incubated chamber at 37ºC. After 6hrs the media was removed, and fresh media was added to the growing biofilms. The strains were grown for another 48hrs in a 37ºC incubator with media being refreshed at 24hrs. After a total of 54hrs, the supernatant containing the dispersed cells was removed and put in a new 96-well microplate. The supernatant was imaged and XTT was added to the biofilm and the supernatant. XTT is a metabolic assay used to determine relative cell abundance by measuring the metabolic output of cells. When added to *C. albicans*, XTT is reduced by the cells resulting in an orange color that is absorbed at OD495. The Tecan Fluent was used to take OD495 readings for both the biofilm and the supernatant.

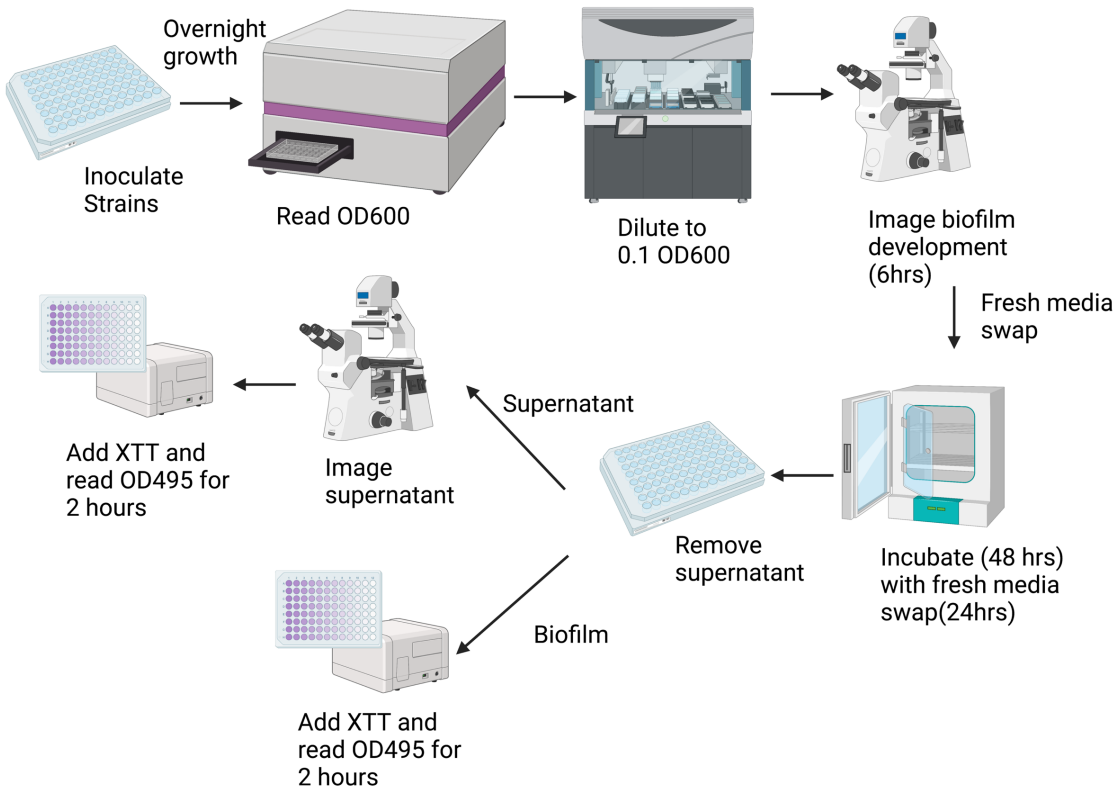

Figure 1. Schematic of the TF mutant screen. Strains were inoculated for overnight growth in a 96-well microplate. Strains were diluted 1:10 and an OD600 reading was taken. Using a liquid handling robot (Tecan Fluent) all strains were diluted to 0.1 OD600 in RPMI+MOPS. The 96-well microplate was then imaged every 30min for 6hrs in an incubated chamber at 37ºC for visualization of biofilm development. After 6hrs media was removed and fresh media was added to the biofilms and plates were incubated for 24hrs. After 24hrs media was removed and fresh media was added. After an additional 24hrs (54hrs total) the supernatant was removed and imaged to capture disperse cells. XTT was then added to both the dispersed cells and the biofilm cells and OD495 readings were taken every 5 minutes for 2 hours. This figure was created using BioRender.com.

From screening the TF mutant library, I found two mutants that had an increased dispersion phenotype when compared to the WT (Fig 2). A one-way ANOVA test was used to determine that there was a difference in mean supernatant XTT between samples ($p<1x10^{-5}$). Tukey's HSD Test

for multiple comparisons found that the mean value of supernatant XTT was significantly different between TF110 and WT ($p<1x10^{-6}$) and TF156 and WT($p<1x10^{-6}$).

Figure 2. Supernatant XTT results from the TF mutant screen. Data is shown after 2hrs of XTT incubation. Each point is one biological replicate and represents 3 technical replicates. Blue stars indicate statistical significance using a Tukey's HSD Test (p<1x10-6).

Additionally, I looked at the dispersive capacity of the strains by dividing the supernatant XTT OD495 by the biofilm XTT OD495. This helped understand the amount of dispersion that occurred relative to the biofilm size. This considers that a larger biofilm has the capacity to disperse more since more cells are present in larger biofilms. I discovered that two mutants dispersed more than WT relative to their respective biofilm sizes (Fig3). A one-way ANOVA test was used to determine that there was a difference in mean dispersive capacity between samples ($p<0.0005$). Tukey's HSD Test for multiple comparisons found that the mean value of dispersive capacities was significantly different between TF110 and WT ($p<0.05$) and TF103 and WT($p<0.005$).

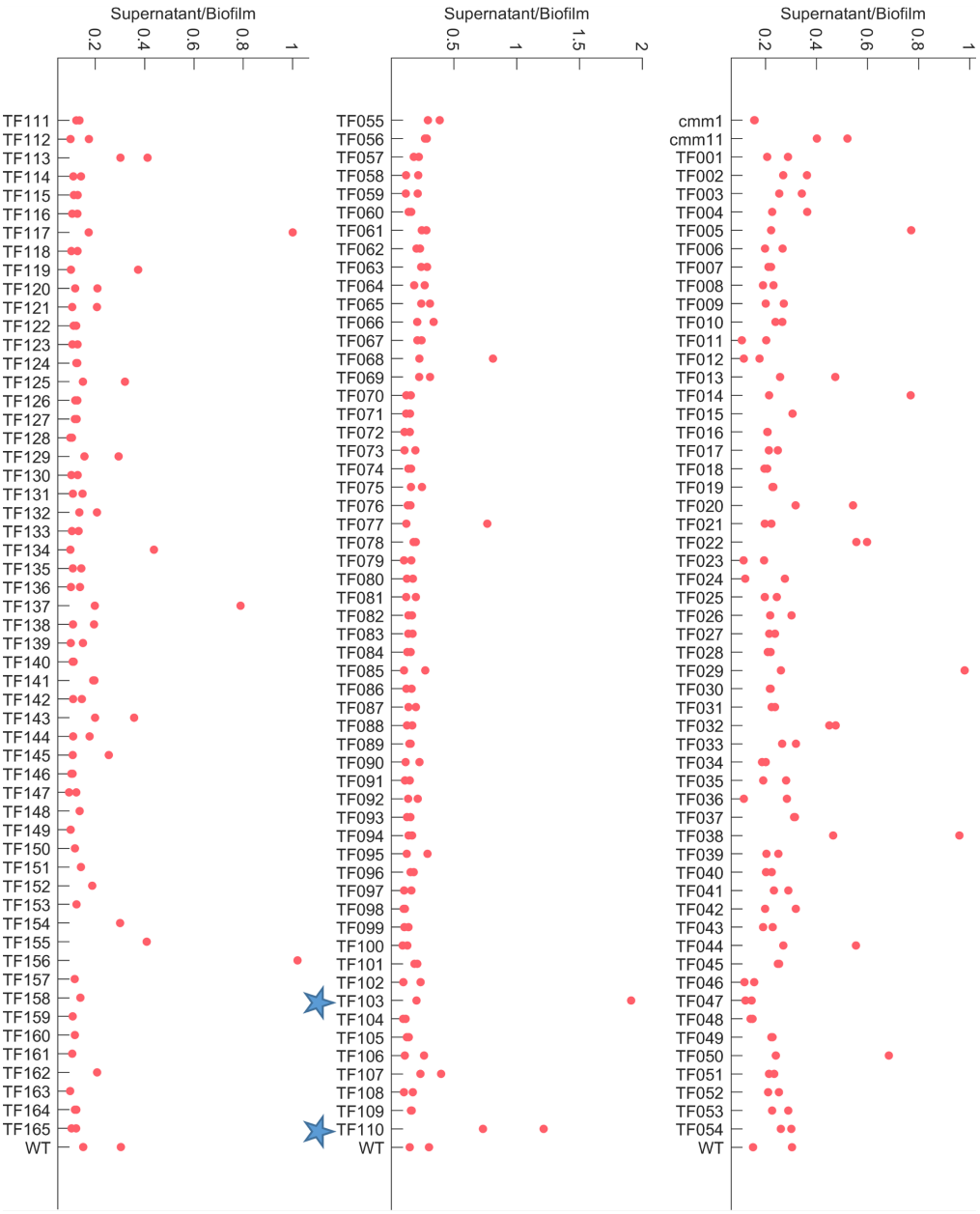

Figure 3. Dispersive capacity from the TF mutant screen. Dispersive capacity is calculated by dividing the XTT results from the supernatant by the XTT results from the biofilm. Both were XTT measurements after 2hrs of incubation. Each point is one biological replicate and represents 3 technical replicates. Blue stars indicate statistical significance using a Tukey's HSD Test ($p<0.05$).

TF103, TF110, and TF156 were all more dispersive than WT. When looking for strains with an increased dispersion phenotype, another consideration is whether the biofilm had hyphal development. We know that dispersed cells are budded from hyphal cells, therefore if a mutant cannot grow hyphae, I excluded that mutant from further analysis. Additionally, dispersive capacity may appear elevated if a section of the biofilm was removed when the supernatant was collected. Since these are not dispersed cells, these mutants were also excluded from further analysis. When looking at the images taken of both biofilm development and the supernatant, I identified that TF156 did not grow hyphae. TF156 is *efg1Δ/Δ*, which has been well characterized to be deficient in hyphal growth [12]–[15], therefore I did not move forward with additional investigation of this mutant. I also noticed that TF103 had large chunks of biofilm and very few yeast form cells in its supernatant. Lastly, TF110 was shown to be more dispersive than WT regardless of whether biofilm size was also compared. TF110, which is *rob1Δ/Δ*, visually displayed hyphal development, and presented more dispersed cells in the supernatant than WT (Fig 4). Rob1 has been characterized in the literature to regulate biofilm development due to deficient biofilm growth when compared to WT. However, *rob1Δ/Δ* has been shown to be capable of hyphal growth [12], [16], which is what I observed in my screen as well. To my knowledge no one has looked at the dispersion phenotype of *rob1Δ/Δ*.

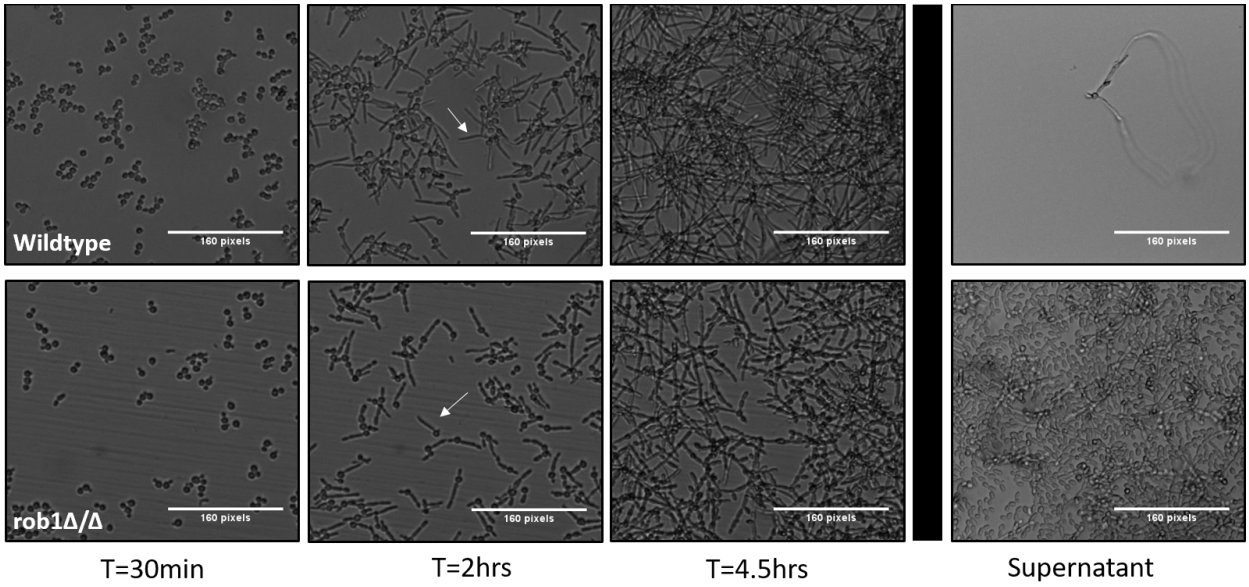

Figure 4. Growth of WT and *rob1Δ/Δ* in the 96-well microplate during the TF mutant screen. White arrows indicate hyphal growth.

To validate that *rob1Δ/Δ* disperses more than WT I grew both strains in our underoil microfluidic droplet. This assay allows visualization of biofilm development and dispersion using microscopy (Chapter 5). Hyphal growth is visually evident in both the WT and *rob1Δ/Δ* strains after 2.5hrs of growth in the underoil microfluidic assay, confirming that *rob1Δ/Δ* has hyphae to bud dispersed cells from (Fig 5). After 15hrs in the underoil microfluidic assay, the *rob1Δ/Δ* mutant displays dispersed cells that cannot be seen in the WT strain. This reflects the results from my TF mutant screen.

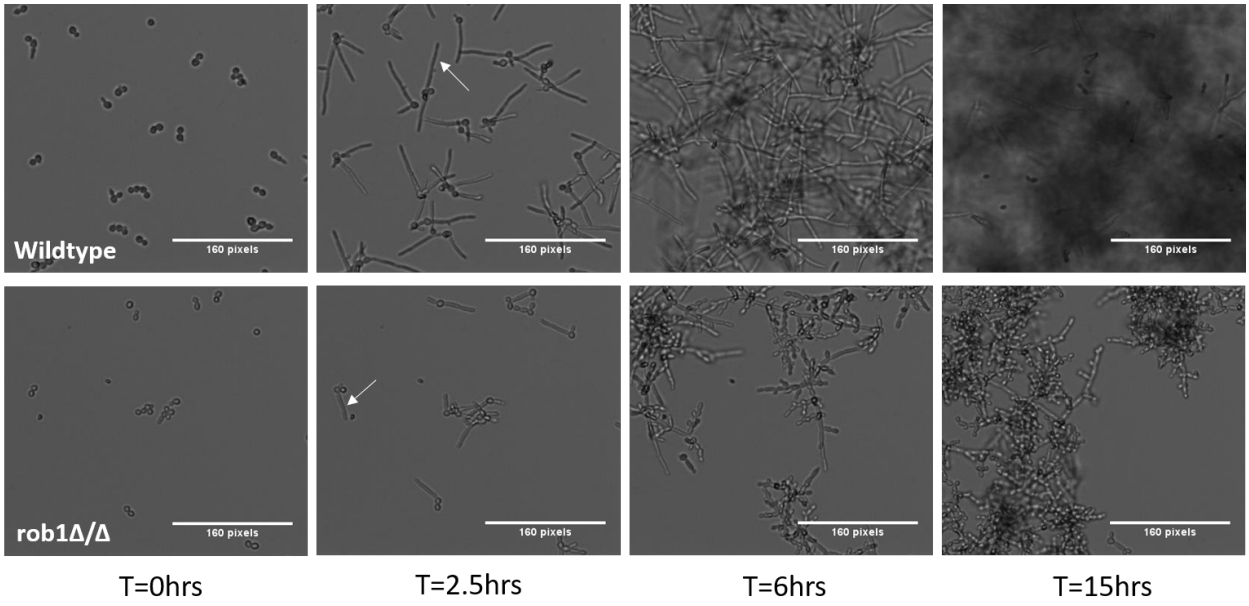

Figure 5. Growth of WT and rob1Δ/ Δ in an underoil microfluidic droplet assay. White arrows indicate hyphal growth.

Using 24 well microplates to collect *rob1Δ/Δ* and WT cells for RNA sequencing

To further understand how *rob1Δ/Δ* disperses more than WT, I decided to study this mutant on a molecular level. I used RNA sequencing to understand gene expression differences both between strains and throughout biofilm development. To collect cells for RNA isolation, strains were seeded into 24 well plates in RPMI+MOPS and incubated at 37ºC except the planktonic samples which were incubated at 30ºC (Fig 6). 24 well microplates were used to ensure enough cells for adequate amounts of RNA. A total of 5 plates were seeded; one plate for each time point that was collected. The planktonic samples were grown for 30mins, and all replicates were collected into individual microcentrifuge tubes. The remaining 4 plates were incubated at 37ºC and collected at 3hrs, 9hrs, 30hrs, and 54hrs. Media was removed, and fresh media was added at 9hrs for the 30hr and 54hr samples, and at 30hrs for the 54hr samples. The 3hr sample collected all the cells from

the well, while the later time points collected the supernatant which includes the dispersed cells, and the biofilm from the well in separate microcentrifuge tubes. As samples were collected, they were centrifuged, supernatant was removed, and samples were flash frozen in liquid nitrogen. Samples were then stored at -80ºC for RNA isolation. 9hr and 30hr supernatant samples were not isolated for the WT strain due to insufficient amounts of cells in the samples.

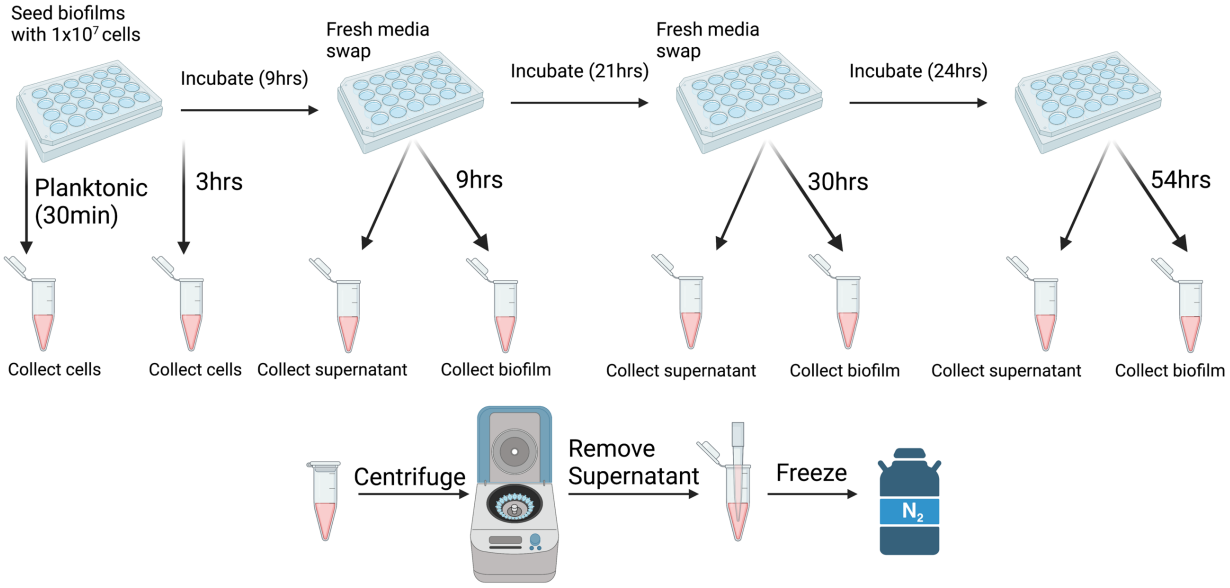

Figure 6. Schematic of collection for RNA sequencing. Strains were grown overnight, enumerated using a hemocytometer, diluted by hand to 1x10^7 cells/mL, and seeded into a 24 well plate. Each collection time was grown in a separate plate. All plates were grown at 37ºC except the planktonic sample which was grown at 30ºC. Planktonic cells were grown for 30 minutes and then collected into a microcentrifuge tube and centrifuged for 30sec at 14,000rpm. The supernatant was then removed, and cells were flash frozen in liquid nitrogen. At 3hrs all cells were collected and processed like the planktonic cells. Then at 9hrs, biofilms and supernatants were collected and processed like the planktonic cells. The remaining time points media was removed and replaced with fresh media. Plates were incubated for 21hrs which is when the 30hr time points supernatant and biofilm was collected and processed like the planktonic cells. Media was removed from the 54hr plate and fresh media was added and the plate was grown for an additional 54hrs. After 54hrs the supernatant and biofilm from the last plate were collected and processed like the planktonic

cells. 8 replicates were grown for each sample per strain. This figure was created using BioRender.com.

Biofilm life stages are distinctly different according to clustering analysis

Clustering of the samples revealed that replicates tend to group together (Fig 7a). When looking at the hierarchical clusters, most replicate samples cluster into their respective groups except for a few supernatant samples that cluster with their respective biofilms. The multidimensional scaling plot (MDS) also indicated that replicates group together which is encouraging for downstream differential gene expression analysis (Fig 7b). Interesting, the MDS plot also indicated that throughout the time course, the samples become more dissimilar with distances between samples becoming greater compared the planktonic sample. Additionally, *rob1Δ/Δ* and wildtype became more dissimilar as the biofilm developed.

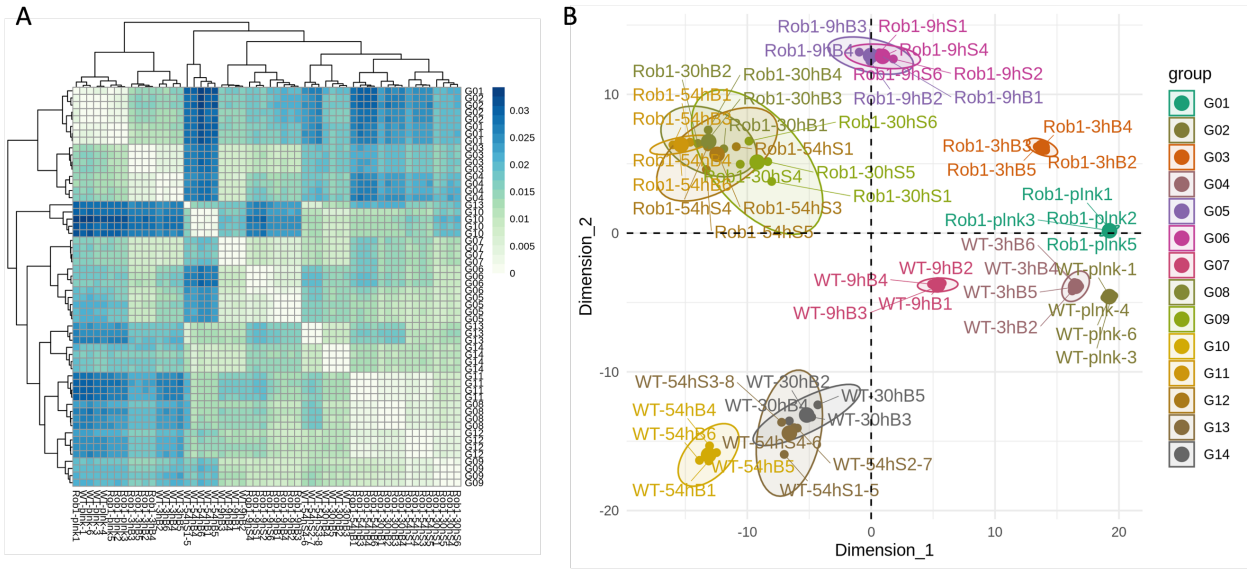

Figure 7. RNA sequencing clustering of all samples. A. Correlation-distance heat mapping between the assigned groups and individual samples. B. Multidimensional scaling plot (MDS) of all the WT and *rob1Δ/Δ* samples. Biofilm and supernatant samples are named as follows: strain name (Rob1 or WT), sampling time (in hours), sample type biofilms (B) or supernatant (S) and

the replicate number. For example, Rob1-30hB2 denotes the second biofilm replicate of the *rob1Δ/Δ* strain sampled at 30 hours. The planktonic samples as labels as follows: strain name, plnk (for planktonic), replicate. For example, WT-plnk-3 denotes the third planktonic replicate sampled for the WT strain.

Clustering analysis of just the WT samples showed clear separation between groups in the correlation-distance heat mapping, with hierarchical clustering showing that replicates all cluster into their respective groups (Fig 8a). Overall, variation between groups looked to be greater than the variation between replicates. The MDS plot for these samples indicated that replicates tend to cluster together, and groups were distinct from other groups apart from the overlap of the 54hr supernatant samples and the 30hr biofilm samples (Fig 8b).

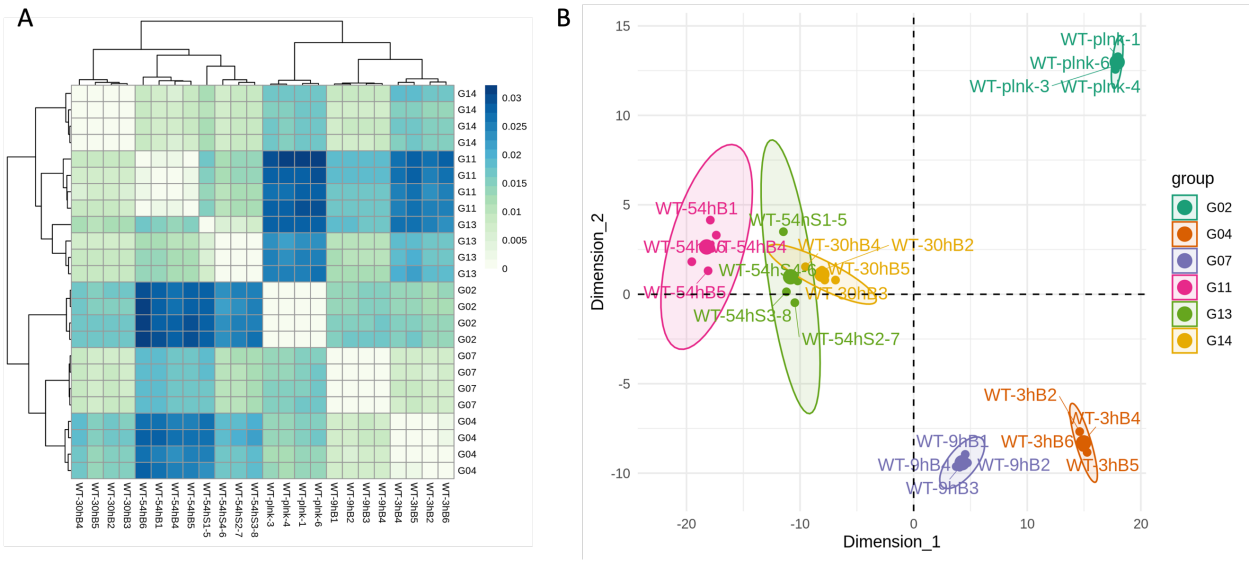

Figure 8. RNA sequencing clustering of the WT samples. A. Correlation-distance heat mapping between the assigned groups and individual samples. B. Multidimensional scaling plot (MDS) of all the WT samples. Biofilm and supernatant samples are named as follows: strain name (WT), sampling time (in hours), sample type biofilms (B) or supernatant (S) and the replicate number. For example, WT-30hB2 denotes the second biofilm replicate of the WT strain sampled at 30

hours. The planktonic samples as labels as follows: strain name, plnk (for planktonic), replicate. For example, WT-plnk-3 denotes the third planktonic replicate sampled for the WT strain.

Clustering data from the *rob1Δ/Δ* samples also clustered replicates together, except for a 9hr supernatant sample that clusters with the 9hr biofilm samples (Fig 9a, indicated on the far right). The correlation-distance heat mapping indicated that variation between groups is greater than the variation within a group due to replicates clustering together hierarchically (Fig 9a). The MDS plot separated groups of different stages of biofilm growth, however supernatant and biofilm samples tended to overlap.

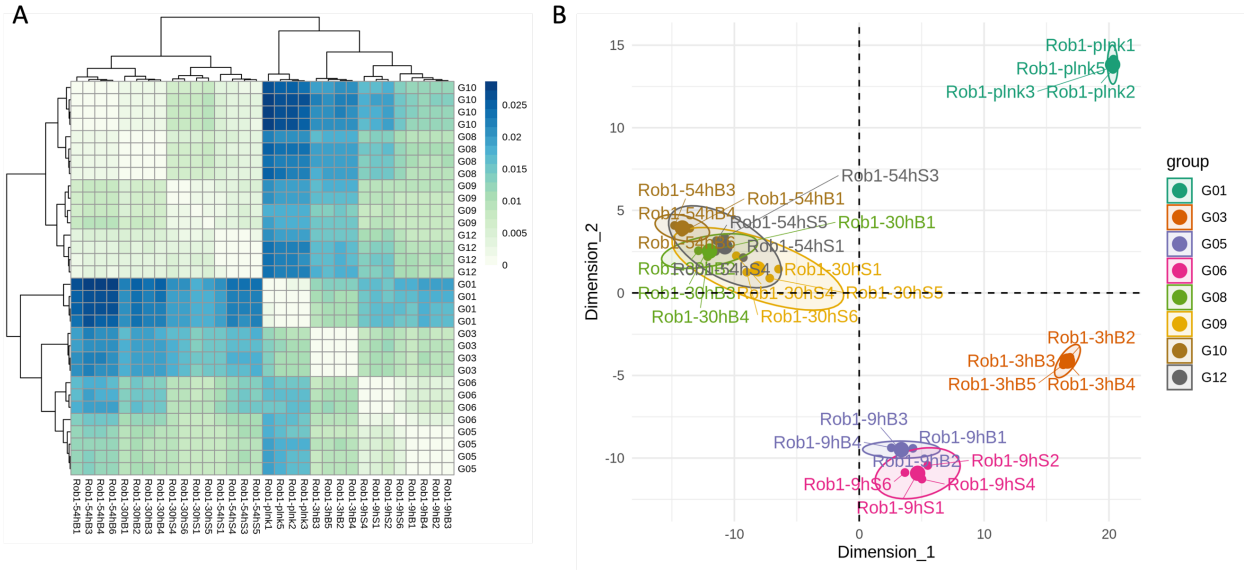

Figure 9. RNA sequencing clustering of the *rob1Δ/Δ* samples. A. Correlation-distance heat mapping between the assigned groups and individual samples. B. Multidimensional scaling plot (MDS) of all the *rob1Δ/Δ* samples. Biofilm and supernatant samples are named as follows: strain name (Rob1), sampling time (in hours), sample type biofilms (B) or supernatant (S) and the replicate number. For example, Rob1-30hB4 denotes the fourth biofilm replicate of the *rob1Δ/Δ* strain sampled at 30 hours. The planktonic samples as labels as follows: strain name, plnk (for

planktonic), replicate. For example, Rob1-plnk3 denotes the third planktonic replicate sampled for the *rob1Δ/Δ* strain.

There are significant differences in gene expression throughout biofilm development and between samples

The WT and *rob1Δ/Δ* planktonic cells had 2,253 statistically significant differentially expressed genes. Of these genes, I found similarities in expression between my study and the Nobile, *et al* (2012) study. In the Nobile, *et al* (2012) study they examined WT and *rob1Δ/Δ* planktonic cells using microarray and RNA sequencing [12]. Genes such as ECE1 and HWP1 were upregulated in WT samples while YWP1 and PRA1 were upregulated in *rob1Δ/Δ* samples which is consistent between my study and Nobile, *et al* (2012). Of the top 50 differentially expressed genes between WT and *rob1Δ/Δ* planktonic cells, I found biofilm formation (11 of 50 genes, correct p=4.72e-06) and biological process involved in interspecies interaction between organisms (16 of 50 genes, correct p=9.00e-07) to be the top functions when analyzed by GO term enrichment (Table S1). These results are not surprising considering that *rob1Δ/Δ* is known to form deficient biofilms.[12] I also found by looking at all the genes that were upregulated in *rob1Δ/Δ* compared to WT, 264 out of 1188 function in the carbohydrate transport pathway by GO term enrichment (corrected p= 8.37e-53) (Table S2). Upregulation data agrees with what was published in Nobile, *et al* (2012).

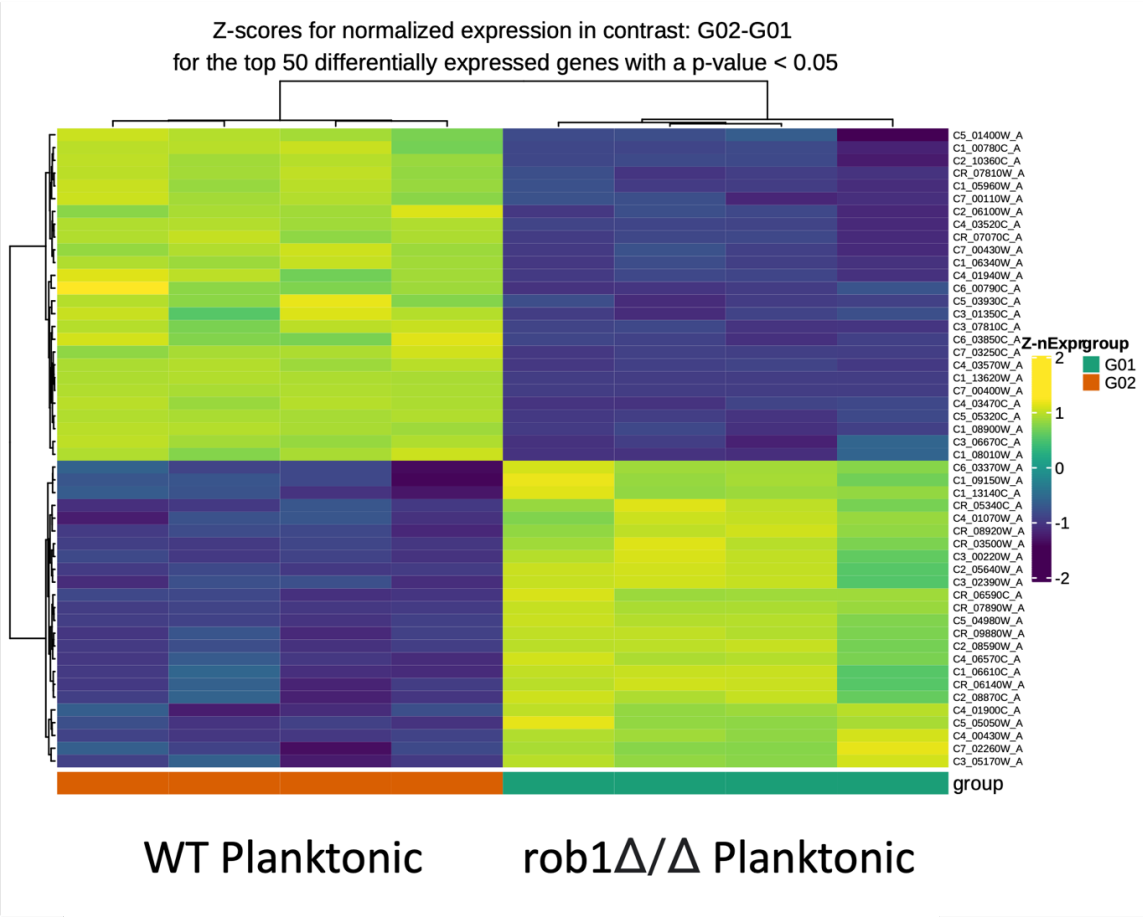

Figure 10. Top 50 differentially expressed genes between *rob1Δ/Δ* planktonic cells and WT planktonic cells. Genes shown have the highest fold change between samples with a false discovery rate correct p <0.05. Color gradient shows differences in the z-score among samples and genes. G01 is the *rob1Δ/Δ* planktonic cell sample while G02 is the WT planktonic sample.

Lastly, I investigated the differential gene expression between 54hr biofilms and 54hr supernatants for both the WT and *rob1Δ/Δ* samples (Fig 11). The *rob1Δ/Δ* samples had 3,117 differentially expressed genes between the biofilm and the supernatant while the WT samples had 3,753 differentially expressed genes. Of the top 50 differentially regulated genes between dispersed and biofilm samples, there were 12 genes that were common between the WT and *rob1Δ/Δ* strains (Table 1). These genes are used in the cellular lipid metabolic process pathways and carbon utilization pathway based on GO term enrichment (Table S3), where carbon utilization is

upregulated in the supernatant samples (correct p =6.66e-9) (Table S4) while lipid biosynthetic process is upregulated in the biofilm samples (corrected p= 0.01010) (Table S5). Although not part of the top 50 differentiated genes between dispersed cells and biofilm cells, it was found that Jen2, Jen1, and Icl1 were upregulated in dispersed cells, which is consistent with what was described in Uppuluri, *et al* [8]. Using GO term enrichment, these three genes are used in the carbohydrate transport pathway (corrected p= 0.00808) (Table S6).

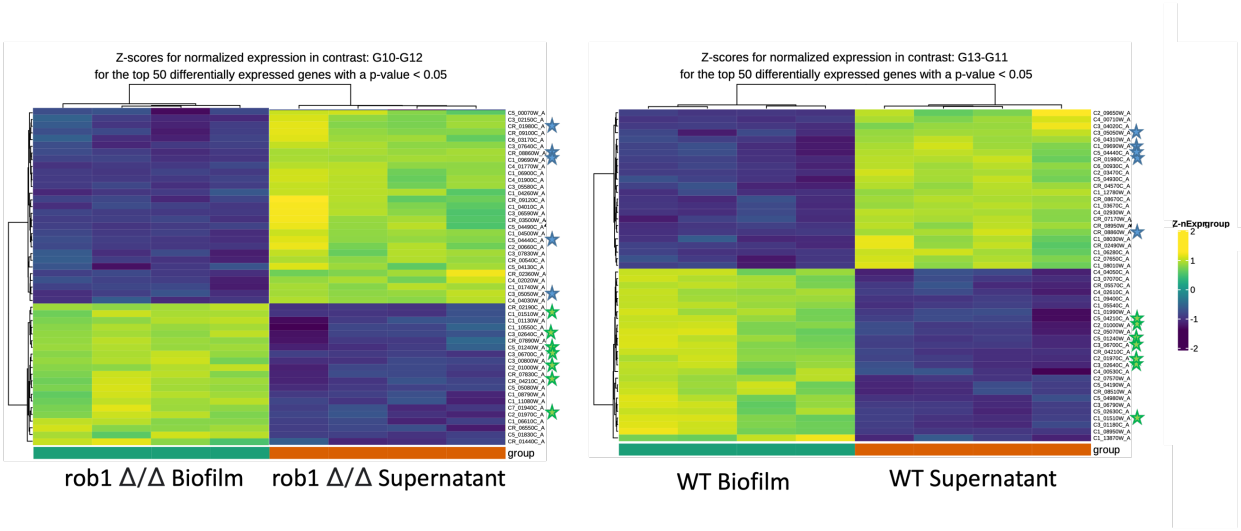

Figure 11. Top 50 differentially expressed genes between 54hr biofilms and 54hr dispersed cells for both WT and *rob1Δ/Δ*. Genes shown have the highest fold change between samples with a false discovery rate correct p <0.05. Color gradient shows differences in the z-score among samples and genes. Blue stars indicate the same gene is upregulated in dispersed cells compared with biofilm cells for both WT and *rob1Δ/Δ* samples. Green stars indicate the same gene is downregulated in dispersed cells compared with biofilm cells for both WT and *rob1Δ/Δ* samples.

Systematic Name	Standard Name	Description
CR_01980C_A	CRC1	Mitochondrial carnitine carrier protein
CR_08860W_A	PDK2	Putative pyruvate dehydrogenase kinase
C1_09690W_A	MLS1	Malate synthase
C5_04440C_A	SFC1	Putative succinate-fumarate transporter
C3_05050W_A	TRY4	C2H2 transcription factor
C1_01510W_A	orf19.3337	Protein of unknown function; merged with orf19.3338
C3_02640C_A	ZCF1	Zn(II)2Cys6 transcription factor
C5_01240W_A	AUR1	Inositolphosphorylceramide (IPC) synthase
C3_06700C_A	orf19.7459	Putative mitochondrial protein with a predicted role in respiratory growth
C2_01000W_A	HGT7	Putative MFS glucose transporter
CR_04210C_A	QDR1	Putative antibiotic resistance transporter
C2_01970C_A	ROD1	A membrane protein with a role in drug tolerance

Table 1. 12 genes differentially regulated in 54hr dispersed cells than 54hr biofilm cells indicated in Fig 11. Genes highlighted in green are upregulated in dispersed cells while genes highlighted in blue are downregulated in dispersed cells.

PES1 is important in the formation of lateral buds [6]–[8]. When comparing WT dispersed cells to hyphal cells, expression was downregulated, which I found surprising since it directly contradicts what has been published [8]. However, PES1 was upregulated in the *rob1Δ/Δ* dispersed cells at 9hrs but downregulated in 54hr dispersed cells when compared to the biofilm. 30hrs showed non-significant differences in PES1 between dispersed cells and biofilm cells. Interestingly, when PES1 expression was compared between *rob1Δ/Δ* and the WT samples, early in development (planktonic and 3hr) PES1 was upregulated in the WT cells. However, in late biofilm and dispersed cells (54hr biofilm and supernatant) PES1 was upregulated in *rob1Δ/Δ*. Additional temporal resolution in dispersion from the WT biofilm is needed to understand PES1's role in dispersion on a temporal scale.

Conclusions

I screened a TF mutant library for dispersion phenotypes using the 96-well microplate assay. From this screen I identified one mutant, *rob1Δ/Δ*, that grew hyphal cells and was significantly more dispersive than WT. I confirmed that the mutant was highly dispersive in our underoil microfluidic droplet assay. The strain showed hyphal development but was incapable of hyphal elongation, which has been recently reported [16]. After hyphal initiation, the strain started to grow lateral buds and pseudohypal cells. These lateral buds would then be released from the biofilm, showing overall greater dispersion than the WT strain.

To identify genes that are either differentially regulated within the biofilm lifecycle, or differentially regulated between the mutant and WT, I completed RNA sequencing of planktonic, early biofilm development, mid-biofilm development, late biofilm development and dispersed cells for both the WT and *rob1Δ/Δ* strains. Analysis showed that replicates of the same group clustered together indicated less variation between replicates than between groups. Additionally, these groups were distinct from each other when using a MDS plot. When comparing the differential gene expression of *rob1Δ/Δ* and WT planktonic cells, I identified that carbohydrate transport (311 genes of 2252, corrected p= 2.90E-18) and small molecule transport (356 genes of 2252, corrected p= 1.17E-12) (Table S7) were both highly upregulated in the mutant using GO term enrichment. Also, some genes that are upregulated in dispersed cells, JEN1, JEN2, and ICL1 also function in the carbohydrate transport pathway.

When testing how carbon abundance affects dispersion, it was found that less carbon supplementation resulted in less dispersion [17]. A person in my lab has investigated the role of

carbon in the underoil microfluidic droplets. It was found that decreasing the amount of carbon in the growth media resulted in earlier dispersion events, which does not replicate what has been previously published. I hypothesize this is difference is due to differences in the growth assays. The previous findings were collected from a macro-flow where fresh media is always available, and the accumulation of quorum sensing molecules is unknown. Therefore, less carbon in the constantly flowing media may result in smaller biofilms that disperse less. This is a contrasting environment from a static assay like the underoil growth assay or 96-well plate where the media is not refreshed and allows for the accumulation of quorum sensing molecules. Interestingly, both the macro-flow assay and the 96-well microplate assay produced dispersed cells that upregulate genes relating to the carbon transport and utilization pathways.

While these are a few interesting examples, additional analysis of the RNA-sequencing data as well as experimentation on specific genes will have to be done to begin further understanding dispersion.

Methods

Strain Growth

Strains from the Homann, *et al* TF mutant library were used in this screen. SC5314 (cmm1) and a clinical isolate (9817) known to be highly dispersive (cmm11) were used as controls for the mutant screen. Strains were grown in YPD (1% yeast extract, 2% Bacto peptone, 2% dextrose) supplemented with uridine (80ug/ml) or RPMI 1640 supplemented with MOPS are listed in the growth methods. Strains are stored in 15% glycerol stocks in the -80°C freezer.

TF mutant screen

Strains were inoculated in 96-well plates overnight in YPD supplemented with uridine. The plates were then diluted 1:10 into RPMI + MOPS and OD600 readings were taken using a Tecan Spark plate reader. Using a script written by a Tecan representative, the Tecan Fluent liquid handling robot was used to dilute all samples to 0.1 OD600 in RPMI+MOPS. Plates were covered with a Breathe-Easy plate seal (Diversified Biotech, BEM-1) and imaged at 10x using brightfield imaging on a Nikon Eclipse TI for 6 hours at 37ºC. After 6 hours media was removed and 200µL of fresh RPMI + MOPS was added to the wells. Strains were grown for an additional 24 hours until media was removed, and fresh media was added again. After another 24 hours (54 hours total) the supernatant was collected and imaged at 10x using brightfield imaging on a Nikon Eclipse TI. 100µL of XTT (90 µL XTT salt (0.5µg/µL),10µL phenazine methosulfate (0.32mg/mL)) was then added to the biofilm and supernatant. Using a script developed in the Tecan software "FluentControl", the Fluent was used to incubate the plates at 37ºC and take XTT OD495 readings every 5 minutes using the Tecan Spark for both the supernatant and biofilm plates. A custom Matlab script was used to analyze the data. Each plate had 3 technical replicate plates.

Underoil microfluidic assay

Strains were grown overnight in YPD supplemented with uridine (80µg/mL) at 30ºC. Cells were then diluted to $1x10^6$ cells/mL in RPMI+MOPS. 1 µL of diluted cells were put in each droplet that had already been established with 1µL of fresh RPMI+MOPS. Slides were fabricated as described in Chapter 5. The underoil microfluidic slide is then put in an 37ºC incubated box on the

microscope (Nikon Eclipse Ti) and 10x magnification images are taken every 30 minutes for 20 hrs. Image analysis is done using ImageJ.

RNA sequencing collection

WT and rob1Δ/ Δ were grown overnight in YPD supplemented with uridine (80µg/mL). Cells were enumerated using a hemocytometer and diluted to $1x10^7$ cells/mL in RPMI +MOPS. 1mL of diluted cells were added to each well which already contained 1mLof RPMI+MOPS. Each collection time was grown in a separate plate. All plates were grown at 37ºC except the planktonic sample which was only grown at 30ºC. Planktonic cells were grown for 30 minutes and then collected into a microcentrifuge tube and centrifuged for 30sec at 14000rpm. The supernatant was then removed, and cells were flash frozen in liquid nitrogen. At 3hrs all cells were collected and processed like the planktonic cells. Then at 9hrs, biofilms and supernatants were collected and processed like the planktonic cells. The remaining time points media was removed and replaced with fresh media. Plates were incubated for 21 additional hours which is when the 30hr time points supernatant and biofilm was collected and processed like the planktonic cells. Media was removed from the 54hr plate and fresh media was added and the plate was grown for an additional 54hrs. After 54hrs the supernatant and biofilm from the last plate were collected and processed like the planktonic cells. 8 replicates were grown for each sample per strain. Frozen cells were stored in the -80ºC freezer until RNA isolation.

RNA Isolation

RNA isolation was done using an adapted protocol of the Purelink RNA mini kit. Samples were thawed on ice in a 4ºC cold room. 50µL of 100% ethanol was added to the cells to help kill the

cells before mechanical disruption was applied. Lysis buffer and glass beads were added, and samples were lysed using a bead beater for 10 minutes. The Purelink RNA mini kit protocol was used for the continuation of the RNA isolation process. Isolations were eluted into 30µL.

This process resulted in RNA that was contaminated with guanidine thiocyanate. To remove this contaminant an ethanol precipitation was completed. 2.5µL of 3M sodium acetate was added to each sample along with 100µL of ice cold 100% ethanol. Samples were stored in the -80ºC freezer for 10 minutes for precipitation. Samples were then centrifuged at 14,000g for 10 minutes at 4ºC.The supernatant was aspirated and 0.5mL of ice cold 70% ethanol was added. Samples were centrifuged at 14,000g for 10 minutes at 4ºC.The supernatant was aspirated, and samples were left open at room temperature for ~10 minutes. 10µL of RNAse free water was added to the samples and they were incubated at 65ºC for 10 minutes.

RNA sequencing

RNA quality and quantity were calculated using an Agilent 2100 Bioanalyzer with a Nanochip or a Picochip, and a Nanodrop ND-2000 Spectrophotometer. Samples passed quality control if their A260/A230 and A260/A280 ratios were >1.8. 100ng-1µg of RNA was used to build libraries. Libraries were built by the UW-Madison Gene Expression center using Truseq mRNA stranded mRNA kit. Library preps were quality checked on the Agilent Tapestation 4200 with D1000 and HS1000 screen tape reagents for a library range >200-1000bp and Adapter dimer (AD) <1%. If the AD > 1% the sample was purified or re-prepped. Final preps had an AD <2%. 100-bp-paired-end sequencing was run with an Illumina Nova seq 6000, which was completed by the UW-Madison DNA Sequencing Facility. Read depth was approximately 40 million reads per sample.

Analysis of the RNA sequencing

Sequencing results were analyzed by the Bioinformatic resource center at UW-Madison. Their methods are listed below.

FASTQ preprocessing

Due to the imperfect nature of the sequencing process and limitations of the optical instruments (batch effects, sequencing error, GC bias, duplicate reads, copy number variation, mapability), base calling has inherent uncertainty associated with it. The magnitude of uncertainty in each base call is represented by an error probability or Phred score. This parameter is denoted formally as Q and is proportional to the probability p that a base call is incorrect, where $Q=-10\log 10\,(p)$.

Any biological inference or conclusion depends on the overall quality of your data. These following quality control (QC) statistics computed on your data are designed to help you evaluate the overall technical quality of your experiment. You should *always* examine if your raw sequence data exhibit good quality and lack obvious problems or biases, which may affect how you can ultimately use it in your research.

Read trimming

The trimming software skewer [18]was used to preprocess raw fastq files. Skewer implements an efficient dynamic programming algorithm designed to remove adapters from Illumina-generated sequence reads.

During sequencing library construction, short oligonucleotides are ligated to the ends DNA fragments to be sequenced, so that they can be combined with primers for PCR amplification. While sequencing the fragments, if the read length is greater than that of the target DNA, the adapter sequence next to the unknown DNA sequence of interest is also sequenced, sometimes only partially. To recover the true target DNA sequence, it is required to identify the adapter sequence and remove it. Moreover, to improve further the quality of the sequence reads, skewer also trims the 3' end of the fragment until a Phred quality of 20 is reached. This is equivalent to a base call accuracy of 99%. More information regarding Phred scores can be obtained from Ewing et al. (1998) and in Ewing and Green (1998). [19], [20]

FASTQ alignment

To identify the transcripts present in a specific sample as well as associated expression levels, the genomic origin of the sequenced cDNA fragments must be determined. The assignment of sequencing reads to the most likely locus of origin is called read alignment or mapping. One challenge of short-read alignment is to map millions of reads accurately in a reasonable amount of time, but in the presence of sequencing errors, genomic variation, incomplete sequencing annotation etc. Many alignment programs exist and employ various strategies meant to find a balance between mapping fidelity, error tolerance, and time.

One challenge of aligning RNASeq data is the spliced alignment of exon-exon-spanning reads, possibly when multiple different transcripts (and isoforms) of the same gene also exist. Some alignment programs address this problem by aligning only to the transcriptome. Although some alternatives exist, this approach is limited to known transcripts and thus requires accurate sequence annotation. In many cases, reads will also overlap with more than one isoform and introduce mapping ambiguity. The most effective current solution uses existing gene annotation for the placement of spliced reads in addition to attempting to identify novel splice events based on reads that cannot be aligned to the reference genome and/or transcriptome.

Read mapping

The trimmed single- or paired-end reads are aligned against the selected reference genome sequence using STAR (Spliced Transcripts Alignment to a Reference) [21]. STAR is a splice-junction aware RNASeq alignment algorithm that uses suffix arrays and a mapping algorithm similar to those used in whole-genome alignment tools to align transcripts to a genomic reference. STAR is substantially faster than other RNASeq aligners, and appears to outperform other aligners in both sensitivity and specificity using both simulated and real (replicated) RNASeq data.[22]

Gene expression

Read quantification

Mapped paired-end reads for both genes and transcripts (isoforms) are counted in each sample using RSEM (RNASeq by Expectation Maximization), described in Li and Dewey (2011).[23]

RSEM uses a statistical model to take into account the uncertainty associated with read mapping, especially in a transcriptome where multiple isoforms may exist. In contrast to R/FPKM (reads/fragments per kilobase per million mapped reads), RSEM implements a TPM (transcripts per million mapped reads) metric to compare differences *between* sequenced sample libraries. The primary rationale is that libraries are not all of the same size and it is necessarily the case that an increase in expression of any particular gene in one library will lead to the exclusion of other genes.

Read filtering

Real RNASeq datasets will be comprised of both expressed and non-expressed genes, which are defined by an annotation model (see section 8, Annotation, for additional information.). Genes with zero or low-abundance counts create problems in RNASeq DGE analyses because small counts do not contain enough information for reliable statistical inference.[24] For analysis methods that require a false discovery rate analysis (FDR), the proportion of genes with very low expression out of the total set of all genes being tested influence considerably the power of detection after multiple testing correction; low-expression genes are usually indistinguishable from sampling noise. Removing (filtering) genes that are expressed at or near zero prior to any DGE analysis reduces the severity of the correction and improves the power of detection. Moreover, if not expressed in any condition, they exhibit no biologically meaningful information, at least within the confines of the experimental context.

Our current workflow uses *filterByExpr*, a function available in edgeR. This function filters those genes failing to meet a threshold of at least 10 read counts or more in a specific number of samples, which is defined as the smallest group sample size in the contrast.

Plots depicting a density distribution of log_2-transformed read counts before and after application of the filtering function are available in Table 4. The distributions are color-coded by the defined contrast group. The vertical dashed line depicts the log_2-CPM threshold used in the filtering step (a CPM value of 1 is equivalent to a log_2-CPM value of 0). Beyond showing the performance of the (independent) filtering, the log_2-CPM plots also serve to indicate per-sample expression distributions, which may be useful as a quality control metric. In general, the distributions should be approximately the same within a specific group. Substantial shifts along either axis may reflect technical (e.g., library size, sample inversion, variation in duplication levels) or biological (e.g., treatment effects) phenomena.

Unsupervised clustering of samples: MDS

One of the most important exploratory plots to examine prior to any differential gene expression (DGE) analysis is an unsupervised multidimensional scaling (MDS) plot. An MDS plot is a visualization of distances among a set of objects. In RNASeq, an MDS plot will show variation among samples such that those with higher dissimilarity are further apart. It is different from a principal components analysis (PCA; PCA is a particular instance of MDS) in that MDS projects data to (usually) a 2D space (i.e. utilize only the first two dimensions) and focuses on distance relationships among scaled objects. In contrast, PCA project a multi-dimensional space onto the directions of maximum variation between samples and genes.

Most importantly, both methods transform a large set of variables (genes) into a smaller one that still contains most of the information. Despite subtle differences, inspection of MDS patterns, with

respect to your sample groupings, can provide clues to the quality of upstream processing procedures (*e.g.,* sample collection; see below), which may affect downstream analyses and/or interpretation. The scaled axes on the *sample-level* MDS plots are computed from contributions of all independently filtered genes and representative of Euclidean distances between samples. The two dimensions depicted are ordered based on how well they fit your samples. If your experiment is well controlled (*e.g.,* uniform sample acquisition and processing yielding a measurable effect), expect to observe the greatest sources of variation *between* the groups (factors) you are contrasting.

Ideally, each factor in the MDS plot will cluster and be separated from other conditions. This indicates that differences between groups (effect size) are larger than differences within groups. In other words, the between-group variance of gene expression is greater than the within-group variance and therefore can be detected reliably. If grouped samples are widely scattered or if one or more samples of an otherwise [expected] cohesive group are distant from each other, these samples can be examined further for sources of error (*e.g.,* sample inversion) or additional and possibly unknown variation (*e.g.,* batch effects, experimental design or possibly true biological variation). If present, technical replicates should located be very close to one another. If you have more than two groups in your experimental design, be sure to carefully examine the contrast-level plots for higher-resolution details.

Unsupervised clustering of samples: Correlation-distance heatmap

Hierarchical clustering is a complementary approach to ordination methods like PCA or MDS. In RNASeq, it seeks to determine whether samples display greater variability between experimental conditions than between replicates of the same condition. While many methods exist to view

clustering relationships, heatmaps (sometimes called Clustered Image Maps; CIMs) work well for RNASeq data. This type of representation is based on a hierarchical clustering of dissimilarities in expected read counts across samples.

Sample relationships are graphically depicted in a 2D image, where each entry is colored on the basis of its dissimilarity to other samples, and where the rows and columns are reordered according to the hierarchical clustering. A dendrogram shows the hierarchical arrangement of the samples produced by the hierarchical clustering (UPGMA).

The heatmaps represent graphically the entire expression data set (gene- and transcript-level, respectively) where the individual values contained in a matrix are represented as colors, themselves representative of a measure of expression dissimilarity. To create the heatmap, the expected read counts were normalized and transformed with a regularized logarithm (rlog) function. Next, the Pearson correlation was computed for each pair of samples and Euclidean distances of the correlation distances determined.

As the Euclidean distance is proportional to the Pearson correlation coefficient, the heatmap will cluster together samples that have positively correlated expression values because large positive correlations correspond to small distances. The branches of the dendrograms on the CIM plots should reflect sample clustering with correlated expression patterns. Although computationally distinct, patterns between the MDS and CIM plots may be visible.

Heatmap of selected DEG Z-scores

A common method of visualizing gene expression data is to display it as a heatmap so that you can simultaneously visualize clusters of samples (i.e., groups) and features (i.e., genes). This can be useful for identifying genes that are commonly regulated, or have biological signatures associated with a particular condition. Often, heatmaps are combined with clustering methods, which group genes and samples together based on the similarity of their gene expression pattern.

Heatmaps for RNASeq data are displayed usually as a grid where each row represents a gene and each column represents a sample. The color and intensity of each grid cell (sample x gene) is used to represent changes in transcript expression. Genes that are upregulated (high expression value) are colored differently than genes that are downregulated (low expression value), thus providing a simultaneous visual representation of gene expression levels across multiple different samples.
A subset of up to 50 of the most differentially expressed genes with an FDR corrected p-value less than 0.05 are selected. Next, both samples and genes are clustered using Euclidean distances. An additional elbow function is applied to estimate the number of gene clusters present. Calculated relationships are depicted by dendrograms drawn at the top (samples) and to the left (genes) of the heatmap. The gradation of color is determined by a Z-score that is computed and scaled across rows of genes normalized by TMM. The Z-score of a given expression value is the number of standard-deviations away from the mean of all the expression values for that gene.

When a gene is expressed differentially in samples among two groups, then the Z-scores will be (mostly) positive in one group and (mostly) negative in the other group, hence the contrast of colors. Clusters of genes with similar or very different expression values are easily visible when scaled in this manner. Depending on the degree of expression change, there should be sharp

contrasts **between** groups; within-group Z-scores should be fairly uniform, hence color gradations should be relatively uniform. However, outliers are often readily apparent and distinguished by discontinuities in both color pattern and cluster relationship. Comparison of the Z-score heatmap with the sample- and contrast-level MDS and CIM plots described earlier may also be informative.

Go term enrichment identification

Systematic names of genes were taken from the differential gene analysis and searched on GO term finder on the Candida Genome Database for process that they affect. [25] (http://www.candidagenome.org/GOContents.shtml) Output processes are reported as well as their corrected p-values.

References

[1] G. Wall, D. Montelongo-Jauregui, B. Vidal Bonifacio, J. L. Lopez-Ribot, and P. Uppuluri, "Candida albicans biofilm growth and dispersal: contributions to pathogenesis," *Curr. Opin. Microbiol.*, vol. 52, pp. 1–6, Dec. 2019.

[2] C. J. Nobile and A. D. Johnson, "Candida albicans Biofilms and Human Disease," *Annu. Rev. Microbiol.*, 2014.

[3] E. P. Fox and C. J. Nobile, "A sticky situation: Untangling the transcriptional network controlling biofilm development in Candida albicans," *Transcription*, vol. 3, no. 6, p. 315, Nov. 2012.

[4] M. Gulati and C. J. Nobile, "Candida albicans biofilms: development, regulation, and molecular mechanisms," *Microbes Infect.*, vol. 18, no. 5, p. 310, May 2016.

[5] J. R. Blankenship and A. P. Mitchell, "How to build a biofilm: a fungal perspective," *Curr. Opin. Microbiol.*, vol. 9, pp. 588–594, 2006.

[6] P. Uppuluri *et al.*, "Dispersion as an important step in the Candida albicans biofilm developmental cycle.," *PLoS Pathog.*, vol. 6, no. 3, p. e1000828, Mar. 2010.

[7] J. Shen, L. E. Cowen, A. M. Griffin, L. Chan, and J. R. Köhler, "The Candida albicans pescadillo homolog is required for normal hypha-to-yeast morphogenesis and yeast proliferation.," *Proc. Natl. Acad. Sci. U. S. A.*, vol. 105, no. 52, pp. 20918–23, Dec. 2008.

[8] P. Uppuluri *et al.*, "Candida albicans Dispersed Cells Are Developmentally Distinct from Biofilm and Planktonic Cells.," *MBio*, vol. 9, no. 4, pp. e01338-18, Sep. 2018.

[9] P. Uppuluri, C. G. Pierce, D. P. Thomas, S. S. Bubeck, S. P. Saville, and J. L. Lopez-Ribot, "The transcriptional regulator Nrg1p controls Candida albicans biofilm formation and dispersion.," *Eukaryot. Cell*, vol. 9, no. 10, pp. 1531–7, Oct. 2010.

[10] N. Robbins *et al.*, "Hsp90 governs dispersion and drug resistance of fungal biofilms.," *PLoS Pathog.*, vol. 7, no. 9, p. e1002257, Sep. 2011.

[11] O. R. Homann, J. Dea, S. M. Noble, and A. D. Johnson, "A Phenotypic Profile of the Candida albicans Regulatory Network," *PLoS Genet.*, vol. 5, no. 12, p. 1000783, Dec. 2009.

[12] C. J. Nobile *et al.*, "A Recently Evolved Transcriptional Network Controls Biofilm Development in Candida

albicans," *Cell*, vol. 148, pp. 126–138, 2012.
[13] S. M. Noble and A. D. Johnson, "Strains and Strategies for Large-Scale Gene Deletion Studies of the Diploid Human Fungal Pathogen Candida albicans," *Eukaryot. Cell*, vol. 4, no. 2, p. 298, Feb. 2005.
[14] M. Řičicová *et al.*, "Candida albicans biofilm formation in a new in vivo rat model," *Microbiology*, vol. 156, no. Pt 3, pp. 909–919, 2010.
[15] M. Y. Huang, C. A. Woolford, G. May, C. Joel Mcmanus, and A. P. Mitchell, "Circuit diversification in a biofilm regulatory network," *PLOS Pathog.*, vol. 15, no. 5, p. e1007787, May 2019.
[16] R. S. Wakade, L. C. Ristow, M. Wellington, and D. J. Krysan, "Intravital imaging based genetic screen reveals the transcriptional network governing Candida albicans filamentation during mammalian infection," *Elife*, vol. 12, Feb. 2023.
[17] P. Uppuluri *et al.*, "Dispersion as an Important Step in the Candida albicans Biofilm Developmental Cycle," *PLOS Pathog.*, vol. 6, no. 3, 2010.
[18] H. Jiang, R. Lei, S. W. Ding, and S. Zhu, "Skewer: A fast and accurate adapter trimmer for next-generation sequencing paired-end reads," *BMC Bioinformatics*, vol. 15, no. 1, pp. 1–12, Jun. 2014.
[19] B. Ewing and P. Green, "Base-Calling of Automated Sequencer Traces Using Phred. II. Error Probabilities," *Genome Res.*, vol. 8, no. 3, pp. 186–194, Mar. 1998.
[20] B. Ewing, L. D. Hillier, M. C. Wendl, and P. Green, "Base-calling of automated sequencer traces using phred. I. Accuracy assessment," *Genome Res.*, vol. 8, no. 3, pp. 175–185, 1998.
[21] A. Dobin *et al.*, "STAR: ultrafast universal RNA-seq aligner," *Bioinformatics*, vol. 29, no. 1, pp. 15–21, Jan. 2013.
[22] P. G. Engström *et al.*, "Systematic evaluation of spliced alignment programs for RNA-seq data," *Nat. Methods 2013 1012*, vol. 10, no. 12, pp. 1185–1191, Nov. 2013.
[23] B. Li and C. N. Dewey, "RSEM: Accurate transcript quantification from RNA-Seq data with or without a reference genome," *BMC Bioinformatics*, vol. 12, no. 1, pp. 1–16, Aug. 2011.
[24] R. Bourgon, R. Gentleman, and W. Huber, "Independent filtering increases detection power for high-throughput experiments," *Proc. Natl. Acad. Sci. U. S. A.*, vol. 107, no. 21, pp. 9546–9551, May 2010.
[25] H. Mi, A. Muruganujan, D. Ebert, X. Huang, and P. D. Thomas, "PANTHER version 14: more genomes, a new PANTHER GO-slim and improvements in enrichment analysis tools," *Nucleic Acids Res.*, vol. 47, no. D1, pp. D419–D426, Jan. 2019.

Supplemental Tables

Table S1. Top 50 differentially expressed genes between WT and *rob1Δ/Δ* planktonic cells.

GOID	GO_term	Cluster frequency	Background frequency	Corrected P-value	False discovery rate
44011	single-species biofilm formation on inanimate substrate	11 out of 50 genes, 22.0%	120 out of 6473 background genes, 1.9%	3.79E-07	0.00%
44419	biological process involved in interspecies interaction between organisms	16 out of 50 genes, 32.0%	344 out of 6473 background genes, 5.3%	9.00E-07	0.00%
90609	single-species submerged biofilm formation	11 out of 50 genes, 22.0%	132 out of 6473 background genes, 2.0%	1.05E-06	0.00%
90605	submerged biofilm formation	11 out of 50 genes, 22.0%	135 out of 6473 background genes, 2.1%	1.34E-06	0.00%
44010	single-species biofilm formation	11 out of 50 genes, 22.0%	138 out of 6473 background genes, 2.1%	1.70E-06	0.00%
42710	biofilm formation	11 out of 50 genes, 22.0%	152 out of 6473 background genes, 2.3%	4.72E-06	0.00%

98630	aggregation of unicellular organisms	11 out of 50 genes, 22.0%	152 out of 6473 background genes, 2.3%	4.72E-06	0.00%
98743	cell aggregation	11 out of 50 genes, 22.0%	152 out of 6473 background genes, 2.3%	4.72E-06	0.00%
44406	adhesion of symbiont to host	7 out of 50 genes, 14.0%	68 out of 6473 background genes, 1.1%	0.00024	0.22%
44403	biological process involved in symbiotic interaction	9 out of 50 genes, 18.0%	140 out of 6473 background genes, 2.2%	0.00031	0.20%
51701	biological process involved in interaction with host	8 out of 50 genes, 16.0%	131 out of 6473 background genes, 2.0%	0.00199	0.36%
1900445	positive regulation of filamentous growth of a population of unicellular organisms in response to biotic stimulus	6 out of 50 genes, 12.0%	83 out of 6473 background genes, 1.3%	0.01252	0.83%
2833	positive regulation of response to biotic stimulus	6 out of 50 genes, 12.0%	83 out of 6473 background genes, 1.3%	0.01252	0.77%
16477	cell migration	2 out of 50 genes, 4.0%	2 out of 6473 background genes, 0.0%	0.01953	1.14%
48870	cell motility	2 out of 50 genes, 4.0%	2 out of 6473 background genes, 0.0%	0.01953	1.07%
1900443	regulation of filamentous growth of a population of unicellular organisms in response to biotic stimulus	6 out of 50 genes, 12.0%	96 out of 6473 background genes, 1.5%	0.02851	1.38%
2831	regulation of response to biotic stimulus	6 out of 50 genes, 12.0%	96 out of 6473 background genes, 1.5%	0.02851	1.29%
98660	inorganic ion transmembrane transport	5 out of 50 genes, 10.0%	67 out of 6473 background genes, 1.0%	0.05042	1.44%
1900428	regulation of filamentous growth of a population of unicellular organisms	8 out of 50 genes, 16.0%	211 out of 6473 background genes, 3.3%	0.0615	1.79%

Table S2. GO term enrichment analysis of upregulated genes in *rob1Δ/Δ* compared to WT in planktonic cells.

GOID	GO_term	Cluster frequency	Background frequency	Corrected P-value	False discovery rate
8643	carbohydrate transport	264 out of 1188 genes, 22.2%	585 out of 6473 background genes, 9.0%	8.37E-53	0.00%
71702	organic substance transport	396 out of 1188 genes, 33.3%	1458 out of 6473 background genes, 22.5%	2.08E-18	0.00%

9056	catabolic process	424 out of 1188 genes, 35.7%	1632 out of 6473 background genes, 25.2%	4.85E-16	0.00%
44248	cellular catabolic process	304 out of 1188 genes, 25.6%	1114 out of 6473 background genes, 17.2%	5.46E-13	0.00%
5975	carbohydrate metabolic process	81 out of 1188 genes, 6.8%	185 out of 6473 background genes, 2.9%	9.03E-13	0.00%
44804	autophagy of nucleus	228 out of 1188 genes, 19.2%	779 out of 6473 background genes, 12.0%	2.27E-12	0.00%
34727	piecemeal microautophagy of the nucleus	227 out of 1188 genes, 19.1%	775 out of 6473 background genes, 12.0%	2.43E-12	0.00%
16237	lysosomal microautophagy	227 out of 1188 genes, 19.1%	781 out of 6473 background genes, 12.1%	6.41E-12	0.00%
51179	localization	515 out of 1188 genes, 43.4%	2177 out of 6473 background genes, 33.6%	1.30E-11	0.00%
51234	establishment of localization	487 out of 1188 genes, 41.0%	2034 out of 6473 background genes, 31.4%	1.32E-11	0.00%
6810	transport	482 out of 1188 genes, 40.6%	2011 out of 6473 background genes, 31.1%	1.70E-11	0.00%
44282	small molecule catabolic process	53 out of 1188 genes, 4.5%	108 out of 6473 background genes, 1.7%	4.62E-10	0.00%
6914	autophagy	245 out of 1188 genes, 20.6%	899 out of 6473 background genes, 13.9%	1.41E-09	0.00%
16042	lipid catabolic process	30 out of 1188 genes, 2.5%	48 out of 6473 background genes, 0.7%	2.70E-08	0.00%
61919	process utilizing autophagic mechanism	247 out of 1188 genes, 20.8%	937 out of 6473 background genes, 14.5%	5.62E-08	0.00%
1901575	organic substance catabolic process	260 out of 1188 genes, 21.9%	1009 out of 6473 background genes, 15.6%	2.02E-07	0.00%
16054	organic acid catabolic process	38 out of 1188 genes, 3.2%	76 out of 6473 background genes, 1.2%	5.90E-07	0.00%
46395	carboxylic acid catabolic process	38 out of 1188 genes, 3.2%	76 out of 6473 background genes, 1.2%	5.90E-07	0.00%
44242	cellular lipid catabolic process	23 out of 1188 genes, 1.9%	36 out of 6473 background genes, 0.6%	3.65E-06	0.00%

16052	carbohydrate catabolic process	27 out of 1188 genes, 2.3%	49 out of 6473 background genes, 0.8%	1.48E-05	0.00%
6508	proteolysis	221 out of 1188 genes, 18.6%	872 out of 6473 background genes, 13.5%	3.74E-05	0.00%
5996	monosaccharide metabolic process	25 out of 1188 genes, 2.1%	45 out of 6473 background genes, 0.7%	4.30E-05	0.00%
19752	carboxylic acid metabolic process	105 out of 1188 genes, 8.8%	348 out of 6473 background genes, 5.4%	4.84E-05	0.00%
32787	monocarboxylic acid metabolic process	55 out of 1188 genes, 4.6%	147 out of 6473 background genes, 2.3%	5.49E-05	0.00%
9062	fatty acid catabolic process	14 out of 1188 genes, 1.2%	18 out of 6473 background genes, 0.3%	0.00012	0.00%
43436	oxoacid metabolic process	105 out of 1188 genes, 8.8%	360 out of 6473 background genes, 5.6%	0.00033	0.00%
72329	monocarboxylic acid catabolic process	21 out of 1188 genes, 1.8%	37 out of 6473 background genes, 0.6%	0.00035	0.00%
6082	organic acid metabolic process	105 out of 1188 genes, 8.8%	361 out of 6473 background genes, 5.6%	0.00038	0.00%
6083	acetate metabolic process	11 out of 1188 genes, 0.9%	13 out of 6473 background genes, 0.2%	0.00079	0.00%
19318	hexose metabolic process	21 out of 1188 genes, 1.8%	39 out of 6473 background genes, 0.6%	0.00118	0.00%
1904659	glucose transmembrane transport	15 out of 1188 genes, 1.3%	23 out of 6473 background genes, 0.4%	0.00177	0.00%
15749	monosaccharide transmembrane transport	17 out of 1188 genes, 1.4%	29 out of 6473 background genes, 0.4%	0.00289	0.00%
8645	hexose transmembrane transport	17 out of 1188 genes, 1.4%	29 out of 6473 background genes, 0.4%	0.00289	0.00%
19395	fatty acid oxidation	11 out of 1188 genes, 0.9%	14 out of 6473 background genes, 0.2%	0.00308	0.00%
34440	lipid oxidation	11 out of 1188 genes, 0.9%	14 out of 6473 background genes, 0.2%	0.00308	0.00%
44281	small molecule metabolic process	182 out of 1188 genes, 15.3%	735 out of 6473 background genes, 11.4%	0.00473	0.00%

34219	carbohydrate transmembrane transport	17 out of 1188 genes, 1.4%	30 out of 6473 background genes, 0.5%	0.00555	0.00%
51666	actin cortical patch localization	53 out of 1188 genes, 4.5%	159 out of 6473 background genes, 2.5%	0.00657	0.00%
1901565	organonitrogen compound catabolic process	193 out of 1188 genes, 16.2%	795 out of 6473 background genes, 12.3%	0.00921	0.00%
42221	response to chemical	137 out of 1188 genes, 11.5%	531 out of 6473 background genes, 8.2%	0.0105	0.00%
50896	response to stimulus	289 out of 1188 genes, 24.3%	1274 out of 6473 background genes, 19.7%	0.01417	0.05%
5976	polysaccharide metabolic process	24 out of 1188 genes, 2.0%	54 out of 6473 background genes, 0.8%	0.01601	0.05%
6635	fatty acid beta-oxidation	9 out of 1188 genes, 0.8%	11 out of 6473 background genes, 0.2%	0.01692	0.05%
70887	cellular response to chemical stimulus	111 out of 1188 genes, 9.3%	417 out of 6473 background genes, 6.4%	0.01982	0.09%
6577	amino-acid betaine metabolic process	7 out of 1188 genes, 0.6%	8 out of 6473 background genes, 0.1%	0.08875	0.27%

Table S3. GO term enrichment data for 12 genes that are commonly differentially expressed between 54hr dispersed cells and 54hr biofilm cells in WT and *rob1Δ/Δ*.

GOID	GO_term	Cluster frequency	Background frequency	Corrected P-value	False discovery rate
15976	carbon utilization	4 out of 12 genes, 33.3%	17 out of 6473 background genes, 0.3%	1.52E-06	0.00%
45733	acetate catabolic process	3 out of 12 genes, 25.0%	8 out of 6473 background genes, 0.1%	2.60E-05	0.00%
6083	acetate metabolic process	3 out of 12 genes, 25.0%	13 out of 6473 background genes, 0.2%	0.00013	0.00%
44255	cellular lipid metabolic process	7 out of 12 genes, 58.3%	443 out of 6473 background genes, 6.8%	0.00037	0.00%
6629	lipid metabolic process	7 out of 12 genes, 58.3%	468 out of 6473 background genes, 7.2%	0.00054	0.00%
72329	monocarboxylic acid catabolic process	3 out of 12 genes, 25.0%	37 out of 6473 background genes, 0.6%	0.0035	0.33%

6631	fatty acid metabolic process	3 out of 12 genes, 25.0%	68 out of 6473 background genes, 1.1%	0.02188	1.71%
16054	organic acid catabolic process	3 out of 12 genes, 25.0%	76 out of 6473 background genes, 1.2%	0.03044	1.75%
46395	carboxylic acid catabolic process	3 out of 12 genes, 25.0%	76 out of 6473 background genes, 1.2%	0.03044	1.56%
9062	fatty acid catabolic process	2 out of 12 genes, 16.7%	18 out of 6473 background genes, 0.3%	0.04552	2.40%
44282	small molecule catabolic process	3 out of 12 genes, 25.0%	108 out of 6473 background genes, 1.7%	0.08549	4.55%

Table S4. GO term enrichment analysis of the 5 genes that are commonly upregulated in 54hr dispersed cells compared to 54hr biofilm cells in WT and *rob1Δ/Δ*.

GOID	GO_term	Cluster frequency	Background frequency	Corrected P-value	False discovery rate
15976	carbon utilization	4 out of 5 genes, 80.0%	17 out of 6473 background genes, 0.3%	6.66E-09	0.00%
45733	acetate catabolic process	3 out of 5 genes, 60.0%	8 out of 6473 background genes, 0.1%	5.07E-07	0.00%
6083	acetate metabolic process	3 out of 5 genes, 60.0%	13 out of 6473 background genes, 0.2%	2.58E-06	0.00%
72329	monocarboxylic acid catabolic process	3 out of 5 genes, 60.0%	37 out of 6473 background genes, 0.6%	6.99E-05	0.00%
6631	fatty acid metabolic process	3 out of 5 genes, 60.0%	68 out of 6473 background genes, 1.1%	0.00044	0.00%
16054	organic acid catabolic process	3 out of 5 genes, 60.0%	76 out of 6473 background genes, 1.2%	0.00062	0.00%
46395	carboxylic acid catabolic process	3 out of 5 genes, 60.0%	76 out of 6473 background genes, 1.2%	0.00062	0.00%
31667	response to nutrient levels	4 out of 5 genes, 80.0%	330 out of 6473 background genes, 5.1%	0.0013	0.00%
9991	response to extracellular stimulus	4 out of 5 genes, 80.0%	335 out of 6473 background genes, 5.2%	0.00138	0.00%
44282	small molecule catabolic process	3 out of 5 genes, 60.0%	108 out of 6473 background genes, 1.7%	0.0018	0.00%

9605	response to external stimulus	4 out of 5 genes, 80.0%	377 out of 6473 background genes, 5.8%	0.00221	0.00%
9062	fatty acid catabolic process	2 out of 5 genes, 40.0%	18 out of 6473 background genes, 0.3%	0.00297	0.00%
32787	monocarboxylic acid metabolic process	3 out of 5 genes, 60.0%	147 out of 6473 background genes, 2.3%	0.00455	0.00%
44242	cellular lipid catabolic process	2 out of 5 genes, 40.0%	36 out of 6473 background genes, 0.6%	0.0122	0.29%
8643	carbohydrate transport	4 out of 5 genes, 80.0%	585 out of 6473 background genes, 9.0%	0.01257	0.27%
16042	lipid catabolic process	2 out of 5 genes, 40.0%	48 out of 6473 background genes, 0.7%	0.02176	0.50%
71702	organic substance transport	5 out of 5 genes, 100.0%	1458 out of 6473 background genes, 22.5%	0.02364	0.59%
19752	carboxylic acid metabolic process	3 out of 5 genes, 60.0%	348 out of 6473 background genes, 5.4%	0.05824	0.89%
43436	oxoacid metabolic process	3 out of 5 genes, 60.0%	360 out of 6473 background genes, 5.6%	0.06431	0.95%
6082	organic acid metabolic process	3 out of 5 genes, 60.0%	361 out of 6473 background genes, 5.6%	0.06483	0.90%

Table S5. GO term enrichment analysis of the 7 genes that are commonly downregulated in 54hr dispersed cells compared to 54hr biofilm cells in WT and *rob1Δ/Δ*.

GOID	GO_term	Cluster frequency	Background frequency	Corrected P-value	False discovery rate
8610	lipid biosynthetic process	4 out of 7 genes, 57.1%	348 out of 6473 background genes, 5.4%	0.0101	20.00%
16129	phytosteroid biosynthetic process	3 out of 7 genes, 42.9%	162 out of 6473 background genes, 2.5%	0.02	14.00%
1902653	secondary alcohol biosynthetic process	3 out of 7 genes, 42.9%	162 out of 6473 background genes, 2.5%	0.02	9.33%
6696	ergosterol biosynthetic process	3 out of 7 genes, 42.9%	162 out of 6473 background genes, 2.5%	0.02	7.00%
97384	cellular lipid biosynthetic process	3 out of 7 genes, 42.9%	162 out of 6473 background genes, 2.5%	0.02	5.60%

16126	sterol biosynthetic process	3 out of 7 genes, 42.9%	165 out of 6473 background genes, 2.5%	0.02111	4.67%
16128	phytosteroid metabolic process	3 out of 7 genes, 42.9%	165 out of 6473 background genes, 2.5%	0.02111	4.00%
6694	steroid biosynthetic process	3 out of 7 genes, 42.9%	165 out of 6473 background genes, 2.5%	0.02111	3.50%
8204	ergosterol metabolic process	3 out of 7 genes, 42.9%	165 out of 6473 background genes, 2.5%	0.02111	3.11%
1902652	secondary alcohol metabolic process	3 out of 7 genes, 42.9%	169 out of 6473 background genes, 2.6%	0.02265	2.80%
16125	sterol metabolic process	3 out of 7 genes, 42.9%	174 out of 6473 background genes, 2.7%	0.02468	2.55%
44255	cellular lipid metabolic process	4 out of 7 genes, 57.1%	443 out of 6473 background genes, 6.8%	0.02566	2.50%
8202	steroid metabolic process	3 out of 7 genes, 42.9%	177 out of 6473 background genes, 2.7%	0.02595	2.31%
46165	alcohol biosynthetic process	3 out of 7 genes, 42.9%	187 out of 6473 background genes, 2.9%	0.03049	2.14%
6629	lipid metabolic process	4 out of 7 genes, 57.1%	468 out of 6473 background genes, 7.2%	0.03167	2.00%
1901617	organic hydroxy compound biosynthetic process	3 out of 7 genes, 42.9%	197 out of 6473 background genes, 3.0%	0.0355	2.12%
6066	alcohol metabolic process	3 out of 7 genes, 42.9%	226 out of 6473 background genes, 3.5%	0.05298	2.94%
1901615	organic hydroxy compound metabolic process	3 out of 7 genes, 42.9%	253 out of 6473 background genes, 3.9%	0.07349	2.89%

Table S6. GO term enrichment analysis of Jen2, Jen1, Icl1.

GOID	GO_term	Cluster frequency	Background frequency	Corrected P-value	False discovery rate
46942	carboxylic acid transport	2 out of 3 genes, 66.7%	73 out of 6473 background genes, 1.1%	0.0041	2.00%
15849	organic acid transport	2 out of 3 genes, 66.7%	74 out of 6473 background genes, 1.1%	0.00422	1.00%

8643	carbohydrate transport	3 out of 3 genes, 100.0%	585 out of 6473 background genes, 9.0%	0.00808	1.33%
15711	organic anion transport	2 out of 3 genes, 66.7%	112 out of 6473 background genes, 1.7%	0.00968	1.00%

Table S7. GO term enrichment analysis of differentially regulated genes in *rob1Δ/Δ* compared to WT in planktonic cells.

GOID	GO term	Cluster frequency	Background frequency	Corrected P-value	False discovery rate
8643	carbohydrate transport	311 out of 2252 genes, 13.8%	585 out of 6473 background genes, 9.0%	2.90E-18	0.00%
44281	small molecule metabolic process	356 out of 2252 genes, 15.8%	735 out of 6473 background genes, 11.4%	1.17E-12	0.00%
51234	establishment of localization	832 out of 2252 genes, 36.9%	2034 out of 6473 background genes, 31.4%	6.40E-09	0.00%
6810	transport	823 out of 2252 genes, 36.5%	2011 out of 6473 background genes, 31.1%	8.21E-09	0.00%
5975	carbohydrate metabolic process	108 out of 2252 genes, 4.8%	185 out of 6473 background genes, 2.9%	7.59E-08	0.00%
51179	localization	876 out of 2252 genes, 38.9%	2177 out of 6473 background genes, 33.6%	1.21E-07	0.00%
46165	alcohol biosynthetic process	108 out of 2252 genes, 4.8%	187 out of 6473 background genes, 2.9%	1.88E-07	0.00%
6364	rRNA processing	361 out of 2252 genes, 16.0%	806 out of 6473 background genes, 12.5%	6.43E-07	0.00%
1901617	organic hydroxy compound biosynthetic process	111 out of 2252 genes, 4.9%	197 out of 6473 background genes, 3.0%	8.11E-07	0.00%
44283	small molecule biosynthetic process	190 out of 2252 genes, 8.4%	381 out of 6473 background genes, 5.9%	9.39E-07	0.00%
6066	alcohol metabolic process	123 out of 2252 genes, 5.5%	226 out of 6473 background genes, 3.5%	1.78E-06	0.00%
8202	steroid metabolic process	101 out of 2252 genes, 4.5%	177 out of 6473 background genes, 2.7%	2.02E-06	0.00%
16129	phytosteroid biosynthetic process	94 out of 2252 genes, 4.2%	162 out of 6473 background genes, 2.5%	2.38E-06	0.00%

1902653	secondary alcohol biosynthetic process	94 out of 2252 genes, 4.2%	162 out of 6473 background genes, 2.5%	2.38E-06	0.00%
6696	ergosterol biosynthetic process	94 out of 2252 genes, 4.2%	162 out of 6473 background genes, 2.5%	2.38E-06	0.00%
97384	cellular lipid biosynthetic process	94 out of 2252 genes, 4.2%	162 out of 6473 background genes, 2.5%	2.38E-06	0.00%
71702	organic substance transport	605 out of 2252 genes, 26.9%	1458 out of 6473 background genes, 22.5%	2.46E-06	0.00%
1902652	secondary alcohol metabolic process	97 out of 2252 genes, 4.3%	169 out of 6473 background genes, 2.6%	2.88E-06	0.00%
1901615	organic hydroxy compound metabolic process	134 out of 2252 genes, 6.0%	253 out of 6473 background genes, 3.9%	3.37E-06	0.00%
16128	phytosteroid metabolic process	95 out of 2252 genes, 4.2%	165 out of 6473 background genes, 2.5%	3.42E-06	0.00%
8204	ergosterol metabolic process	95 out of 2252 genes, 4.2%	165 out of 6473 background genes, 2.5%	3.42E-06	0.00%
16072	rRNA metabolic process	368 out of 2252 genes, 16.3%	835 out of 6473 background genes, 12.9%	4.85E-06	0.00%
34470	ncRNA processing	378 out of 2252 genes, 16.8%	862 out of 6473 background genes, 13.3%	5.87E-06	0.00%
16126	sterol biosynthetic process	94 out of 2252 genes, 4.2%	165 out of 6473 background genes, 2.5%	8.95E-06	0.00%
6694	steroid biosynthetic process	94 out of 2252 genes, 4.2%	165 out of 6473 background genes, 2.5%	8.95E-06	0.00%
16125	sterol metabolic process	98 out of 2252 genes, 4.4%	174 out of 6473 background genes, 2.7%	9.48E-06	0.00%
6629	lipid metabolic process	221 out of 2252 genes, 9.8%	468 out of 6473 background genes, 7.2%	1.68E-05	0.00%
462	maturation of SSU-rRNA from tricistronic rRNA transcript (SSU-rRNA, 5.8S rRNA, LSU-rRNA)	281 out of 2252 genes, 12.5%	620 out of 6473 background genes, 9.6%	2.24E-05	0.00%
42254	ribosome biogenesis	384 out of 2252 genes, 17.1%	886 out of 6473 background genes, 13.7%	2.42E-05	0.00%
22613	ribonucleoprotein complex biogenesis	395 out of 2252 genes, 17.5%	915 out of 6473 background genes, 14.1%	2.52E-05	0.00%

34660	ncRNA metabolic process	403 out of 2252 genes, 17.9%	936 out of 6473 background genes, 14.5%	2.53E-05	0.00%
27	ribosomal large subunit assembly	65 out of 2252 genes, 2.9%	105 out of 6473 background genes, 1.6%	2.99E-05	0.00%
30490	maturation of SSU-rRNA	283 out of 2252 genes, 12.6%	627 out of 6473 background genes, 9.7%	3.27E-05	0.00%
42274	ribosomal small subunit biogenesis	286 out of 2252 genes, 12.7%	636 out of 6473 background genes, 9.8%	4.24E-05	0.00%
44255	cellular lipid metabolic process	209 out of 2252 genes, 9.3%	443 out of 6473 background genes, 6.8%	5.00E-05	0.00%
42273	ribosomal large subunit biogenesis	250 out of 2252 genes, 11.1%	546 out of 6473 background genes, 8.4%	5.52E-05	0.00%
9987	cellular process	1696 out of 2252 genes, 75.3%	4602 out of 6473 background genes, 71.1%	6.21E-05	0.00%
469	cleavage involved in rRNA processing	226 out of 2252 genes, 10.0%	488 out of 6473 background genes, 7.5%	8.98E-05	0.00%
6396	RNA processing	398 out of 2252 genes, 17.7%	932 out of 6473 background genes, 14.4%	0.0001	0.00%
966	RNA 5'-end processing	198 out of 2252 genes, 8.8%	421 out of 6473 background genes, 6.5%	0.00016	0.00%
34471	ncRNA 5'-end processing	197 out of 2252 genes, 8.7%	419 out of 6473 background genes, 6.5%	0.00018	0.00%
967	rRNA 5'-end processing	197 out of 2252 genes, 8.7%	419 out of 6473 background genes, 6.5%	0.00018	0.00%
90501	RNA phosphodiester bond hydrolysis	229 out of 2252 genes, 10.2%	500 out of 6473 background genes, 7.7%	0.00022	0.00%
90305	nucleic acid phosphodiester bond hydrolysis	233 out of 2252 genes, 10.3%	511 out of 6473 background genes, 7.9%	0.00027	0.00%
32787	monocarboxylic acid metabolic process	82 out of 2252 genes, 3.6%	147 out of 6473 background genes, 2.3%	0.00032	0.00%
472	endonucleolytic cleavage to generate mature 5'-end of SSU-rRNA from (SSU-rRNA, 5.8S rRNA, LSU-rRNA)	195 out of 2252 genes, 8.7%	417 out of 6473 background genes, 6.4%	0.00035	0.00%
36260	RNA capping	198 out of 2252 genes, 8.8%	426 out of 6473 background genes, 6.6%	0.00049	0.00%

8152	metabolic process	1564 out of 2252 genes, 69.4%	4231 out of 6473 background genes, 65.4%	0.00065	0.00%
90502	RNA phosphodiester bond hydrolysis, endonucleolytic	216 out of 2252 genes, 9.6%	474 out of 6473 background genes, 7.3%	0.00089	0.00%
16042	lipid catabolic process	34 out of 2252 genes, 1.5%	48 out of 6473 background genes, 0.7%	0.00102	0.00%
478	endonucleolytic cleavage involved in rRNA processing	215 out of 2252 genes, 9.5%	473 out of 6473 background genes, 7.3%	0.0012	0.00%
479	endonucleolytic cleavage of tricistronic rRNA transcript (SSU-rRNA, 5.8S rRNA, LSU-rRNA)	215 out of 2252 genes, 9.5%	473 out of 6473 background genes, 7.3%	0.0012	0.00%
463	maturation of LSU-rRNA from tricistronic rRNA transcript (SSU-rRNA, 5.8S rRNA, LSU-rRNA)	197 out of 2252 genes, 8.7%	429 out of 6473 background genes, 6.6%	0.00158	0.00%
470	maturation of LSU-rRNA	197 out of 2252 genes, 8.7%	431 out of 6473 background genes, 6.7%	0.00238	0.00%
1901360	organic cyclic compound metabolic process	746 out of 2252 genes, 33.1%	1902 out of 6473 background genes, 29.4%	0.00255	0.00%
44242	cellular lipid catabolic process	27 out of 2252 genes, 1.2%	36 out of 6473 background genes, 0.6%	0.00268	0.00%
42255	ribosome assembly	69 out of 2252 genes, 3.1%	125 out of 6473 background genes, 1.9%	0.00556	0.00%
44419	biological process involved in interspecies interaction between organisms	160 out of 2252 genes, 7.1%	344 out of 6473 background genes, 5.3%	0.00772	0.00%
44282	small molecule catabolic process	61 out of 2252 genes, 2.7%	108 out of 6473 background genes, 1.7%	0.00792	0.00%
71704	organic substance metabolic process	1379 out of 2252 genes, 61.2%	3716 out of 6473 background genes, 57.4%	0.00841	0.00%
41	transition metal ion transport	31 out of 2252 genes, 1.4%	45 out of 6473 background genes, 0.7%	0.00877	0.00%
9062	fatty acid catabolic process	16 out of 2252 genes, 0.7%	18 out of 6473 background genes, 0.3%	0.00887	0.00%
16054	organic acid catabolic process	46 out of 2252 genes, 2.0%	76 out of 6473 background genes, 1.2%	0.01055	0.00%
46395	carboxylic acid catabolic process	46 out of 2252 genes, 2.0%	76 out of 6473 background genes, 1.2%	0.01055	0.00%

6631	fatty acid metabolic process	42 out of 2252 genes, 1.9%	68 out of 6473 background genes, 1.1%	0.01337	0.00%
6082	organic acid metabolic process	165 out of 2252 genes, 7.3%	361 out of 6473 background genes, 5.6%	0.01956	0.00%
6826	iron ion transport	22 out of 2252 genes, 1.0%	29 out of 6473 background genes, 0.4%	0.02075	0.00%
43436	oxoacid metabolic process	164 out of 2252 genes, 7.3%	360 out of 6473 background genes, 5.6%	0.02642	0.00%
44238	primary metabolic process	1333 out of 2252 genes, 59.2%	3596 out of 6473 background genes, 55.6%	0.02646	0.00%
19752	carboxylic acid metabolic process	159 out of 2252 genes, 7.1%	348 out of 6473 background genes, 5.4%	0.02965	0.00%
1901135	carbohydrate derivative metabolic process	172 out of 2252 genes, 7.6%	381 out of 6473 background genes, 5.9%	0.03083	0.00%
72329	monocarboxylic acid catabolic process	26 out of 2252 genes, 1.2%	37 out of 6473 background genes, 0.6%	0.03181	0.00%
459	exonucleolytic trimming involved in rRNA processing	16 out of 2252 genes, 0.7%	19 out of 6473 background genes, 0.3%	0.03794	0.00%
90503	RNA phosphodiester bond hydrolysis, exonucleolytic	16 out of 2252 genes, 0.7%	19 out of 6473 background genes, 0.3%	0.03794	0.00%
8610	lipid biosynthetic process	158 out of 2252 genes, 7.0%	348 out of 6473 background genes, 5.4%	0.04865	0.00%
71826	protein-RNA complex organization	97 out of 2252 genes, 4.3%	198 out of 6473 background genes, 3.1%	0.05981	0.03%
44085	cellular component biogenesis	529 out of 2252 genes, 23.5%	1339 out of 6473 background genes, 20.7%	0.08694	0.05%
9156	ribonucleoside monophosphate biosynthetic process	15 out of 2252 genes, 0.7%	18 out of 6473 background genes, 0.3%	0.09275	0.05%
9161	ribonucleoside monophosphate metabolic process	15 out of 2252 genes, 0.7%	18 out of 6473 background genes, 0.3%	0.09275	0.05%

Chapter 7. Conclusions and Future Directions

Stephanie H Geller wrote this chapter.

This thesis describes tools built to the study dispersion from *C. albicans* biofilms, the screening of a transcription factor (TF) mutant library, and RNA sequencing of a hyper dispersive mutant. Specifically, I introduced two optogenetic tools built in *S. cerevisiae* to control gene expression with light and tested a similar optogenetic tool in *C. albicans*. To develop these tools, I added light-controlled components to an existing modular cloning toolkit for *S. cerevisiae* and expanded the toolkit to function with *C. albicans*. I also developed and used an underoil microfluidic assay for studying the process of dispersion. Lastly, I discovered a hyper dispersive *C. albicans* mutant by screening a TF knockout library. I then performed mRNA-seq on the hyper dispersive mutant and its parent strain to identify genes potentially important for dispersion. This work improves our ability to effectively study dispersion in *C. albicans* and provides a high-quality mRNA-seq dataset to inform future studies of dispersion and the development of new therapeutics for treating *C. albicans* infections.

Optogenetic tools built in *S. cerevisiae*

Optogenetic systems use genetically encoded, light-controlled effector proteins to perturb cellular processes [1]–[3]. They can be powerful tools for studying protein interactions, evaluating protein production, and controlling pathways used in important applications like biofuel production [1], [2], [4], [5]. Optogenetics is a powerful tool for studying dispersion as it can be used to control gene expression with both spatial and temporal precision. This can result in normal biofilm development until light is applied, changing the expression of a specific gene of interest.

In Chapter 2, I introduced an optogenetic tool for repressing gene expression with light using dCas9 fused to a light-inducible nuclear localization signal (LINuS). Therefore, dCas9-LINuS

enters the nucleus in response to blue light and is directed to target genes by a guide RNA where it represses gene expression via steric hindrance [6]. I also added the repressor domain Mxi1 to dCas9-LiNUS to further repress gene expression. The tool was able to achieve up to 10-fold repression of gene expression, but with substantial variation among cells. Subsequent investigation by another lab member, showed that fluorescent proteins tagged with LiNUS are either poorly expressed or highly degraded in yeast cells, possibly because its nuclear localization signal (NLS) includes a sequence (KKKRK) resembling a D-box degron motif [7], [8]. It is therefore possible that dCas9-LiNUS is subject to similar effects, which should be investigated further. If the protein is being degraded, this could lead to less repression of the gene of interest since there would be less dCas9-LiNUS available to bind to the DNA. If so, a newer, more optimized optogenetic tool like CLASP, which uses a different NLS, may result in greater repression of the gene of interest through more protein availability [9]. CLASP features a light inhibited plasma membrane anchoring system which would decrease background repression from "leakiness" (unwanted activation in the dark), and an optimized *S. cerevisiae* NLS that would allow for potentially better repression from increased abundance of the optogenetic tool.

In Chapter 3, I described an optogenetic tool for inducing gene expression using the light-inducible heterodimerizers CRY2 and CIB1. In this tool, CRY2 is fused to a Zif268 DNA binding domain (DBD) and CIB1 is fused to a VP16 activation domain. I used this tool to activate a fluorescent reporter, mRuby2, under the control of a synthetic promoter pZIF, which includes a Zif268 binding site. When excited by light, CRY2 undergoes a conformation change and binds CIB1, recruiting the activation domain to pZIF to induce mRuby2 expression. With this tool, mRuby2 expression was dependent on the intensity and the duty cycle of administered light. A limitation of this tool

for studying *C. albicans* dispersion is that—by design—it binds only the pZIF promoter, not *C. albicans* genes. This means that when investigating a gene of interest, normal expression of this gene will be disrupted when it is put under the control of the pZIF. This may cause a change in biofilm formation, much like ones seen by using gene knockouts or overexpression experiments. However, future studies could use this tool to study the role of *C. albicans* genes in dispersion by modifying their promoters to bind Zif268, such as using pZIF.

Future studies could build on these tools to study *C. albicans* dispersion by combining a light-controlled dCas9 with the VP16 activation domain or a repressor domain such as Mxi1. Such a tool could thus be targeted to any *C. albicans* gene containing a PAM sequence. Optogenetic control of this dCas9 construct could be achieved using CLASP, a successor to LINuS that is much more effective in *S. cerevisiae*. With this tool, *C. albicans* strains could grow normally in the dark, but could be illuminated to perturb target genes as the biofilm develops. Alternately, CRY2 and CIB1 could be used to reconstitute a split dCas9 in response to light, however a potential drawback of this approach is that constitutively nuclear dCas9 fragments could sterically hinder the gene of interest during biofilm growth, resulting in non-normal expression of the gene during biofilm development [10], [11].

Development of the *C. albicans* toolkit and optogenetic tool

In Chapter 4, I tested if CRY2/CIB1-based optogenetic tool like that developed for *S. cerevisiae* in Chapter 3, could be used to control gene expression in *C. albicans*. I chose a CRY2/CIB1-based system as they had already been used in *C. albicans* to control proteins binding [1]. I had previously found that optimization of CRY2 and CIB1 expression levels was necessary for optimal

performance in *S. cerevisiae*. I therefore ported a set of well-characterized constitutive promoters from *S. cerevisiae* to *C. albicans* with the aim of using them to tune CRY2 and CIB1 levels. As part of this process, I measured the strength of these promoters in *C albicans*, which has not been previously explored. Many constitutive *S. cerevisiae* promoters functioned in *C. albicans*, though none were as strong as the native *C. albicans* promoters pENO1 and pACT1. I also screened a set of *S. cerevisiae* terminators in *C. albicans* and found no significant differences in reporter gene expression among them, as was the case in *S. cerevisiae*. Because tools for genetically modifying *C. albicans* are limited (e.g., there is no known origin of replication) I incorporated these promoters, terminators, and some components for building optogenetic tools into a modular cloning toolkit, which I expanded upon to allow the rapid assembly of plasmids for integration into a safe harbor locus in the *C. albicans* genome. I did not test the *S. cerevisiae* promoters in *C. albicans* cells grown in biofilm forming conditions. Since gene perturbations would need to occur during biofilm growth to directly study dispersion, future experiments should measure the performance of these promoters in biofilm forming conditions to determine if they are appropriate for studies of *C. albicans* dispersion. We know that gene expression changes as the biofilm develops, which could result in a promoter that causes high expression of the gene of interest during planktonic growth, to be lowly expressed during biofilm growth. If these promoters do not drive expression of the optogenetic tools during biofilm development, they would not be suitable for studying dispersion. Additionally, we know from Chapter 3 that the ratio of CRY2:CIB1 is important for optimal output of the gene of interest. Therefore, we would need to choose promoters that cause high and medium expression in the biofilm growth, which, as stated, may not be the same promoters that cause high and medium expression during planktonic growth.

After determining the strength of *S. cerevisiae* promoters and terminators in *C. albicans*, I built a CRY2/CIB1-based optogenetic tool for controlling gene expression in *C. albicans*. I tested the tool with the Zif268 or LexA DNA binding domains and the VP64 activation domain. However, no version of this tool appeared to induce the expression of a fluorescent reporter in response to light. I was unable to determine why these constructs did not work but, among other reasons, it's possible that my DNA binding domains may not function in *C. albicans* as would be expected based on the literature or that my activation domain does not properly recruit transcriptional machinery to the promoter. Because this optogenetic tool did not work, I also created TFZIF, to test the performance of a simpler construct with just the Zif268 DNA binding domain, a constitutive NLS, and a VP16 or VP64 activation domain. However, TFZIF also did not activate a fluorescent reporter in *C. albicans*, which indicated that the problems were not simply due to the light sensitive components. Future efforts to make such a tool in *Candida* should therefore investigate the function of each individual component, test different linker sequences, and confirm that the entire construct is expressed and localizes to the nucleus. Future efforts to optimize such a tool could also use the truncated CRY2PHR protein, which is more effective than CRY2 for light activated gene expression in *S. cerevisiae* [12].

While testing my optogenetic tool in *C. albicans,* I also noticed that the samples exposed to light fluoresced more strongly than dark samples, regardless of whether a fluorescent reporter was present. This indicates that light induces auto-fluorescence in *C. albicans*. Since autofluorescence has also been reported in *C. albicans* exposed to stressful conditions like oxidative stress, I hypothesize that the light conditions used are causing a stress-induced autofluorescence [13]–[15]. Testing different light intensities and duty cycles would test my hypothesis and potentially identify

less stressful light doses for future optogenetic experiments. Such experiments could be performed using the automated high-throughput light induction system "LUSTRO" to test many light doses at once [16].

Underoil microfluidic assay for studying dispersion

Currently there are three assays for testing the dispersion of *C. albicans* biofilms: a 96-well microplate assay, a micro-flow assay, and a macro-flow assay [17]–[20]. All these assays have caveats that limit their utility for studying large libraries of mutants for dispersion phenotypes. These caveats include: throughput limitations, the inability to collect cells for further analysis, the introduction of variability through necessary human interventions, and the absence of flow. Therefore in Chapter 5, I introduced an underoil microfluidic assay for visualizing biofilm growth and dispersion. This approach uses plasma treatment and silanization to create two different surface chemistries on a slide that allow many self-contained droplets of media to be deposited on the slide, each acting like a well of a microplate. I demonstrated that *C. albicans* can grow biofilms and disperse in these droplets, and using visual scoring, I was able to detect differences between a highly dispersive strain and a moderately dispersive strain, as confirmed by a traditional XTT dispersion assay. It was difficult to distinguish less dramatic differences in dispersion between strains by simple visual scoring. However, given recent improvements in computer vision, future studies should be able to use image processing software to identify hyphae and yeast from underoil images of *C. albicans* dispersion [21]–[23] [24].

The underoil assay allows the introduction of flow through the biofilm. By creating channels with outlets of different sizes, it is possible to create a pressure gradient in the channel that results in

media flow to one of the outlets. It is also possible to time the introduction of flow through the channel. This is achieved by adding a valve to the channel, effectively splitting it into two sections. Adding media to the valve then connects the two sections and causes media to flow through the channel to the larger outlet port. With collaborators, I demonstrated that this flow is sufficient to carry dispersed cells away from the biofilm.

The environment in the underoil microfluidic assay differs from a 96-well plate or the macro-flow assay and it is currently unknown exactly how this affects biofilm development. However, through visualization, I have demonstrated that all the life stages of *C. albicans* biofilm development occur in this assay. However, I also noticed that the *C. albicans* life cycle appears to be sped up in the underoil microfluidic droplets, with dispersion starting around 8 hours after seeding, compared to at least 24 hours in a 96-well microplate. I hypothesize that this is a result of a resource limitation in the underoil environment, though future studies are needed to investigate this behavior. These studies could either dropout or supplement resources to determine their effects on dispersion in either environment. For example, in Chapter 6 I discovered that dispersed cells have increased gene expression of genes related to the carbohydrate transport process. Therefore, I can investigate the effects of different amounts of carbohydrate supplementation on dispersion. Additionally, because of the small size of the droplets, the local concentration of any quorum sensing molecules would ride quickly. This could be investigated through supplementing these molecules into the growth media, or by taking spent media from a dispersing biofilm, filtering it to remove any cells, and supplementing the media back. This would result in media that has the same resources as fresh media, but any molecules that the cells released would also be present.

Lastly, while all stages of biofilm development are present in the underoil assay, it is not known how gene expression differs in this environment. RNA sequencing can be used to determine differences in gene expression in the underoil microfluidic assay and the 96 well assay by collecting cells from different stages of biofilm development, as well as just planktonic cells growing and observing which genes may be differentially regulated in the underoil microfluidic assay. I would start by looking at differences during planktonic growth, because this is where I may find a resource limitation in the underoil microfluidic assay by differential regulation of genes related to the uptake or processing of these resources. I could then look at differences in biofilm development and maturation that may lead to an explanation for early dispersion.

Screening the TF mutant library and subsequent RNA sequencing of a hyper dispersive mutant

In Chapter 6, I screened a TF knockout mutant library for highly dispersive phenotypes. From this screen I identified a mutant, *rob1Δ/Δ*, that is highly dispersive while retaining the ability to form hyphae. Rob1 is one of 6 transcription factors known to regulate biofilm development. The *rob1Δ/Δ* mutant was deficient in producing elongated hyphae, but not in the ability to initiate hyphal development [25], [26]. A drawback of the TF mutant screen is that it used traditional XTT assays, which have high technical variation, making it difficult to distinguish subtle differences in dispersion phenotypes [27]. In addition, XTT cannot distinguish different cell morphologies and is therefore unable to identify defects in biofilm growth such as the lack of hyphae formation.

I next used mRNA-seq to measure the *rob1Δ/Δ* mutant and its parent strain (WT) at different stages of development. For both strains, I collected and measured both biofilm and supernatant with

dispersed cells at select timepoints. Clustering of measurements indicated that variation between replicates (4 per group) was less than the variation between groups. An MDS plot also indicated distinct gene expression profiles for cells at different stages of biofilm development, though expression differences between corresponding supernatant and biofilm samples were less distinct. My measurements of differential gene expression throughout the *C. albicans* life cycle broadly agreed with those of Nobile, *et al* (2012) and Uppuluri, *et al* (2018) [25], [28]. Interestingly, many carbohydrate transport genes were upregulated in the highly dispersive *rob1Δ/Δ* compared to WT, which agrees with Nobile *et al* (2012) [25]. The *rob1Δ/Δ* and WT had 12 genes in common among the 50 genes whose expression changed the most between biofilm samples and dispersion samples. Based on GO term enrichment, these genes are involved in lipid metabolism and carbon utilization pathways: carbon utilization was upregulated in the dispersed cells and lipid metabolism was upregulated in the biofilm cells. Uppuluri, *et al* (2018) found that Jen2, Jen1, and Icl1 were upregulated in dispersed cells [28], all of which are involved in the carbohydrate transport process according to GO term enrichment [29]. From this, I hypothesize that differences in carbohydrate transport may distinguish dispersed cells and that carbohydrate availability affects dispersion. There is evidence that dispersion is affected by glucose concentration [30] and recent experiments using the underoil microfluidic assay support this hypothesis. Perturbing genes in the carbohydrate transport pathway using a gene induction system would help us understand the role that this pathway plays in dispersion. Additionally, it is interesting that the strain that disperses more (*rob1Δ/Δ)* has upregulated carbohydrate transport. Understanding what benefits and drawbacks this gives to the strain through experimentation using different carbohydrate concentrations may also give insight into how dispersion is affected by carbon availability.

Future studies should also investigate the role Rob1 using a gene induction system. Because Rob1 is necessary for normal biofilm growth, a *rob1Δ/Δ* mutant may show a dispersive phenotype without being directly linked to dispersion. Understanding the role of Rob1 in dispersion can unlock knowledge of the pathways critical for dispersion. The role of Rob1 can be further analyzed by comparing my RNA sequencing results to the ChIP-chip data in Nobile, *et al* (2012) [25] to determine the regulation of the genes that are known to be affected by Rob1. The WT and *rob1Δ/Δ* samples will have information about how these genes are affected during biofilm development with or without Rob1 affecting regulation.

Lastly, my mRNA-seq measurements constitute a vast trove of data and should be analyzed further to identify additional differences between strains throughout the different stages of biofilm development. While I focused on analyzing the dispersing biofilms and the dispersed cells, investigating the differences between early-stage biofilms and dispersing biofilms could give an insight into the pathways that are upregulated to lead to the creation of dispersed cells. I hypothesize that there is a regulated genetic switch from developing a biofilm to creating dispersed cells, but the regulation of the switch is unknown. Gene expression differences between a developing biofilm and a dispersing biofilm could indicate a cause for this switch such as resource limitation, but likely this will have to be explored experimentally by testing dropout and supplementations of different resources such as carbon, nitrogen, or oxygen. Understanding the regulation of biofilm development and dispersion may lead to the ability to halt dispersion, which could be very beneficial in a healthcare setting.

Conclusions

C. albicans dispersion is an understudied process that affects the virulence of an infection [28], [30], [31]. Our understanding of dispersion had been limited by a lack of appropriate tools. In this thesis, I describe tools built to aid the study of dispersion. I also identified a TF mutant, *rob1Δ/Δ*, with a hyper dispersive phenotype. Through RNA sequencing, I found that the carbohydrate transport and utilization processes should be investigated further to understand their role in biofilm development and dispersion. While I focus on changes of genes relating to the carbohydrate transport pathway, additional analysis of my mRNA-seq measurements should be completed to identify additional pathways to study. While there is more to be discovered, the additional tools and information provided in this thesis can help advance our knowledge of dispersion.

References

[1] P. M. Silva, C. Puerner, A. Seminara, M. Bassilana, and R. A. Arkowitz, "Secretory Vesicle Clustering in Fungal Filamentous Cells Does Not Require Directional Growth," *Cell Rep.*, vol. 28, no. 8, pp. 2231-2245.e5, Aug. 2019.

[2] N. Moreno Morales, M. T. Patel, C. J. Stewart, K. Sweeney, and M. N. McClean, "Optogenetic Tools for Control of Public Goods in Saccharomyces cerevisiae," *mSphere*, vol. 6, no. 4, Aug. 2021.

[3] J. Melendez, M. Patel, B. L. Oakes, P. Xu, P. Morton, and M. N. McClean, "Real-time optogenetic control of intracellular protein concentration in microbial cell cultures," *Integr. Biol.*, vol. 6, no. 3, p. 366, Mar. 2014.

[4] J. M. López, L. Duran, and J. L. Avalos, "Physiological limitations and opportunities in microbial metabolic engineering," *Nat. Rev. Microbiol. 2021*, pp. 1–14, 2021.

[5] F. Salinas, V. Rojas, V. Delgado, E. Agosin, and L. F. Larrondo, "Optogenetic switches for light-controlled gene expression in yeast," *Appl. Microbiol. Biotechnol.*, vol. 101, no. 7, pp. 2629–2640, Apr. 2017.

[6] D. Niopek *et al.*, "Engineering light-inducible nuclear localization signals for precise spatiotemporal control of protein dynamics in living cells," *Nat. Commun.*, vol. 5, no. 1, p. 4404, Dec. 2014.

[7] N. E. Davey and D. O. Morgan, "APC/C degron respository," 2016. .

[8] N. E. Davey and D. O. Morgan, "Building a regulatory network with short linear sequence motifs – lessons from the degrons of the anaphase-promoting complex," *Mol. Cell*, vol. 64, no. 1, p. 12, Oct. 2016.

[9] S. Y. Chen *et al.*, "Optogenetic Control Reveals Differential Promoter Interpretation of Transcription Factor Nuclear Translocation Dynamics," *Cell Syst.*, vol. 11, no. 4, p. 336, Oct. 2020.

[10] X. Huang *et al.*, "A Light-Inducible Split-dCas9 System for Inhibiting the Progression of Bladder Cancer Cells by Activating p53 and E-cadherin," *Front. Mol. Biosci.*, vol. 7, p. 445, Jan. 2021.

[11] B. Zetsche, S. E. Volz, and F. Zhang, "A Split Cas9 Architecture for Inducible Genome Editing and Transcription Modulation," *Nat. Biotechnol.*, vol. 33, no. 2, p. 139, 2015.

[12] M. J. Kennedy, R. M. Hughes, L. A. Peteya, J. W. Schwartz, M. D. Ehlers, and C. L. Tucker, "Rapid blue-light-mediated induction of protein interactions in living cells," *Nat. Methods*, vol. 7, no. 12, pp. 973-U48, Dec. 2010.

[13] M. Monici, "Cell and tissue autofluorescence research and diagnostic applications," *Biotechnol. Annu. Rev.*, vol. 11, no. SUPPL., pp. 227–256, Jan. 2005.

[14] R. Maslanka, M. Kwolek-Mirek, and R. Zadrag-Tecza, "Autofluorescence of yeast Saccharomyces cerevisiae cells caused by glucose metabolism products and its methodological implications," *J. Microbiol. Methods*, vol. 146, pp. 55–60, Mar. 2018.

[15] J. Surre, C. Saint-Ruf, V. Collin, S. Orenga, M. Ramjeet, and I. Matic, "Strong increase in the autofluorescence of cells signals struggle for survival," *Sci. Reports 2018 81*, vol. 8, no. 1, pp. 1–14, Aug.

2018.
[16] Z. P. Harmer and M. N. McClean, “Lustro: High-throughput optogenetic experiments enabled by automation and a yeast optogenetic toolkit,” *bioRxiv*, p. 2023.04.07.536078, Apr. 2023.
[17] A. McCall and M. Edgerton, “Real-Time Approach to Flow Cell Imaging of Candida albicans Biofilm Development.,” *J. fungi (Basel, Switzerland)*, vol. 3, no. 1, Mar. 2017.
[18] R. Zarnowski *et al.*, “Coordination of fungal biofilm development by extracellular vesicle cargo,” *Nat. Commun. 2021 121*, vol. 12, no. 1, pp. 1–9, Oct. 2021.
[19] P. Uppuluri, A. K. Chaturvedi, and J. L. Lopez-Ribot, “Design of a Simple Model of Candida albicans Biofilms Formed under Conditions of Flow: Development, Architecture, and Drug Resistance,” *Mycopathologia*, vol. 168, no. 3, pp. 101–109, 2009.
[20] P. Uppuluri and J. L. Lopez-Ribot, “An easy and economical in vitro method for the formation of Candida albicans biofilms under continuous conditions of flow.,” *Virulence*, vol. 1, no. 6, pp. 483–7, 2010.
[21] G. Nagy *et al.*, “Time-lapse video microscopy and image analysis of adherence and growth patterns of Candida albicans strains,” *Appl. Microbiol. Biotechnol.*, vol. 98, no. 11, pp. 5185–5194, Apr. 2014.
[22] A. Cardini, E. Pellegrino, E. Del Dottore, H. A. Gamper, B. Mazzolai, and L. Ercoli, “HyLength: a semi-automated digital image analysis tool for measuring the length of roots and fungal hyphae of dense mycelia,” *Mycorrhiza*, vol. 30, no. 2–3, pp. 229–242, May 2020.
[23] Q. Shen, M. U. F. Kirschbaum, M. J. Hedley, and M. C. Arbestain, “Testing an Alternative Method for Estimating the Length of Fungal Hyphae Using Photomicrography and Image Processing,” *PLoS One*, vol. 11, no. 6, p. e0157017, Jun. 2016.
[24] V. Bettauer *et al.*, “A Deep Learning Approach to Capture the Essence of Candida albicans Morphologies,” *Microbiol. Spectr.*, vol. 10, no. 5, Oct. 2022.
[25] C. J. Nobile *et al.*, “A Recently Evolved Transcriptional Network Controls Biofilm Development in Candida albicans,” *Cell*, vol. 148, pp. 126–138, 2012.
[26] R. S. Wakade, L. C. Ristow, M. Wellington, and D. J. Krysan, “Intravital imaging based genetic screen reveals the transcriptional network governing Candida albicans filamentation during mammalian infection,” *Elife*, vol. 12, Feb. 2023.
[27] J. E. Nett, M. T. Cain, K. Crawford, and D. R. Andes, “Optimizing a Candida Biofilm Microtiter Plate Model for Measurement of Antifungal Susceptibility by Tetrazolium Salt Assay,” *J. Clin. Microbiol.*, vol. 49, no. 4, p. 1426, Apr. 2011.
[28] P. Uppuluri *et al.*, “Candida albicans Dispersed Cells Are Developmentally Distinct from Biofilm and Planktonic Cells.,” *MBio*, vol. 9, no. 4, pp. e01338-18, Sep. 2018.
[29] H. Mi, A. Muruganujan, D. Ebert, X. Huang, and P. D. Thomas, “PANTHER version 14: more genomes, a new PANTHER GO-slim and improvements in enrichment analysis tools,” *Nucleic Acids Res.*, vol. 47, no. D1, pp. D419–D426, Jan. 2019.
[30] P. Uppuluri *et al.*, “Dispersion as an Important Step in the Candida albicans Biofilm Developmental Cycle,” *PLOS Pathog.*, vol. 6, no. 3, 2010.
[31] G. Wall, D. Montelongo-Jauregui, B. Vidal Bonifacio, J. L. Lopez-Ribot, and P. Uppuluri, “Candida albicans biofilm growth and dispersal: contributions to pathogenesis,” *Curr. Opin. Microbiol.*, vol. 52, pp. 1–6, Dec. 2019.